PLEASE NOTE:

In all cases this material has been filmed in the best possible way from the available copy. Problems encountered with this document have been identified here with a check mark ✓.

1. Glossy photographs ✓
2. Colored illustrations _____
3. Photographs with dark background ✓
4. Illustrations are poor copy _____
5. Print shows through as there is text on both sides of page _____
6. Indistinct, broken or small print on several pages _____ throughout _____
7. Tightly bound copy with print lost in spine _____
8. Computer printout pages with indistinct print _____
9. Page(s) _____ lacking when material received, and not available from school or author _____
10. Page(s) _____ seem to be missing in numbering only as text follows _____
11. Poor carbon copy _____
12. Not original copy, several pages with blurred type _____
13. Appendix pages are poor copy _____
14. Original copy with light type _____
15. Curling and wrinkled pages ✓
16. Other _____

THE UNIVERSITY OF OKLAHOMA

GRADUATE COLLEGE

INTERMETALLIC COMPOUND FORMATION IN SOFT SOLDERS

A DISSERTATION

SUBMITTED TO THE GRADUATE FACULTY

in partial fulfillment of the requirements for the

degree of

DOCTOR OF PHILOSOPHY

BY

EVERETT WARNER BROTHERS

Norman, Oklahoma

1979

INTERMETALLIC COMPOUND FORMATION

IN SOFT SOLDERS

APPROVED BY

DISSERTATION COMMITTEE

ACKNOWLEDGEMENTS

I sincerely wish to express appreciation to Dr. Robert J. Block, for his support, guidance, and patience while developing the capabilities necessary to pursue these studies. My associations with Dr. Block, while attempting to acquire an infinitesimal amount of his expertise as metallurgist and metallographer, will be retained as a prized asset.

My gratitude is expressed to Mrs. Rita R. Edwards for conducting the wetting rate experiments, and her detailed summary of the results as presented in Appendix B; Mr. J. D. Brewer for preparation of the excellent micrographs; Mr. W. R. Coleman for his assistance in developing the experimental techniques; and Dr. C. L. Stroud for helpful discussions regarding various aspects of the electrochemistry. Also, my gratitude is expressed to Ms. La Vonne Whitney and the previously mentioned members of the Failure Analysis Laboratory staff for the professional preparation of this manuscript.

I am indebted to my wife Peggy, and my children, Diane and Kathy, who have endured throughout my graduate studies by sincerely understanding my commitment and providing encouragement without which this work would have been impossible.

Finally, I would like to thank Western Electric Company, Inc., for the Engineering and Science Fellowship and for their continued support.

ABSTRACT

The morphology and formation of intermetallic compounds within "soft" soldered connections to substrate materials common to the electronics industry have been documented. Microstructural analyses of the soldered connections have been performed revealing the presence of intermetallic compounds. These compounds have been identified using scanning electron microscopy and energy dispersive X-ray analysis techniques.

A series of experiments with gold plated substrates has been conducted. These experiments demonstrate the reliability problems often associated with thick gold platings. The brittle characteristics of soldered connections to thick gold platings appear to be the result of the formation of intermetallic compound layers. Detachment of the solder fillet from the substrate is found to be related to the presence of $AuSn_2$ intermetallic compounds. Porosity in the solder fillet is shown to be associated with the thickness and type of gold plating. A discussion of porosity in terms of the decomposition of a co-deposited polymer produced in cobalt hardened gold platings is presented.

Area spread tests and wetting rate studies have been conducted to observe the effects of the various "soft" solder alloys. Three different tin-lead solder alloys, 50/50 - 60/40 - 63/37, and a

proprietary antimonial alloy, have been applied to substrates consisting of copper, brass, and gold. Detailed analyses of the results of these studies provide new and additional information regarding the nature of the metallurgical processes involved when soldering with tin based alloys. The formation of a phase corresponding to the Sb_2Sn_3 compound is observed when utilizing the antimonial alloy.

TABLE OF CONTENTS

LIST OF TABLES

LIST OF FIGURES

FIGURE Page

FIGURE Page

FIGURE Page

FIGURE Page

FIGURE Page

FIGURE Page

FIGURE Page

APPENDIX B

FIGURE Page

INTERMETALLIC COMPOUND FORMATION IN SOFT SOLDERS

CHAPTER I

INTRODUCTION

Soldering is a metallurgical process by which metals are joined to produce electrical and mechanical connections. The joining process is achieved by the application of a liquid filler metal or alloy which forms a bond with the substrate surfaces. In most joint configurations surface tension and capillary action cause the melted solder to be drawn into the spaces between the metals to be joined. The solder wets the substrates while molten and reacts with them to form the bond. The simplest metallurgical bond might simply involve a sharp interface and shared grain boundaries between the solidified solder and substrate.

The nature of the interface between substrate and solder is seldom, if ever, simply a sharp transition between the two metals. The solid substrate may dissolve one or more components from the solder producing a surface of greatly altered character and composition; or components from the substrate itself may be dissolved and incorporated

in the solder. Obviously both processes are capable of occurring simultaneously, depending on the metals involved.

The electronics industry is a principal user of soft solders. A filler metal composed of tin and lead is common, with extensive use of the near-eutectic 60/40 alloy (60 wt.% Sn - 40 wt.% Pb). The phase equilibria which govern the dissolution processes occurring when a solder joint is made become complicated when tin is involved. The complications are a direct result of the strong tendency of tin to form intermetallic compounds with a wide variety of other metals. Many of these metals find themselves in common usage as substrate materials upon which soldering must be carried out. A compilation of phase diagrams and structural data is included as Appendix A.

Intermetallic compounds are capable of influencing the mechanical and electrical behavior of soldered joints because of their brittle characteristics. The distribution of the compounds in the soldered joint is critical to determining their influence. As uniformly distributed and isolated particles within the solder mass, the presence of intermetallics may be rather benign. The mechanical and electrical properties of the solder will largely be governed by the continuous solder phases. The comparatively large wetted areas of the soldered joints are capable of minimizing the effects of reaction products which would act to raise the electrical resistivity of the solder.

An entirely different situation is obtained when the compounds form as continuous layers at the solder substrate interface. Under these conditions the intermetallic compounds can interrupt electrical circuits with material of very high resistivity effectively isolating

the metals which were to be electrically joined. The influence upon mechanical behavior of brittle layers which surround the substrate metals should be immediately obvious.

The performance of soldered joints made with tin-lead based filler metals is further complicated by continued reaction in the solid state. Because the solder alloys are low melting, diffusion within the solder and with common substrate metals is relatively fast at room temperature. Recrystallization in strained joints will occur as well as precipitation of various alloy and compound phases. These processes can give rise to delayed failures in components which have been tested and accepted at the time of manufacture.

This paper describes a series of experiments with near-eutectic tin-lead and tin-lead-antimony solders. The work deals primarily with the microstructures of the soldered joints, the intermetallic compounds which form and their relationship to the soldering process. The presentation is divided into sections dealing with specific phases of the investigation. Appropriate background material, description of the experimental procedures and a discussion of the results are included in each section.

Microstructure of Solder Alloys

The solders used in this study were four common alloys 50/50, 60/40, 63/37 tin-lead and a propietary antimonial alloy consisting of 52-Sn 45-Pb and 3-Sb by weight. The last alloy had been developed as a cost effective alternative for traditional near-eutectic solders, in an effort to meet the rising costs of tin. Figures 1, 2, and 3 show the structures obtained from small preforms of 60/40, 63/37, and the antimonial

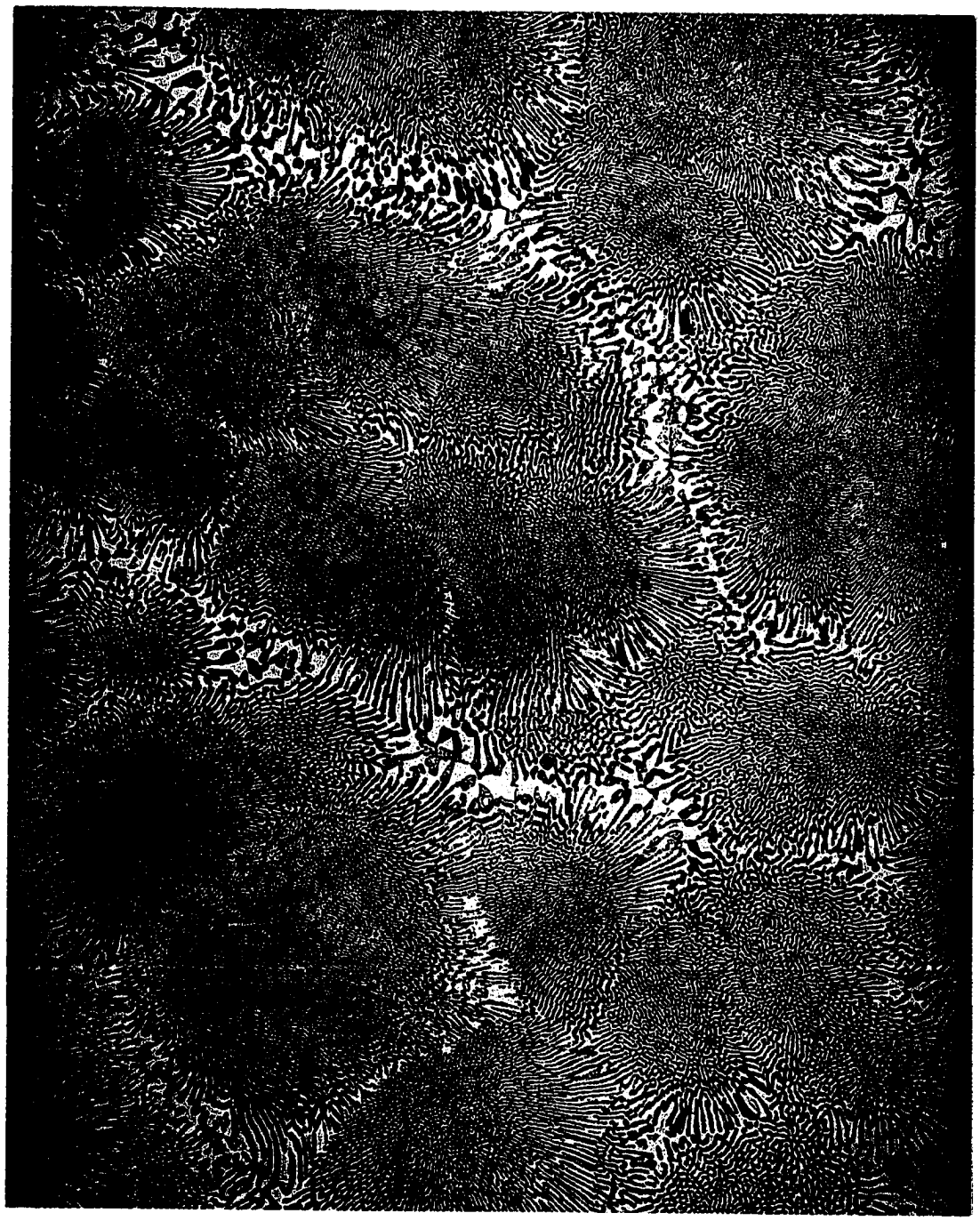

Figure 1. 200X - Peroxide and Glycol Etch
Virgin 60/40 solder alloy after reflowing at
215°C for 80 seconds.

Figure 2. 300X - Peroxide and Glycol Etch
Virgin 63/37 solder alloy after reflowing at
215°C for 80 seconds.

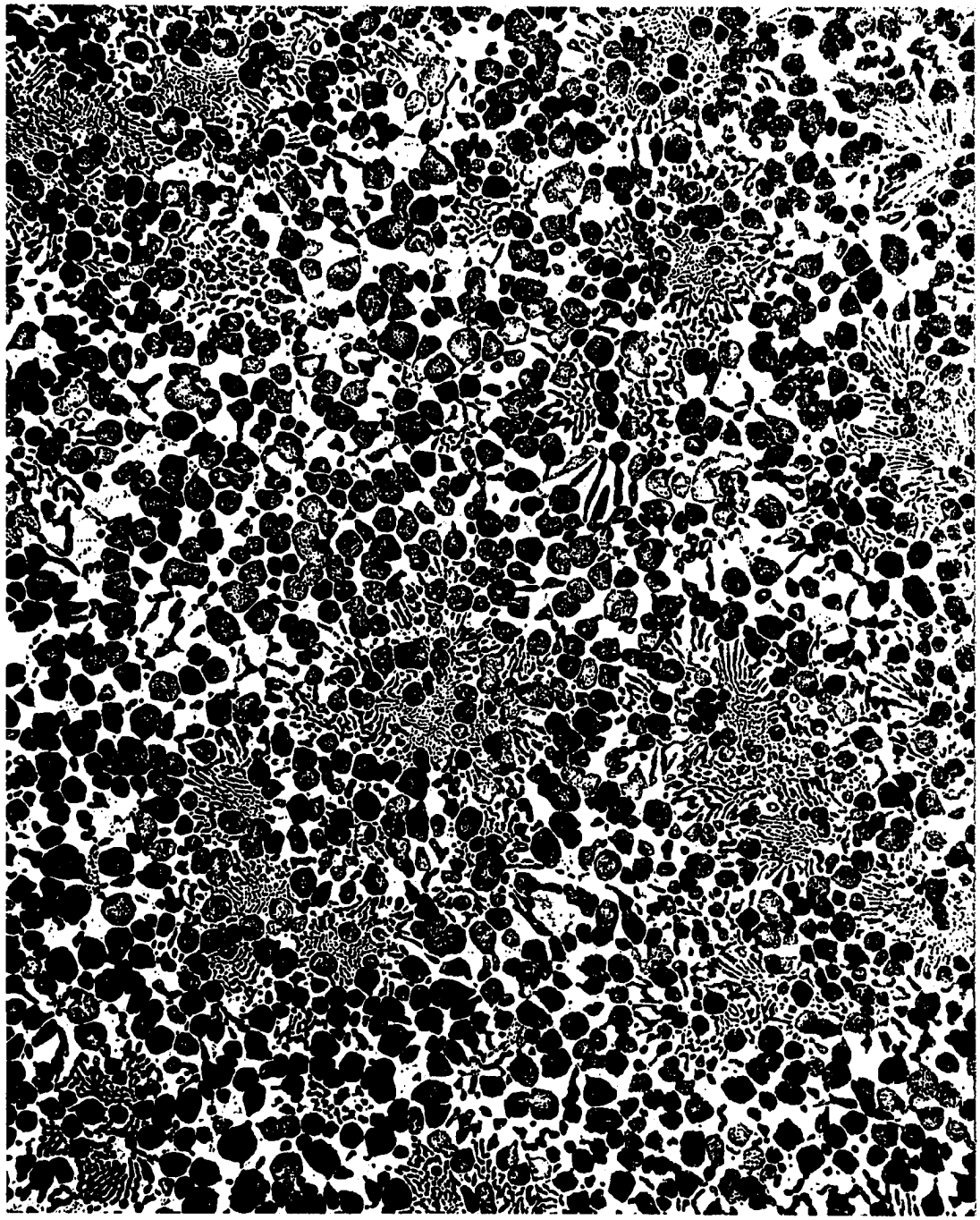

Figure 3. 200X - Peroxide and Glycol Etch
Virgin antimonial solder alloy after reflowing
at 215°C for 80 seconds.

solders after melting at 215°C and resolidifying. In the process of reflowing, the cooling rates subsequent to melting were probably slower than would be obtained from commercial soldering processes due to the large thermal mass of the preforms combined with the teflon containers in which reflowing was accomplished.

The two tin-lead alloys (Figures 1 and 2) exhibited a fine eutectic structure with some evidence of excess α, the dark, lead rich phase, in the hypoeutectic alloy. The ternary alloy showed some evidence of the lamellar eutectic mixture; however, a significant fraction of the α phase appeared as roughly spherical masses in a β (tin rich) matrix. The differences in the phase distributions appear to be most likely due to the antimony and its effect on interfacial energies and diffusion rates.

The low melting temperatures of solder alloys make them particularly susceptible to microstructural changes with aging at ambient temperatures. Figures 4, 5, and 6 demonstrate the effects of a 7-day aging period at 100°C. Assuming ordinary rate theory of the form:

$$\text{Rate} = Ae^{-Q/RT}$$

where Rate = reaction rate
A = rate constant
Q = activation energy
R = gas constant
T = temperature (°K)

and an activation energy of approximately 20,000 cal/mol, the artificial aging treatment corresponded to about 20 years at room temperature. The tin-lead solders show a significant degree of spherodizing of the α phase in the eutectic. Likewise in the antimonial solder the lamellar

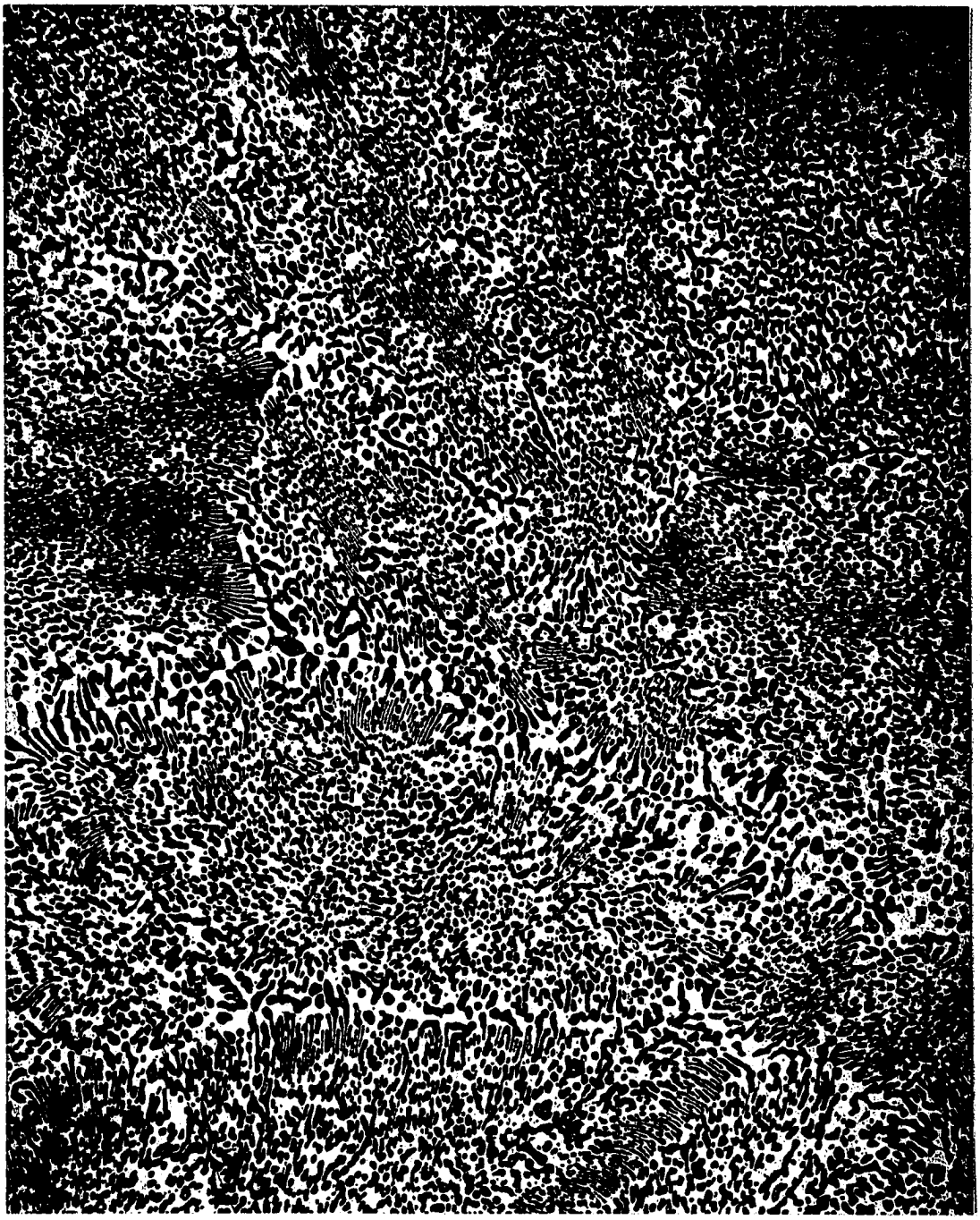

Figure 4. 200X - Peroxide and Glycol Etch
The 60/40 solder alloy of Figure 1
after aging for 7 days at 100°C.

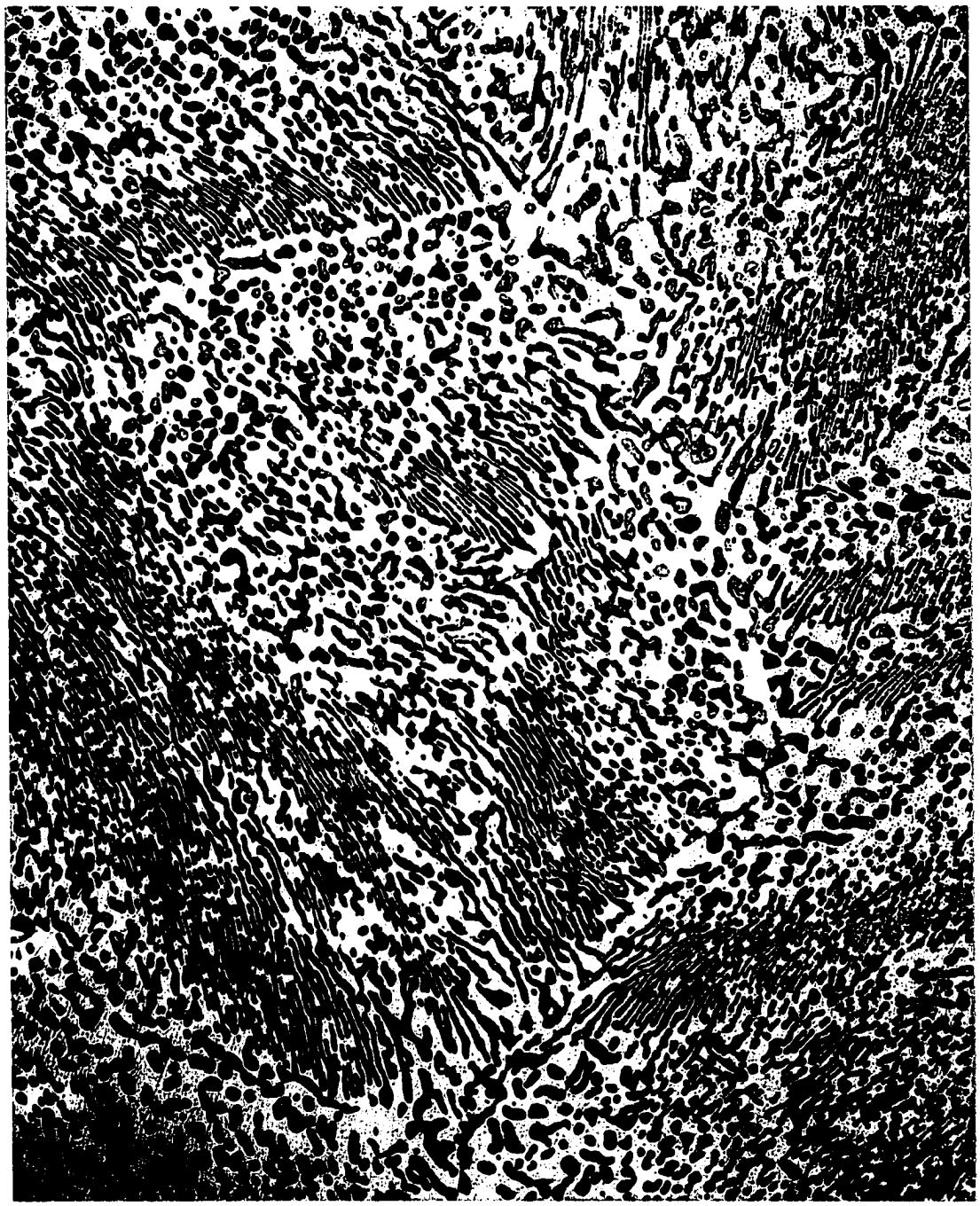

Figure 5. 300X - Peroxide and Glycol Etch
The 63/37 solder alloy of Figure 2 after aging for 7 days at 100°C.

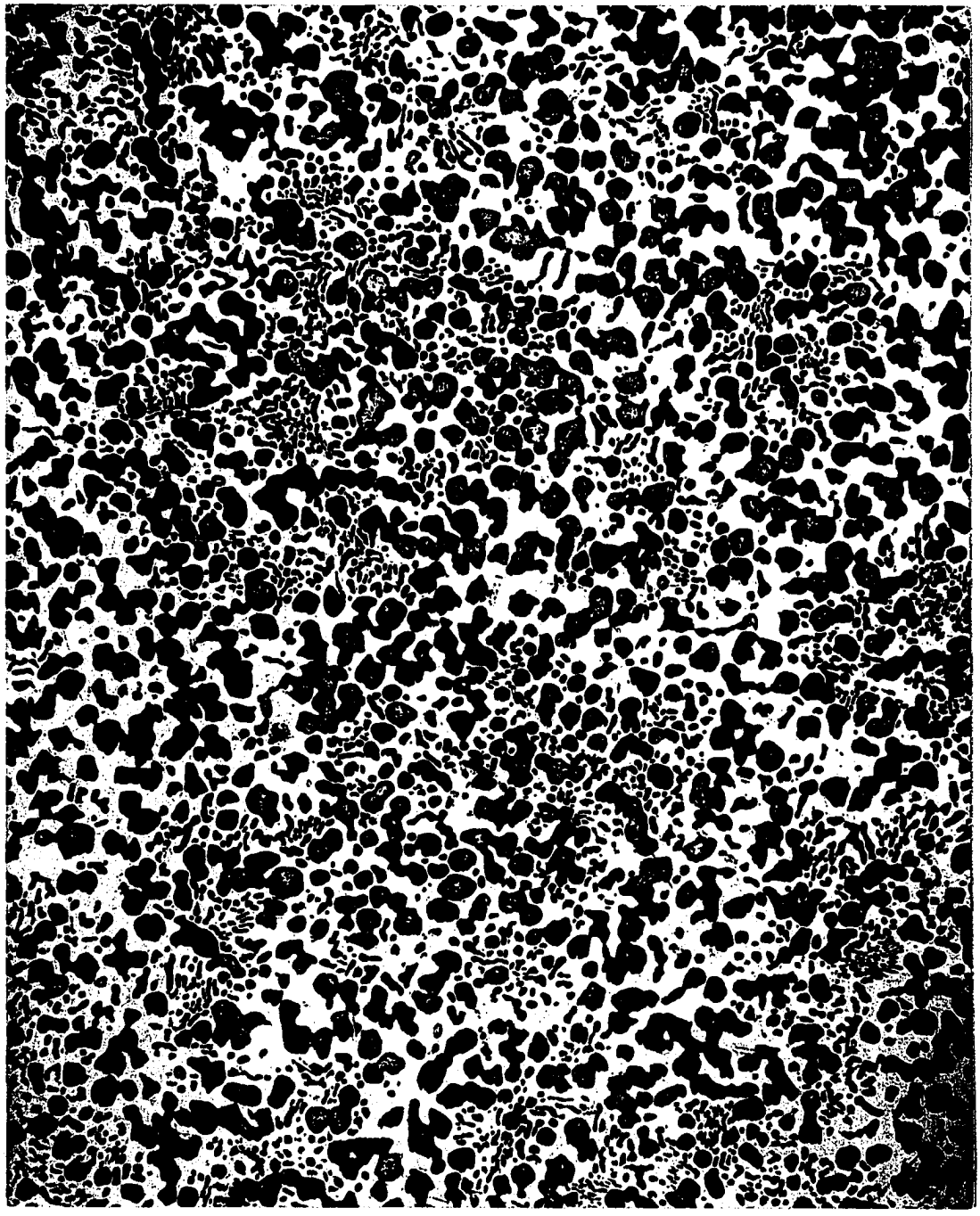

Figure 6. 200X - Peroxide and Glycol Etch
The antimonial solder alloy of Figure 3 after aging for 7 days at 100°C.

portion of the eutectic has also spherodized. In addition, all solders showed microstructural changes in the α phase. These are evidenced by the formation of particles of tin rich β. The β particles are apparent within the dark α islands, seen most easily in Figure 5. The characteristics of the α phase are more clearly demonstrated with the higher resolution of the Scanning Electron Microscope (SEM). Figure 7 is an SEM micrograph of an aged mass of reflowed 60/40 solder. The β phase appears as the dark isolated regions as well as the long structures running from the top to the bottom of the photograph. The particles of β shown within the α mass were not observed in freshly reflowed solders.

The microstructures described above are relatively simple and predictable on the basis of the tin-lead phase diagram. The apparent precipitation of β within the α phase may simply be a readjustment of composition toward equilibrium, delayed because of the cooling rate imposed by the conditions of the experiment. While providing a baseline against which comparisons may be made, structures as simple as these are seldom obtained in commercial soldering operations. Instead, interactions with the substrate and the presence of contaminants complicate the structures leading to interpretation difficulties and the greater problem of soldering failures.

Etching of Solder Alloys

In order to reveal all of the microconstituents present in the solder alloys studied, reliable etching procedures had to be developed. The effects of different etching methods are most clearly demonstrated by comparisons of photomicrographs obtained during several phases of this study. Comparisons of optical and SEM micrographs are also useful

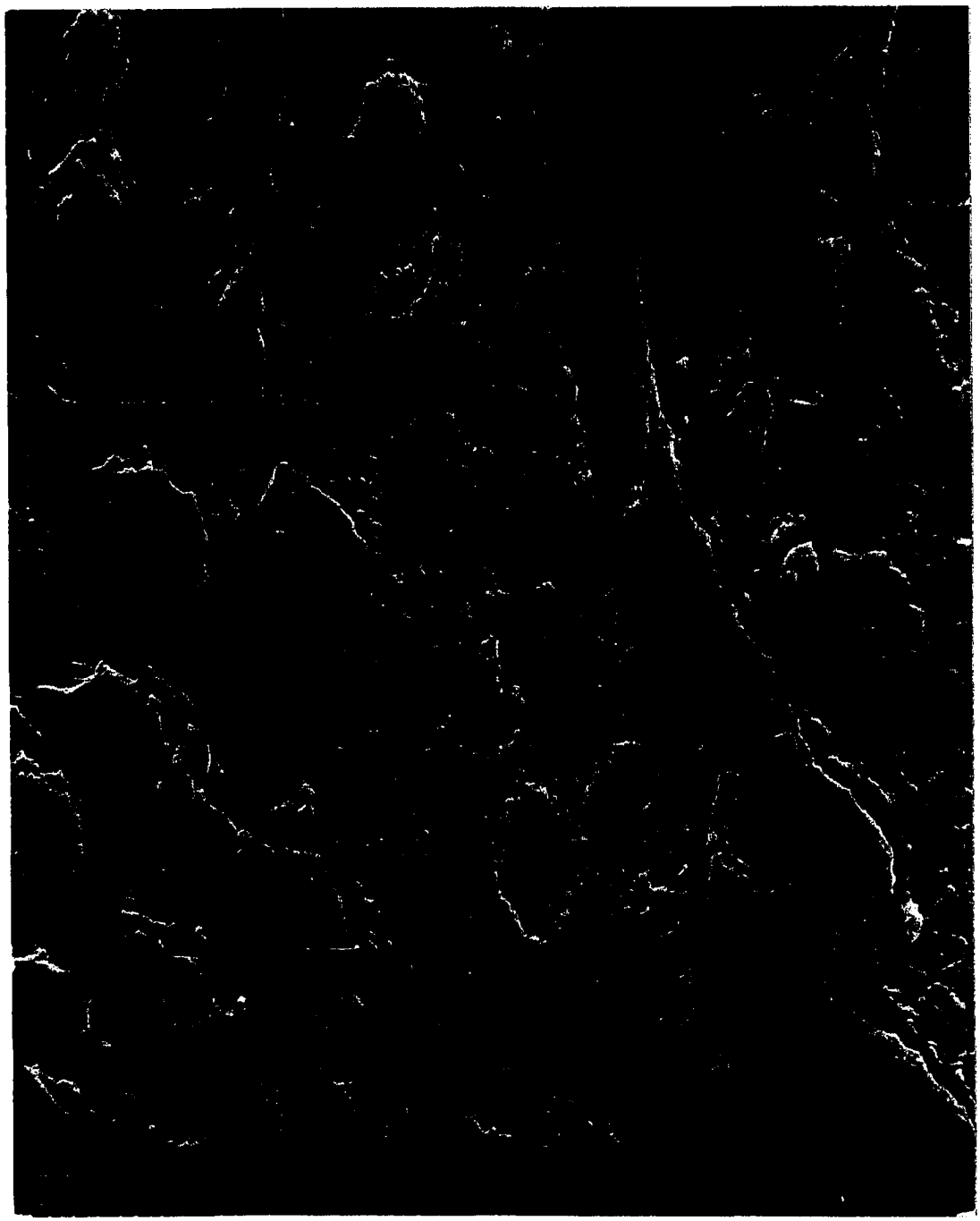

Figure 7. 5600X - Peroxide and Nital (2%) Etch
An SEM micrograph of a 60/40 solder mass aged for 7 days at 100°C. β phase tin precipitates are shown in the α phase mass.

at this point in order to recognize the different appearance of various phases as observed by the two different techniques.

Figure 8 is an optical micrograph showing a typical 60/40 solder fillet applied to a circuit board. A gold plated terminal pin is shown running vertically at the right edge of the photograph and a copper land area appears at the bottom left. The structure was etched in NH_4OH - H_2O_2 commonly used for copper based alloys. The dark dendritic proeutectic phase is lead rich α, contained in an α-β eutectic. The structure differs from Figure 1 because of differences in the cooling rates and interactions with the substrate metals. These latter effects will be discussed as a principle topic of this study.

Figure 9 shows the same solder fillet after an additional etching treatment in 2% nital. The structure has darkened considerably revealing an occasional bright needle or circular particle as indicated by arrows N and C. These note the appearance of intermetallic compounds $AuSn_4$ and Cu_6Sn_5 formed within the structure. Figure 10 shows the appearance of a solder fillet containing a much higher concentration of intermetallic compounds. A comparison of Figures 11 and 12 demonstrates that in the absence of the nital etch these structures are very difficult to observe.

The scanning electron microscope reverses the phase "coloration" in tin-lead alloys. Figure 13 is the same solder fillet shown in Figure 9. As seen in the photomicrograph, the proeutectic α in a nital etched 60/40 solder appears bright while the β phase is dark. Intermetallic compounds take on various degrees of brightness depending on the particular compounds being viewed. Figure 14 shows the same solder

Figure 8. 200X - Peroxide Etch
An optical micrograph of a .5 micron gold plated terminal pin soldered with the 60/40 alloy to a copper plated circuit land.

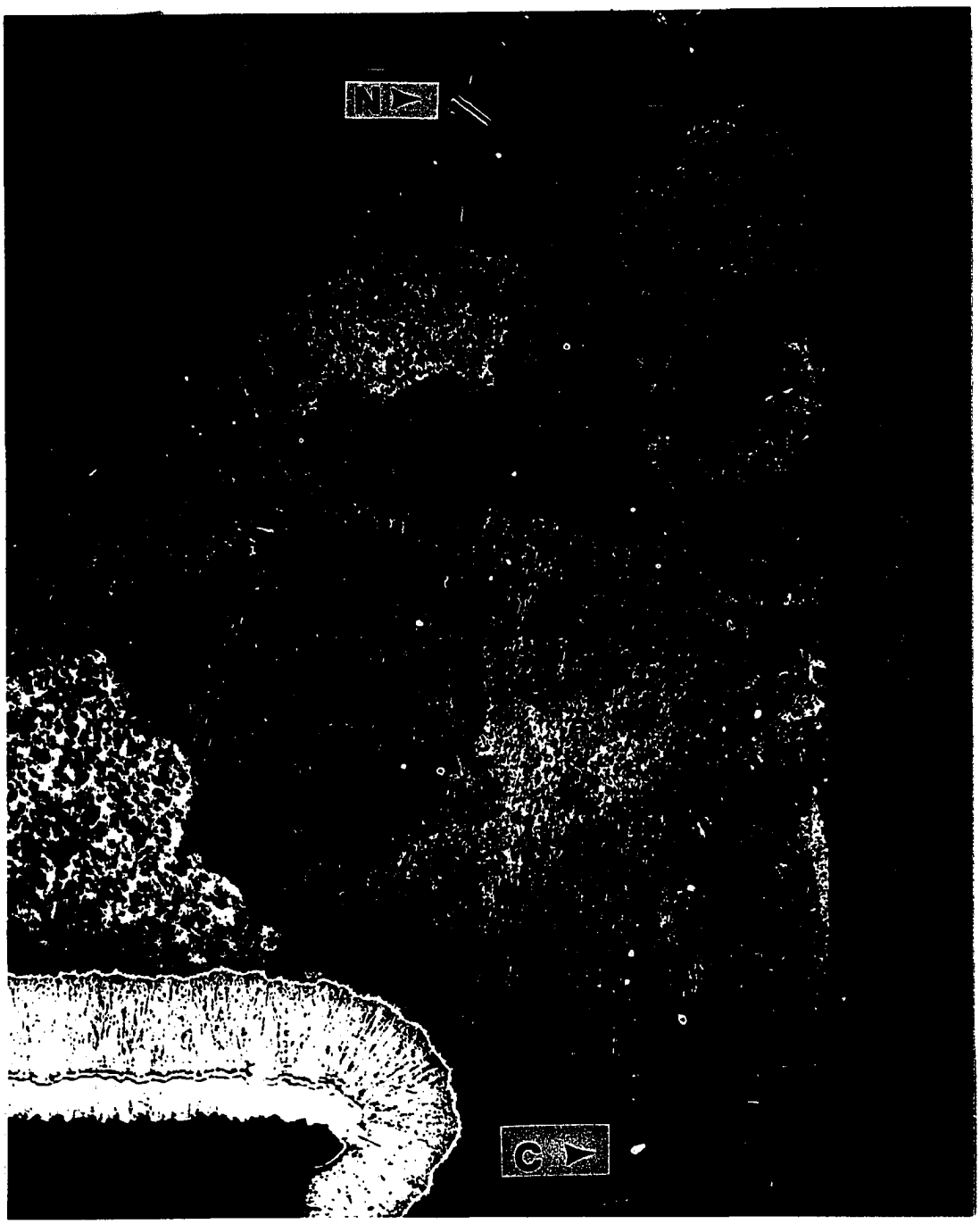

Figure 9. 200X - Peroxide and Nital (2%) Etch
An optical micrograph of the solder fillet shown in Figure 8 after nital etching. Isolated intermetallic compounds of $AuSn_4$ and Cu_6Sn_5 are revealed.

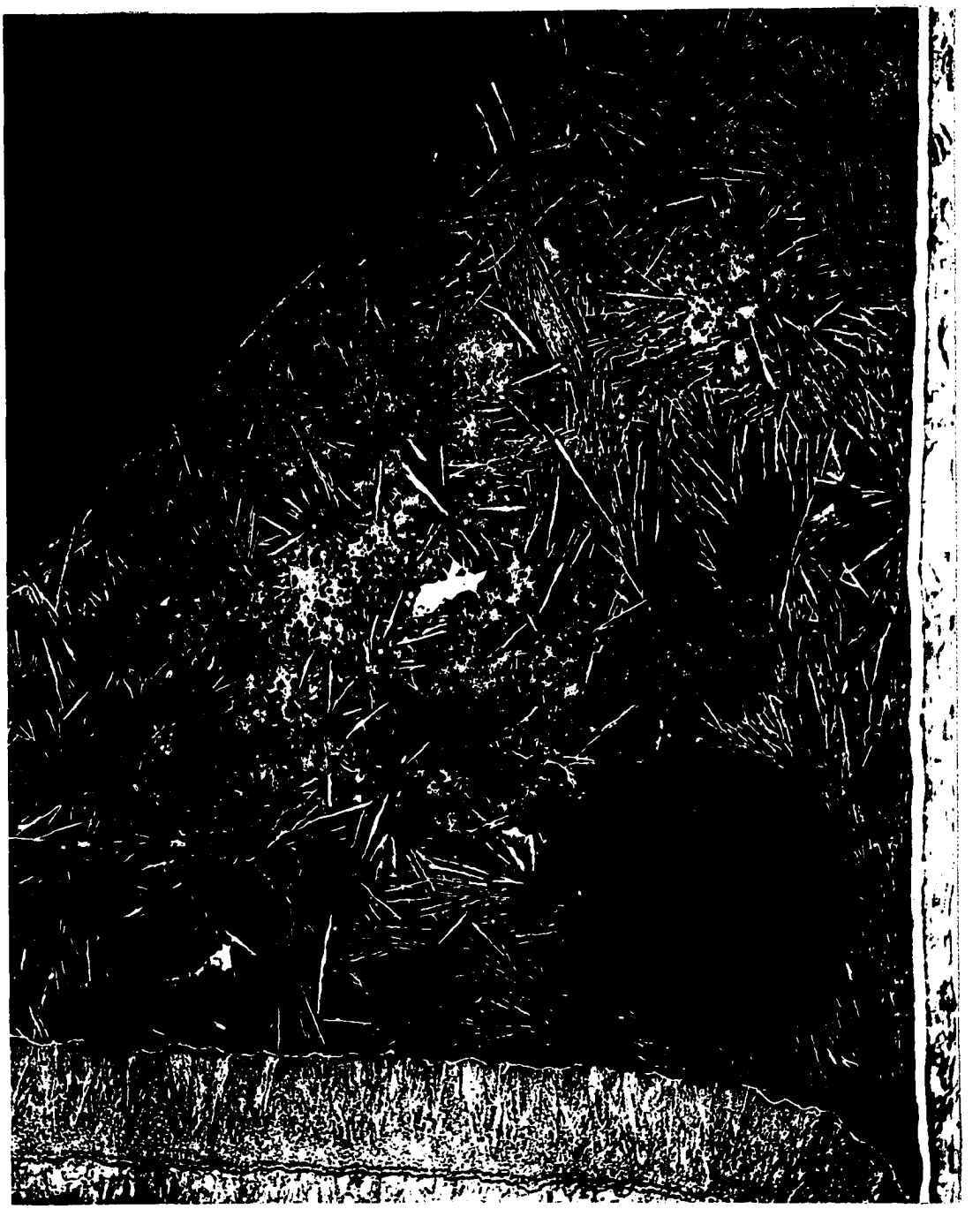

Figure 10. 200X - Peroxide and Nital (2%) Etch
An optical micrograph of a 2.5 micron gold plated terminal pin soldered with 60/40 solder to a copper plated circuit land. Excessive $AuSn_4$ compounds are shown.

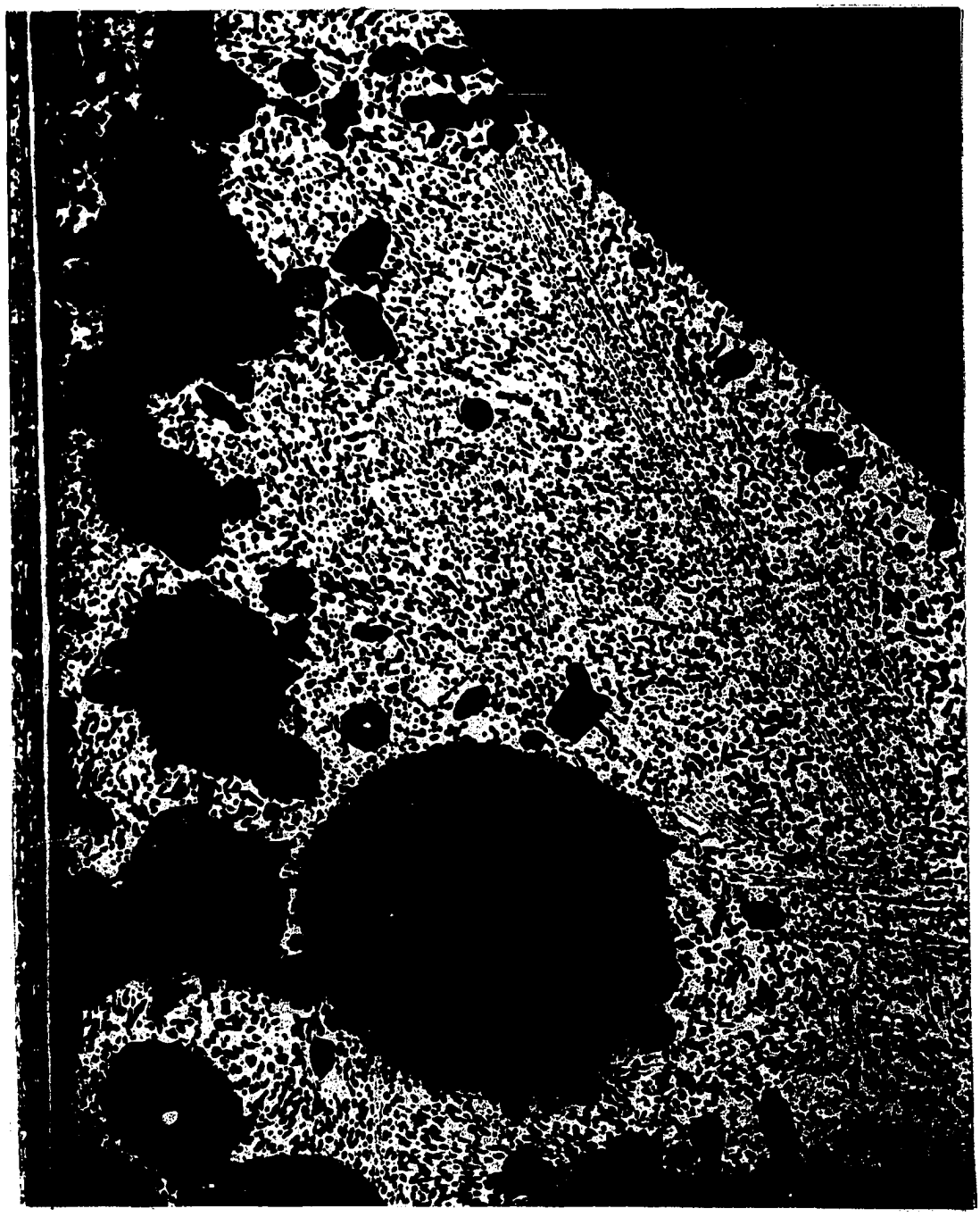

Figure 11. 200X - Peroxide Etch
A 2.5 micron gold plated terminal pin soldered with 60/40 solder to a copper plated circuit land. Note the appearance of striations in the fillet and the porosity.

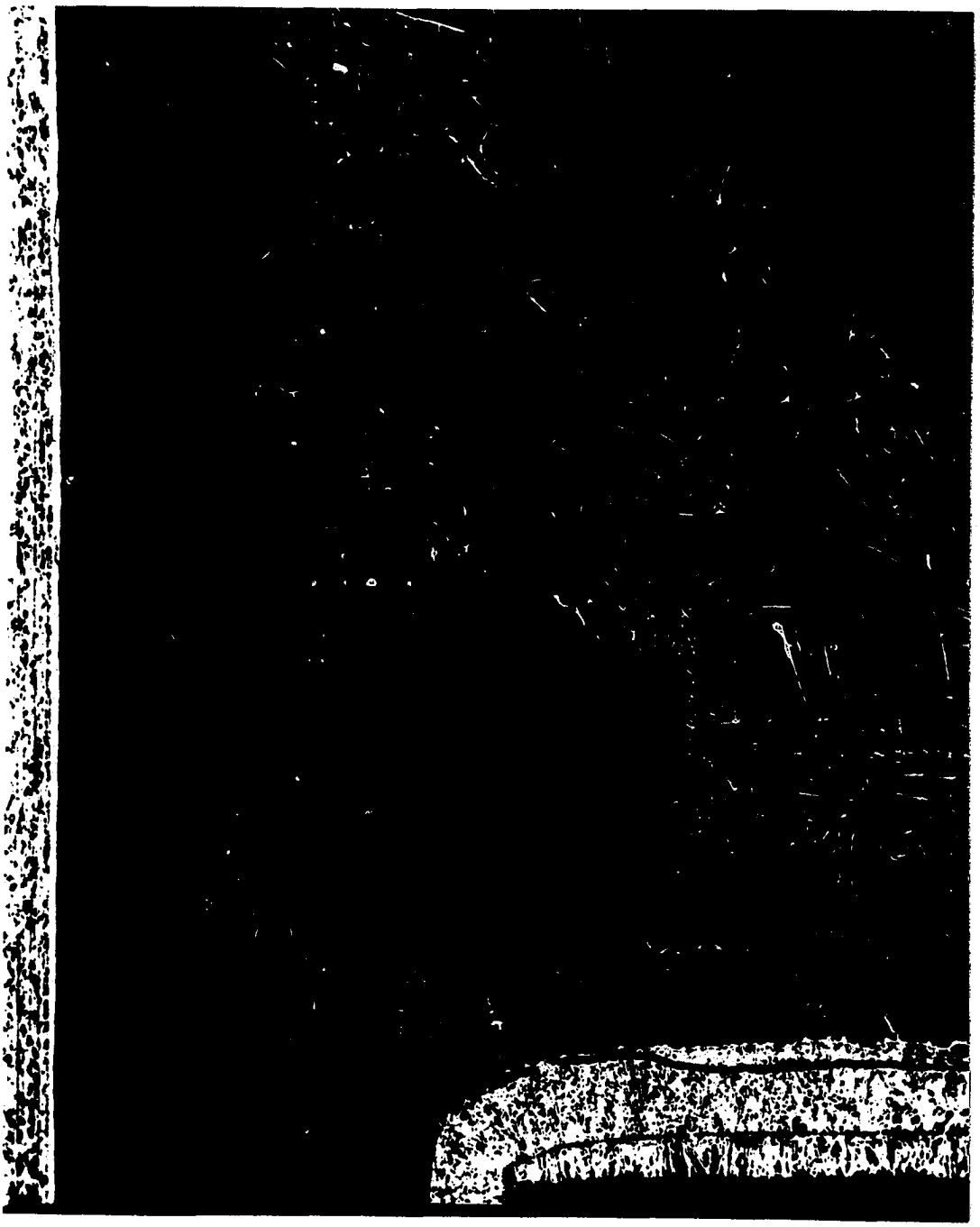

Figure 12. 200X - Peroxide and Nital Etch
The same area as shown in Figure 11 after nital etching. The striations are now seen as bright needle appearing structures.

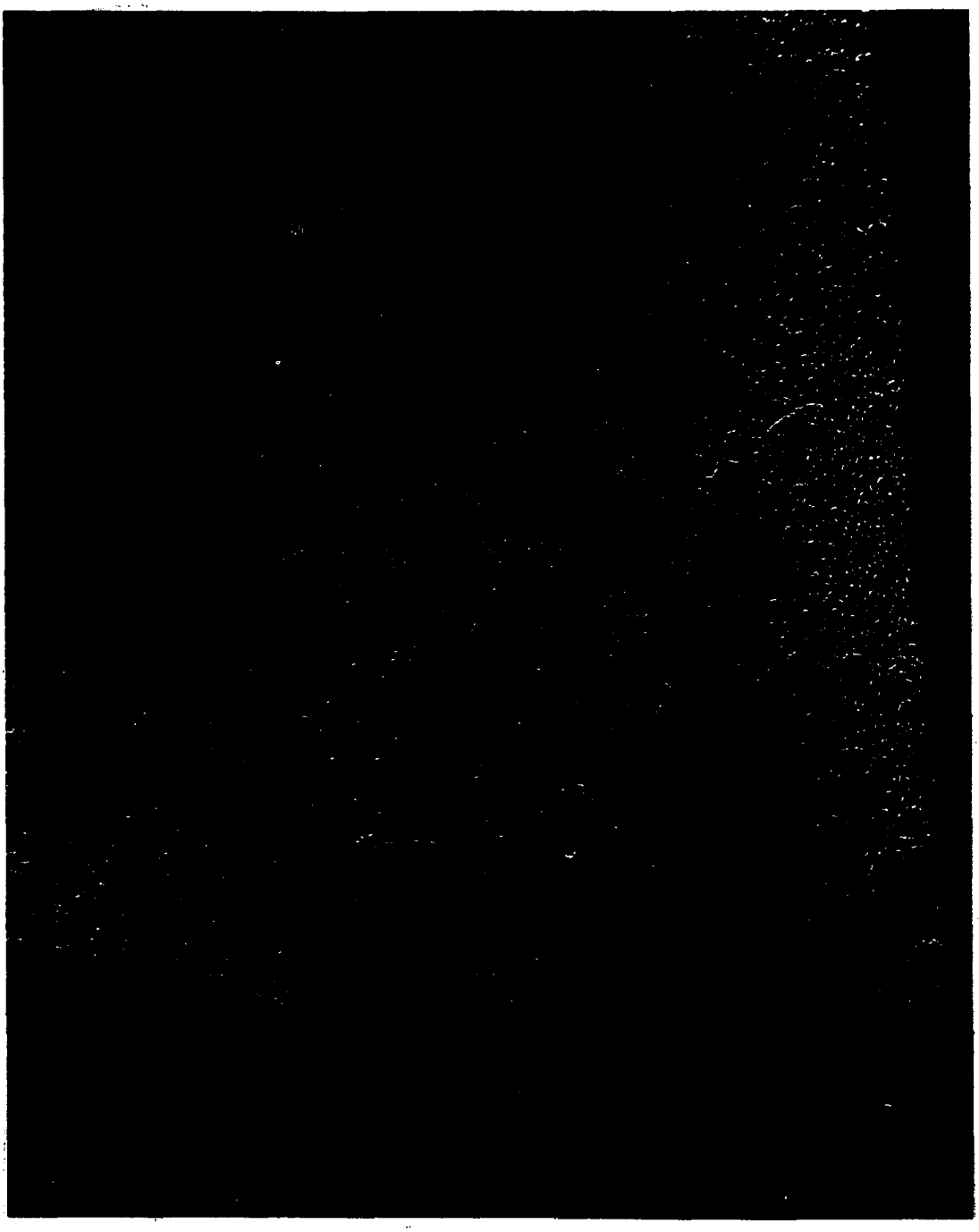

Figure 13. 200X - Peroxide and Nital Etch
An SEM micrograph of the area shown in Figure 9. Very few intermetallic compounds can be seen.

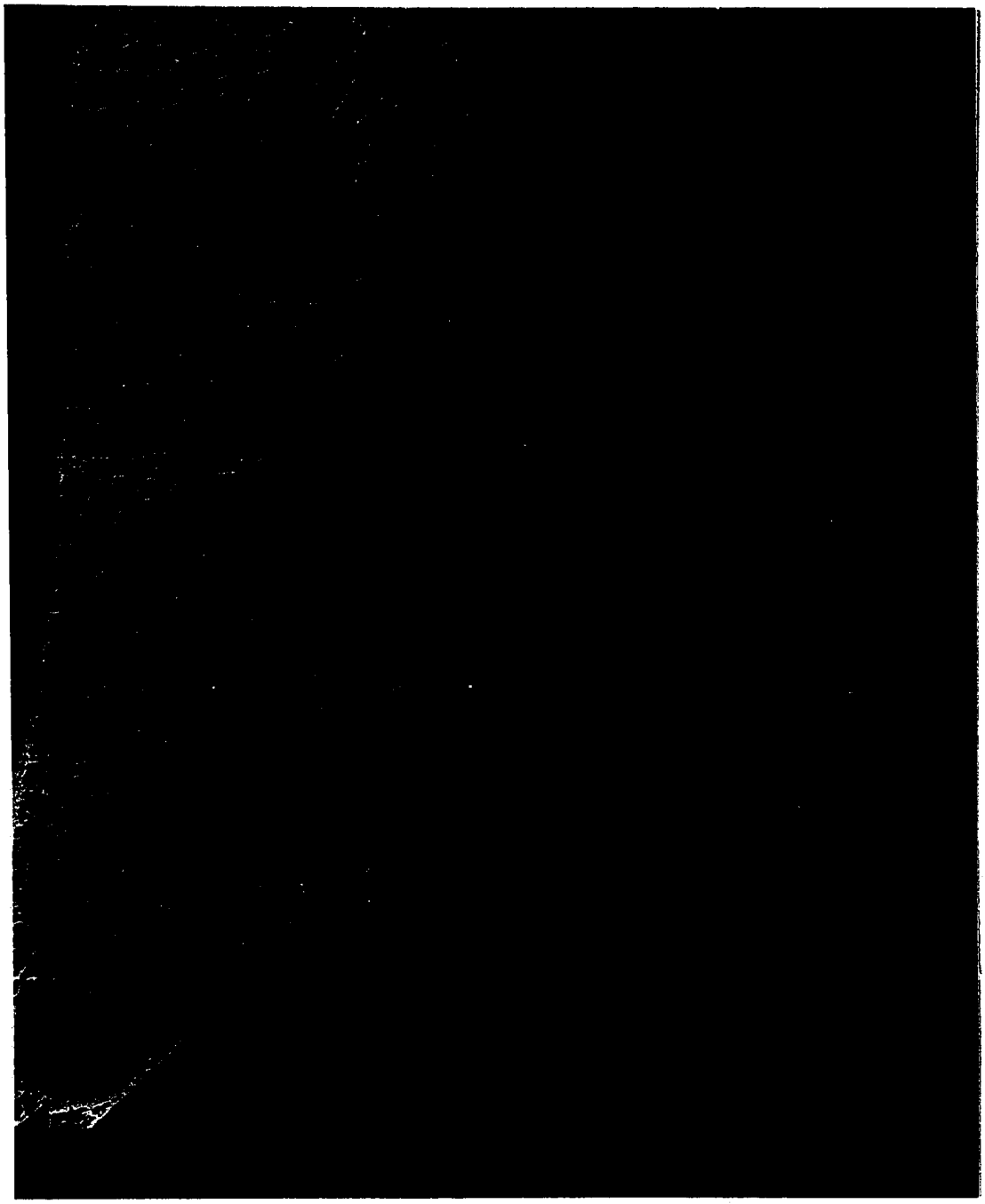

Figure 14. 150X - Peroxide and Nital Etch
An SEM micrograph of the area shown in Figure 10. The needlelike structures are $AuSn_4$ intermetallic compounds.

fillet seen in Figure 10. The terminal pin is at the lower right and the land at the upper right. The intermetallic compounds again appear bright and in greater relief against the rest of the structure.

Intermetallic Compound Formation in Sn-Pb and Sn-Pb-Sb Solders

The formation of intermetallic compounds in the tin-lead based solders applied to various substrates has been reported in a number of references (1-4). The most complete listing of the compounds which form may be found in Manko (5) and Bailey and Watkins (6), or may be deduced from inspection of the appropriate phase diagrams (Appendix A). Compounds involving materials which are used in the electronics industry are of the greatest significance as are compounds of common impurity elements. In this phase of the work, attention was focused upon the metallographic appearance of intermetallic compounds formed in solder alloys.

Intermetallic compounds are formed by the dissolution of substrate metals in molten or solid solder masses. The simplest method of producing the compounds involves the application of the solder to pure metal, alloy, or plated substrates. The compounds form as an interfacial layer at the solder substrate boundary as well as isolated particles within the solder mass. Artificial aging at elevated temperatures has been shown to enhance compound formation as well as to change the nature of some of the compounds which have formed directly upon cooling. These studies include the results obtained from experiments with the tin-lead-antimony solder (52 Sn, 45 Pb, 3 Sb) described above.

Copper-Tin Intermetallic Compounds

The alloy system Cu-Sn predicts four intermetallic compounds: δ - $Cu_{31}Sn_8$, ε - Cu_3Sn, η and η' - Cu_6Sn_5, and ζ - $Cu_{20}Sn_6$. Cu_6Sn_5 undergoes an ordering transition ($\eta \rightarrow \eta'$) in the neighborhood of 187°C. The transformation was discussed in detail by Bever (7). The formation of copper-tin intermetallic compounds is perhaps of the greatest commercial significance due to the large number of copper and copper clad electronic circuits which are soldered by wave or dipping processes using recirculatory solder baths. The dissolution rate of copper at normal soldering temperatures is quite high and contamination of the solder bath with copper-tin intermetallics is common.

Figure 15 shows a typical solder joint made with 60/40 solder applied to a pure copper substrate. The solder mass appears near the top of the photomicrograph and the substrate at the bottom. The normal lamellar character of the eutectic is shown near the center of the field. A thin, continuous band of light etching material is seen within the solder at the boundary with the substrate. A scanning electron microscope equipped with an energy dispersive X-ray microanalysis system (EDS) was utilized in determining the composition of the band, which corresponded to Cu_6Sn_5.

A higher magnification view of a Cu_6Sn_5 boundary layer is shown in Figure 16. Here some of the angularity and faceting of the band becomes apparent. This characteristic of intermetallic compounds formed as interfacial layers permits their recognition. Unfortunately, there is not a great deal of difference between the appearance of the Cu_6Sn_5 band and compounds of other elements which form at the solder

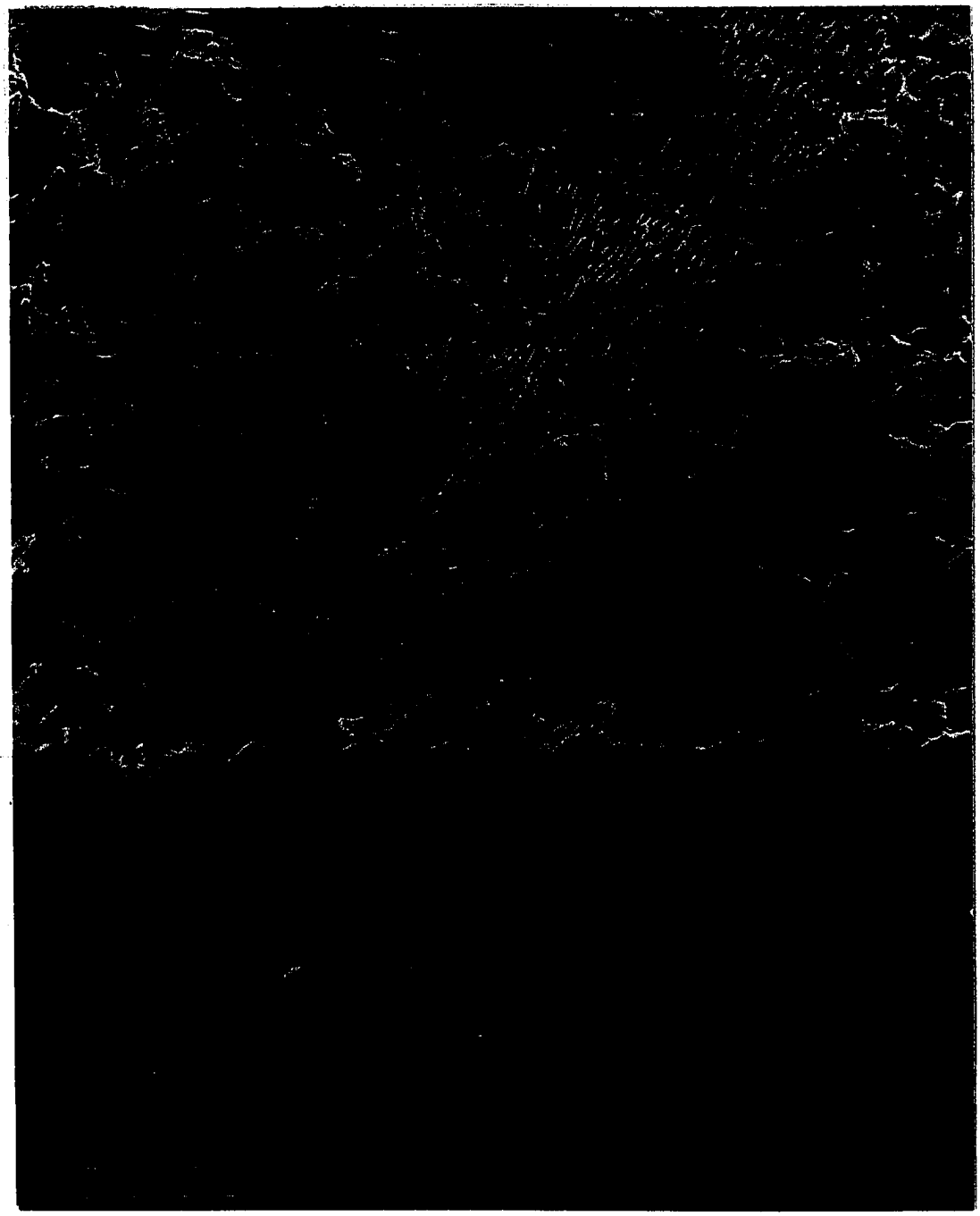

Figure 15. 1680X - Peroxide and Nital Etch 60/40 solder applied to a copper substrate. The thin band of material between the solder (top) and the copper substrate (bottom) is the Cu_6Sn_5 intermetallic compound.

Figure 16. 2800X – Peroxide and Nital (2%) Etch
A larger magnification of a band of Cu_6Sn_5 compounds. Solder fillet (left) and copper substrate (right).

substrate boundary. Consequently, the EDS is required for identification.

Cu_6Sn_5 intermetallic compounds form within the solder mass in areas remote from the substrate. The particles can be formed easily either directly upon cooling the solder or after artificial aging. Figure 17 shows a typical example of these isolated Cu_6Sn_5 intermetallic compounds. The compound forms as a slender structure often with an "eye" in the needle as seen in Figure 18. The eye is a consequence of an axial cavity which extends to one side of the needle, or is intercepted by the plane of polish. The axial cavity is shown in Figure 19. This photomicrograph also demonstrates the hexagonal shape which is typical of the Cu_6Sn_5 compound when it is formed remote from the solder substrate interface. The shape notwithstanding, the compound was cited incorrectly by Manko as being orthorhombic. Hansen (8) and Bever indicate the structure as ($B8_1$) hexagonal, NiAs type. Cu_6Sn_5 needles are often observed in close association with the boundary layer of compound. Figure 20 shows a typical example. The large needle has been broken off at its intersection with the plane of polish and ridges have developed on its surface, probably due to etching. A number of smaller needles, demonstrating a hexagonal shape, are also apparent near the interface.

The Cu_6Sn_5 intermetallic compound does not appear to be limited to the hexagonal shape. Figures 21, 22, and 23 show the compound as rods of circular cross section which had formed in the antimonial solder applied to a copper substrate and aged for a week at 100°C. The rod shown in Figure 21 has the axial cavity characteristic of Cu_6Sn_5.

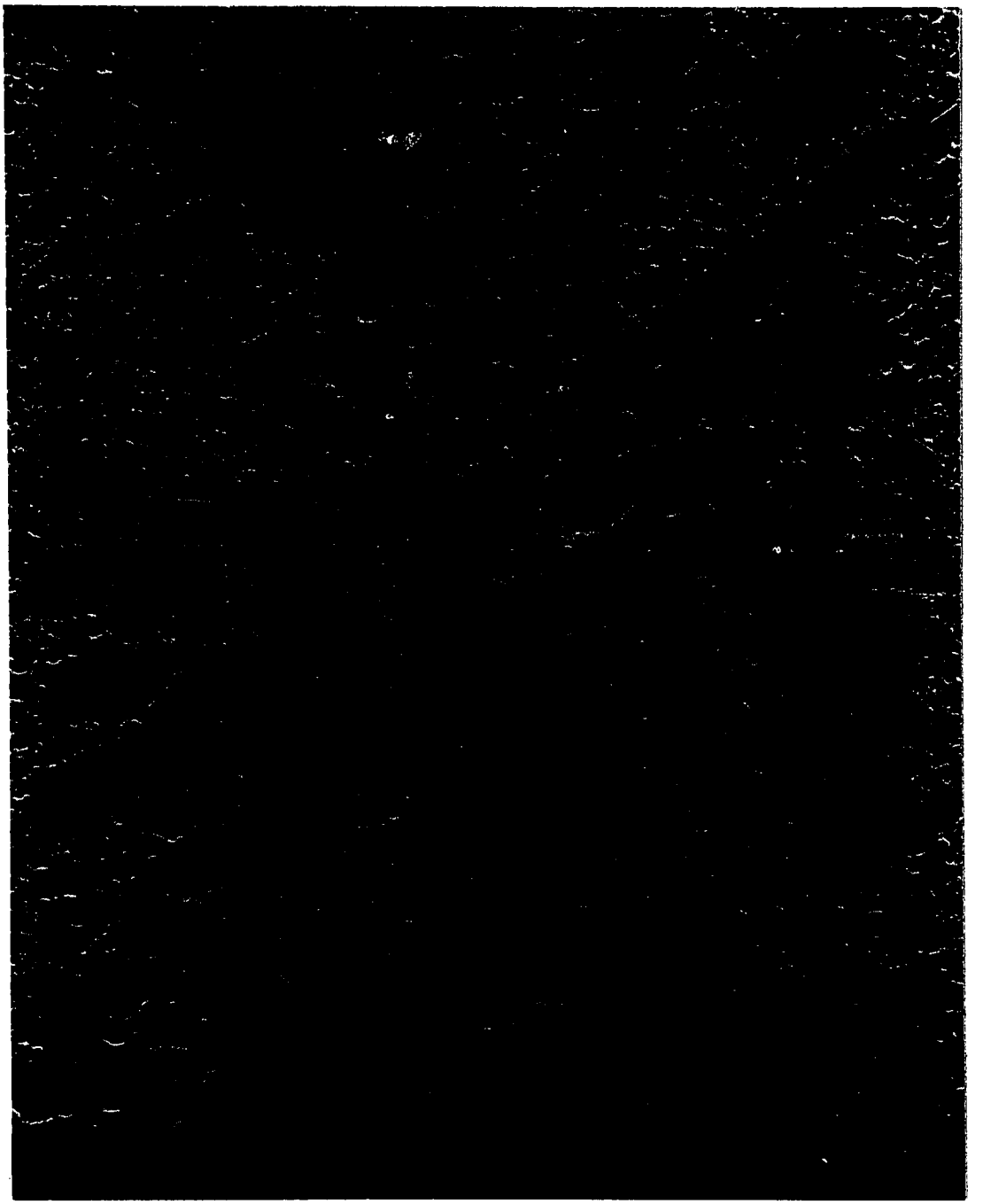

Figure 17. 1120X - Peroxide and Nital Etch
60/40 solder applied to a copper substrate.
Isolated Cu_6Sn_5 intermetallic compounds are
shown in the solder mass remote from the
interface.

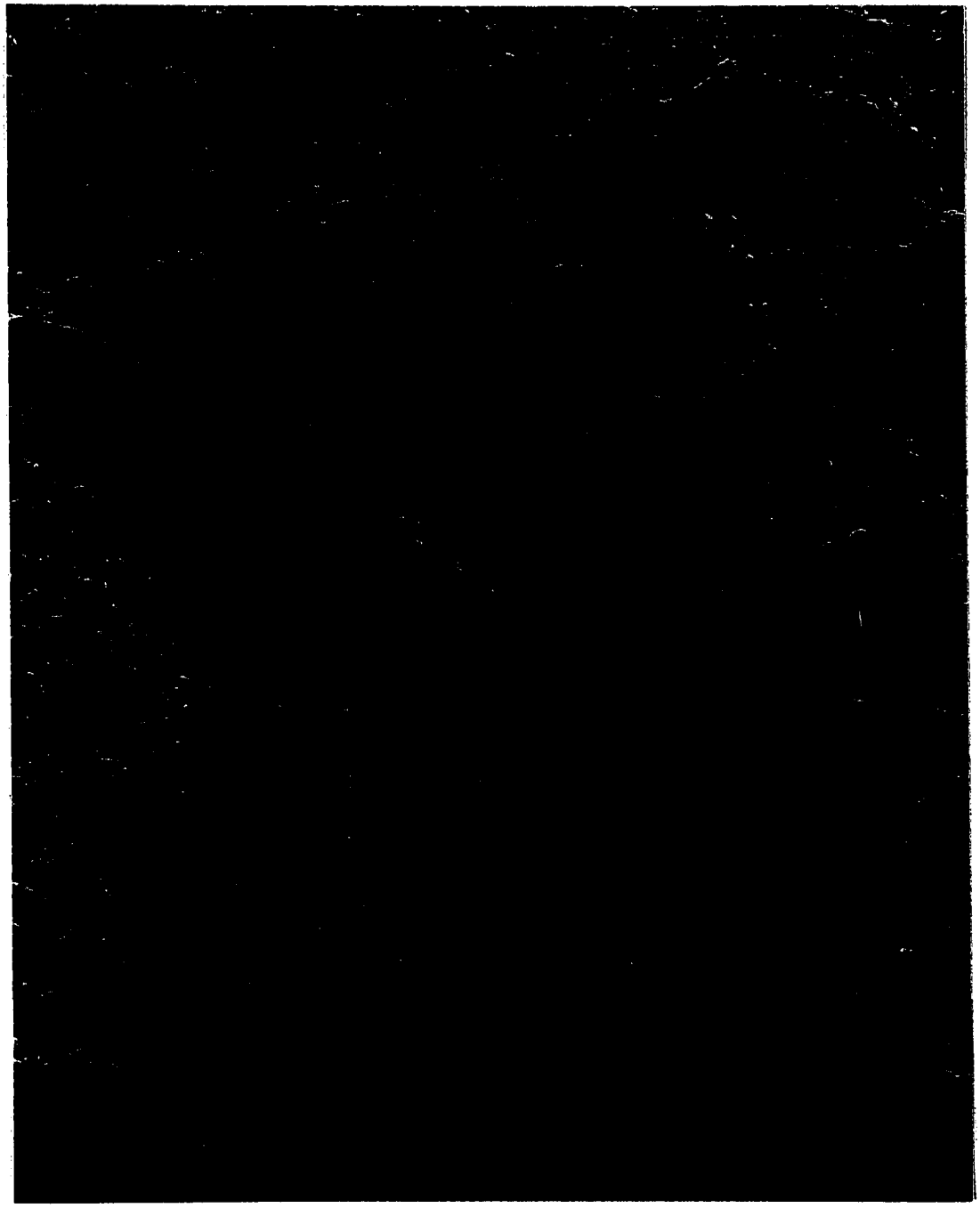

Figure 18. 1400X - Peroxide and Nital Etch
An isolated Cu_6Sn_5 intermetallic compound formed in the mass of 60/40 solder and remote from the interface.

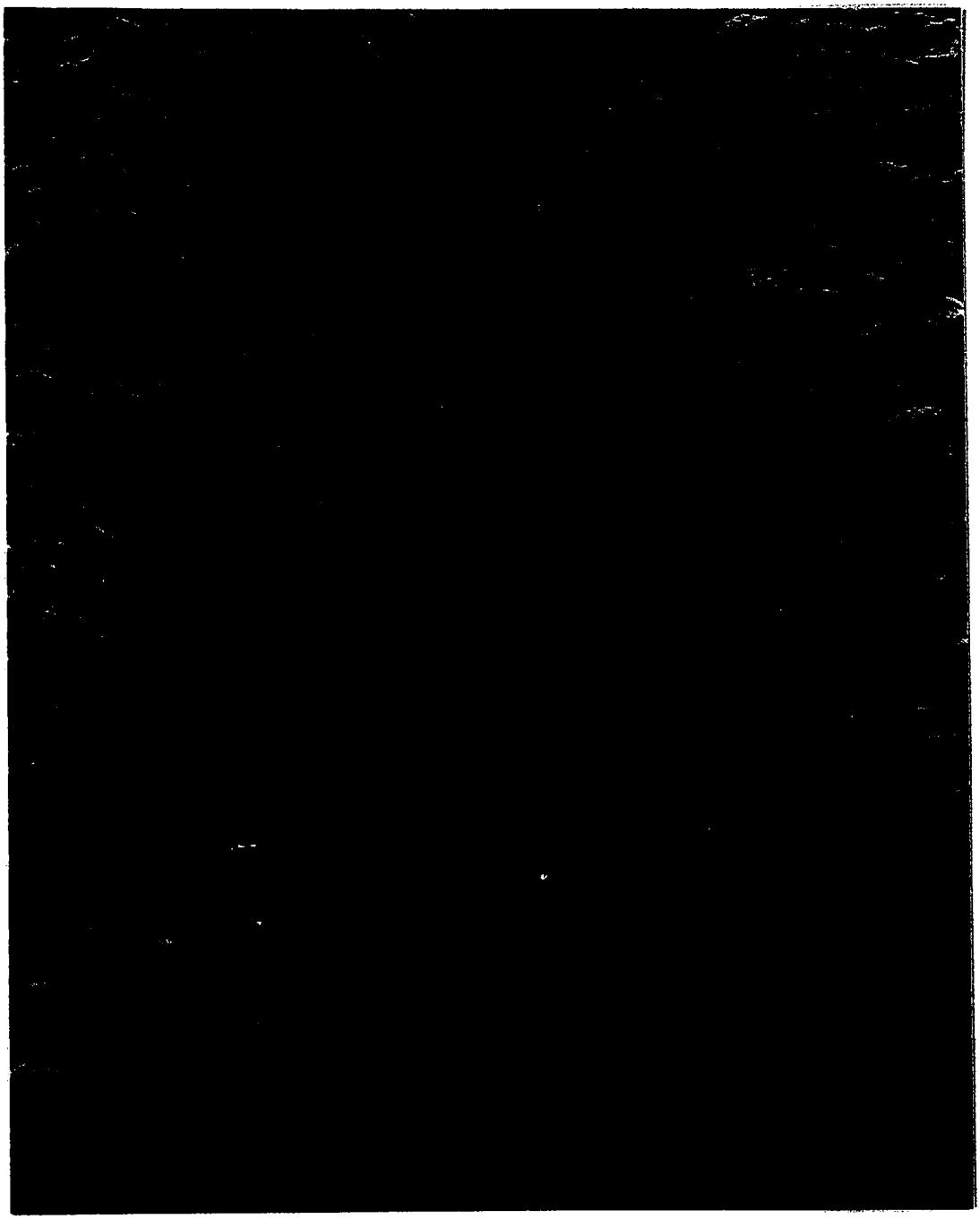

Figure 19. 2800X - Peroxide and Nital Etch
An isolated Cu_6Sn_5 intermetallic compound formed remote from the interface in 60/40 solder applied to copper. The hexagonal shape, with a cavity near the center, is shown.

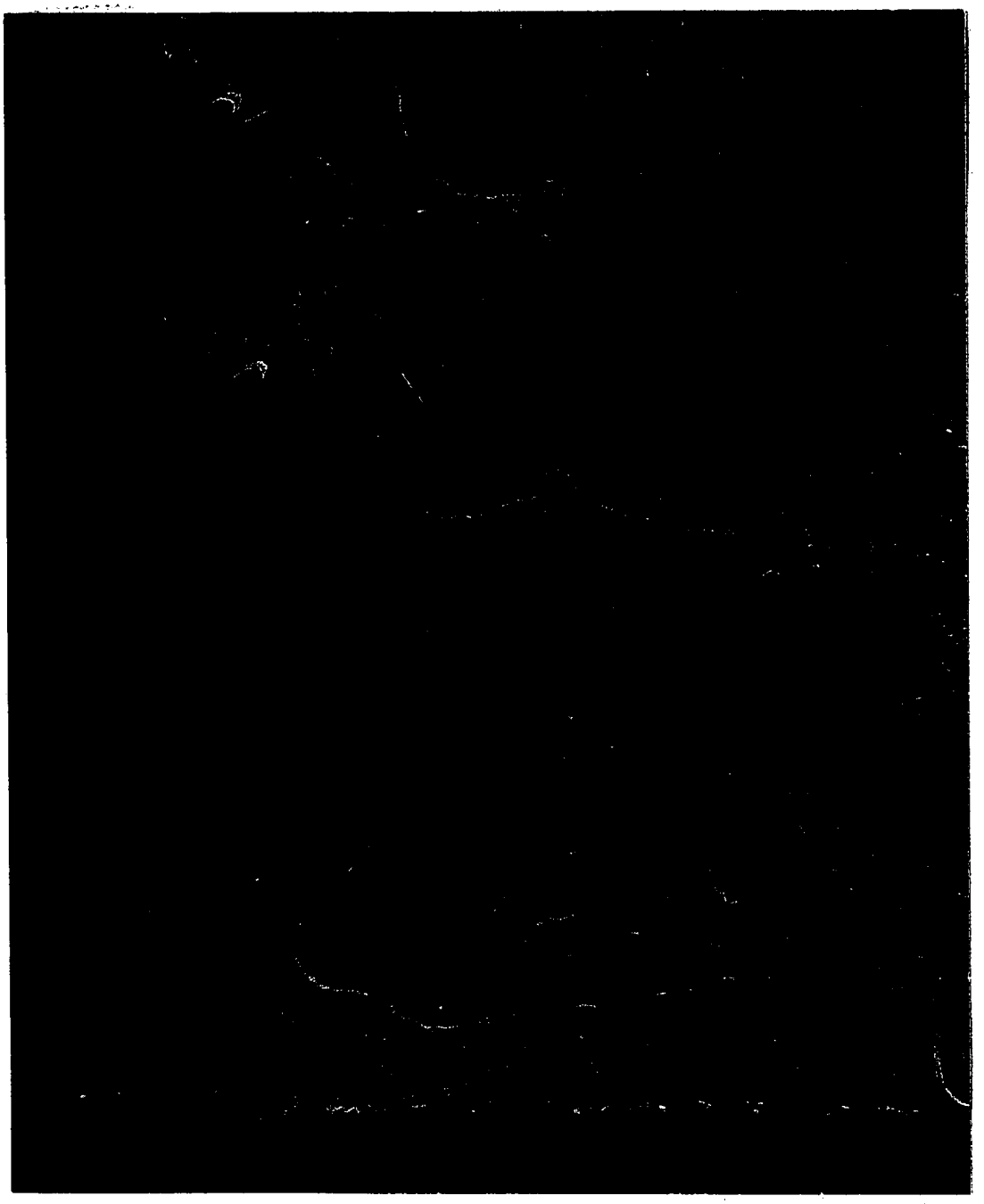

Figure 20. 2800X - Peroxide and Nital (2%) Etch
A broken Cu_6Sn_5 compound extending into the 60/40 solder mass from the Cu_6Sn_5 interface.

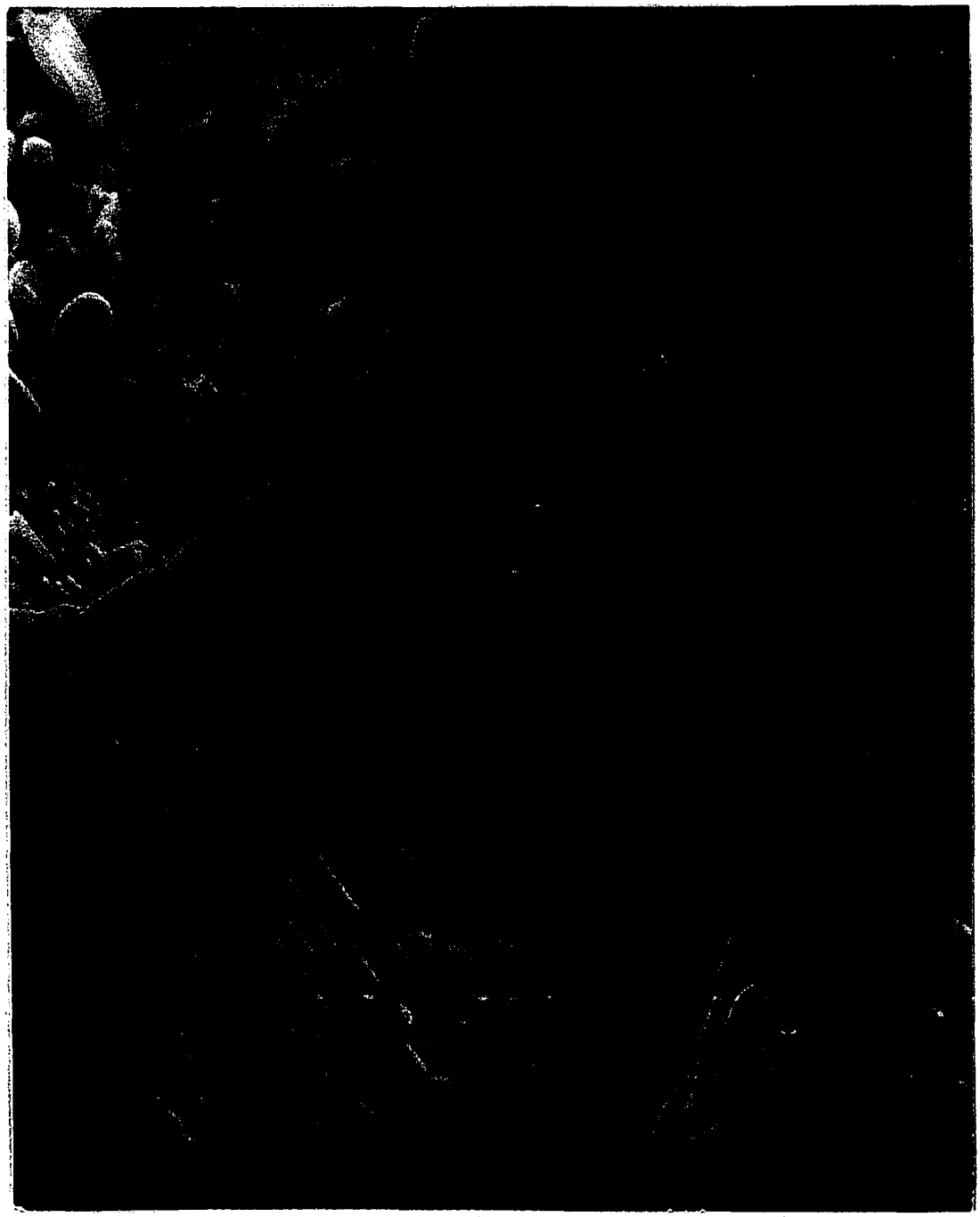

Figure 21. 5600X - Peroxide-Glycol-Nital Etch
Antimonial solder aged for 7 days at 100°C.
A rod of Cu_6Sn_5 having a circular cross section with a hole.

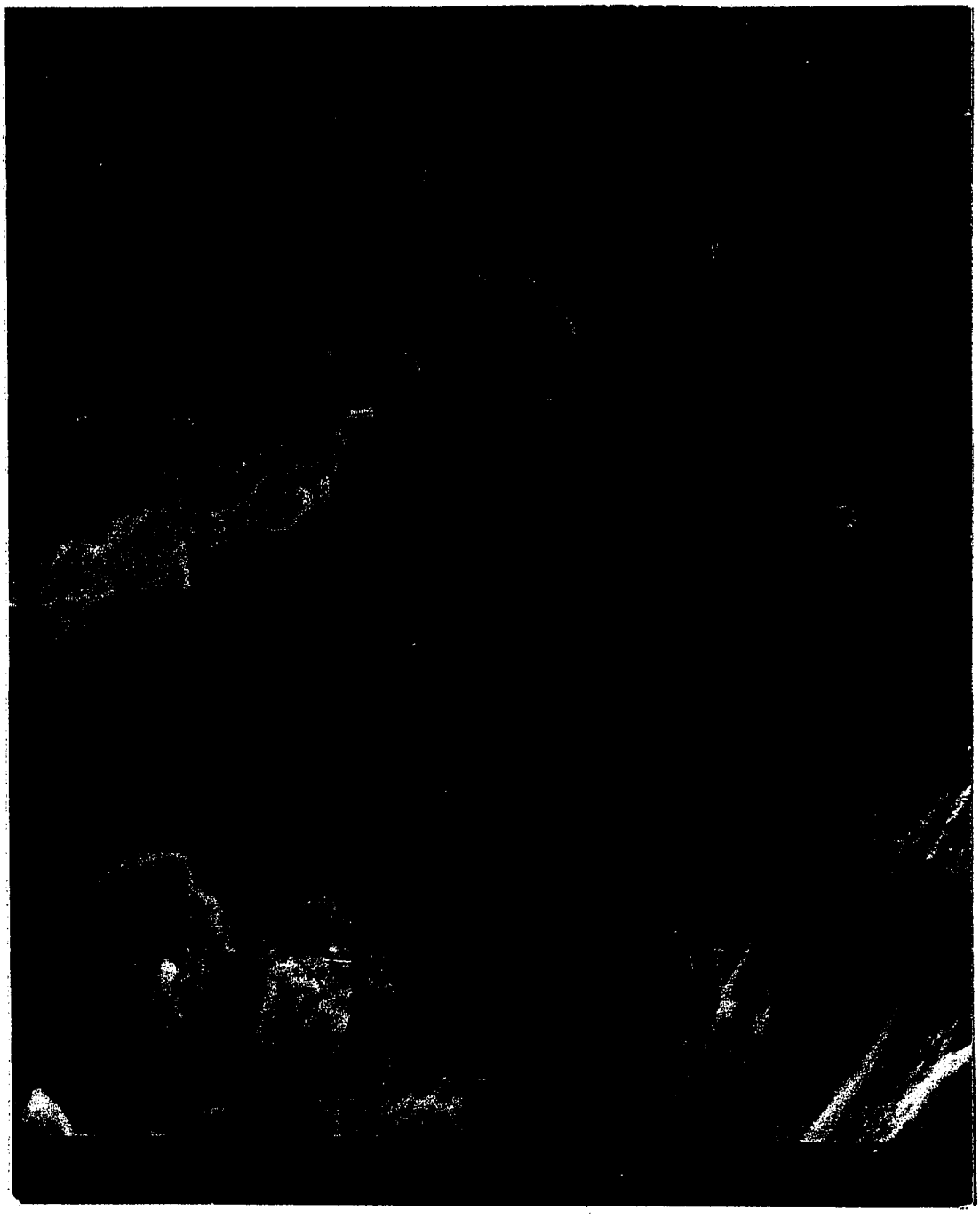

Figure 22. 12,600X - Peroxide-Glycol-Nital Etch Antimonial solder aged for 7 days at 100°C. A rod of Cu_6Sn_5 having a circular cross section without a hole.

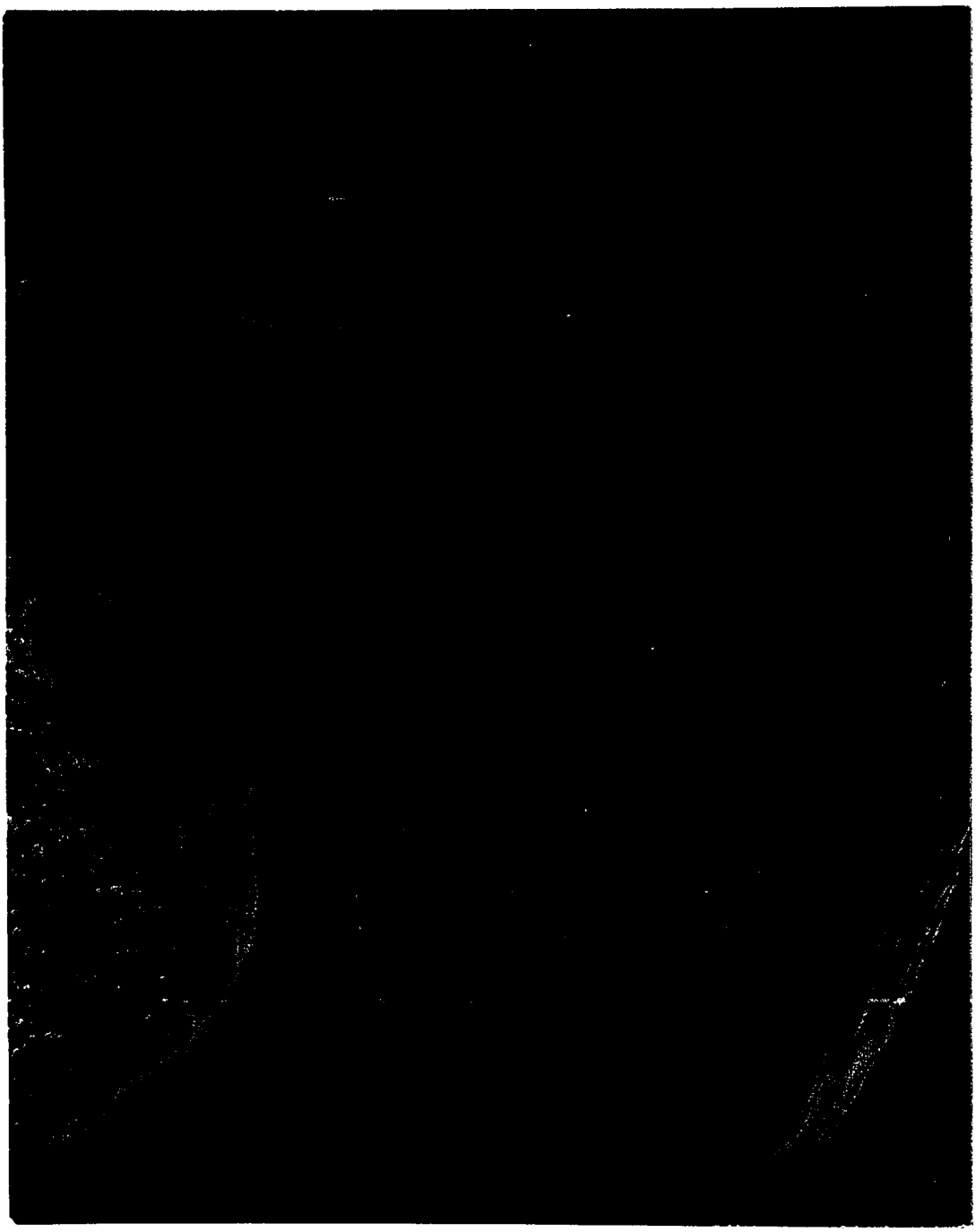

Figure 23. 5600X - Peroxide-Glycol-Nital Etch Antimonial solder aged for 7 days at 100°C. Cu_6Sn_5 intermetallic compounds with random orientations which exhibited brittle characteristics.

The end of the rod shown at the left of Figure 23 has been fractured in the handling of the specimen. The brittle character of the fracture is indicative of the behavior of the compound.

The only intermetallic compound of copper and tin which was observed in any of the experiments was Cu_6Sn_5. Reference to the Cu-Sn phase diagram (Appendix A) indicates that $Cu_{31}Sn_8$ and $Cu_{20}Sn_6$ do not exist in equilibrium at room temperature. Cu_3Sn is predicted at room temperature. Simple analysis of the composition gradients which exist in soldered joints suggests that Cu_3Sn would most likely form between the Cu_6Sn_5 layer and the substrate.

The influence of copper-tin intermetallic compound formation toward decreasing soldered joint reliability has been known for some time and acknowledged in industrial practice. The source of the problem can be readily understood on the basis of the photomicrographs presented here. Cu_6Sn_5 was determined by Bever to be principally metallic on the basis of its bonding. However, experience has shown it to be an embrittling agent in the soldered joint. Isolated particles of Cu_6Sn_5 probably do not affect joint performance greatly as long as the interparticle separations are fairly large. They may, in some circumstances, be beneficial in as much as they would serve to precipitation harden the solder mass. The effect here would be very limited since isolated needle precipitates are not very efficient hardeners. Compound embrittlement of soldered joints is more likely caused by the compact layer which forms at the soldered substrate interface. A localized brittle phase in this critical region has a disproportionate influence on the mechanical properties of the system.

Intermetallic compound formation may also affect the electrical properties of solder joints. The compound layer can create partially isolated boundaries as described above. These may become very significant in certain microelectronic applications.

Gold-Tin Intermetallic Compound Formation

The phase diagram for the system gold tin appeared in Hansen and was subsequently modified by the ASM (9). The intermetallic compounds which exist at room temperature are δ - AuSn, γ - $AuSn_2$ and β - $AuSn_4$. The morphology of the compounds which were observed will be discussed here; but a detailed discussion of the processes which influence the formation of Au-Sn intermetallics will be treated later.

Figure 24 shows the boundary layer of intermetallic compounds which were formed when 60/40 solder was applied to a terminal pin plated with 2.5 microns of nickel and overlayed with 25 microns of gold. The compound layer appears thicker than Cu_6Sn_5 but not as densely populated with angular particles. A somewhat more magnified view is shown in Figure 25. Analysis performed by the EDS indicated that the boundary layer consisted of $AuSn_4$. The isolated angular particles which appear within the solder fillet were also identified as $AuSn_4$. $AuSn_4$ is reported to be face centered orthorhombic.

The morphology of the intermetallic compounds which result when solders are applied to gold plated substrates varied widely. Figures 26 and 27 show $AuSn_4$ intermetallic compounds within a 50/50 tin-lead solder fillet applied on a pure gold plated substrate. The compound forms as

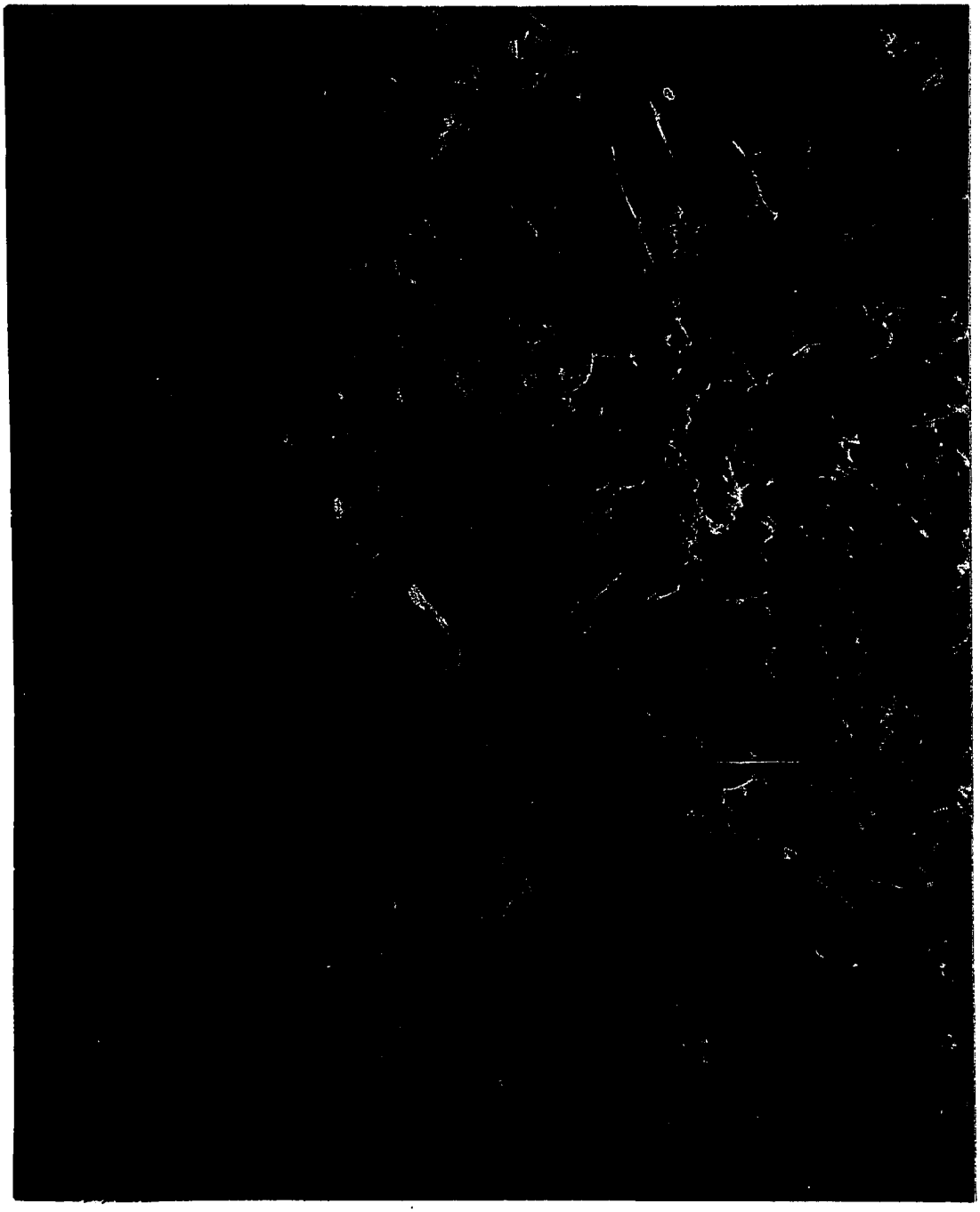

Figure 24. 700X - Peroxide and Nital Etch
60/40 solder applied to a terminal pin with 25.0 microns of gold plating and aged for 7 days at 100°C.

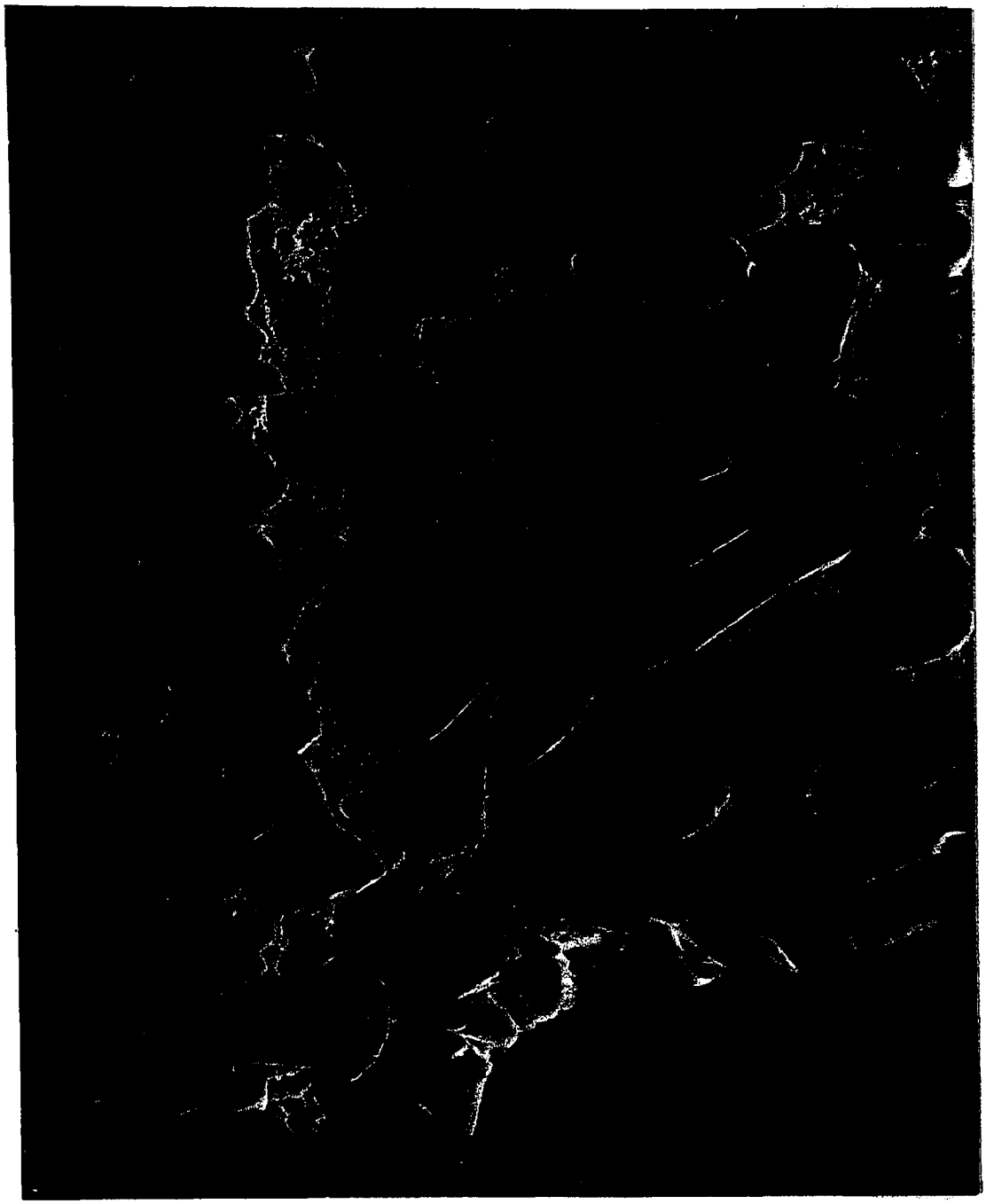

Figure 25. 1400X - Peroxide and Nital Etch
A more magnified view of the area seen in Figure 24.

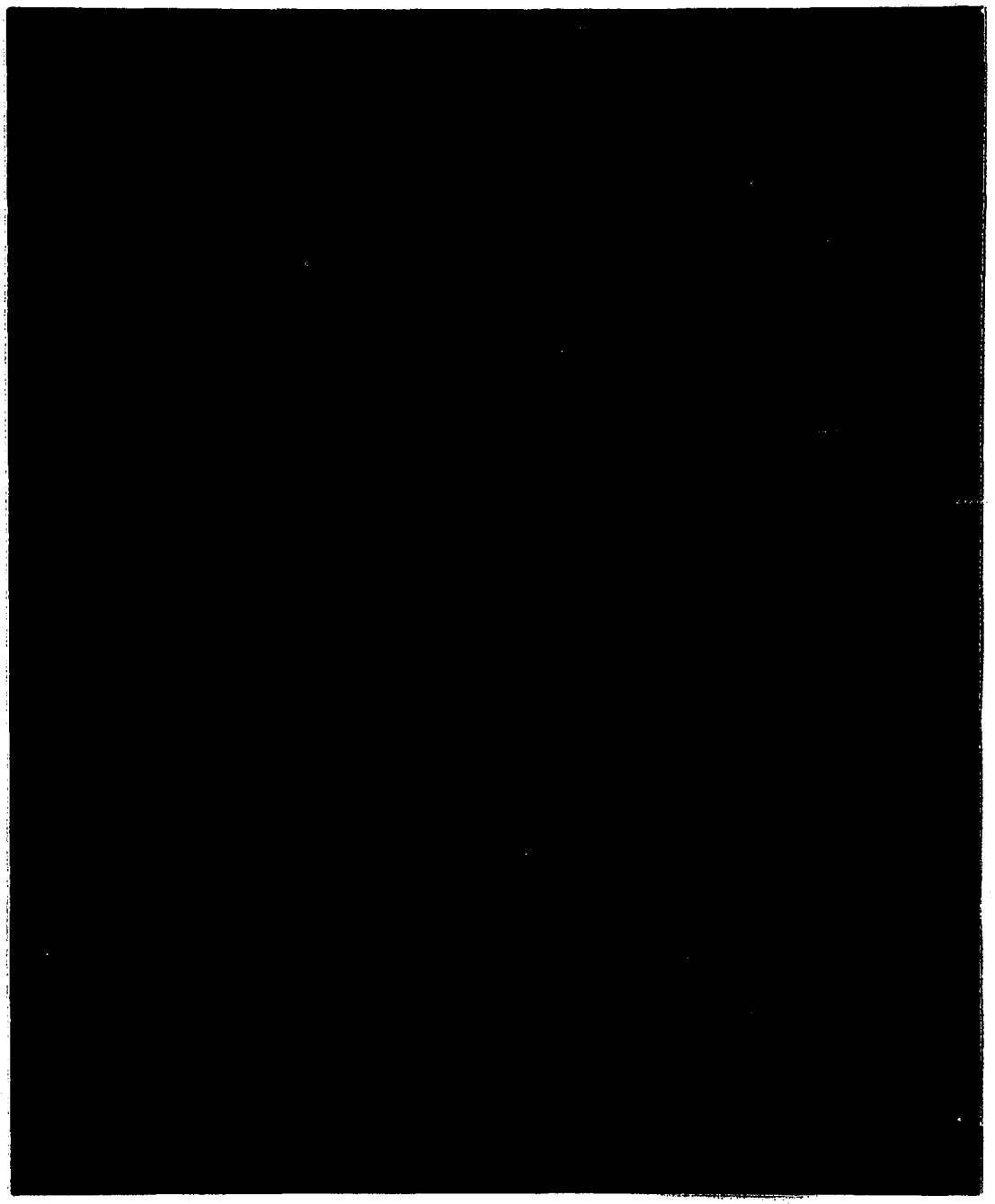

Figure 26. 1120X - Peroxide and Nital Etch
$AuSn_4$ intermetallic compounds are shown
in the 50/50 solder mass.

Figure 27. 8400X - Peroxide and Nital Etch
$AuSn_4$ compounds are shown at a higher magnification in the 50/50 solder mass.

very thin plates which appear as fine needles. Similar structures were obtained in 60/40 solder fillets as shown in Figures 28 and 29.

Other Intermetallic Compounds

A variety of intermetallic compounds were formed by applying solders to pure metals or substrates coated with the elements of interest. In each case the intermetallic compound of the substrate metal and tin which formed was the compound which comprised the largest proportion of tin.

The silver-tin phase diagram, Appendix A, predicts one intermetallic compound, γ - Ag_3Sn, of orthorhombic symmetry. The ζ phase is a hexagonal solid solution of tin in silver covering a range of compositions from about $Ag_{4.5}Sn$ to $Ag_{5.5}Sn$. Figures 30 and 31 show typical clusters of isolated Ag_3Sn intermetallic compounds formed in a 60/40 solder fillet applied to a silver substrate.

The system Pt-Sn predicts a series of intermetallic compounds to be stable at room temperature. However, $PtSn_4$ was the only compound observed. Figures 32 and 33 show the interface which was observed when 60/40 solder was applied to a platinum coated substrate. The compounds appear as rectangular blocks, consistent with their reported orthorhombic (10) symmetry. An isolated $PtSn_4$ intermetallic compound is shown in Figure 34. The two circular dots left of center are the locations where the electron beam was directed during X-ray microanalysis. Palladium-tin is also capable of forming a number of intermetallic compounds. The tin rich compound, $PdSn_4$, will form in solder applied to palladium substrates. Figure 35 shows a few dispersed intermetallic compounds in a

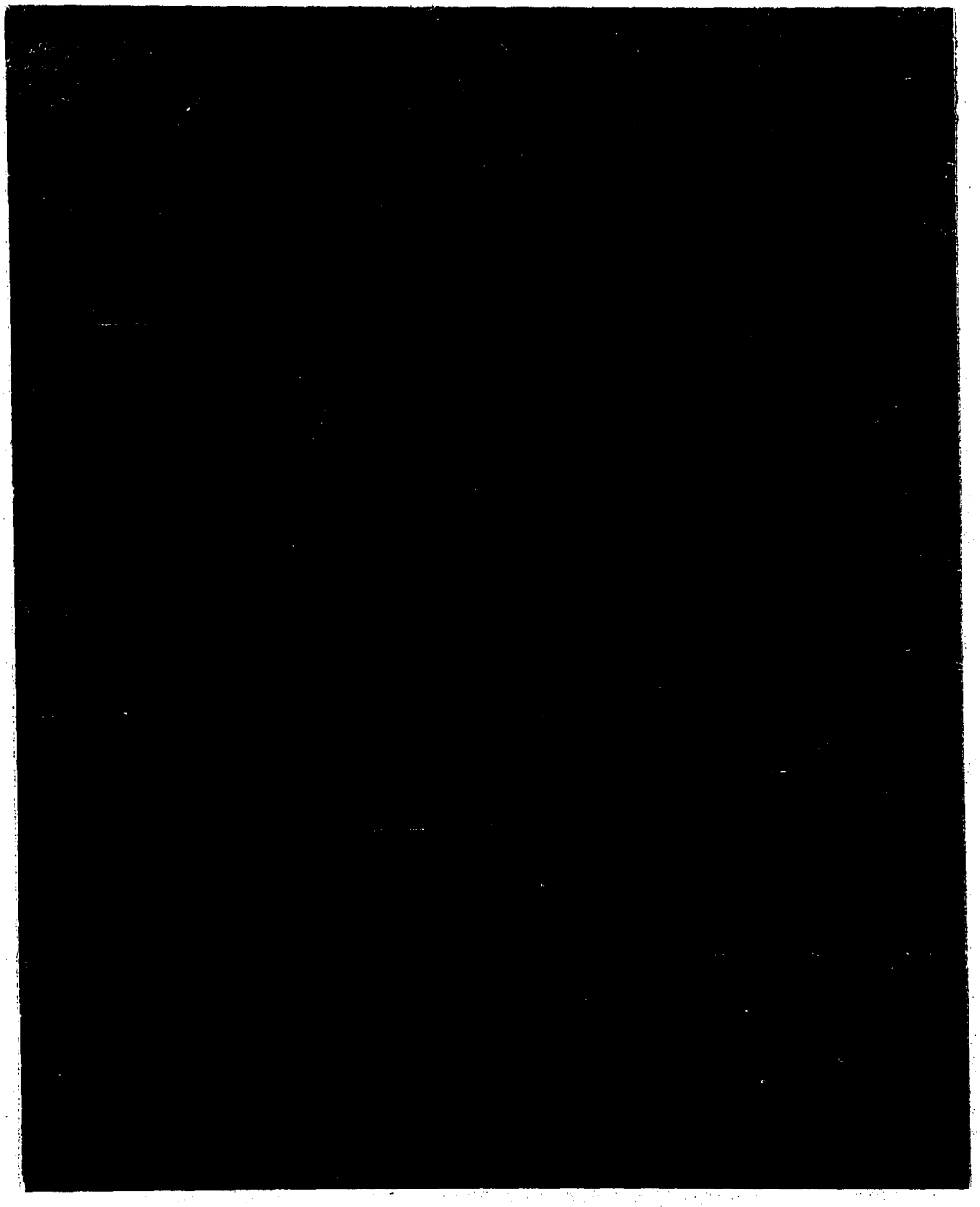

Figure 28. 1120X - Peroxide and Nital Etch $AuSn_4$ intermetallic compounds formed in a 60/40 solder mass when applied to a pure gold plated substrate.

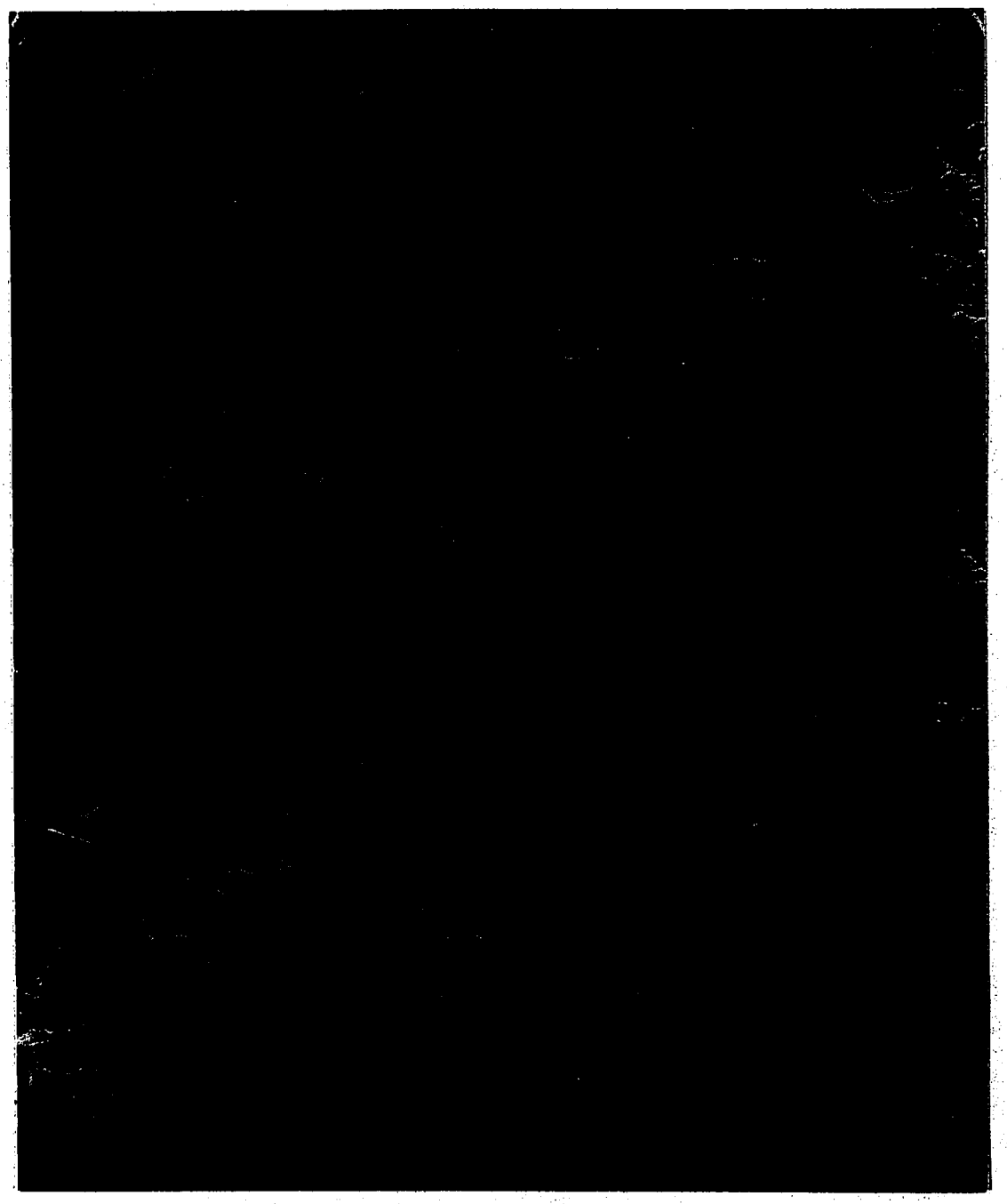

Figure 29. 1400X - Peroxide and Nital Etch
The plate like $AuSn_4$ compounds are shown in various orientations.

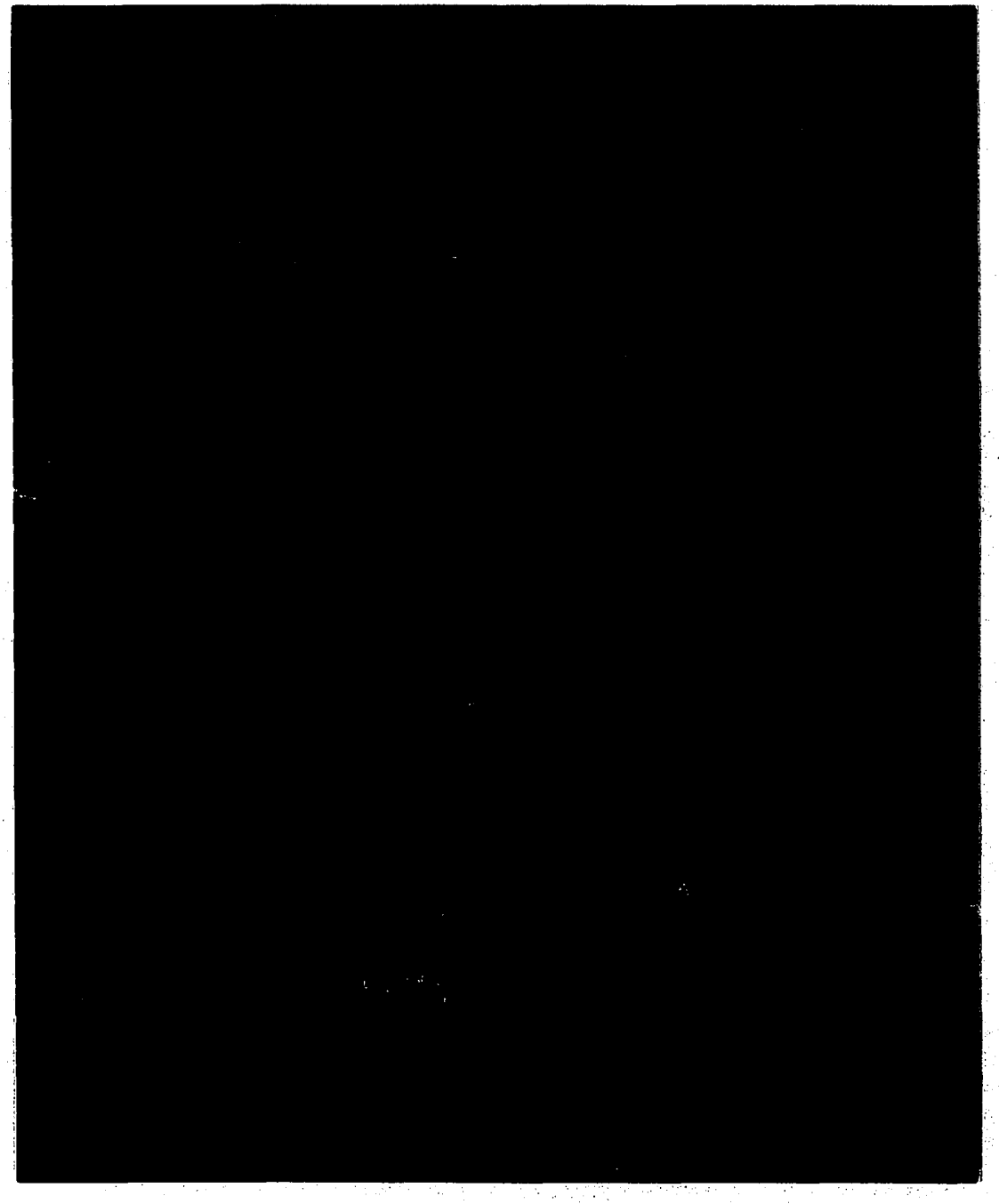

Figure 30. 1400X - Peroxide and Nital Etch Ag_3Sn intermetallic compounds formed in a 60/40 solder which was applied to a pure silver substrate.

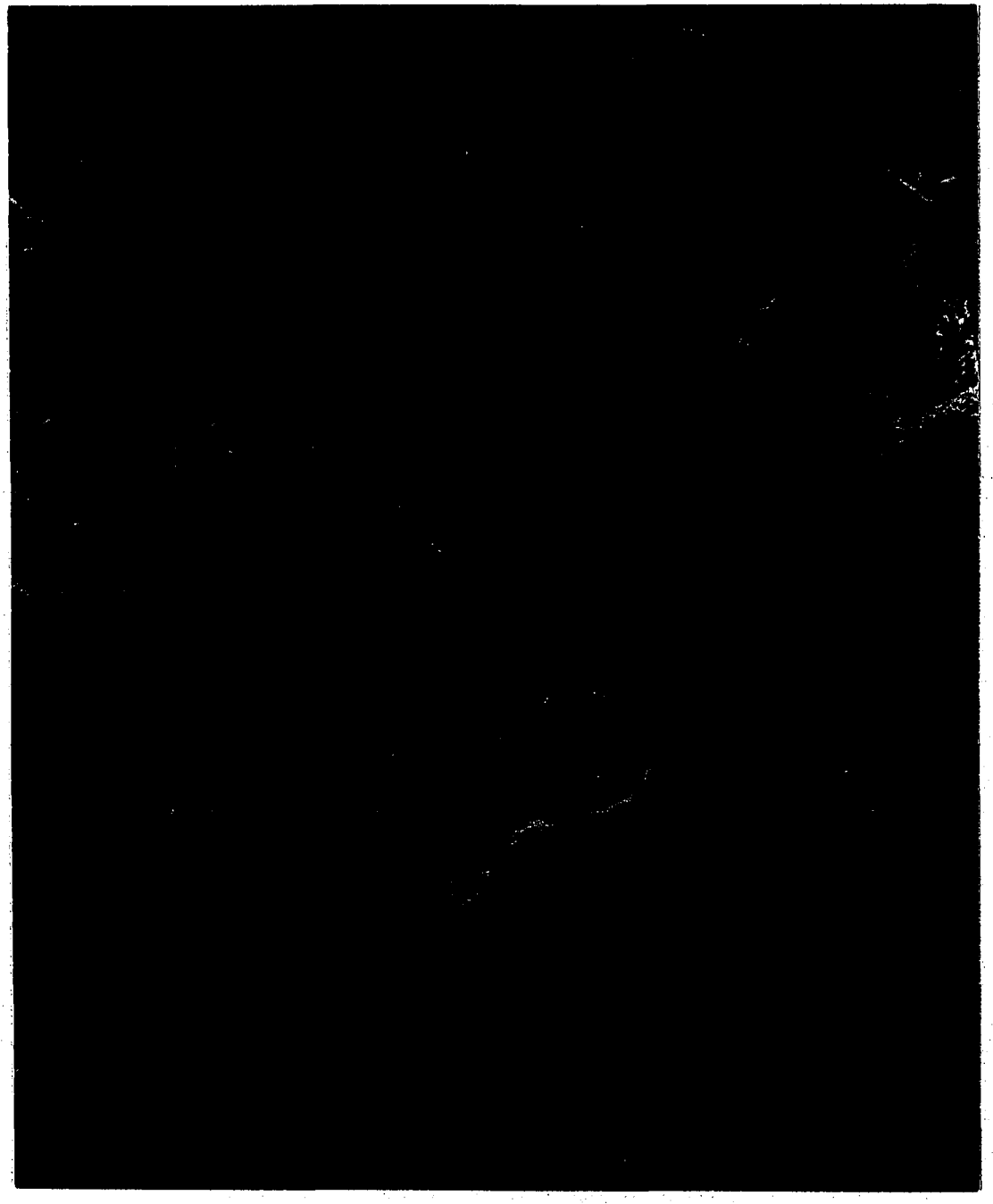

Figure 31. 2800X - Peroxide and Nital Etch Ag_3Sn intermetallic compounds in a mass of 60/40 solder.

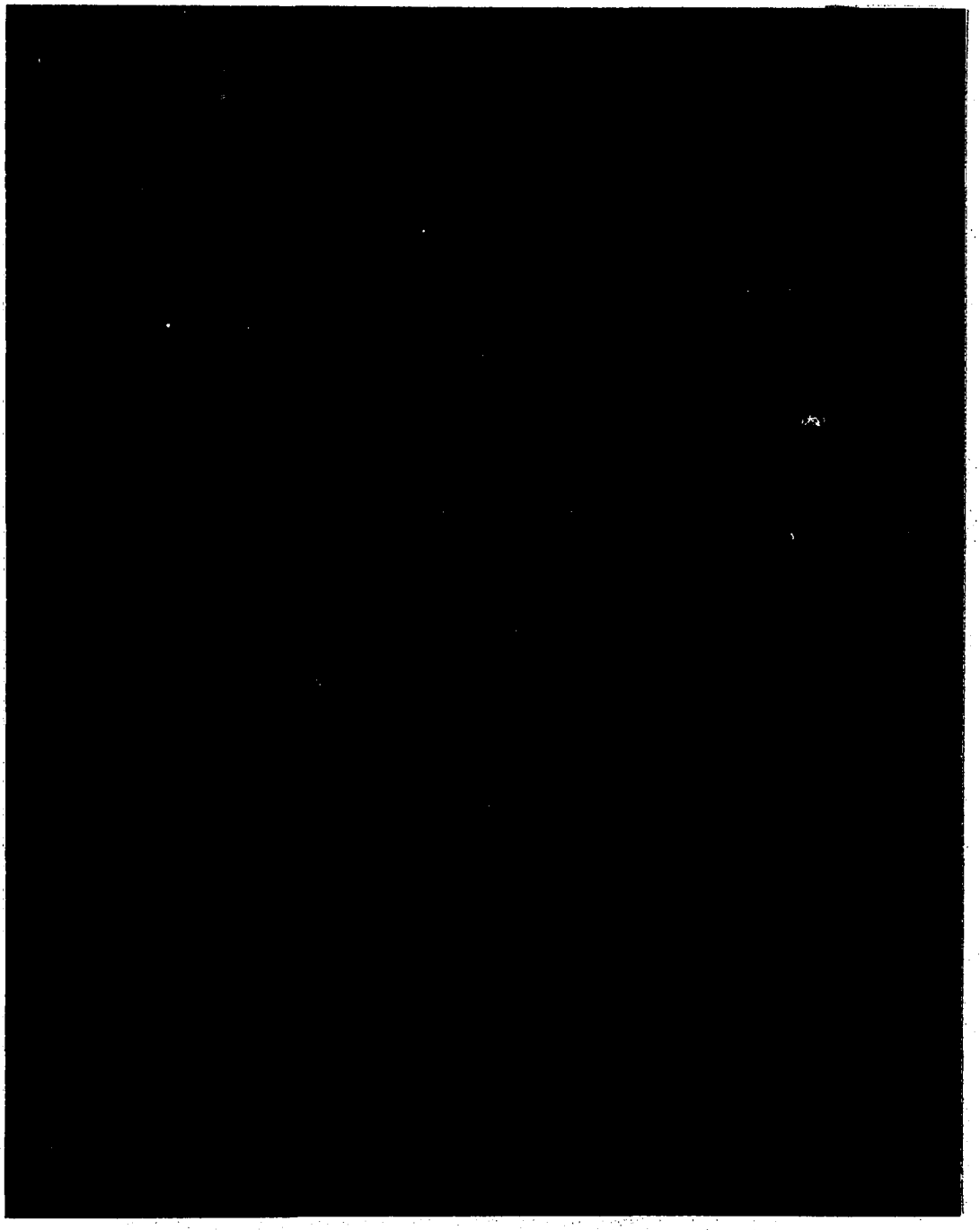

Figure 32. 1400X - Peroxide and Nital Etch 60/40 solder applied to a pure platinum substrate. $PtSn_4$ intermetallic compounds formed at the interface.

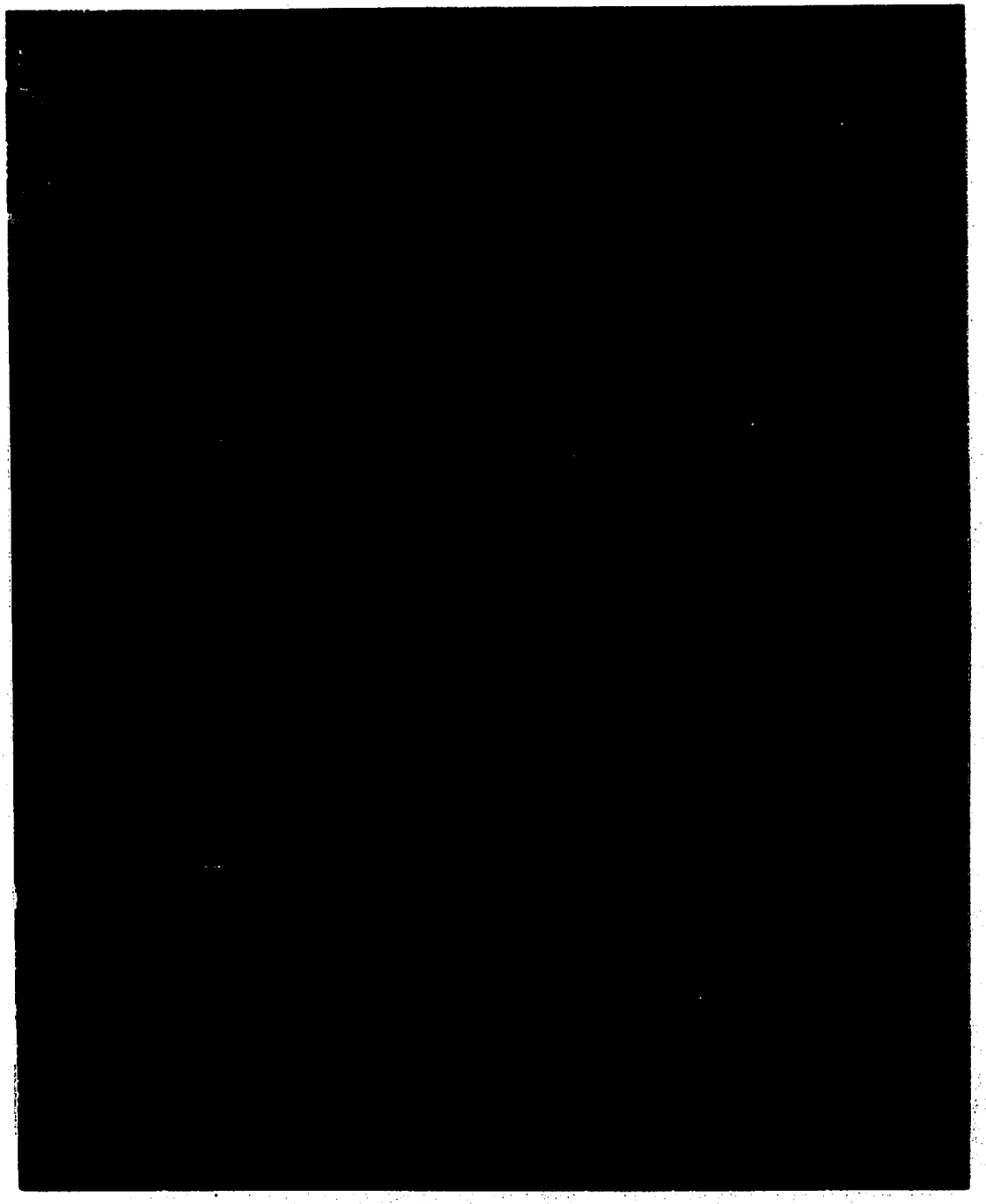

Figure 33. 8400X - Peroxide and Nital Etch
A more magnified view of Figure 32 and the $PtSn_4$ compounds formed at the interface of 60/40 solder applied to a pure platinum substrate.

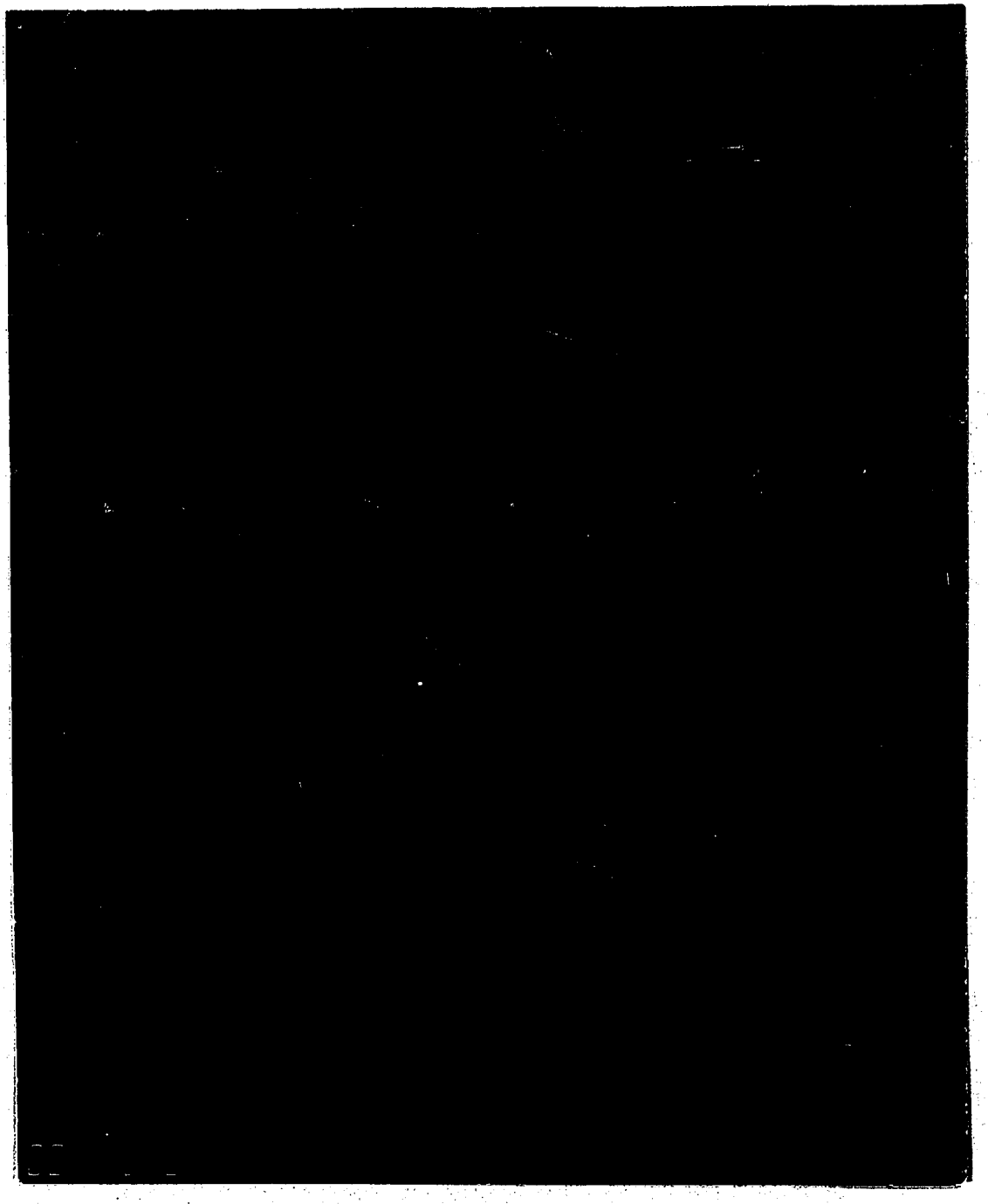

Figure 34. 11,200X - Peroxide and Nital Etch
An isolated $PtSn_4$ intermetallic compound formed in a 60/40 solder mass remote from the interface.

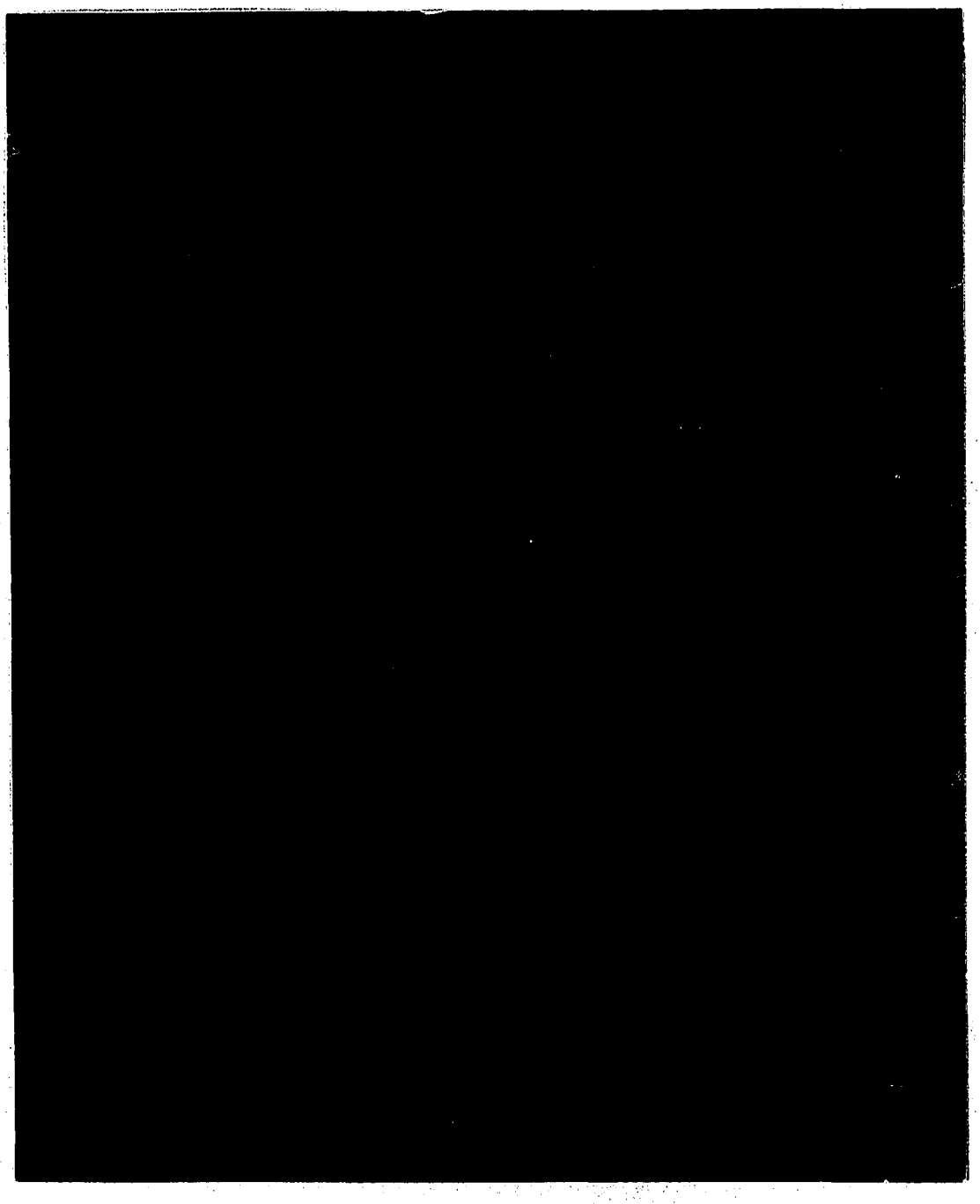

Figure 35. 1260X - Peroxide and Nital Etch $PdSn_4$ intermetallic compounds formed in a 60/40 solder mass when applied to a pure palladium substrate.

60/40 solder fillet. Enlarged views of typical examples of the intermetallic compounds are shown in Figures 36 and 37.

Nickel is commonly used as a diffusion barrier for copper substrates which are gold plated for use in connector applications. The nickel is intended to reduce diffusion of copper through the gold plating and, thereby, maintain a stable and low resistance contact surface. The function of the gold is to provide a non-degrading solderable surface. The nature of the separate roles of these layers will be discussed in some detail later. Here it is noted that nickel is not immune from reaction with solder. The tin rich intermetallic compound Ni_3Sn_4 forms primarily along the solder substrate boundary as shown in Figure 38. The sample shown was heavily etched, resulting in a ledge between the substrate nickel plating and the solder fillet. The blocky particles shown in greater detail in Figures 39 and 40 are Ni_3Sn_4. Some of the particles in Figure 38 appear to show hexagonal symmetry, suggesting copper (Cu_6Sn_5) contamination. However, Ni_3Sn_4 is reported to be monoclinic (11) and the shape of the isolated particle shown in Figures 41 and 42 demonstrate angles which could generate external surfaces which appear hexagonal.

Iron and iron based alloys are generally used as containers for molten solder in commercial soldering equipment and as inert platings to prevent solder attack. The most familiar of the latter class are iron plated soldering tips. Iron-tin intermetallic compounds were in the fillets and at the interface of 60/40 solder applied to pure nickel substrates. Figure 43 shows examples of compound formation in both regions. The near surface compounds, shown in more detail in

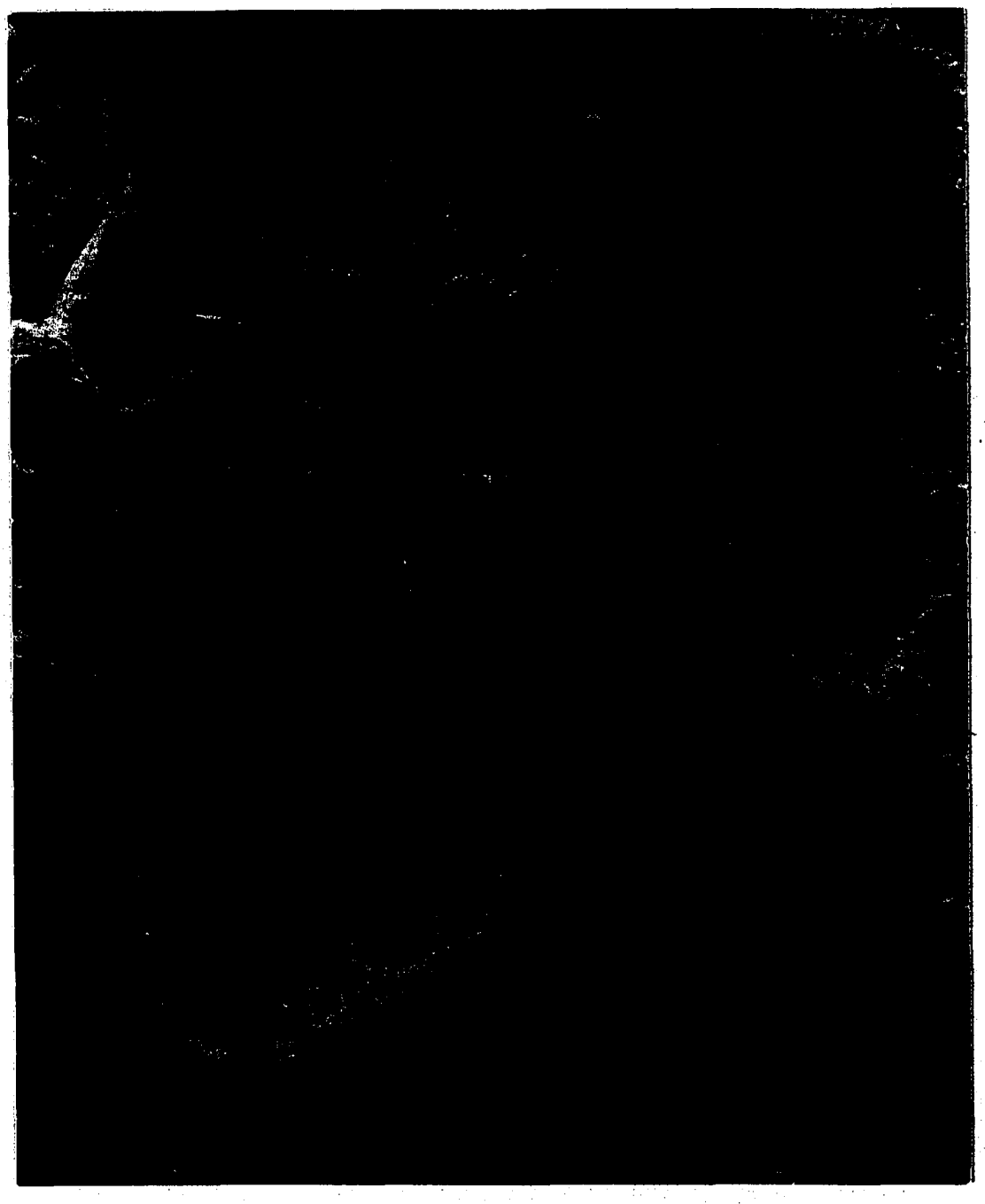

Figure 36. 7000X - Peroxide and Nital Etch $PdSn_4$ intermetallic compound formed in a mass of 60/40 solder remote from the interface.

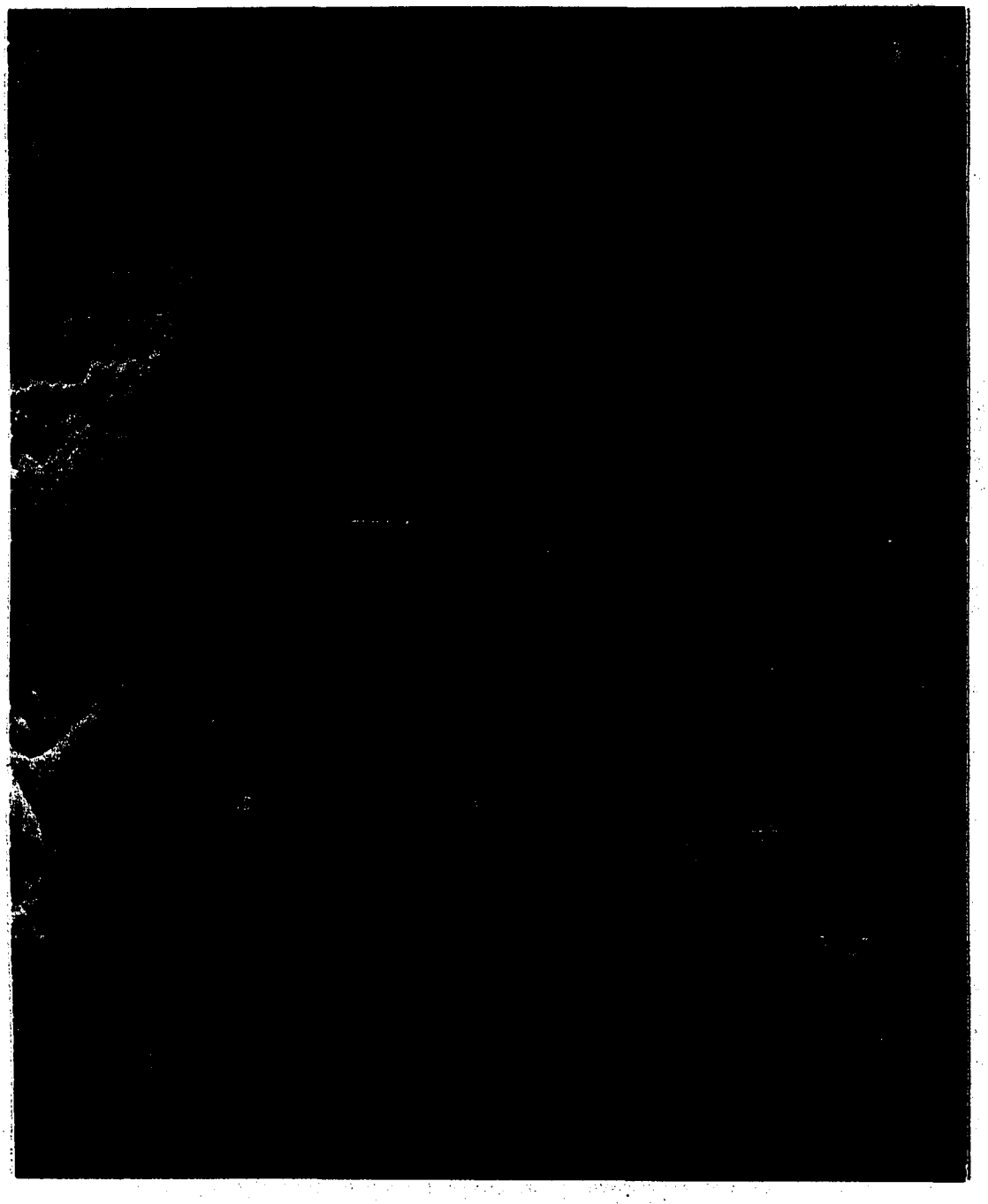

Figure 37. 7000X - Peroxide and Nital Etch
A $PdSn_4$ intermetallic compound in
a mass of 60/40 solder.

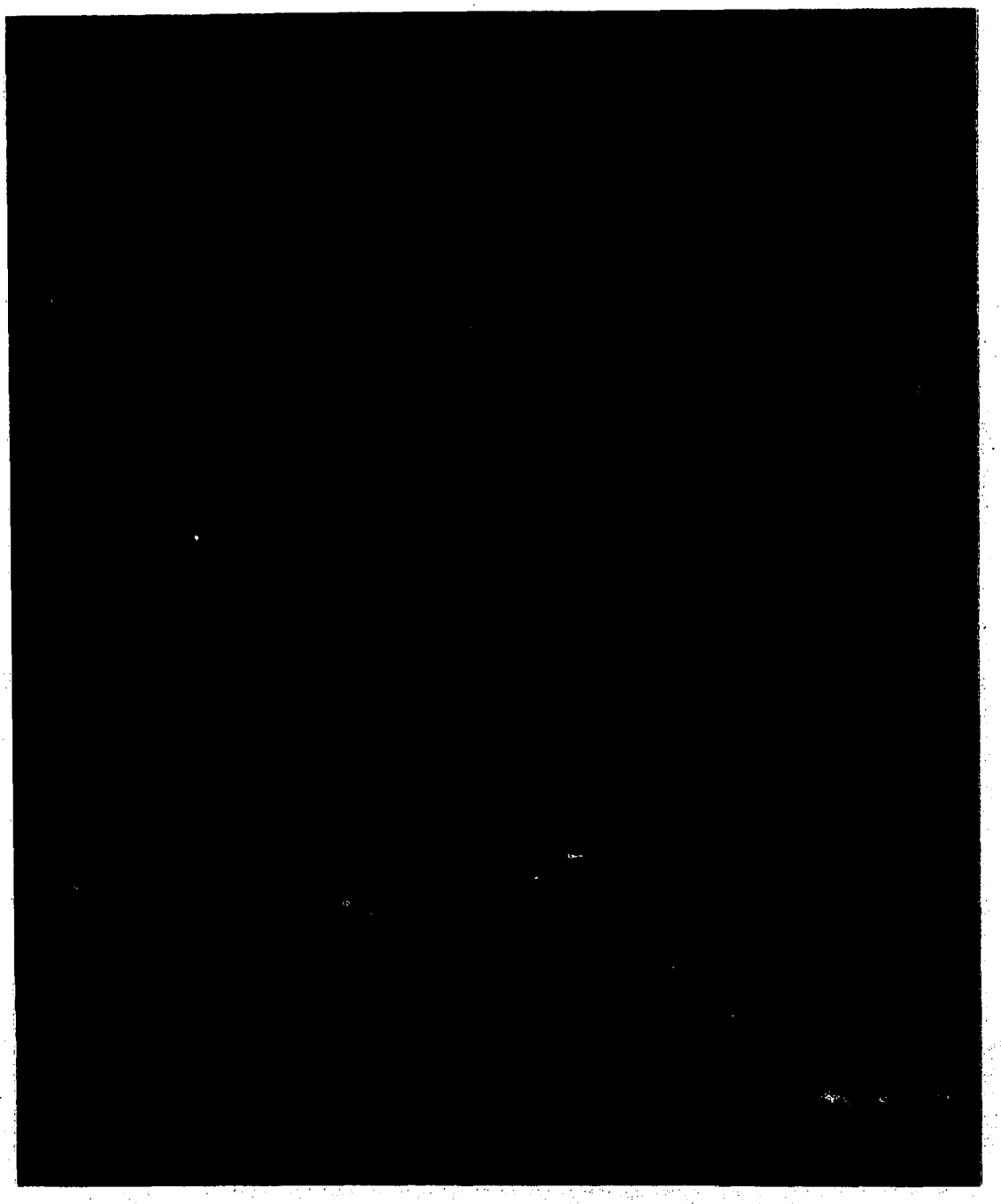

Figure 38. 2800X - Peroxide and Nital Etch 60/40 solder applied to a pure nickel substrate using a hand soldering iron. Ni_3Sn_4 intermetallic compounds formed near the interface.

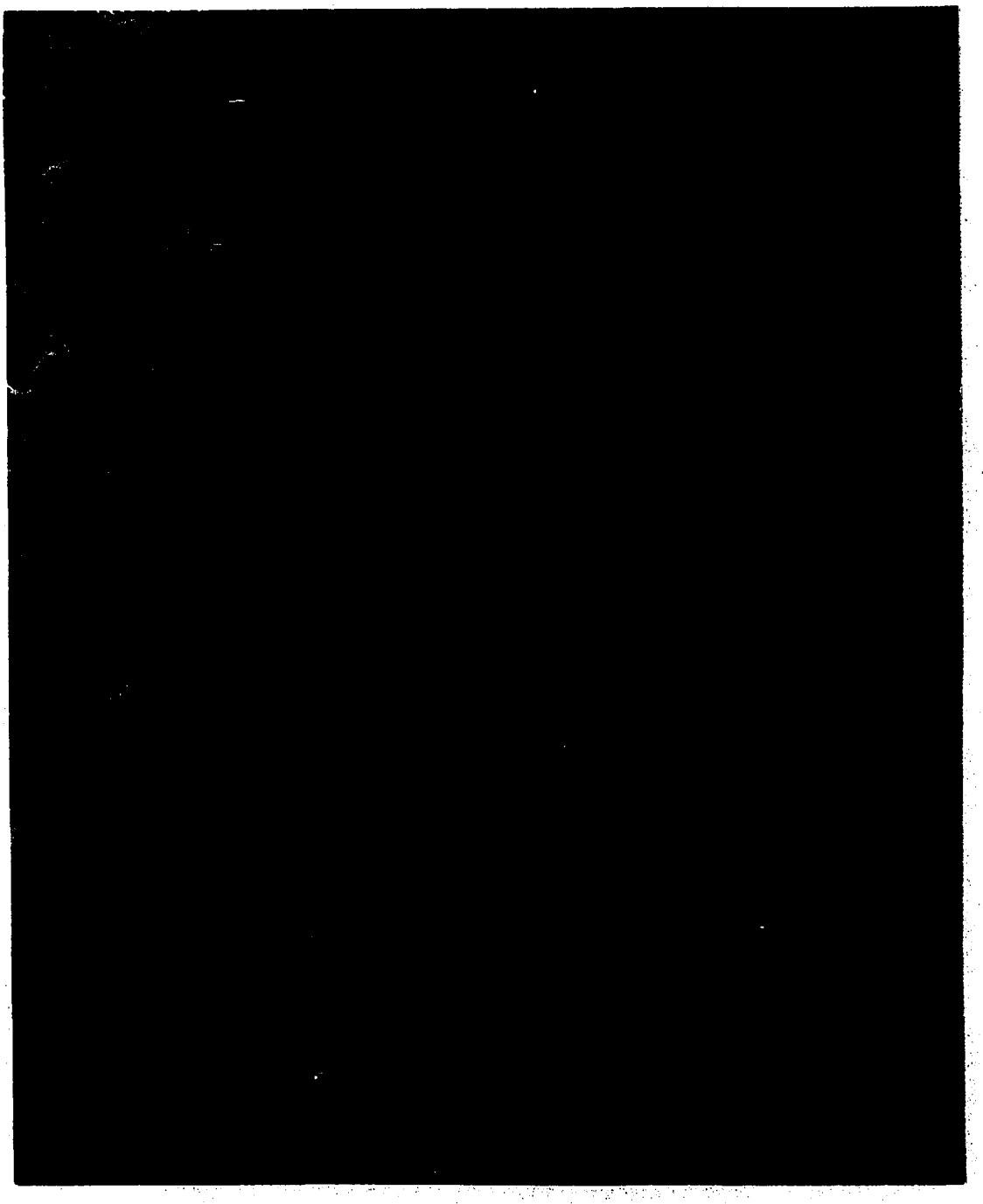

Figure 39. 9800X - Peroxide and Nital Etch
The blocky particles near the interface as shown in Figure 38 are Ni_3Sn_4 intermetallic compounds which formed during soldering.

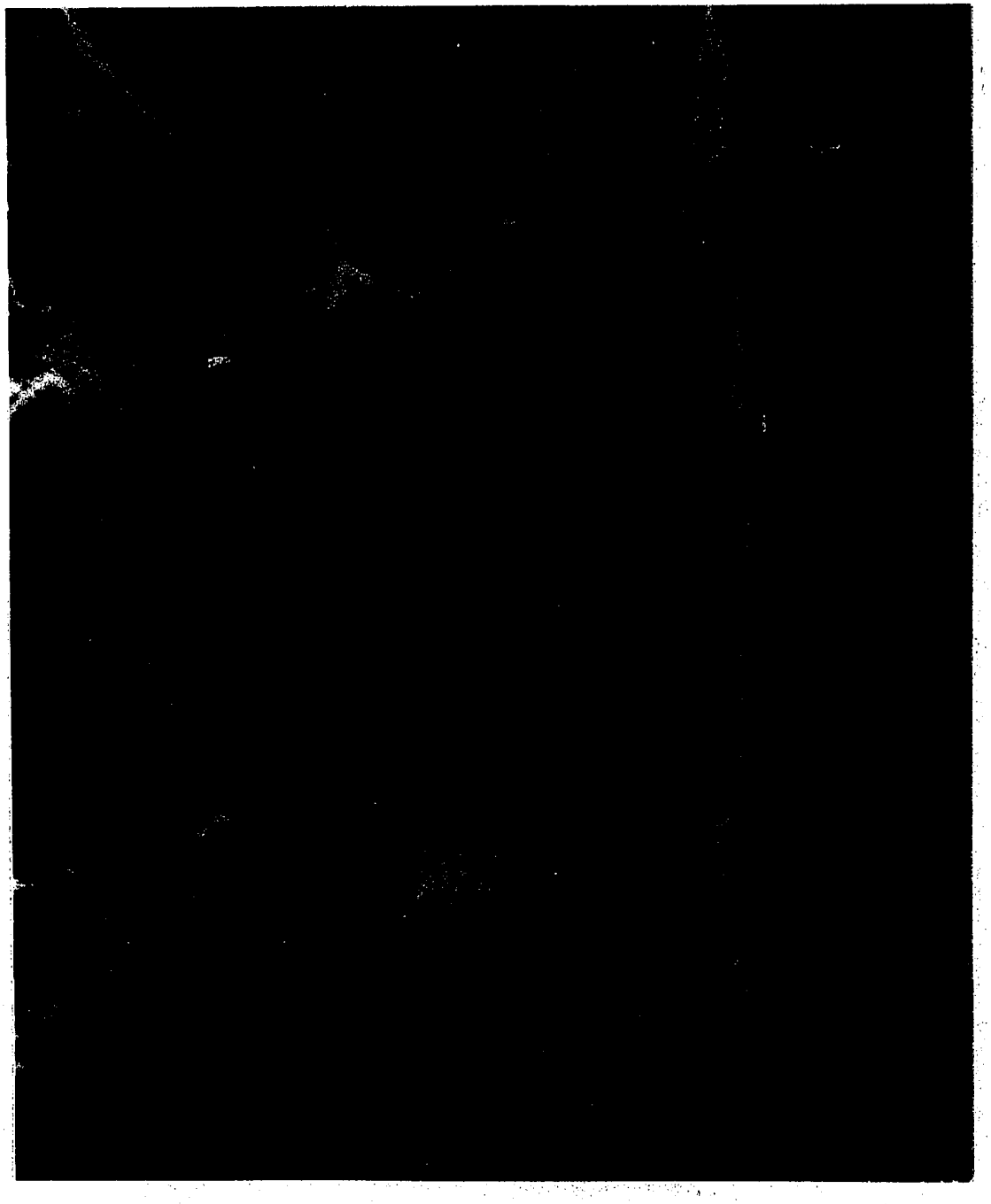

Figure 40. 11,200X - Peroxide and Nital Etch
A magnified area of Figure 39 of the Ni_3Sn_4 intermetallic compounds.

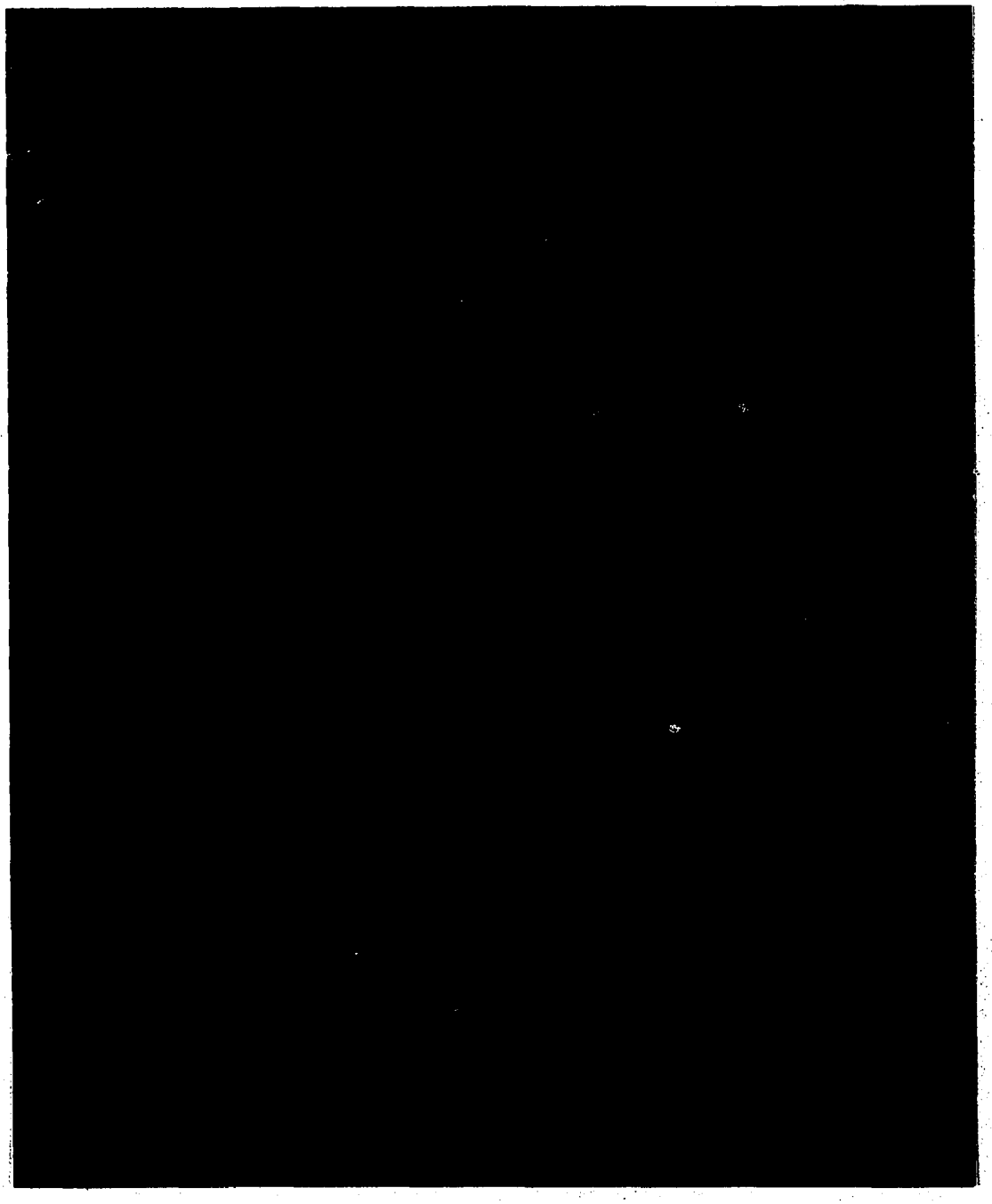

Figure 41. 1400X - Peroxide and Nital Etch
An isolated Ni_3Sn_4 intermetallic compound.

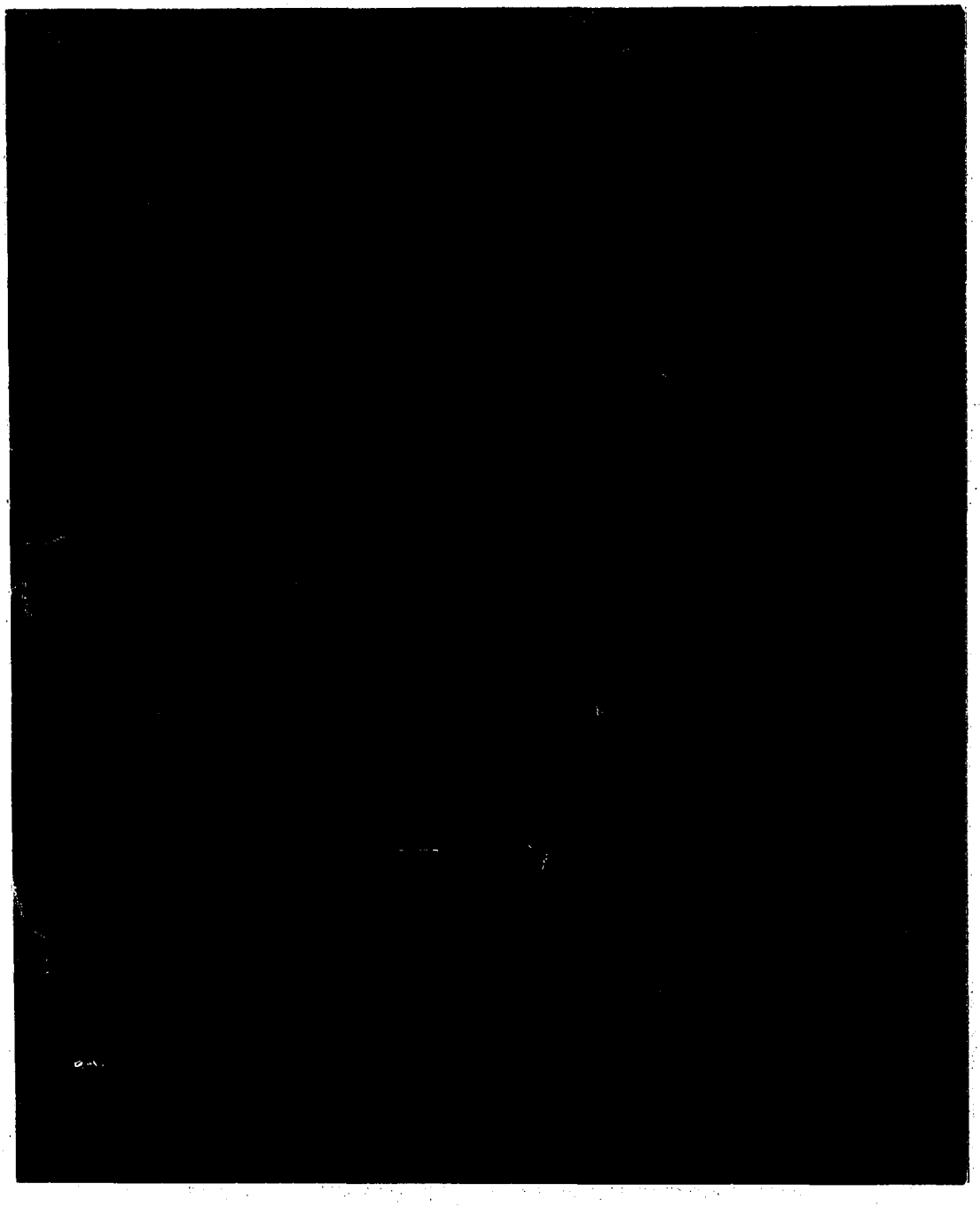

Figure 42. 7000X - Peroxide and Nital Etch
A magnified area of Figure 41 of the Ni_3Sn_4 intermetallic compound.

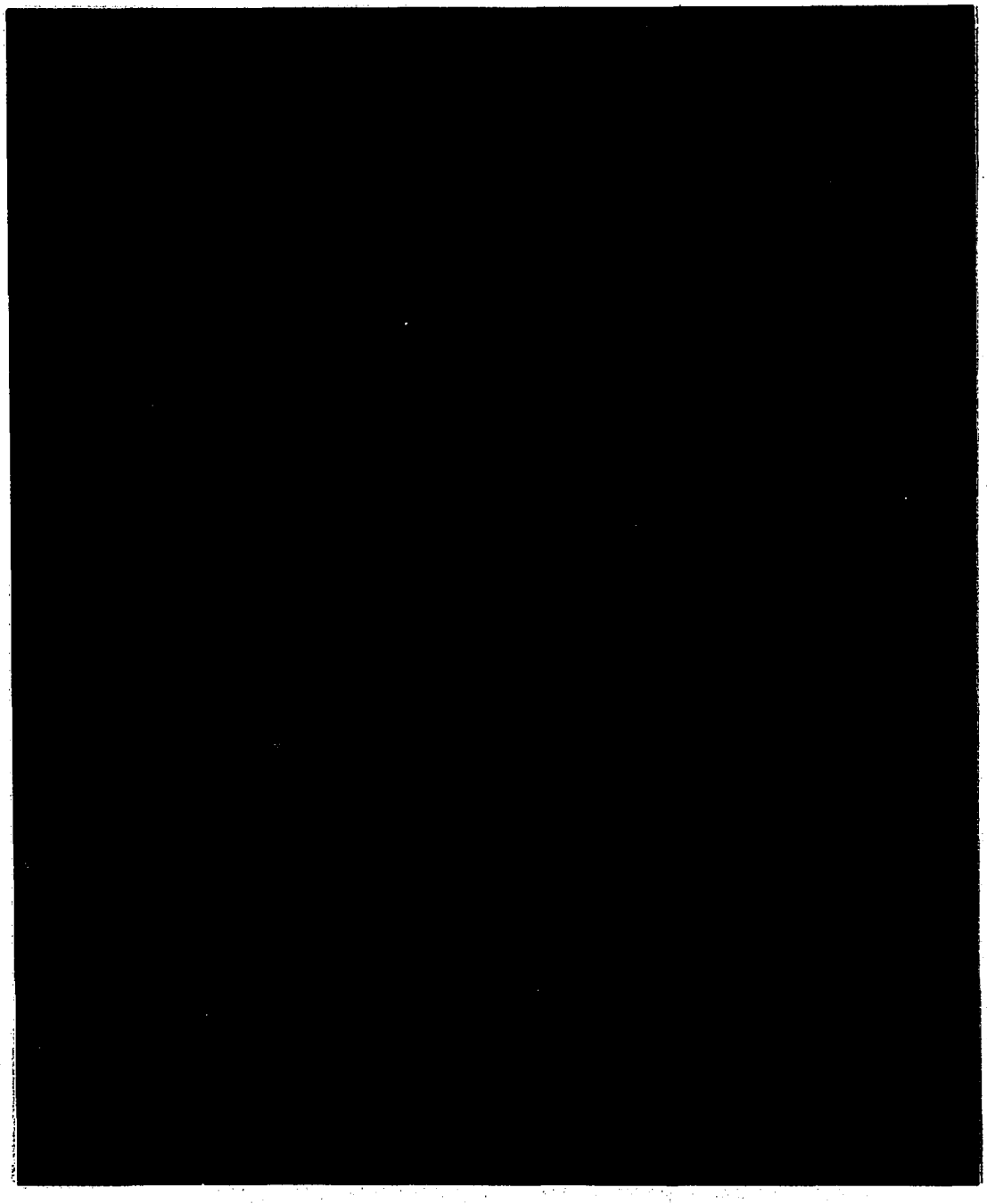

Figure 43. 280X - Peroxide and Nital Etch
Intermetallic compounds corresponding to $FeSn_2$ + 1 a/o % nickel. A hand soldering iron was used during soldering.

Figures 44 and 45, contained tin and iron in atomic proportions corresponding to $FeSn_2$. This is the tin rich intermetallic compound reported to have a body centered tetragonal structure (12). A low level of nickel contamination (less than one atomic percent) was detected in the interfacial compound.

The massive compound cluster seen in the fillet in Figure 43 is shown at higher magnification in Figure 46. EDS analysis revealed tin, iron and nickel in atomic proportions 20:10:1. Apparently the compound $FeSn_2$ was formed in a fillet of 60/40 solder applied to a copper substrate, as shown in Figure 47. The iron was probably incorporated as a contaminant in the solder. Cu_6Sn_5 compounds are also shown in the micrograph. A particle of $FeSn_2$ was also noted in a fillet of the antimonial solder. The particle shown in Figure 48 was also most probably formed from contaminants in the solder.

Contaminants in solders are capable of inducing intermetallic compound formation. Figure 49 shows a platelike particle having a composition which corresponded to As_2Sn_3. The compound was formed in a 60/40 solder fillet applied to a copper substrate. The hexagonal particle shown in the photomicrograph is Cu_6Sn_5. Arsenic was probably an impurity in the substrate.

Intermetallic compound formation involving antimony is possible in antimonial solders. The antimony-tin system does not predict any intermetallic compound formation (Appendix A). The β' phase is centered on the composition SbSn, with a total β and β' composition range extending from approximately Sb_2Sn_3 to Sb_2Sn. The crystal structure is rhombohedral with nearly orthogonal axes. The compositions of antimonial

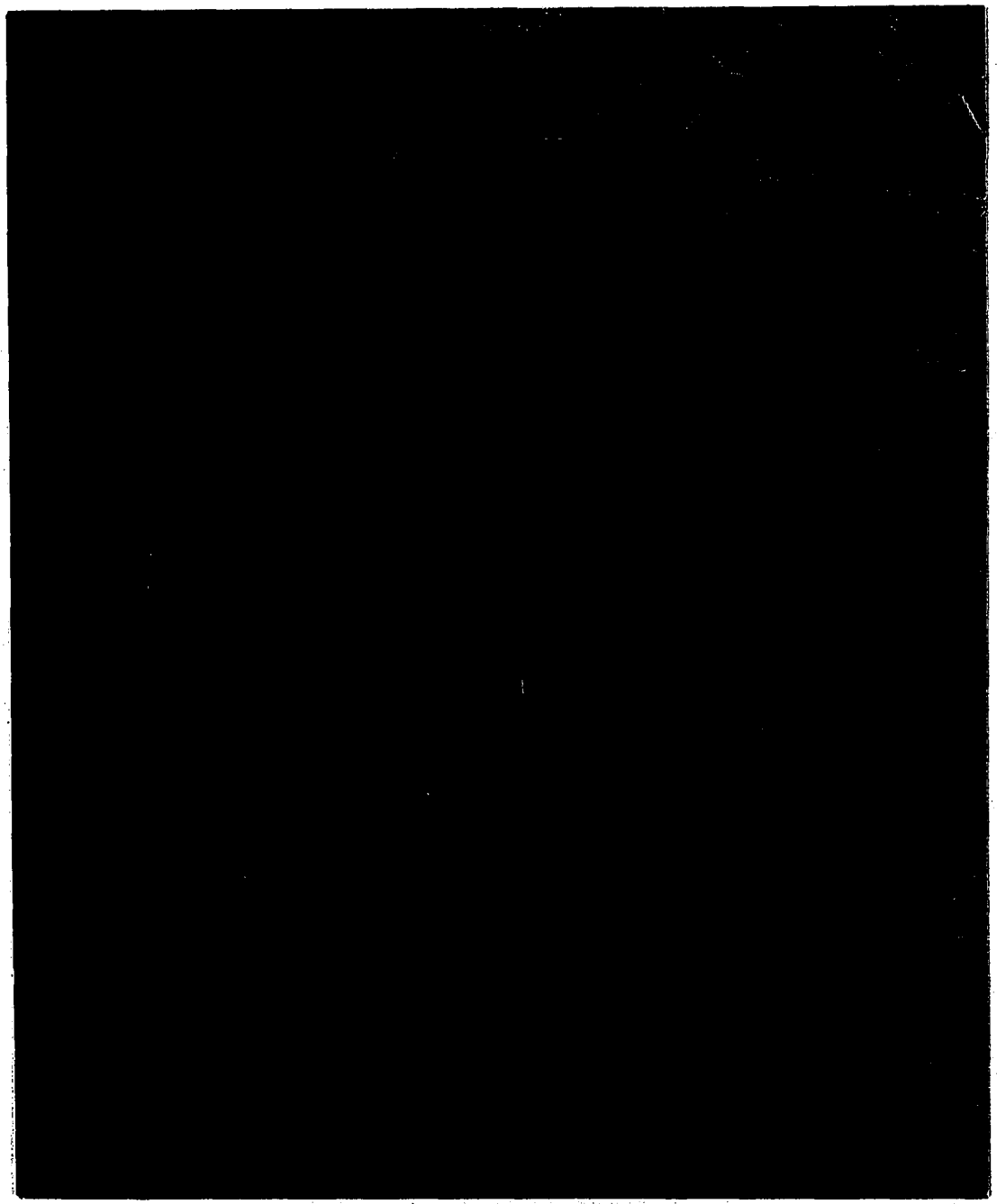

Figure 44. 2800X - Peroxide and Nital Etch
The near surface compounds shown in Figure 43.

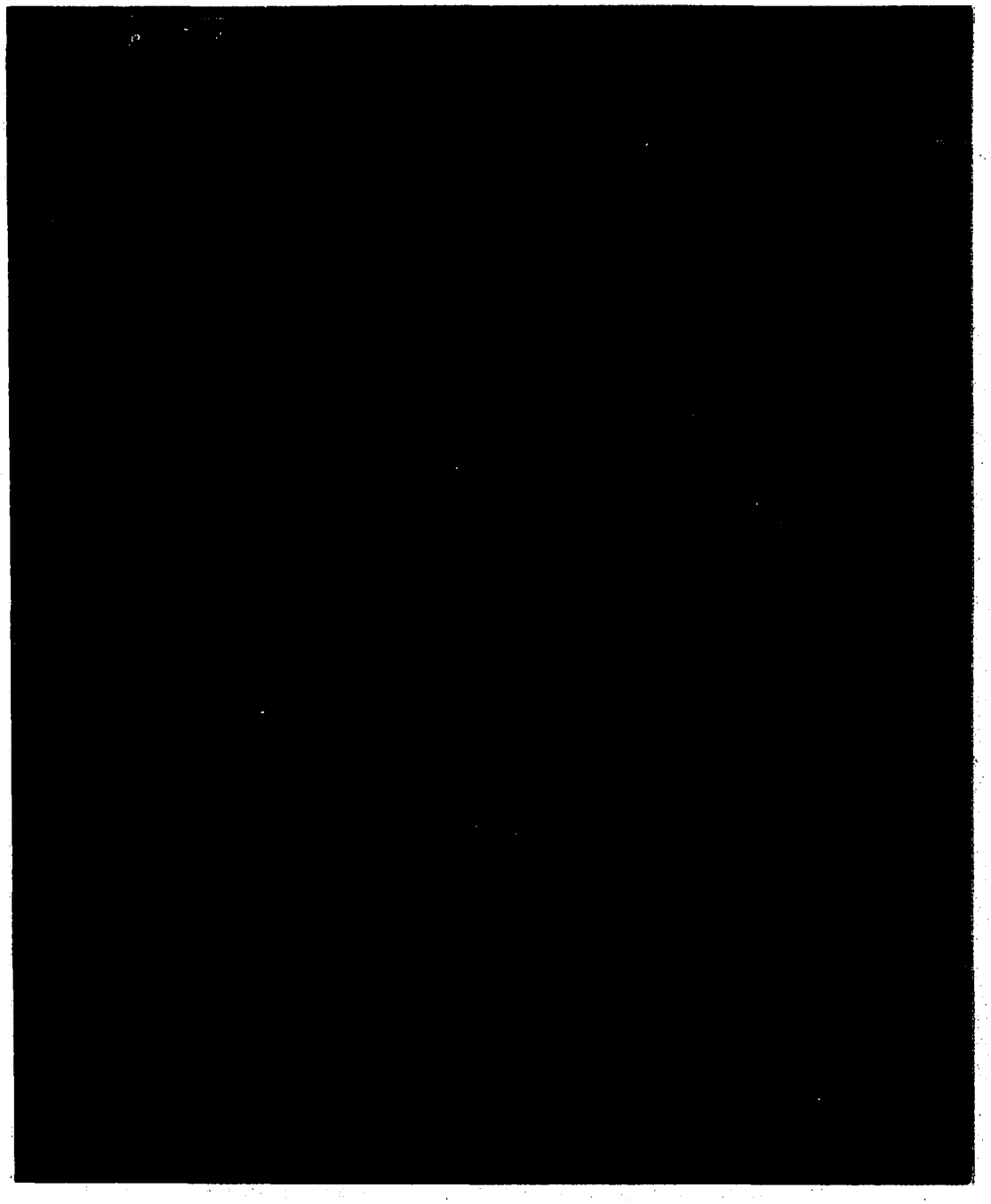

Figure 45. 1400X - Peroxide and Nital Etch
A $FeSn_2$ + 1 a/o% nickel compound near
the substrate and solder mass interface.

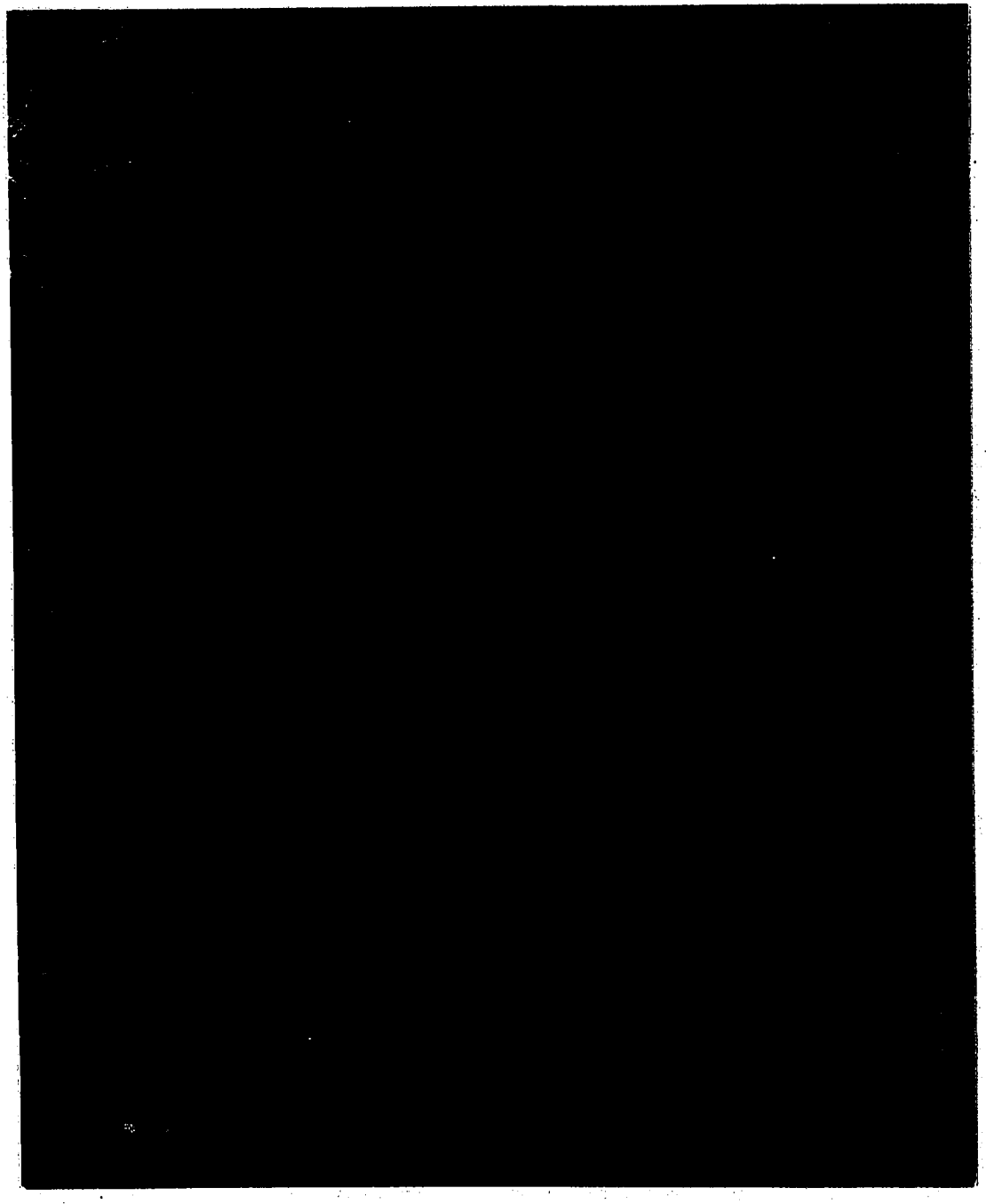

Figure 46. 1400X - Peroxide and Nital Etch
The massive compound shown in Figure 43 is shown at higher magnification. EDS analysis revealed atomic proportions of Sn:Fe:Ni of 20:10:1.

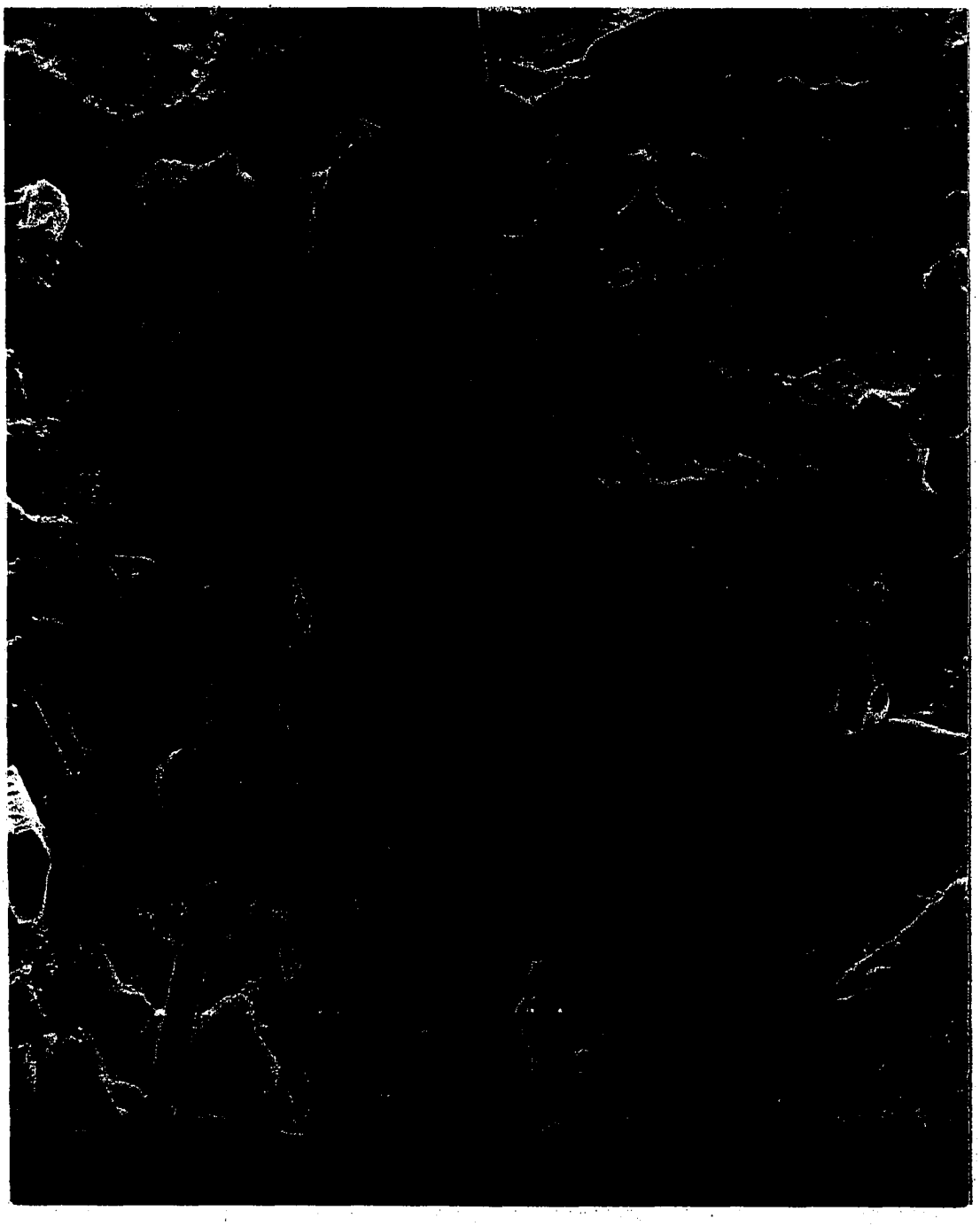

Figure 47. 3080X - Peroxide and Nital Etch
The massive compound is $FeSn_2$.
The intermetallic compound is predicted by the Fe-Sn binary phase diagram.

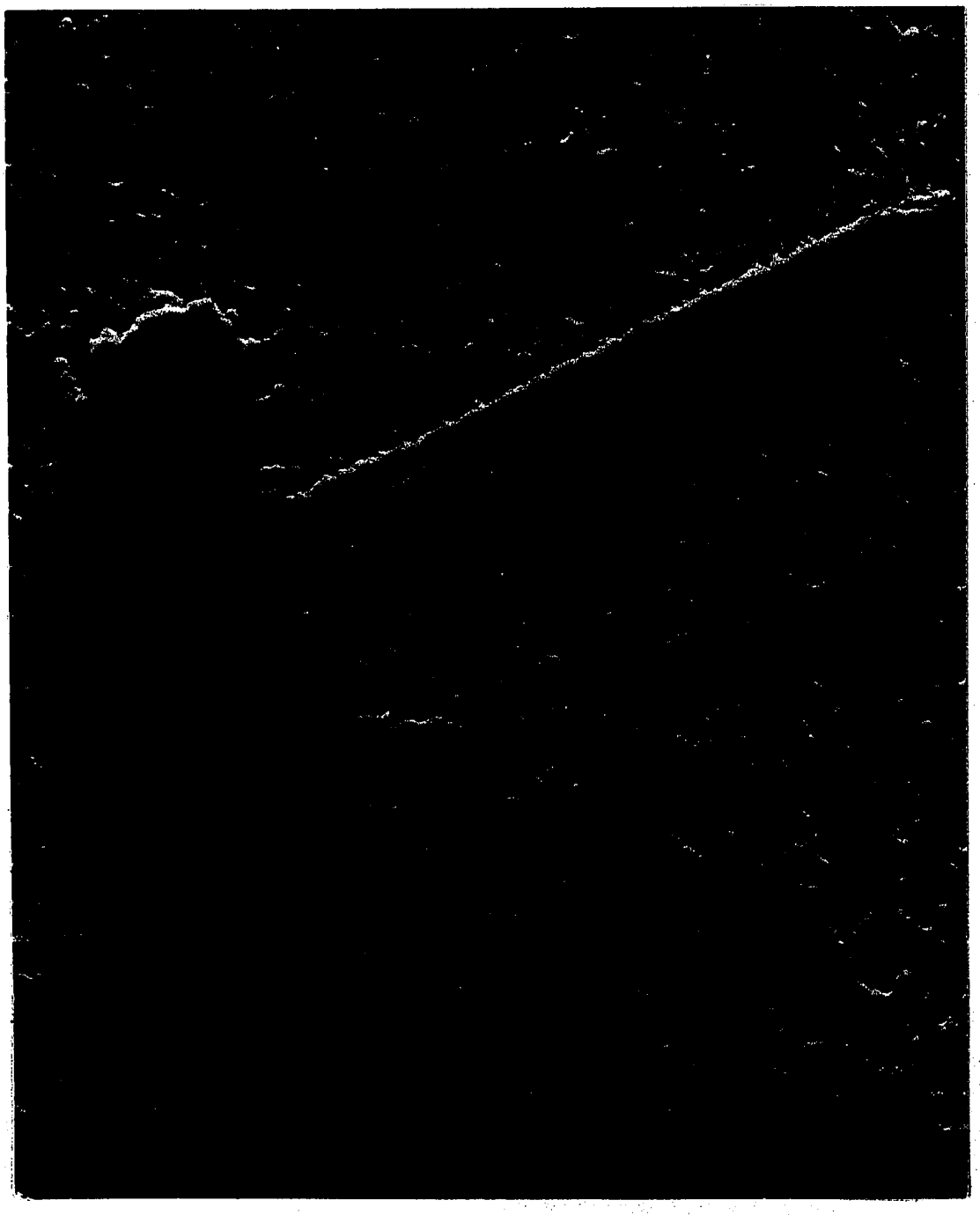

Figure 48. 1400X - Peroxide and Nital Etch
An $FeSn_2$ intermetallic compound in an antimonial solder mass.

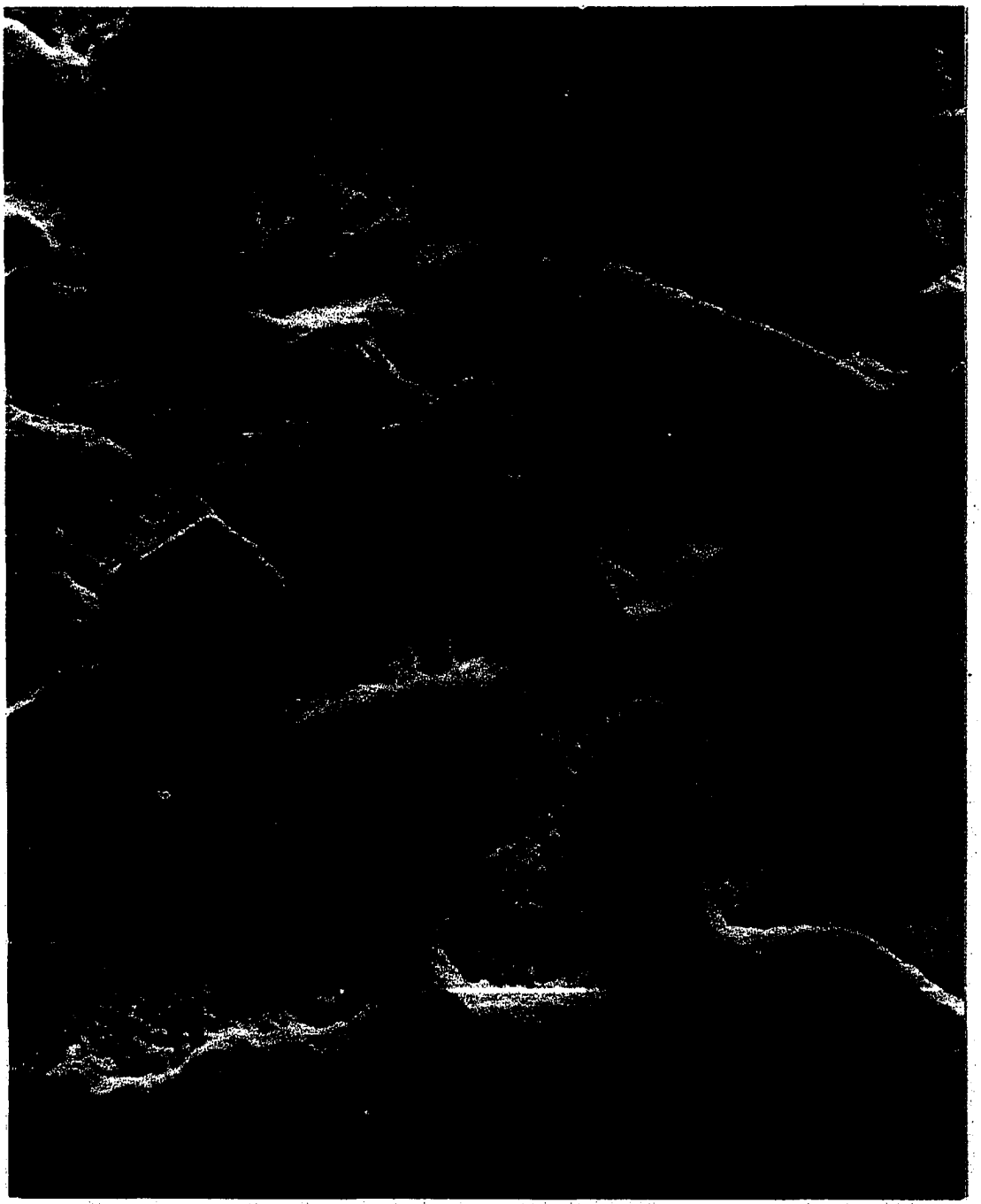

Figure 49. 4200X - Peroxide and Nital Etch
The hexagonal structure is Cu_6Sn_5 and the rectangular structure is As_2Sn_3.

solders are balanced so that the antimony content will not exceed the solid solubility limit in tin (approximately three atomic or weight percent). Precipitation of sufficient tin-based intermetallic compounds was capable of raising the effective antimony concentration in the antimonial solder used in this study. The result was the formation of β' at a composition corresponding to Sb_2Sn_3.

Figures 50 and 51 show the appearance of β' in an antimonial solder fillet formed on a brass substrate and subsequently aged for a week at 100°C. Figures 52 and 53 show β' in an antimonial solder formed on a gold plated substrate. In both cases, considerable intermetallic compound formation (Cu_6Sn_5 and $AuSn_4$) was noted elsewhere in the alloy. Apparently these depleted the tin content of the alloy facilitating the formation of Sb_2Sn_3.

It has been reported periodically that difficulties have been encountered with antimonial solders applied to zinc bearing substrates (13). Likewise, the use of antimony in solders has been suspect because of a supposed increased disposition toward intermetallic compound formation. There are no known intermetallic compounds of tin and zinc and none were observed. However, the antimony zinc system is capable of producing two compounds: β - SbZn and ε - Sb_3Zn_4 both of which are stable at room temperature. Their structures are orthorhombic and monoclinic or hexagonal respectively.

Figure 54 shows the antimonial solder applied to a pure zinc substrate. A thin interfacial layer of blocky, antimony-zinc compounds was noted. The angular particles in the solder fillet remote from the substrate were identified as Sb_3Zn_4. Other examples of this compound are shown in Figures 55 and 56.

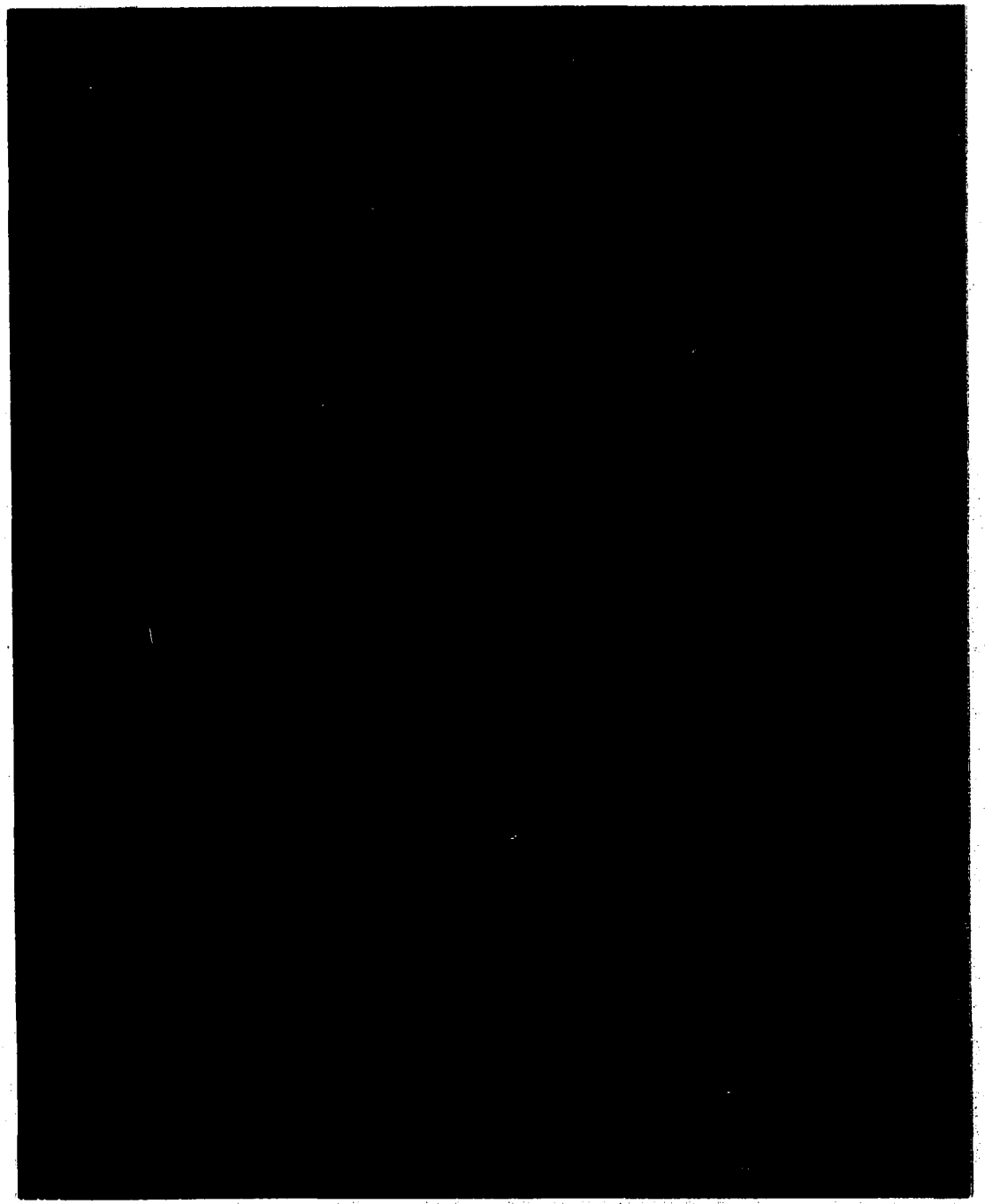

Figure 50. 1400X - Peroxide and Nital Etch Antimonial solder applied to α brass and aged for 7 days at 100°C. The cubic appearing areas correspond to Sb_2Sn_3 by EDS and WDS.

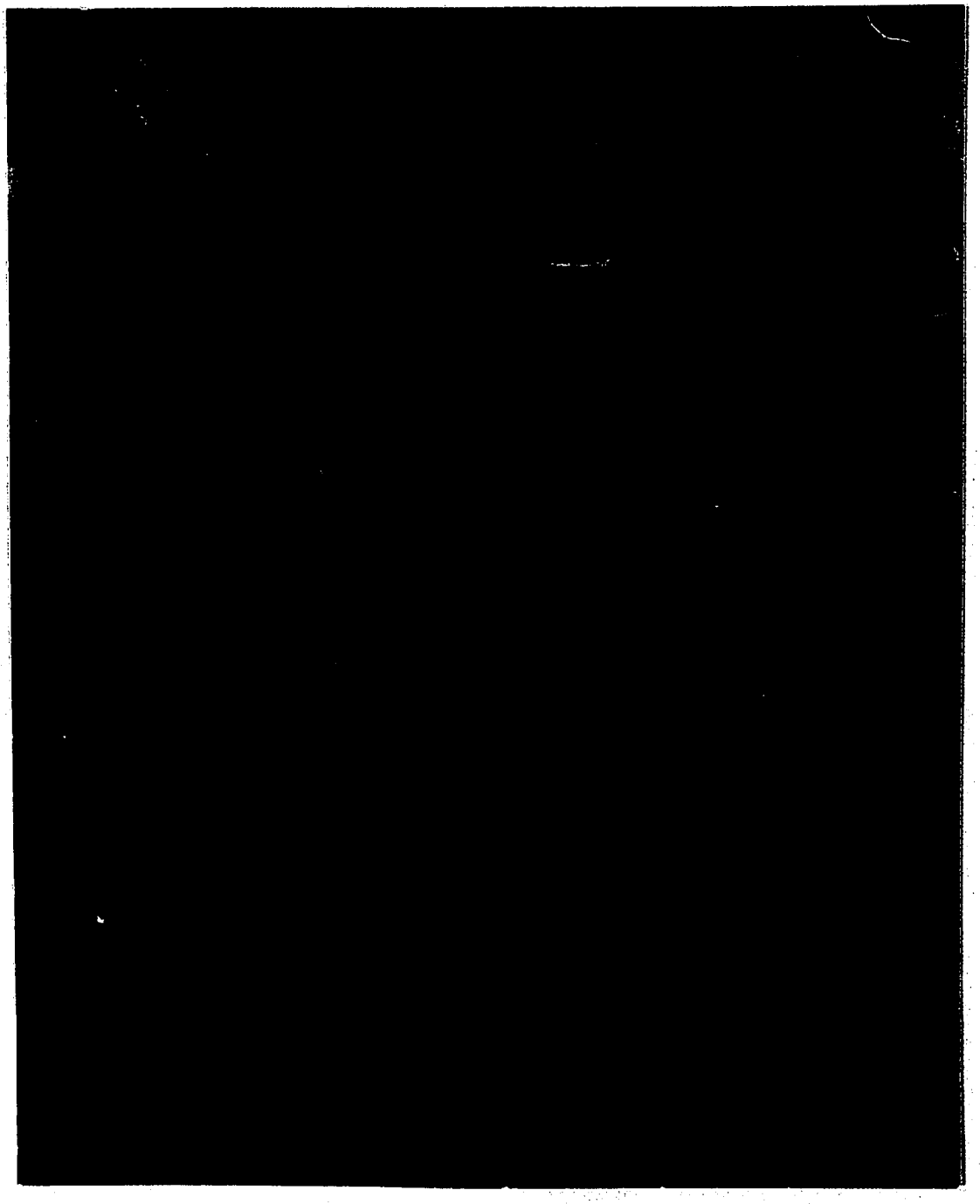

Figure 51. 5600X - Peroxide and Nital Etch
A magnified area of Figure 50.

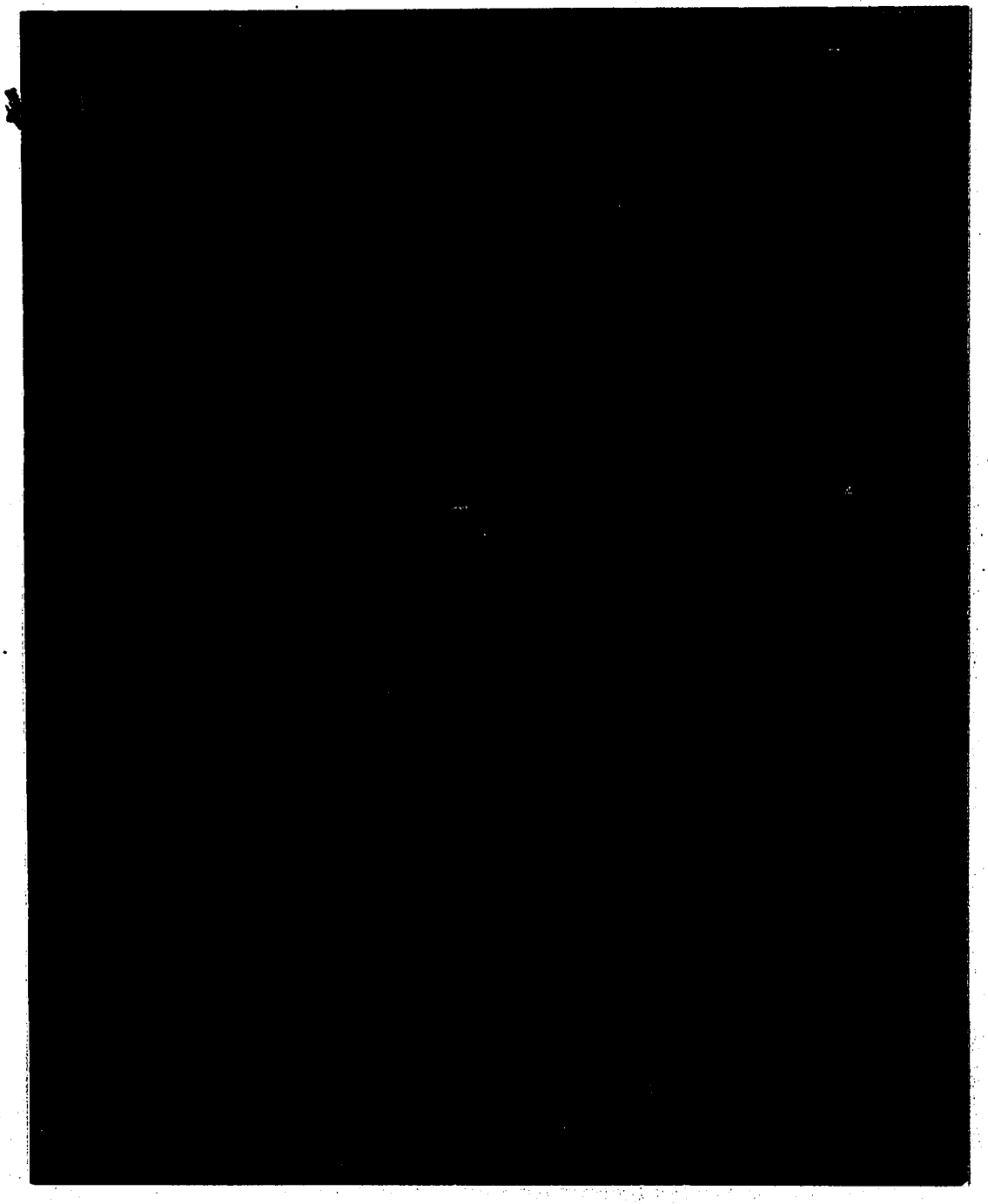

Figure 52. 1400X - Peroxide and Nital Etch Sb_2Sn_3 formation in an antimonial solder mass applied to a 2.5 micron gold plated terminal pin.

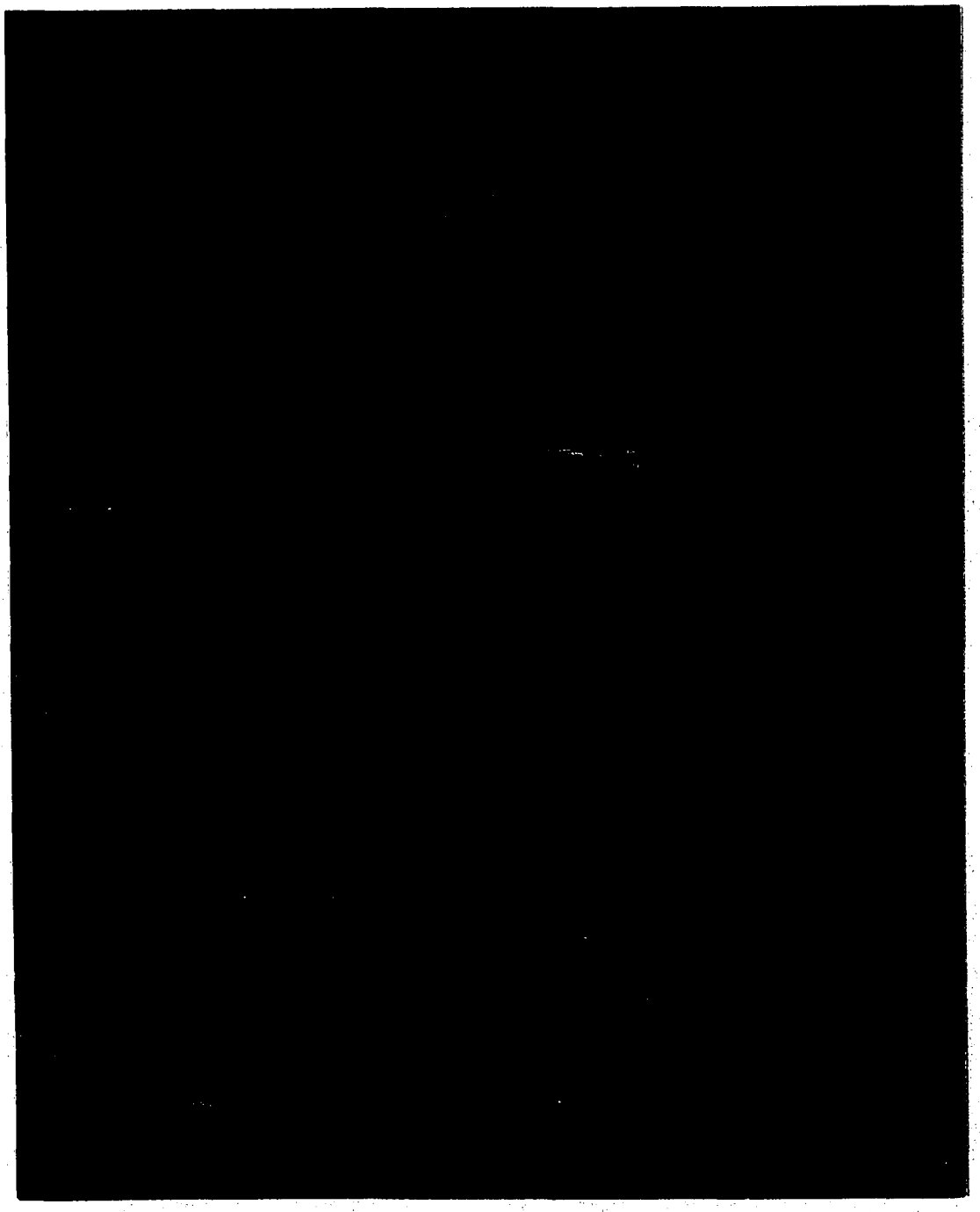

Figure 53. 12,600X - Peroxide and Nital Etch a magnified view of the Sb_2Sn_3 compound shown in Figure 52.

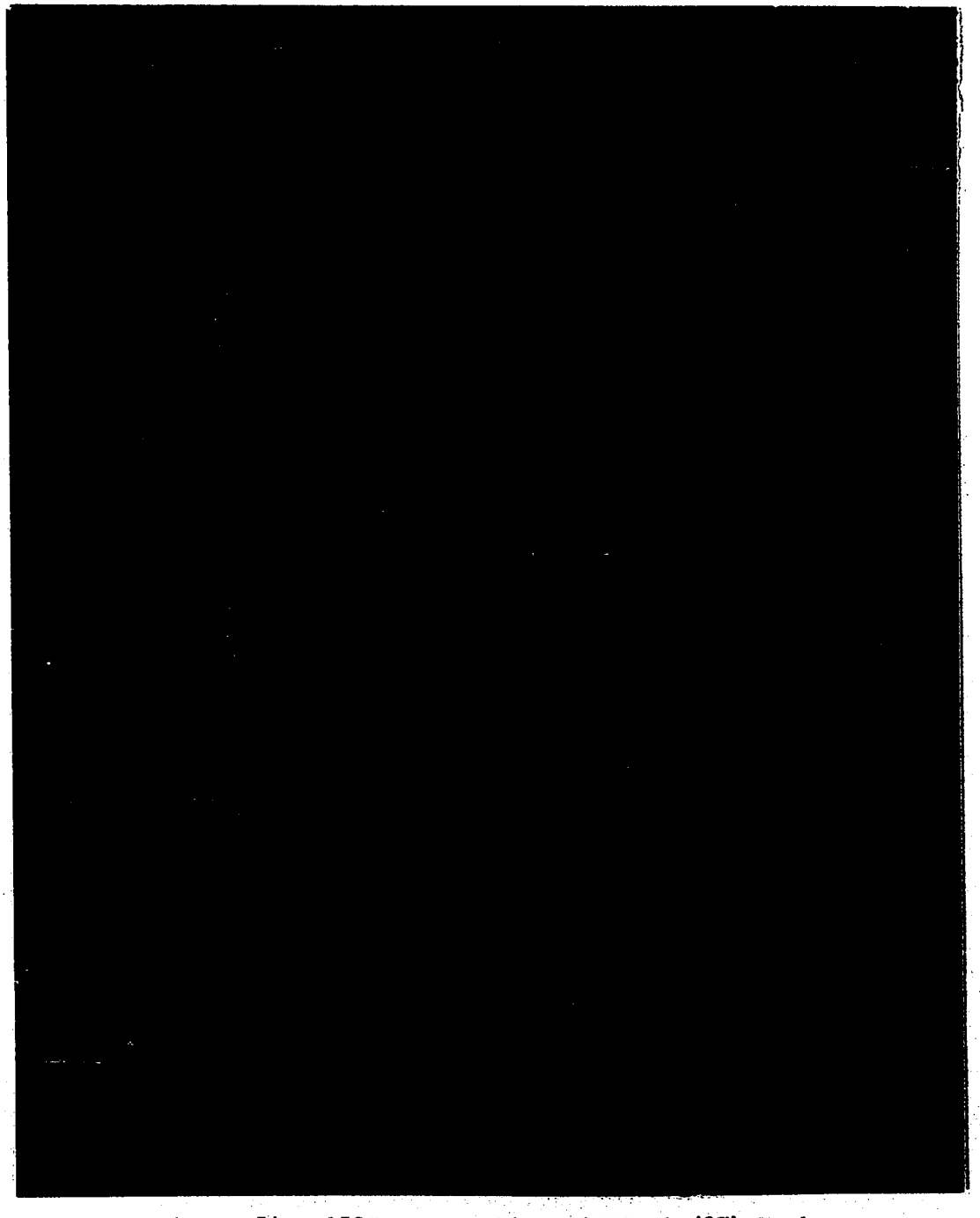

Figure 54. 150X - Peroxide and Nital (2%) Etch Antimonial solder applied to a pure zinc substrate. The sample was aged for nine months at room temperature.

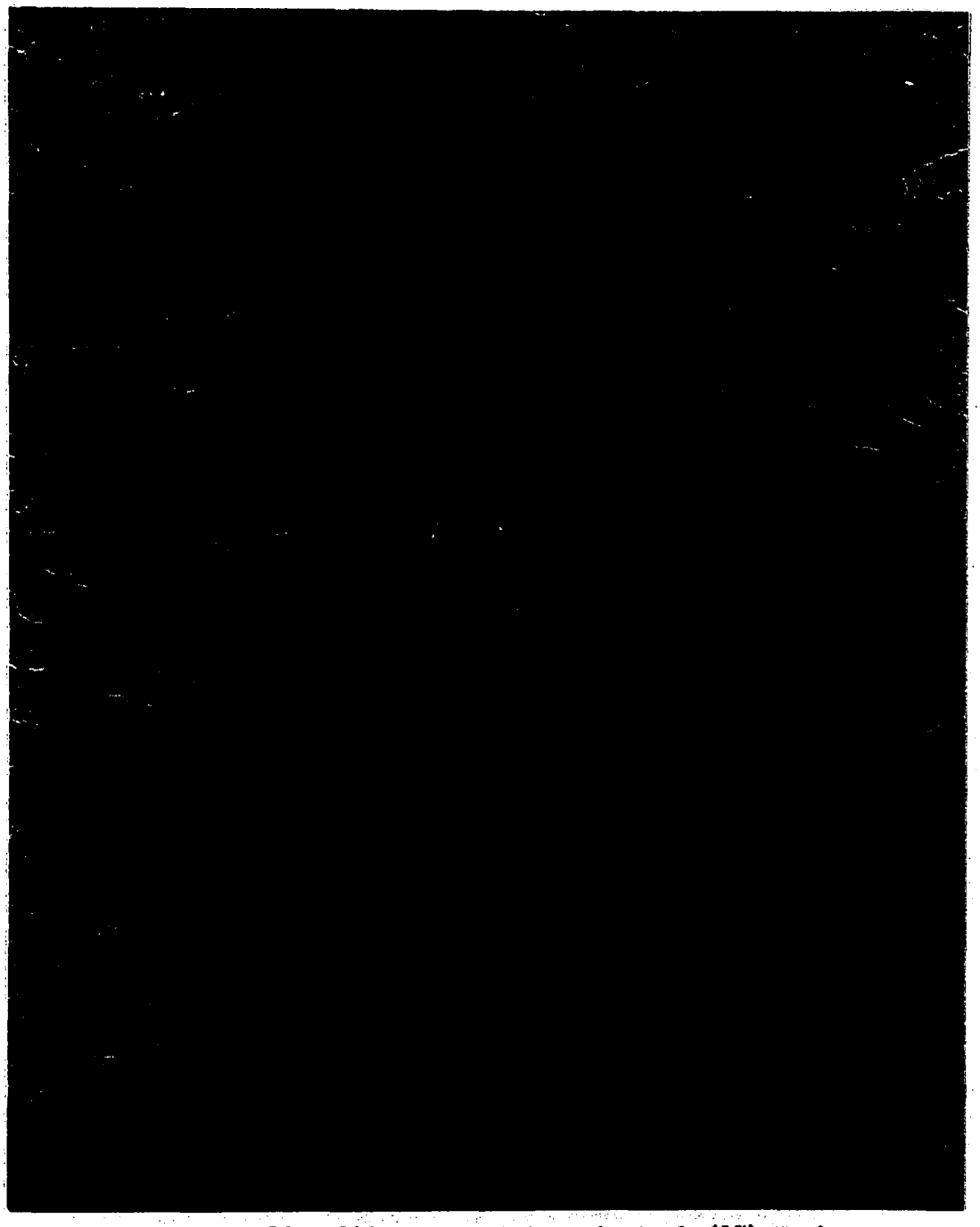

Figure 55. 840X - Peroxide and Nital (2%) Etch Antimonial solder applied to a pure zinc substrate. The compounds shown in the solder mass, remote from the interface, correspond to Sb_3Zn_4. These compounds were formed with freshly prepared joints.

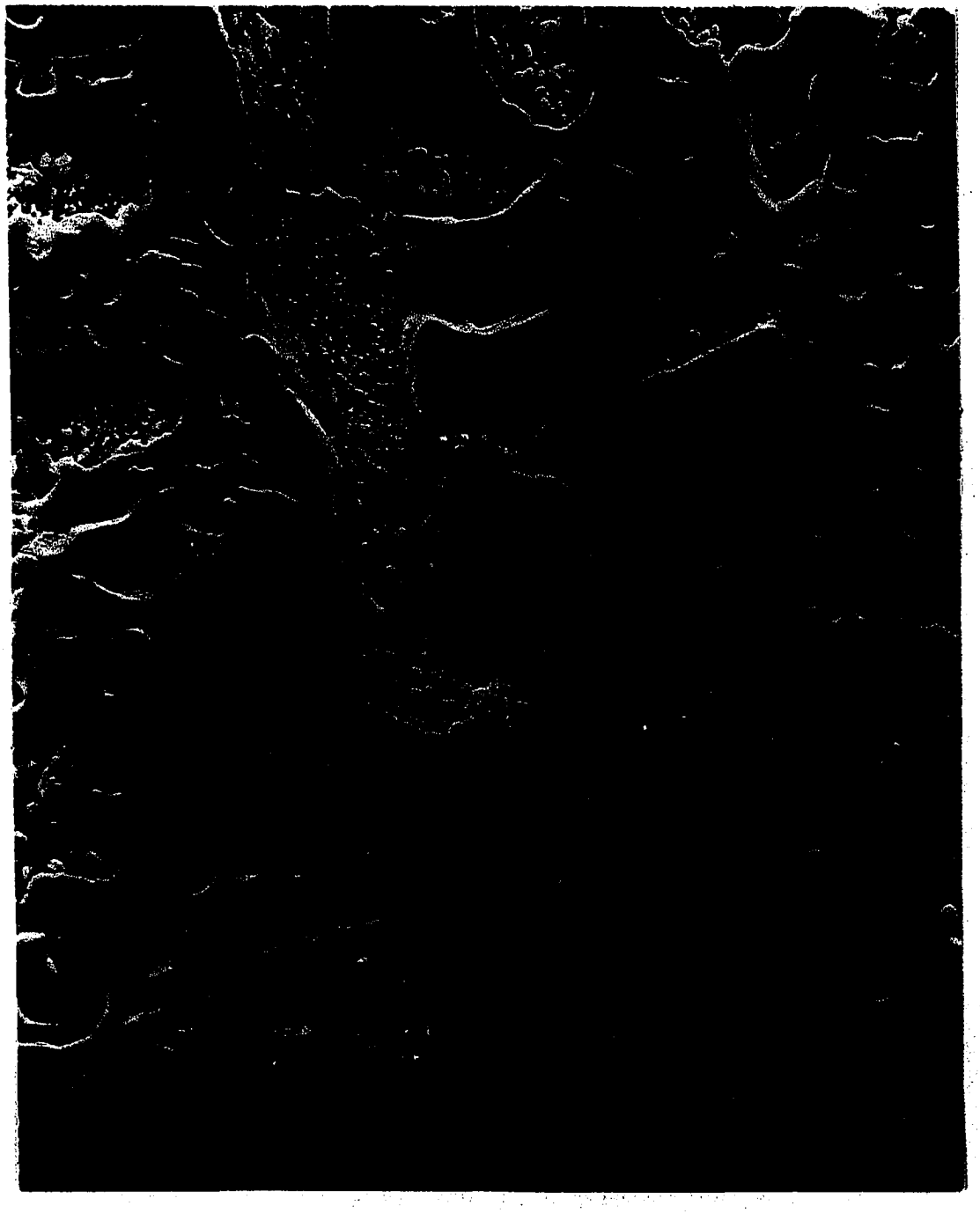

Figure 56. 560X - Peroxide and Nital (2%) Etch
An enlargement of the area shown in Figure 55. The compounds shown correspond to Sb_3Zn_4.

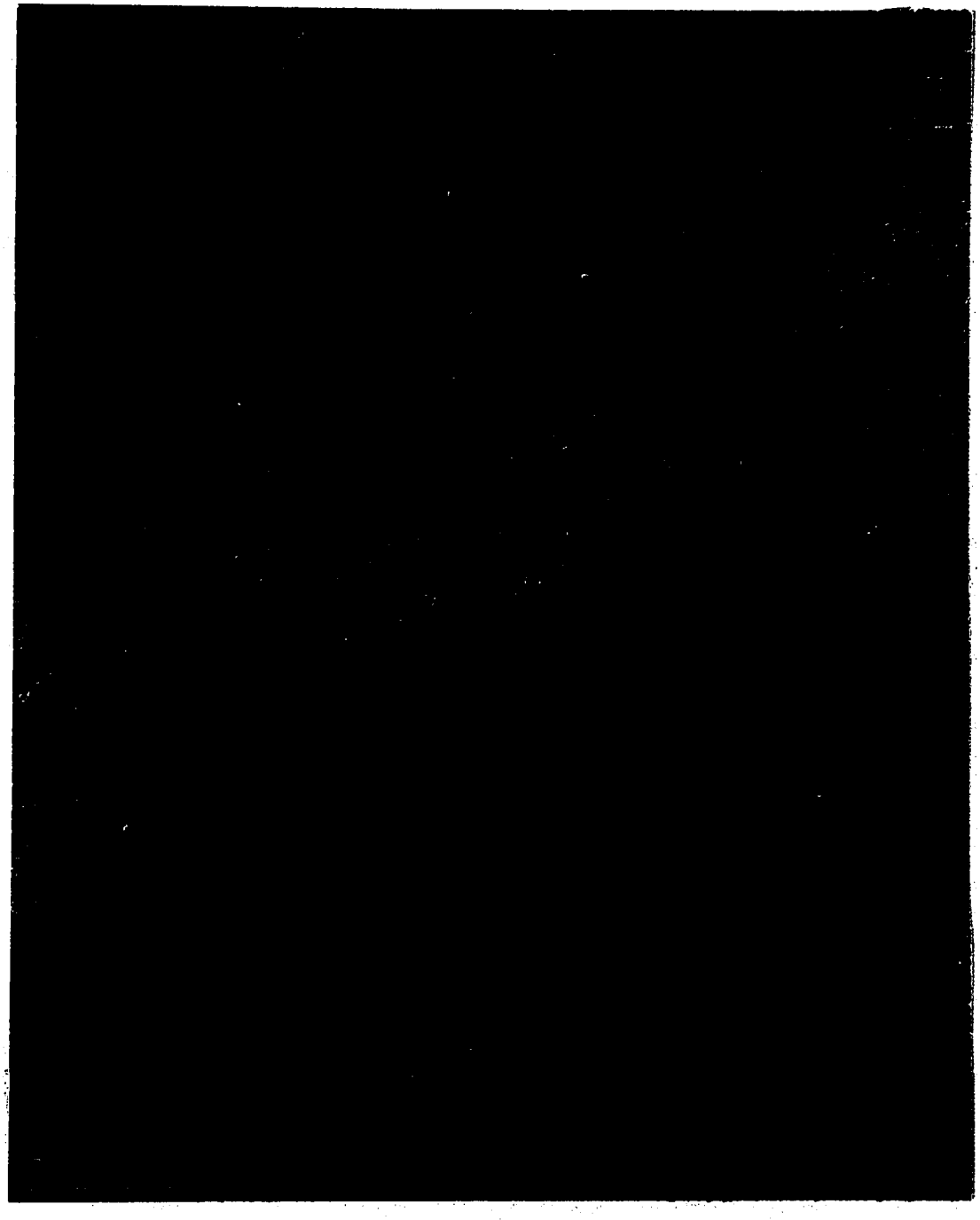

Figure 57. 560X - Peroxide and Nital (2%) Etch
The antimonial solder mass shown in Figure 54, remote from the interface. The intermetallic compounds shown correspond to SbZn. The sample was aged for nine months at room temperature.

The sample shown in Figure 54 was aged at room temperature for about nine months. The aging treatment resulted in the formation of SbZn compounds as shown in Figure 57. These compounds were not noted within a few weeks of applying the antimonial solder to the zinc substrate.

CHAPTER II

SOLDERING TO GOLD PLATED SUBSTRATES

Introduction

Gold plated terminals and connectors are employed in the electronics and communication industries because of their stable, low resistance and noncorroding properties. Copper based alloys are frequently used for the base material, with a nickel layer applied as a diffusion barrier against substrate erosion by the liquid and fillet contamination after extended periods subsequent to soldering. The gold coatings are usually applied as a soft gold strike followed by a cobalt hardened plating to resist abrasive wear during handling and use. This is particularly important for connector pins which are subject to connect-disconnect cycles and to which lead wires must be soldered.

Soldering to gold plated surfaces with soft solders can produce unexpected results. Although the gold is very easily wetted by tin-lead based solders the performance of the joints is often disappointing. Solder connections showing mechanical weakness and unreliable electrical performance are commonly experienced. The connections obtained with gold plated substrates have been reported to produce joints which appear "cold" even though adequate soldering temperatures have been achieved.

A cold joint typically has an appearance similar to that of Figure 58. The electron micrograph shows the solder fillet adjacent to the terminal pin in a multilayered circuit board. The reliability and brittle character of such joints have been described by several authors (14, 15, 16).

It is now well accepted in the literature that the source of the problem is the ease with which intermetallic compounds of gold and tin form in molten and solid solders. However, the processes which lead to compound formation and degradation of the joint are not universally acknowledged.

The dissolution rates of pure metals commonly used as solderable substrate coatings have been investigated by Bader (17). The results of these studies demonstrate that gold dissolves quicker than silver, palladium, copper, nickel, and platinum in 60/40 solder at all temperatures. At typical soldering temperatures, in the neighborhood of 200°C, the radial dissolution rate was found to be about 1 micron per second. Other investigators have reported dissolution rates as high as 10 microns per second (18). The residence times at soldering temperatures commonly used in mass production operations would be predicted to dissolve gold platings thinner than 3 microns.

Nonmetallic impurities in hard gold platings have been observed by Munier (19). These were found to be carbonaceous in character and were believed to be produced by the plating process. The principal material most probably is a polymer codeposited from the cyanide plating bath. Investigations of the plating parameters which affect the amount of codeposited polymer have been made by Holt and Stanyer (20), and the mechanisms which produce the polymer have been studied by Cohen, West, and Antler (21).

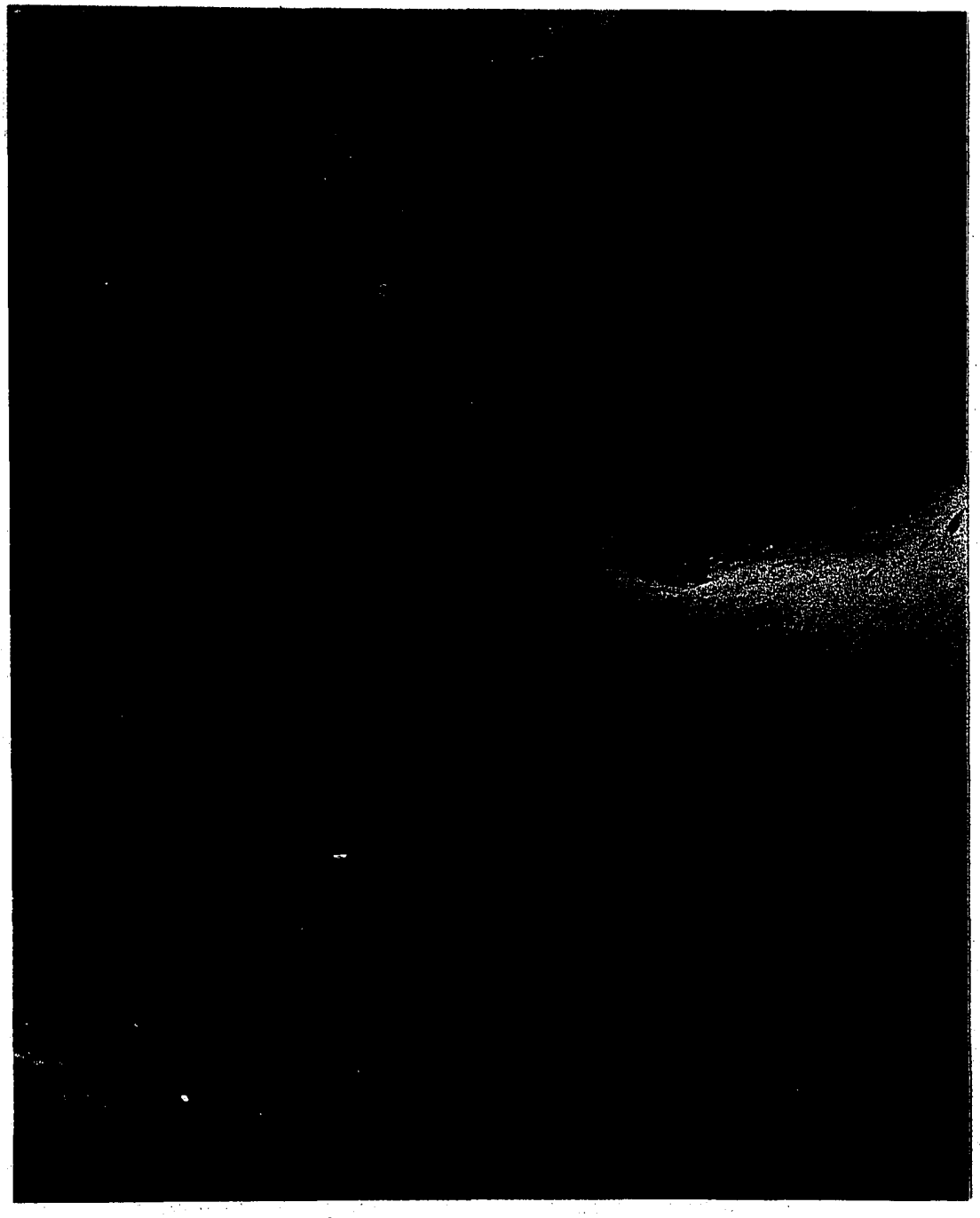

Figure 58. 85X
A 60/40 solder mass applied to a 2.5 micron thick gold plated terminal pin. The appearance of this joint is typical of a "cold" solder joint as evidenced by the cracking.

Experimental

The studies reported here involve the investigation of structures produced when 60/40 solder was applied to gold plated terminal pins. The solder was obtained as a preformed ring which was sized to fit the 0.025 inch square (cross section) pins. The terminals were fabricated from 92% copper - 8% nickel alloy prepared with the nickel, soft and hard gold finish described above. Three different thicknesses of gold plating, 0.5, 2.5, and 25 microns, were studied. Plating was carried out in a Selrex CI (cobalt hardened) solution. Soldering was accomplished in an industrial condensation apparatus which maintained a constant temperature of 215°C and fixed soldering time of eighty seconds.

In order to conveniently handle the small samples, the soldered terminal pins were mounted in lucite or Koldmount according to standard metallographic practice. The heating cycles associated with each of the mounting procedures were estimated to be equivalent to 1 or 2 months aging at room temperature. Samples which were examined in cross section were wet polished and etched in equal parts of 3% H_2O_2 and NH_4OH (conc.). Subsequent treatment of 2% nital was found to enhance the relief between intermetallic compounds and the β phase in the matrix.

Results and Discussion

Figure 59 is an optical micrograph showing an overall view of a typical solder joint applied to a terminal having a 0.5 micron gold plating. The solder shows good wetting of the terminal pin (at the top of the solder fillet) and the expected near-eutectic microstructure in

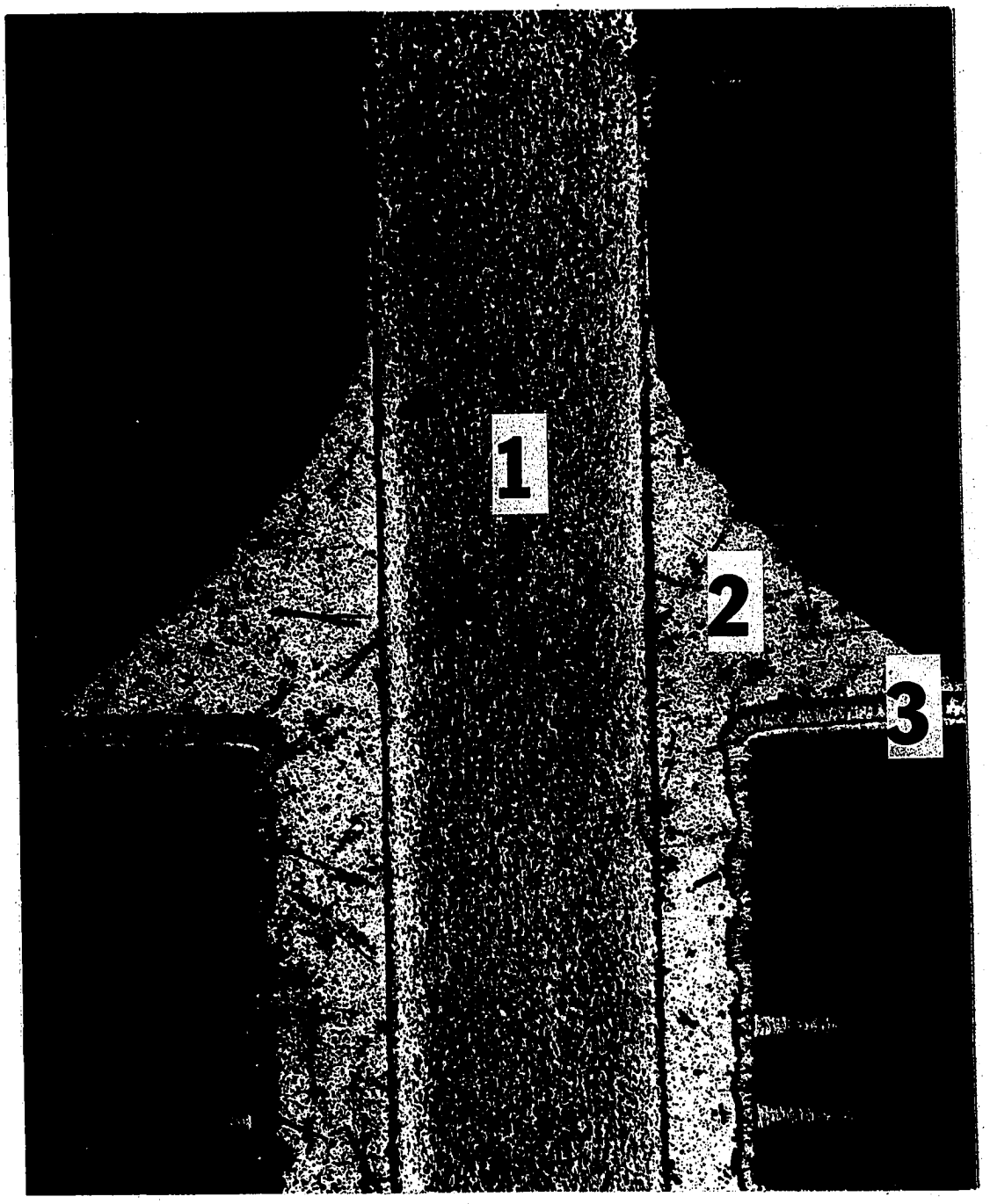

Figure 59. 50X - Peroxide Etch
A 60/40 solder mass applied to a .5 micron thick gold plated terminal pin to connect the terminal to the printed circuit board. (1) terminal pin, (2) solder fillet, (3) copper land.

the solder mass. This is the same joint described earlier with reference to Figure 8. The locations of the terminal pin, solder fillet and land area of the printed circuit board are indicated by numbers on the photograph.

Figure 60 is an optical micrograph showing a 60/40 solder fillet formed on a terminal pin having a 25 micron hard gold plating. The solder mass is generally porous and shows extensive intermetallic compound formation. Figures 61 and 62 show closer views of the right side of the fillet. Solder joints applied to thick, hard gold coatings usually show fillets of this same character.

Detailed examination of the adhesion obtained at the top of the solder fillet in Figures 60 and 63 demonstrates the phenomenon of dewetting. The solder is seen to be detached from the gold plating on the terminal pin. Harding and Pressly (22) have observed the solder to initially wet gold surfaces and then draw back leaving a rough appearing fillet. Etching the sample shown in Figure 63 resulted in the structure revealed in Figure 64. Here a massive accumulation of $AuSn_4$ intermetallic compounds may be noted in the dewetted region. Figures 65 and 66 are optical micrographs showing another example of large scale dewetting associated with massive $AuSn_4$ intermetallic compound formation. Figures 67, 68, and 69 are SEM micrographs of 60/40 solder applied to a thick, hard gold coated terminal. The gap between the substrate and $AuSn_4$ intermetallic compound layer is immediately obvious.

Commercial producers of soldered products involving gold plated substrates have, for some time, recognized that joint reliability was somehow associated with the thickness of the gold coatings. Plated

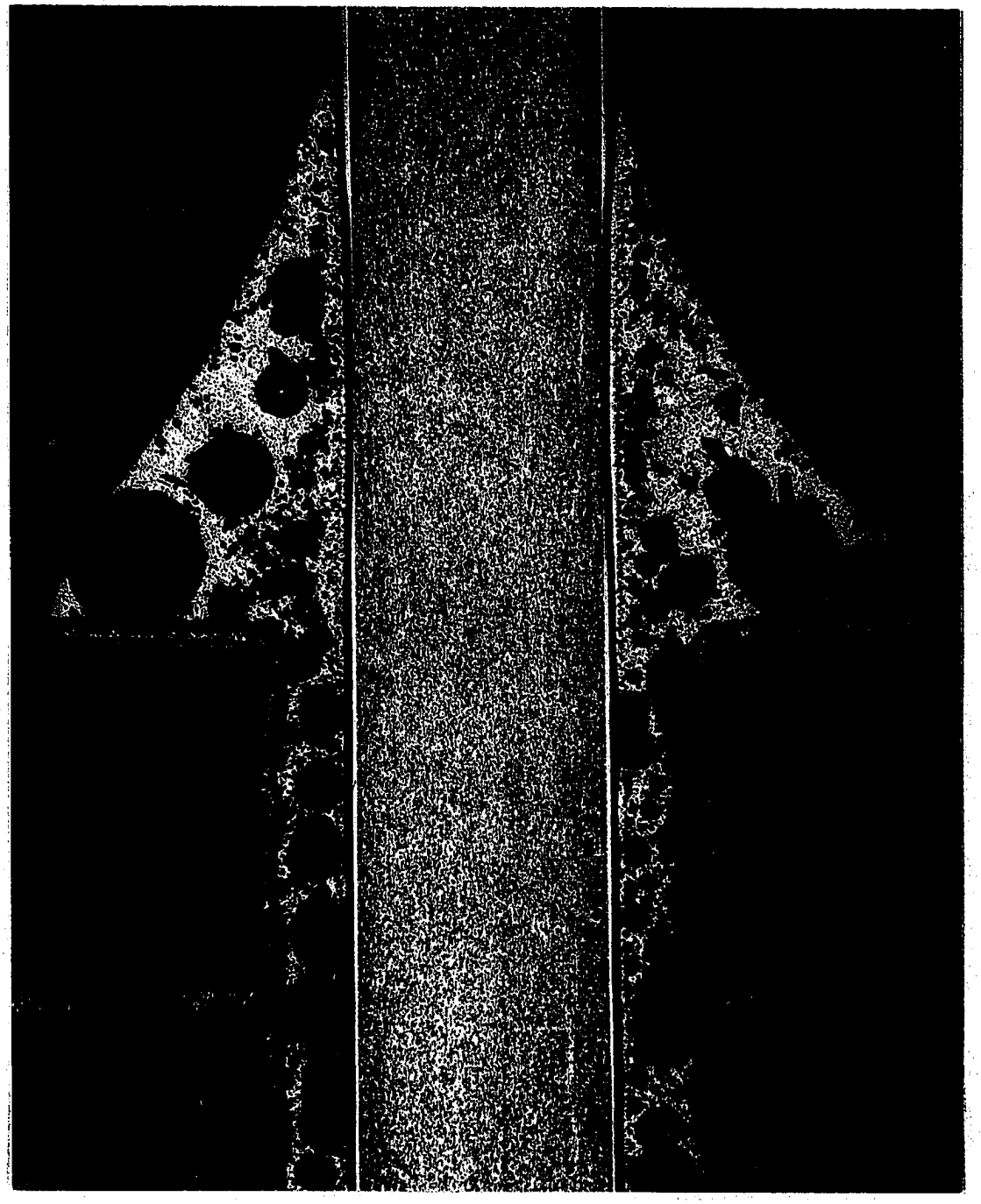

Figure 60. 50X - Peroxide Etch
A 60/40 solder mass applied to a 25 micron thick gold plated terminal pin in a printed circuit board. Extensive intermetallic compounds and excessive porosity are evident. Dewetting near the top of the fillet is also evident.

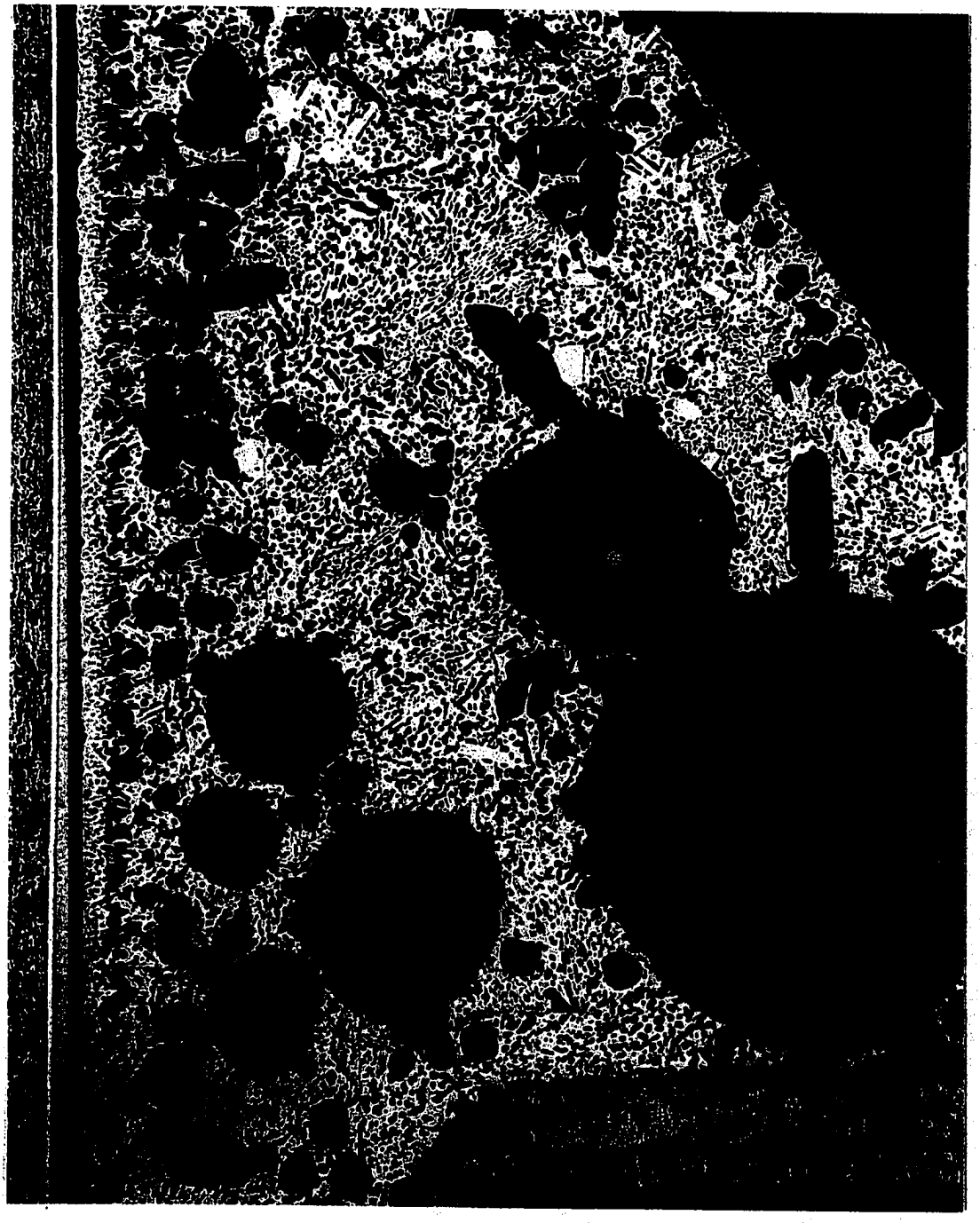

Figure 61. 200X - Peroxide Etch
An area of the solder fillet shown in Figure 60. The sample was aged for 7 days at 100°C.

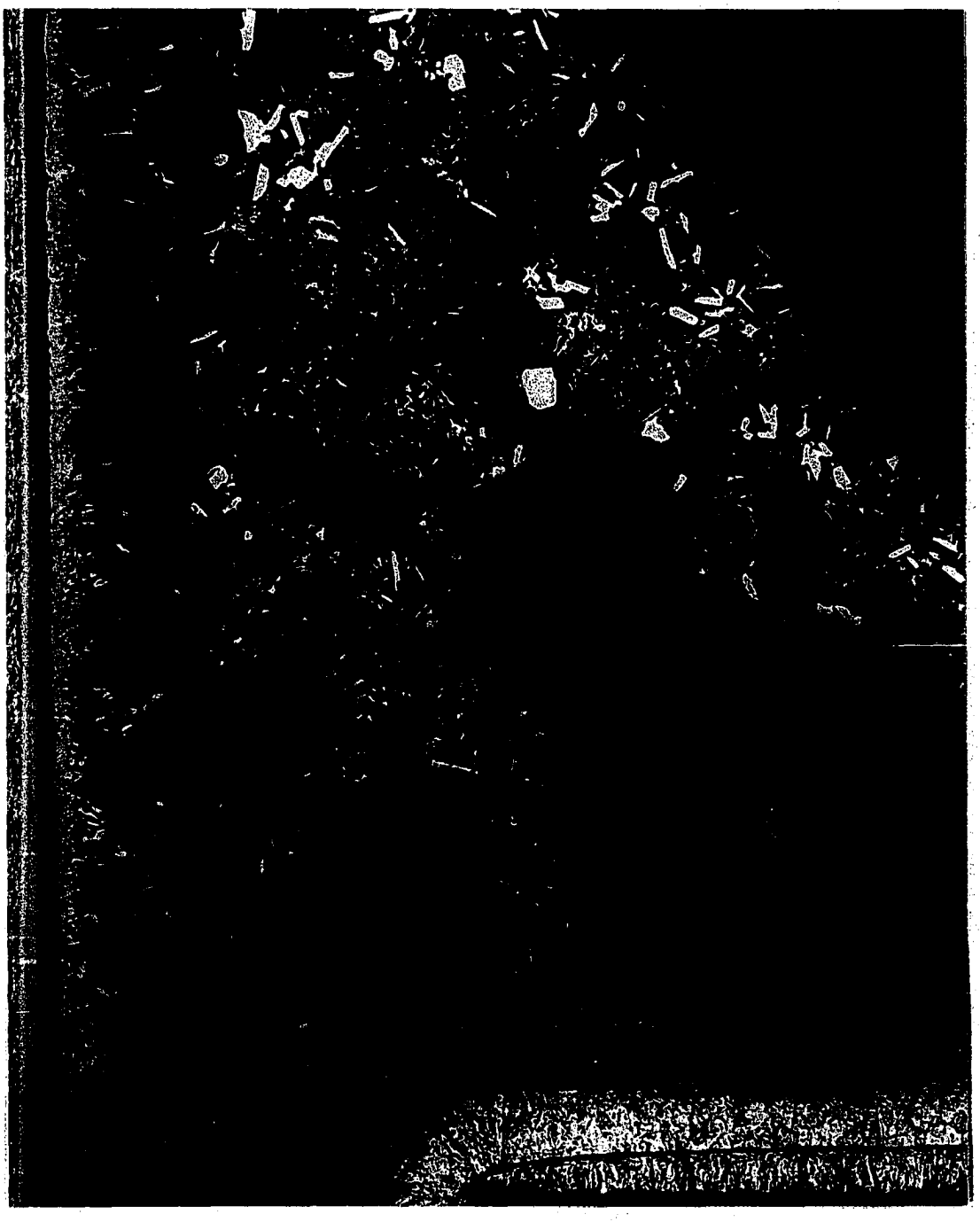

Figure 62. 200X - Peroxide and Nital (2%) Etch
Massive and excessive intermetallic compounds of $AuSn_4$ are observed in the 60/40 solder fillet.

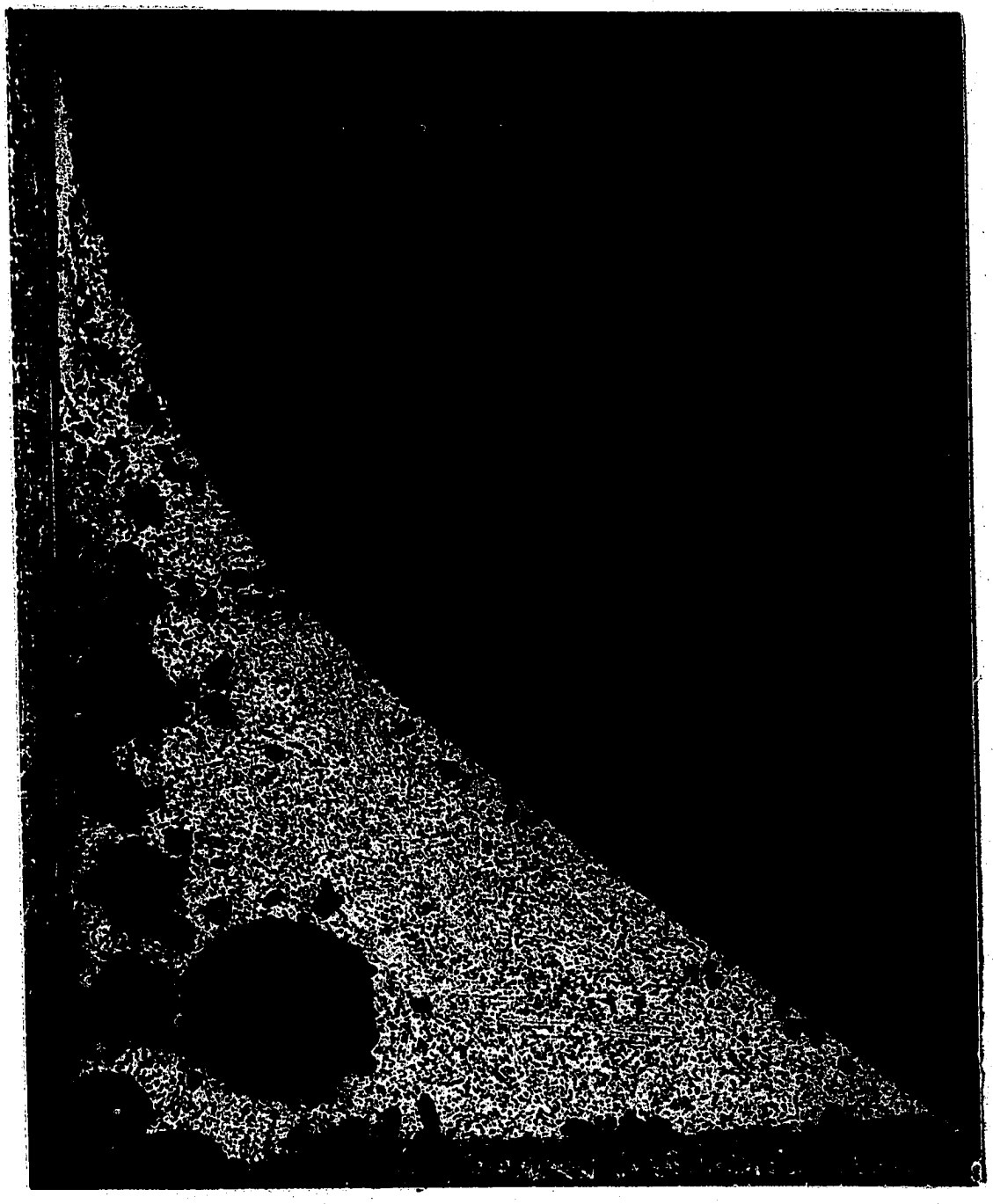

Figure 63. 200X - Peroxide Etch
60/40 solder applied to a 2.5 micron thick gold plated terminal pin for connection to a copper land of a printed wiring board. Porosity is evident in the solder fillet and dewetting appears near the top of the fillet.

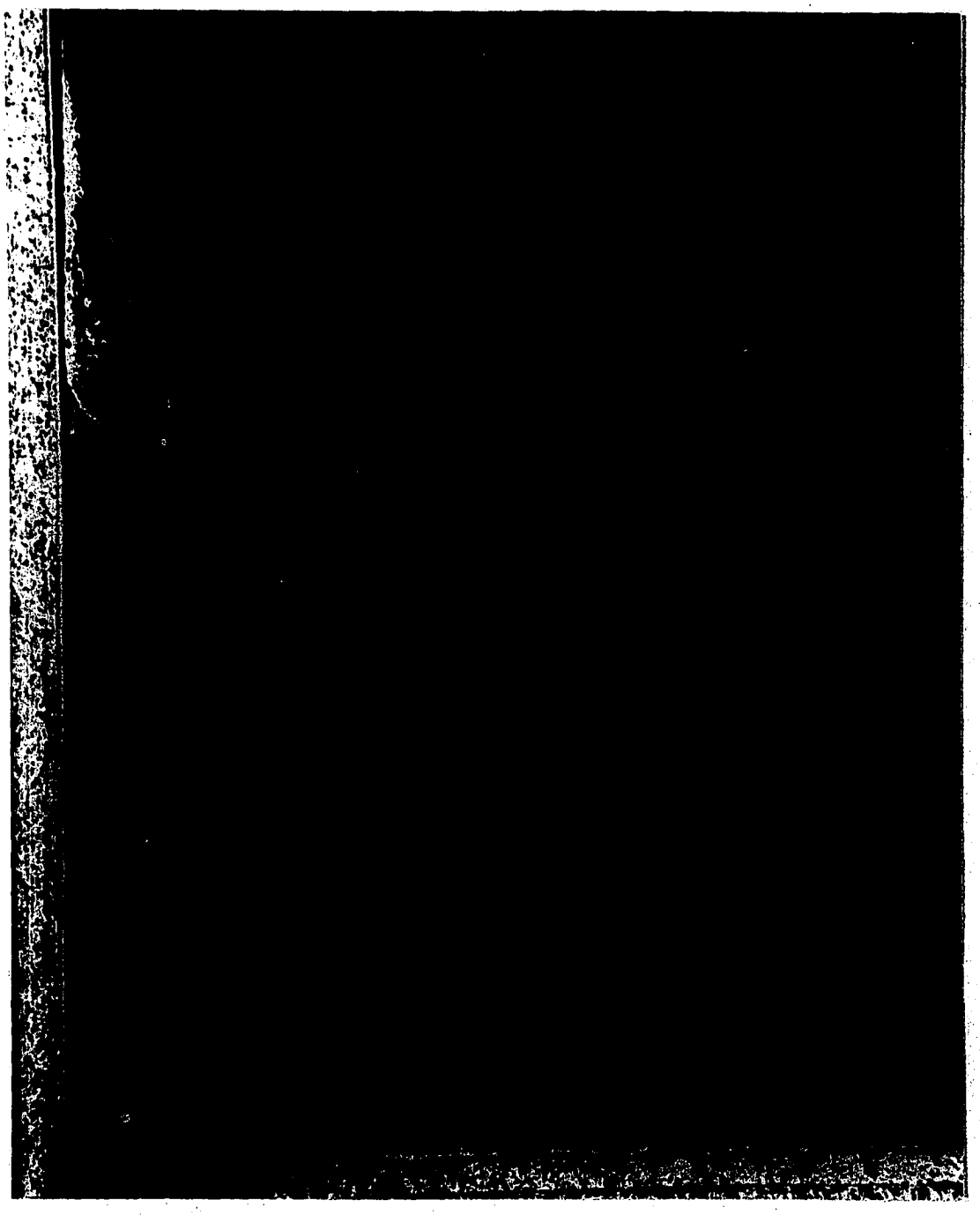

Figure 64. 200X - Peroxide and Nital (2%) Etch
The same area shown in Figure 63 after nital etching. The presence of $AuSn_4$ intermetallic compounds is evident.

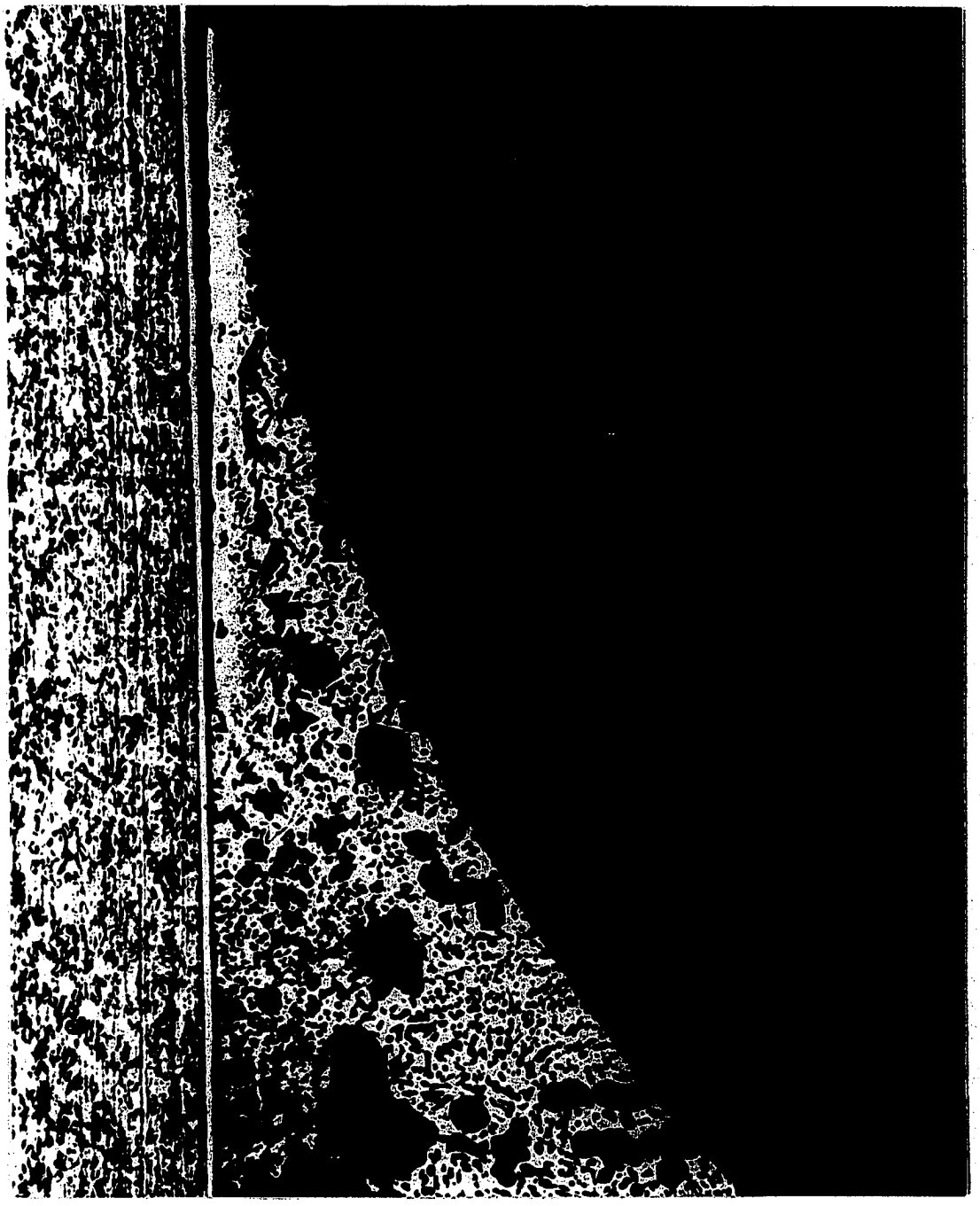

Figure 65. 200X - Peroxide Etch
The same solder fillet shown in Figures 63 and 64 before the nital etch. The area shown reveals dewetting near the top of the fillet.

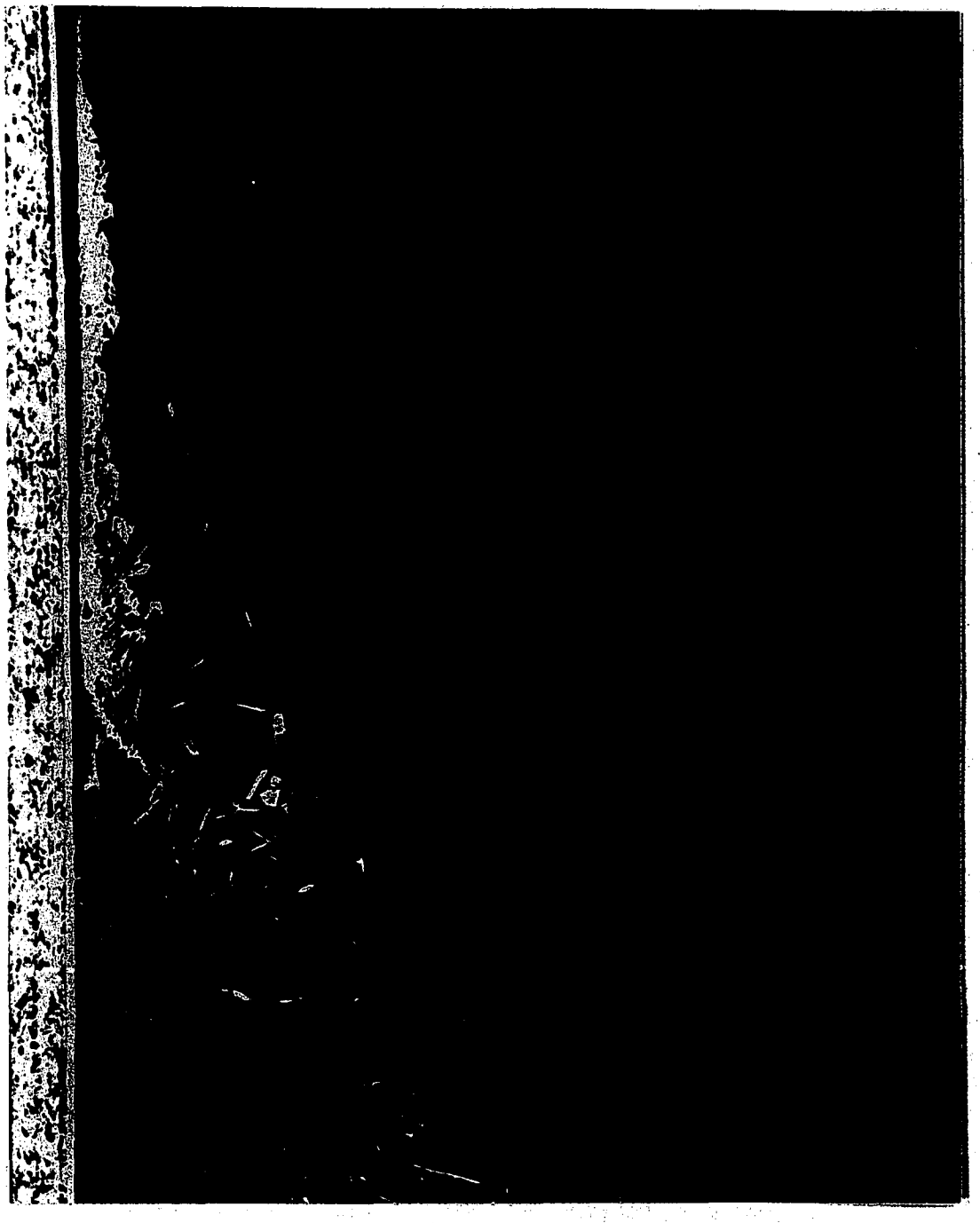

Figure 66. 200X - Peroxide and Nital (2%) Etch
The same area shown in Figure 65 after nital etching. Dense and massive intermetallic compounds are shown in the dewetted area.

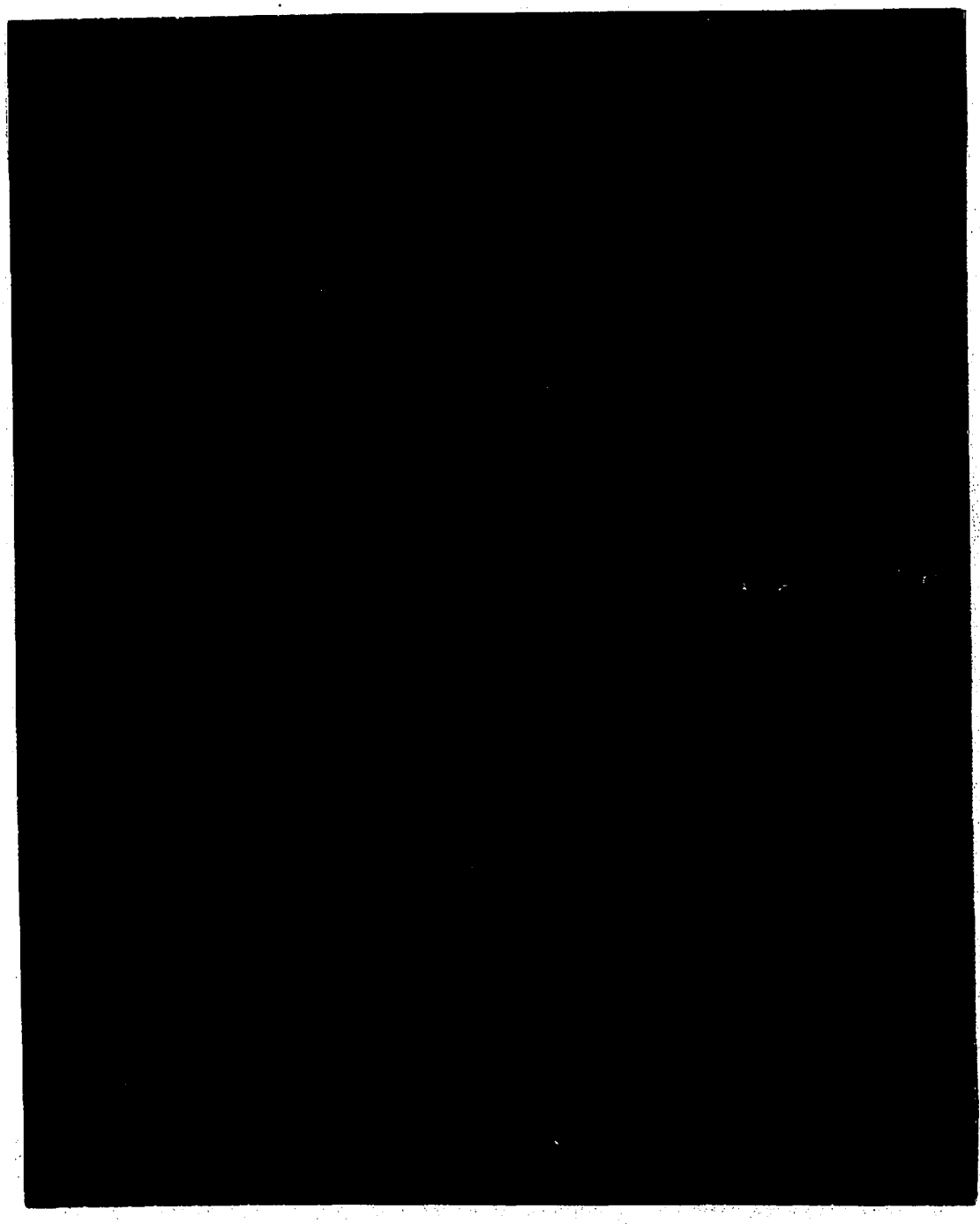

Figure 67. 70X - Peroxide and Nital (2%) Etch
An SEM micrograph of the solder fillet shown in Figures 63, 64, 65 and 66. The porosity and intermetallic compounds are evident.

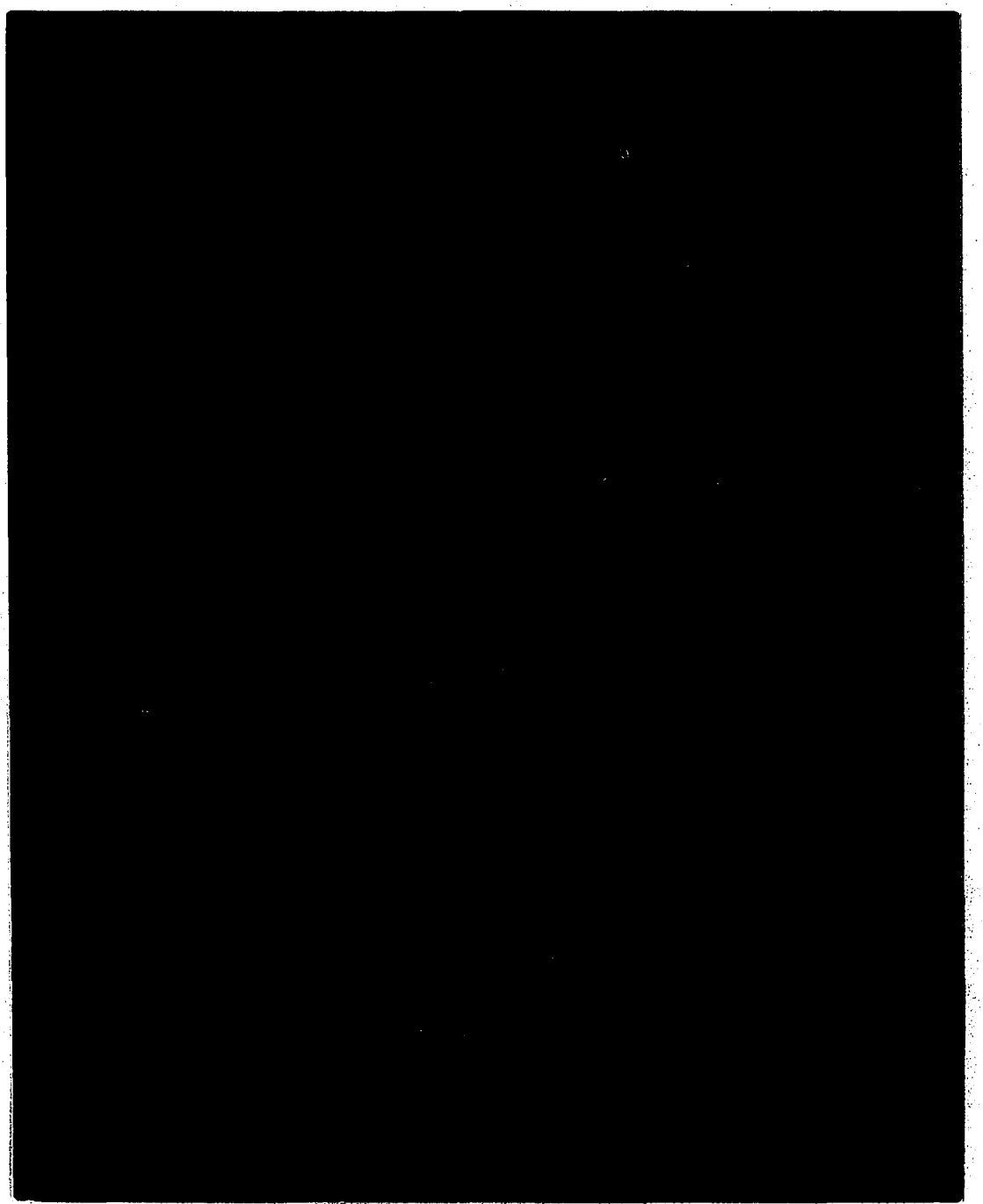

Figure 68. 140X - Peroxide and Nital (2%) Etch
An SEM micrograph of the dewetted area shown in the optical micrographs of Figures 65 and 66.

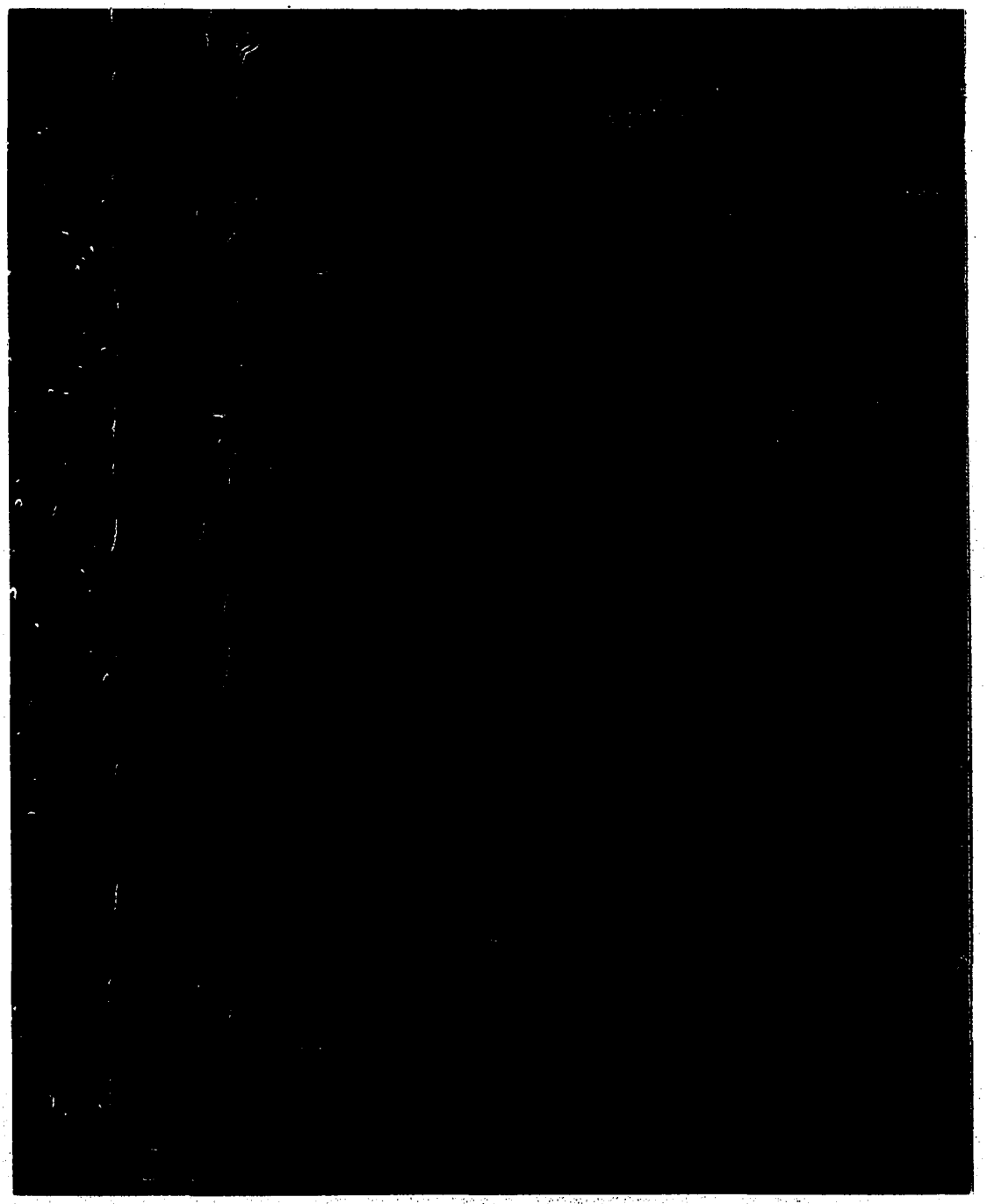

Figure 69. 1400X - Peroxide and Nital (2%) Etch An SEM micrograph of the area shown in Figure 68. Dewetting is clearly evident and excessive and dense intermetallic $AuSn_4$ compounds are observed.

layers thinner than 1 or 2 microns generally produced trouble free joints. As the plating thickness was increased the gold did not fully dissolve in the solder and embrittlement resulted. The continuing trend toward microelectronics will undoubtedly reduce the acceptable thickness of gold coatings. As the solder fillets become smaller they will more easily saturate with gold and open circuits caused by complete detachment of dewetted particles of solder are predictable.

Figure 70 is an SEM micrograph showing dewetting of the top of a solder fillet. A feathery formation of $AuSn_4$ intermetallic compound is seen growing out of the plating on the left side of the micrograph. A thin, compact layer of gold-tin intermetallic is also visible in the solder mass and at the detached boundary. This layer is demonstrated by the corresponding X-ray map of gold shown in Figure 71. The map also shows that the gold plating had not completely dissolved from the pin in the dewetted area.

Figure 72 shows an area in the thick region of a solder fillet applied to a 25 micron gold plated terminal, as seen in Figures 60, 61, and 62. A layer of gold-tin intermetallic compound had formed and became detached from the gold plated substrate. X-ray microanalysis indicated that the composition of the layer corresponded to $AuSn_2$. This is the same composition noted in the detached region of solder shown in Figure 70.

The addition of small amounts of antimony to the 60/40 composition appears to suppress the formation of $AuSn_2$. Figure 73 shows the interface region within a 51% Sn - 46% Pb - 3% Sb solder fillet applied to a terminal having a 25 micron plating. The intermetallic compound

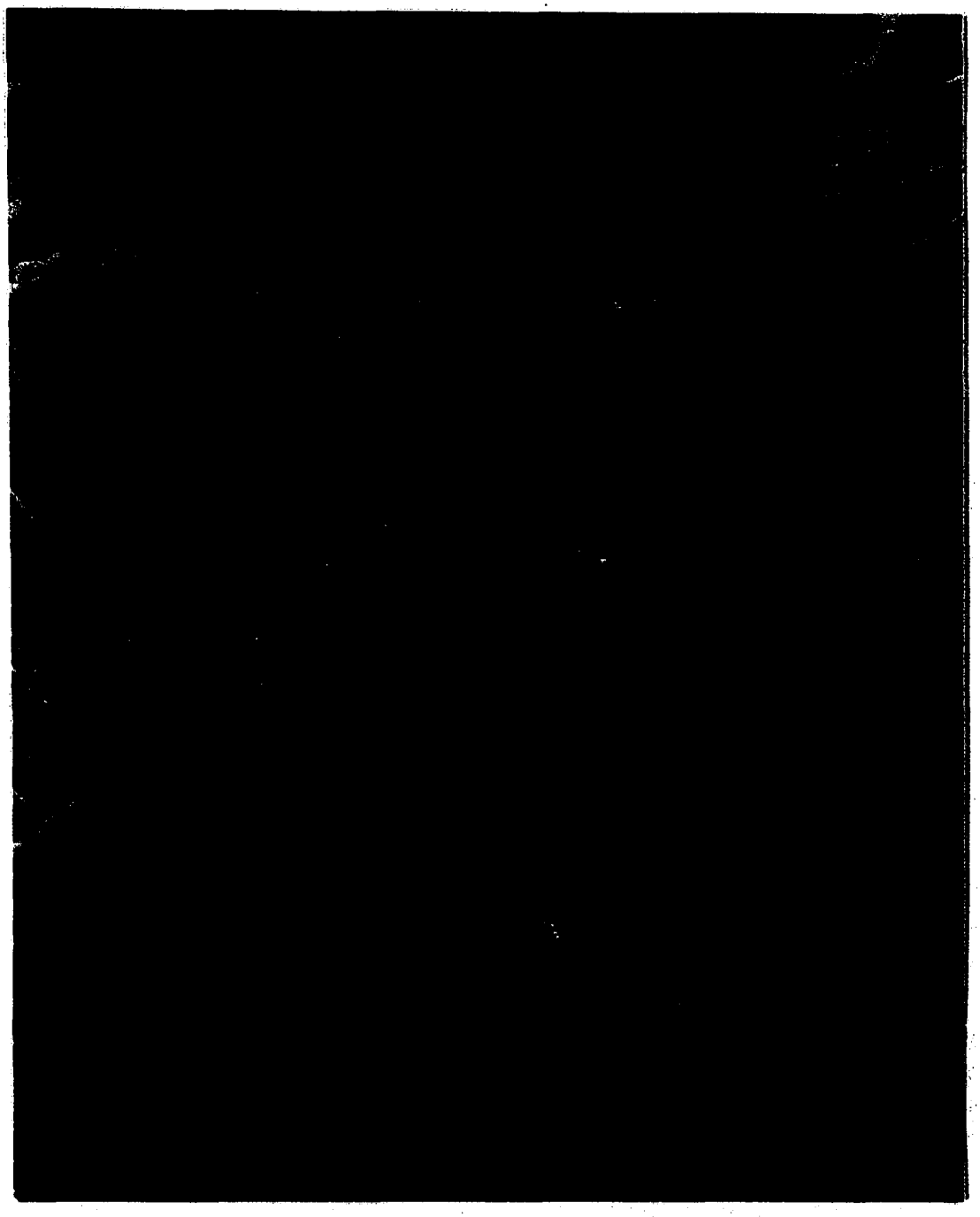

Figure 70. 980X - Peroxide and Nital (2%) Etch
An SEM micrograph showing dewetting at the top of a solder fillet. The $AuSn_4$ intermetallic compounds are seen growing out of the gold plating. This is an area near the top of a fillet.

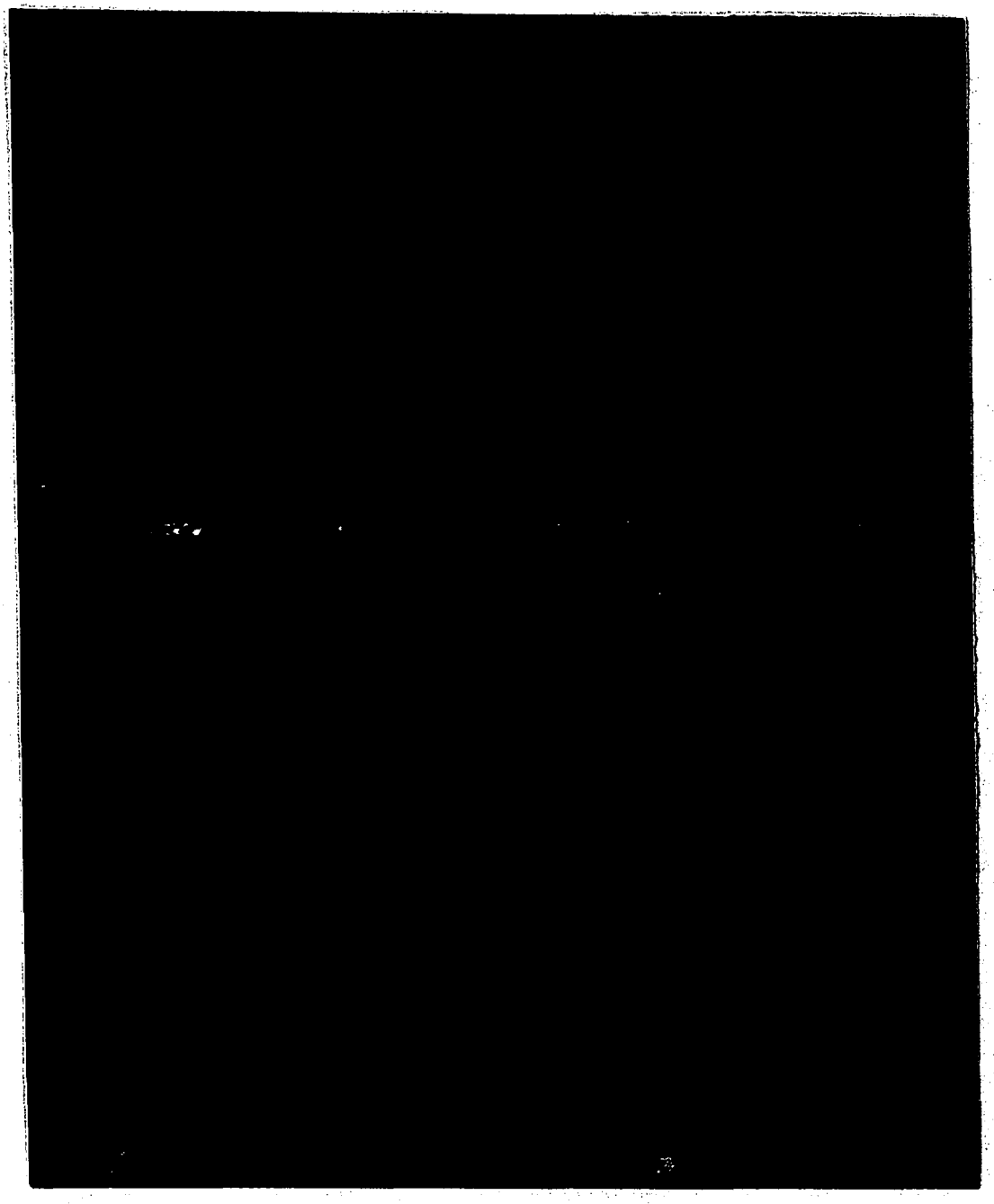

Figure 71. 980X - EDS-X-Ray Mapping of Au
An x-ray mapping of gold indicating the location of Au by white dots. This mapping corresponds to the micrograph shown in Figure 70. The gold plating on the terminal was completely dissolved into the solder mass in the areas that did not exhibit dewetting.

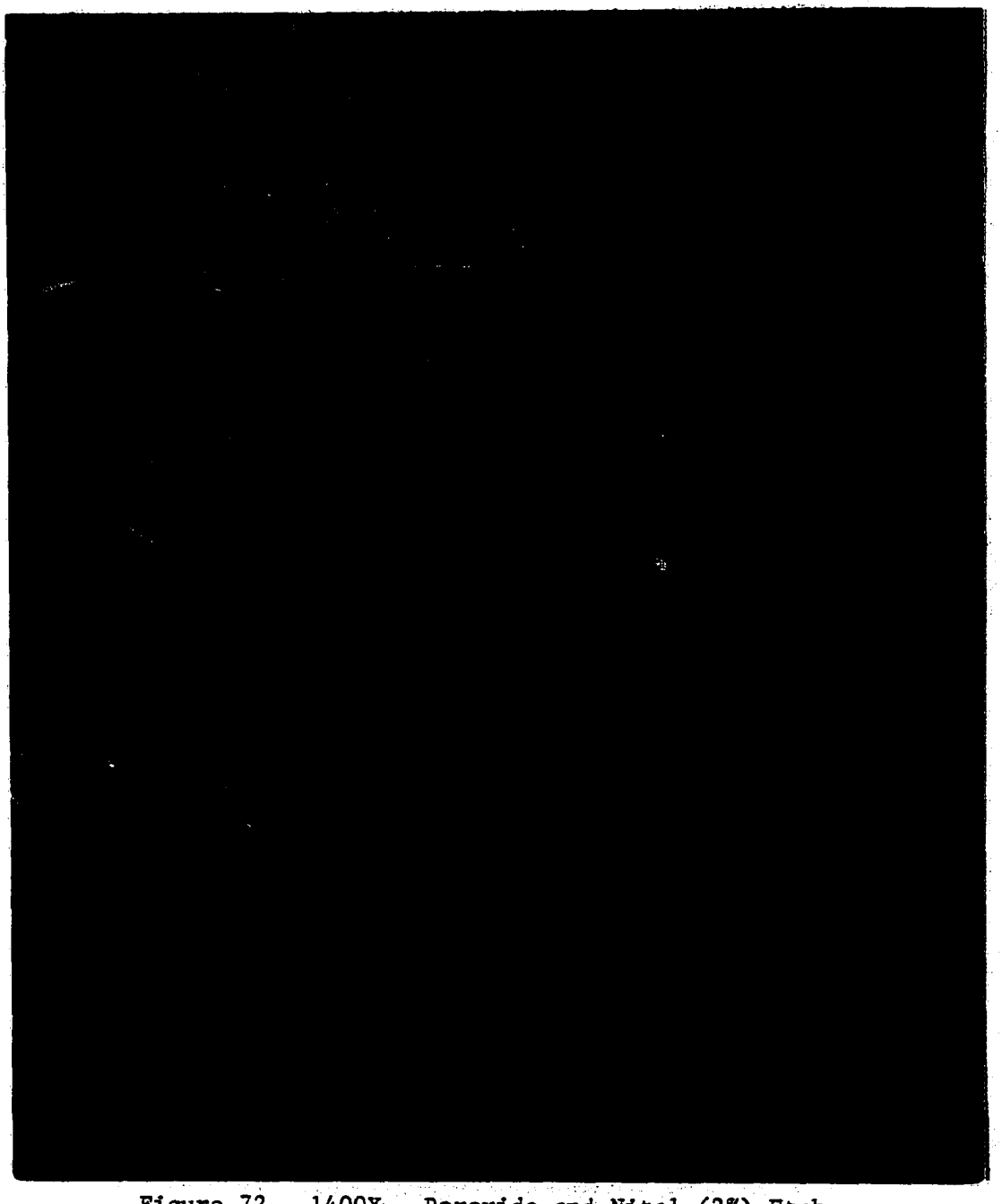

Figure 72. 1400X - Peroxide and Nital (2%) Etch An SEM micrograph of the detached interface shown in Figures 60, 61 and 62. The composition of this intermetallic compound layer near the surface corresponded to $AuSn_2$. The gold thickness remaining after soldering with 60/40 for 80 seconds was 17 microns.

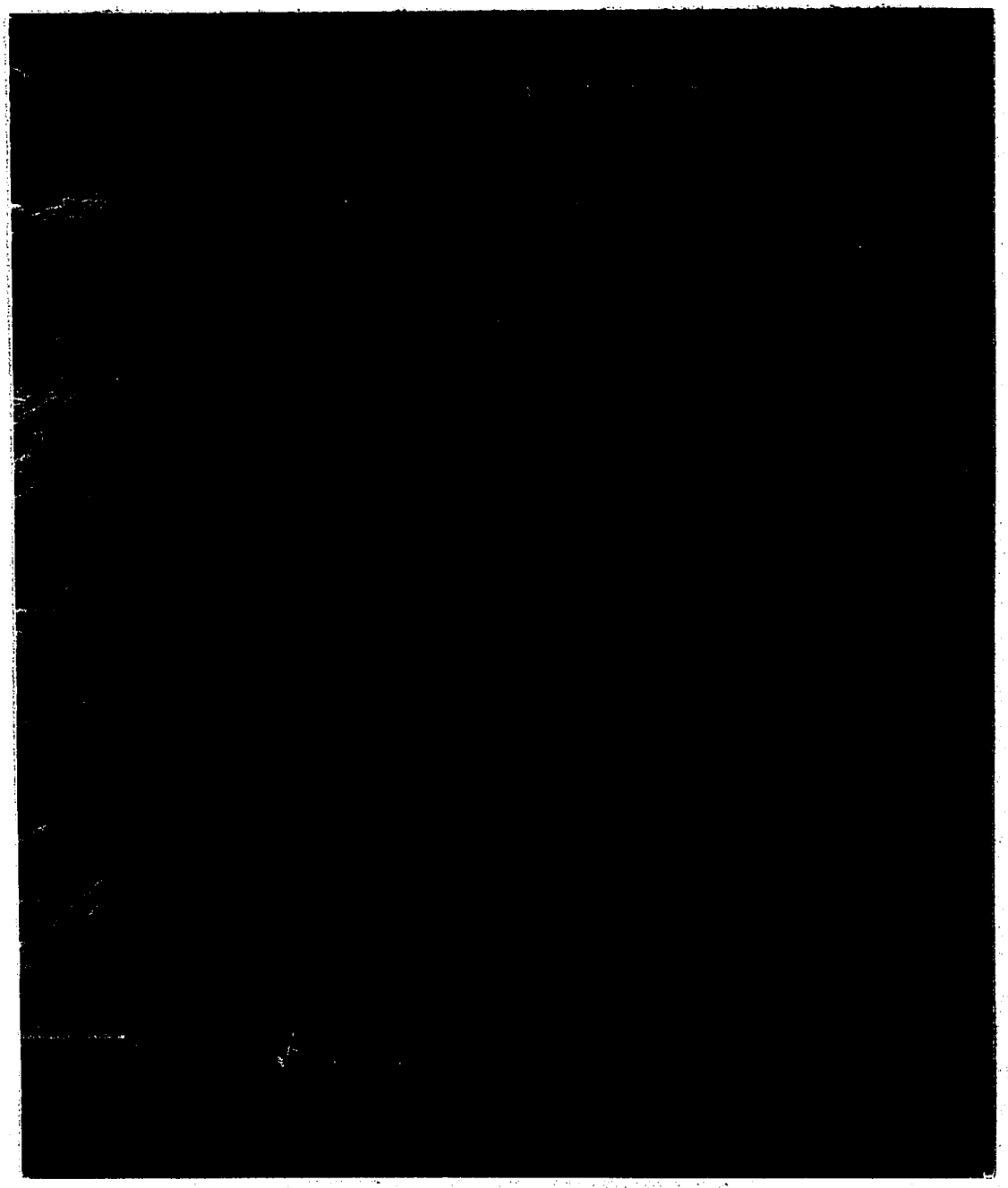

Figure 73. 1400X - Peroxide and Nital (2%) Etch
An SEM micrograph of an antimonial solder applied to a 25 micron gold plating. The gold plating remaining after an 80 second soldering time was 20.5 microns. It is evident that dewetting similar to that shown in Figure 72 did not occur.

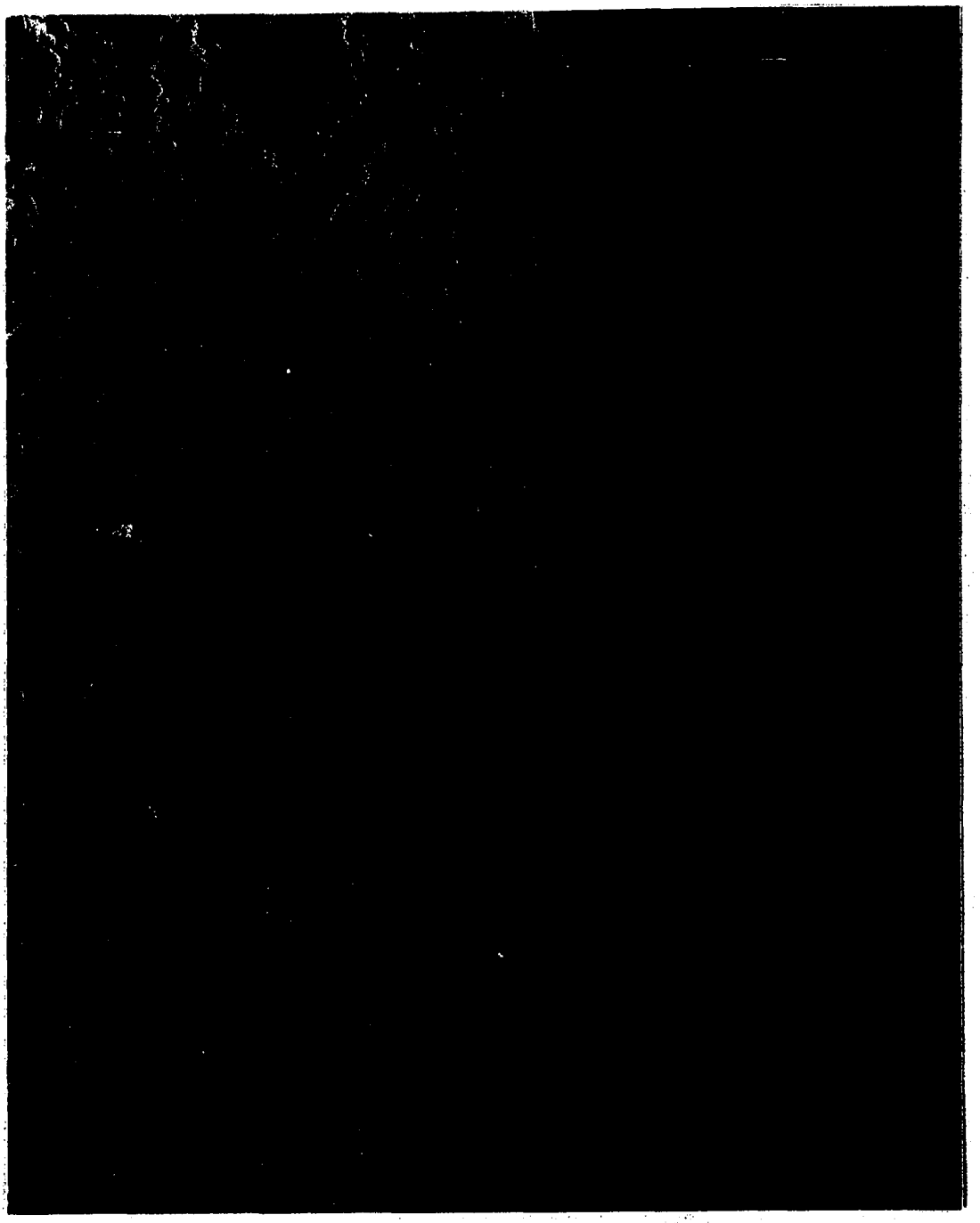

Figure 74. 420X - Peroxide and Nital (2%) Etch 60/40 solder applied to a 2.5 micron gold plated terminal pin. The gold was plated from a plating solution using cobalt as a hardening element. The porosity is evident along the solder-plating interface.

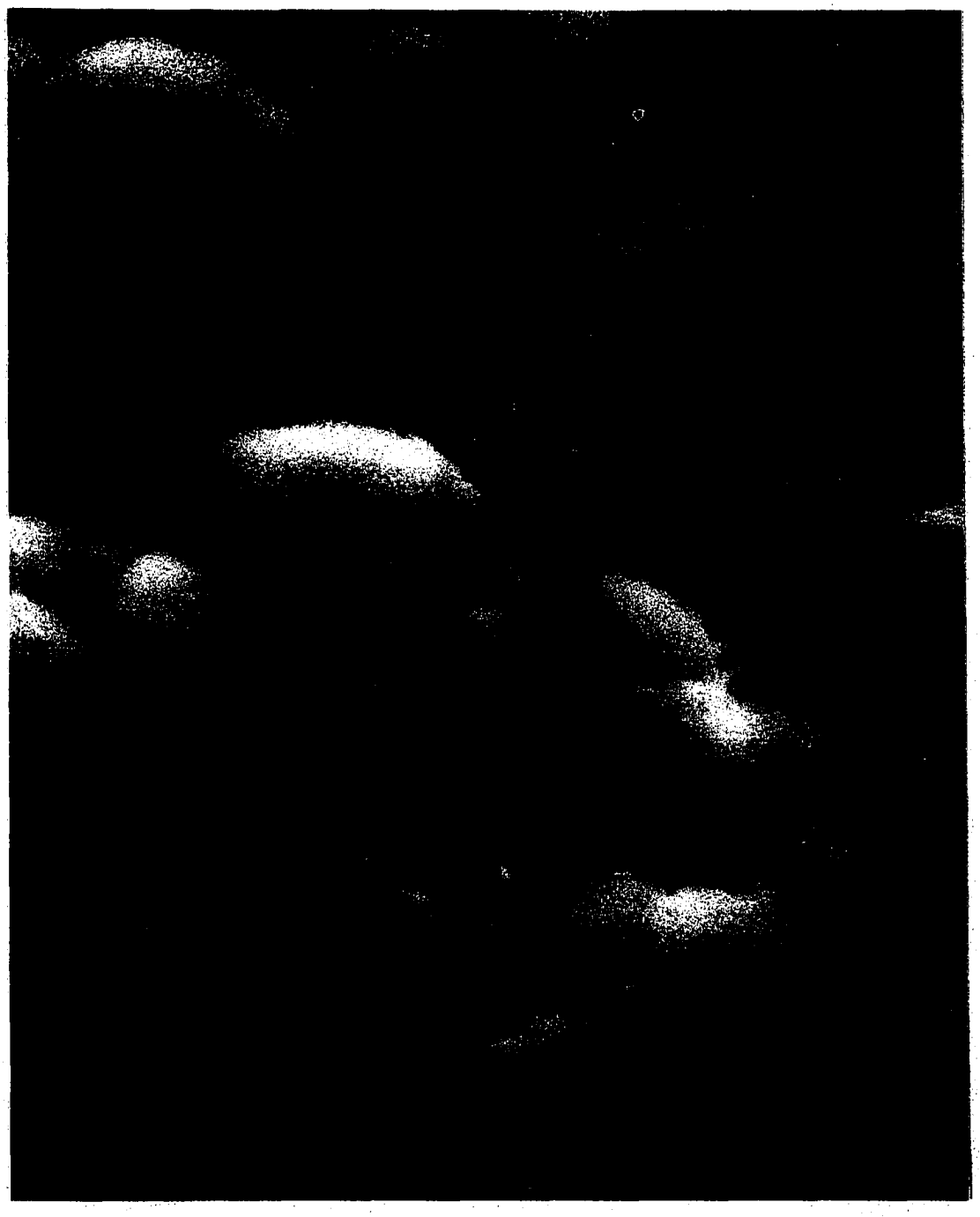

Figure 75. 9800X
The structure shown is believed to be a polymer emerging from within a pore in a cobalt hardened gold plating.

layer has not separated from the substrate. X-ray microanalysis indicated that the composition of this layer was close to $AuSn_2$ but did not correspond to any simple stoichiometry of gold and tin. Aging for 7 days at 100°C converted the intermetallic layer to $AuSn_2$ and invariably produced detachment similar to Figure 72.

Extensive porosity was noted in solders applied to terminals having gold platings thicker than 0.5 microns. Typical examples were presented in Figures 60, 63 and 67. The sample shown in Figure 60 had been aged for 7 days at 100°C, however, such treatment would not affect the porosity. Figure 74 shows a solder fillet applied to a 2.5 micron gold plated terminal. The porosity appears to be associated with the solder-terminal interface. If a codeposited polymer is produced in the hard gold plating, then one might expect its decomposition in the molten solder. Apparently the quantities of polymer produced with thick gold layers are sufficient to create the porosity commonly observed when these terminals are soldered. Here it is interesting to note the lack of porosity obtained with the 0.5 micron gold coating shown in Figure 59. Direct observation of the polymer was made by Munier who was able to isolate a clear transparent layer covering the entire cathode area of the plating system. Observations made during this investigation of a porous hard gold deposit indicated that polymer had exuded from within the coating. Figure 75 shows an example of this observation.

CHAPTER III

WETTING OF SUBSTRATES BY SOFT SOLDERS

Introduction

The rates at which molten solder spreads on substrate surfaces and the area produced by spreading have been used as a measure of solderability. It is now certain that the performance of the solder joint is in no way related to spread rate; however, this criterion persists because of the need to produce soldered joints quickly in commercial production. The theoretical considerations governing wetting of solid surfaces by molten metals was treated by Wassink (23); and a series of experiments by Bailey and Watkins demonstrated the importance of alloying in a diffusion layer ahead of the advancing liquid front.

In the experiments described below, the spread rates of 60/40, 63/37, and the antimonial solders on gold, copper, and brass substrates were compared. In addition, the nature of the solid and wetted areas adjacent to the interface was examined with the SEM and EDS.

Experimental

Solder preforms were applied to clean substrates and melted in the condensation soldering apparatus described earlier. Where flux was

required, a proprietary chemical Alpha 611 (Alpha Metals, Newark, NJ) was used. This is a mildly activated flux of a type generally used for electronic applications. The soldering temperature was maintained at 215°C and times were varied from 5 to 80 seconds. The areas over which the solders spread were compared qualitatively and the contact angle through the solder after solidification was determined by cross sectioning the samples.

Results and Discussion

Figure 76 shows a typical series of test samples obtained for 60/40, 63/37, and the antimonial solders applied to fluxed copper substrates. The differences in areas over which the solder had spread in a 5-second exposure period suggest that the wetting rates of the three alloys are somewhat different, with 60/40 giving the highest rate and the antimonial solder the lowest. However, the areas obtained after an 80 second reaction time on fluxed copper substrates, shown in Figure 77, appear to be about the same. Apparently the molten solder spreads very rapidly until its equilibrium contact angle is established. The area over which the solder has spread appears to be more likely a function of the amount of solder available to the substrate rather than the exposure time. The results of tests conducted on fluxed cartridge brass substrates are shown in Figure 78. In these tests the 60/40 alloy showed the greatest spread, and the 63/37 solder and antimonial alloy were about equal.

The results of the solid contact angle measurements of solders on copper and brass substrates are presented in Table I. These data are

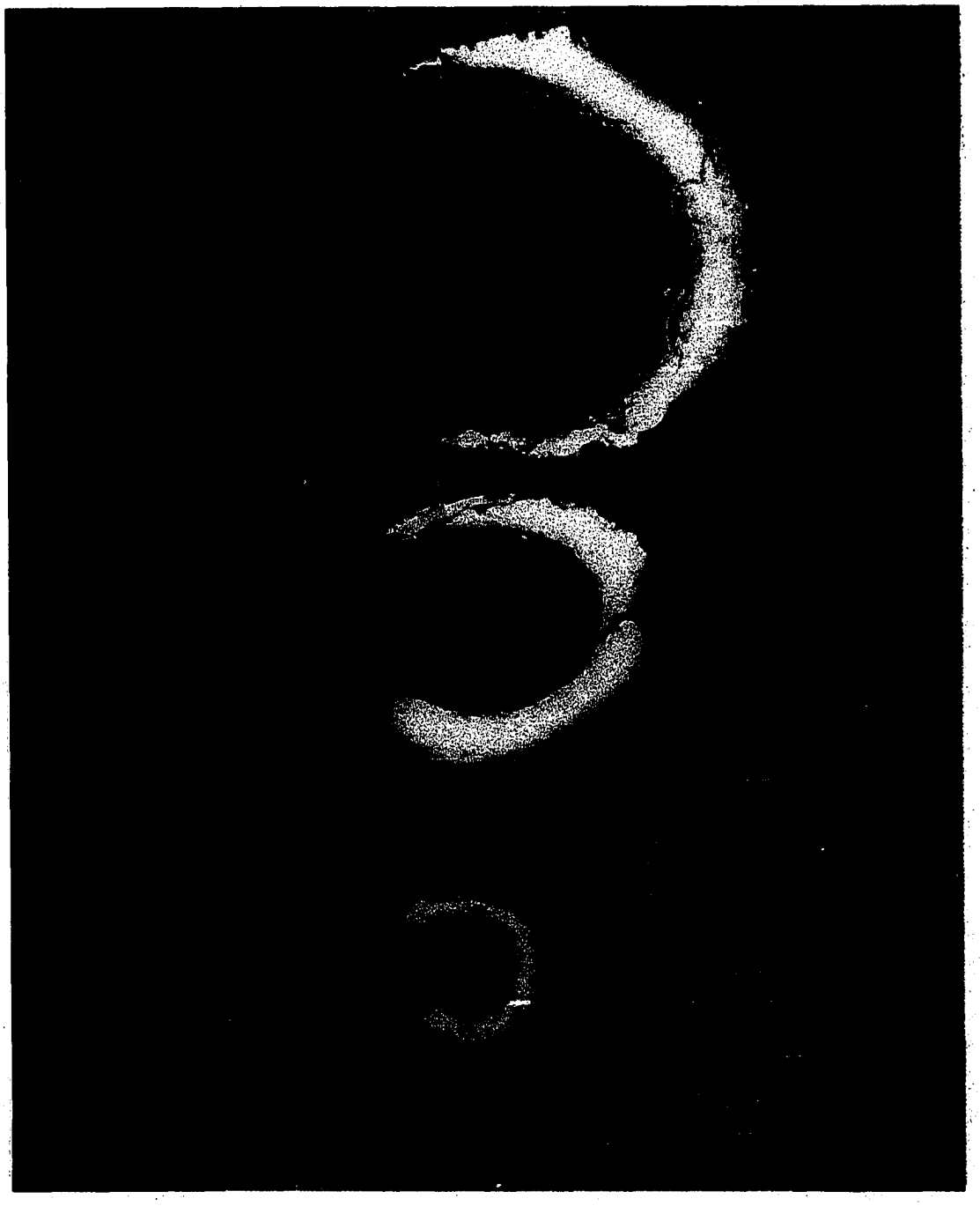

Figure 76. 10X
Solder preforms which were reflowed at 215°C with a soldering time of 5 seconds on a cleaned and fluxed pure copper substrate. 60/40 (top) - 63/37 (middle) - antimonial (bottom).

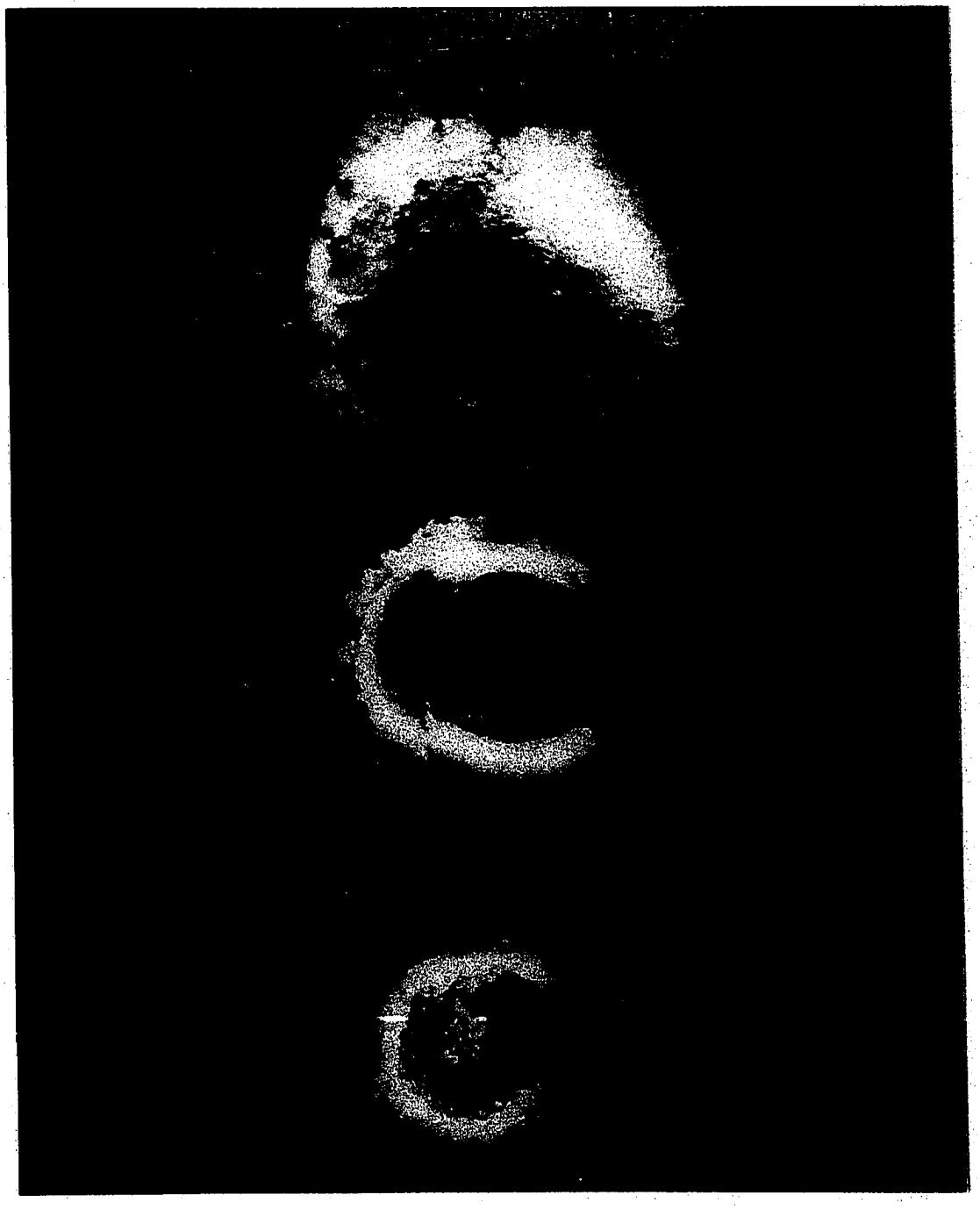

Figure 77. 10X
Solder preforms which were reflowed at 215°C with a soldering time of 80 seconds on a cleaned and fluxed pure copper substrate. 60/40 (top) - 63/37 (middle) - antimonial (bottom).

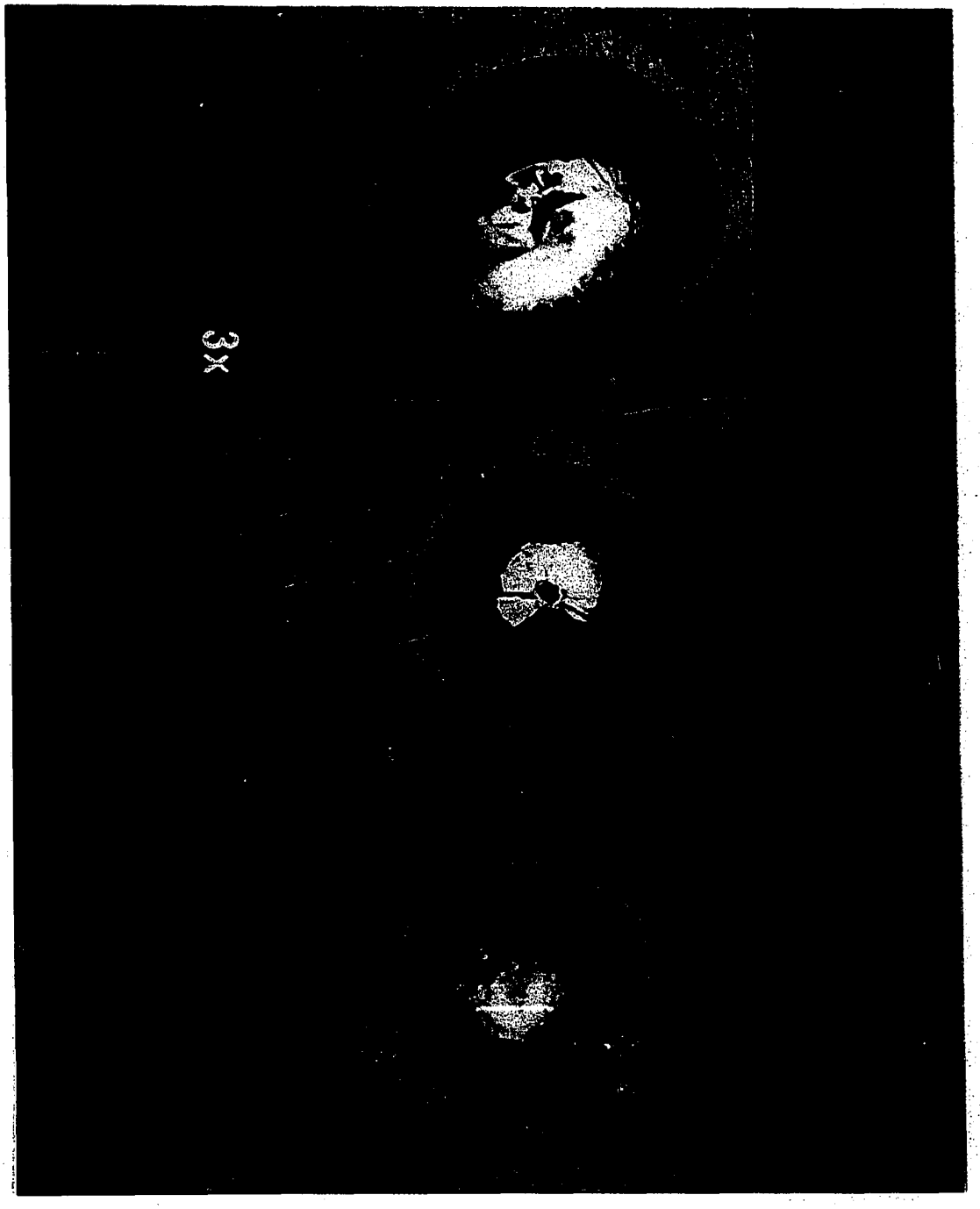

Figure 78. 10X
Solder preforms which were reflowed at 215°C with a soldering time of 80 seconds on a cleaned and fluxed cartridge brass substrate. 60/40 (top) - 63/37 (middle) - antimonial (bottom).

TABLE I: Measurement of Contact Angles
80-Second Reaction Time

	Copper Substrate	Brass Substrate
60/40 Solder	3°	27°
63/37 Solder	13°	35°
Antimonial Solder	21°	33°

consistent with the results of the area spread tests. Low contact angle is associated with large area of spread.

The results of similar area spread tests are presented in Figures 79-83. Here substrates coated with thick layers of pure and cobalt hardened gold were compared with and without the use of flux. The results showed the greatest area of spread was obtained with the 60/40 solder and the smallest with the antimonial alloy. The effects of flux is shown in Figure 82 where a copper substrate was cleaned with HCl just prior to soldering. Chemical reactions during soldering with various substrates and types of fluxes has been reported in a series of papers by Kihara (24).

The rates at which liquid solders wet substrate surfaces can be determined by a different experimental technique. The method involves a measurement of the buoyant force exerted by a molten solder bath on a strip of substrate metal which is inserted to a predetermined depth. The results of measurements carried out on a series of substrate surfaces are included in Appendix B.

The complex nature of the processes which occur as the advancing solder interface wets the substrate is demonstrated by Figure 84. Here the edge of a solidified pool of 60/40 solder which has spread on a fluxed copper substrate is shown in an electron micrograph. The solder mass appears on the left and the copper substrate on the right. Proeutectic α dendrites may be noted in the solder, and the etched grain structure of the substrate is evident. The boundary between the solder mass and substrate consist of two separate regions which are shown at higher magnification in Figure 85. These two regions appear to

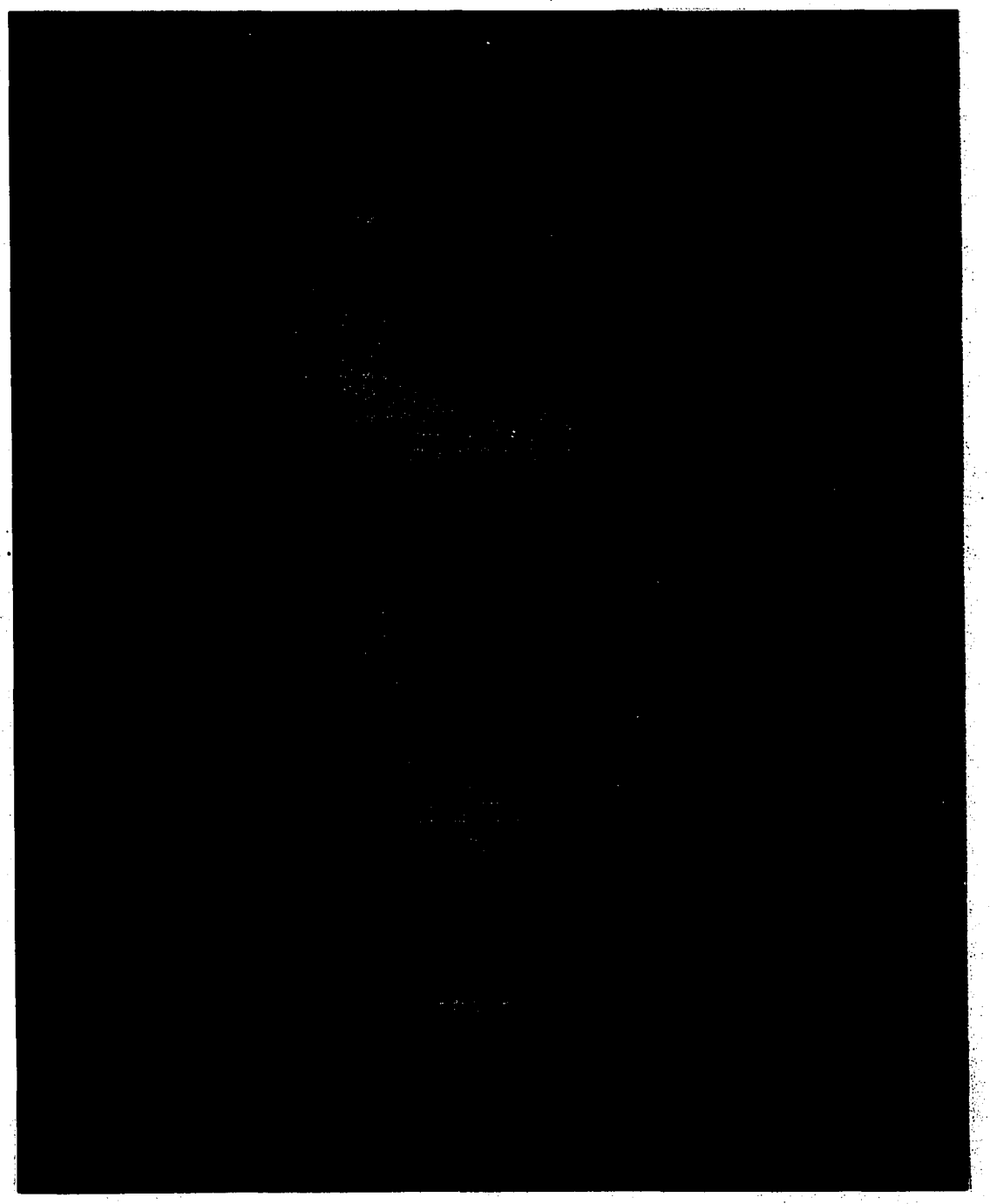

Figure 79. 10X
Solder preforms which were reflowed at 215°C with a soldering time of 80 seconds on a cleaned and fluxed pure gold substrate. 60/40 (top) - 63/37 (middle) - antimonial (bottom).

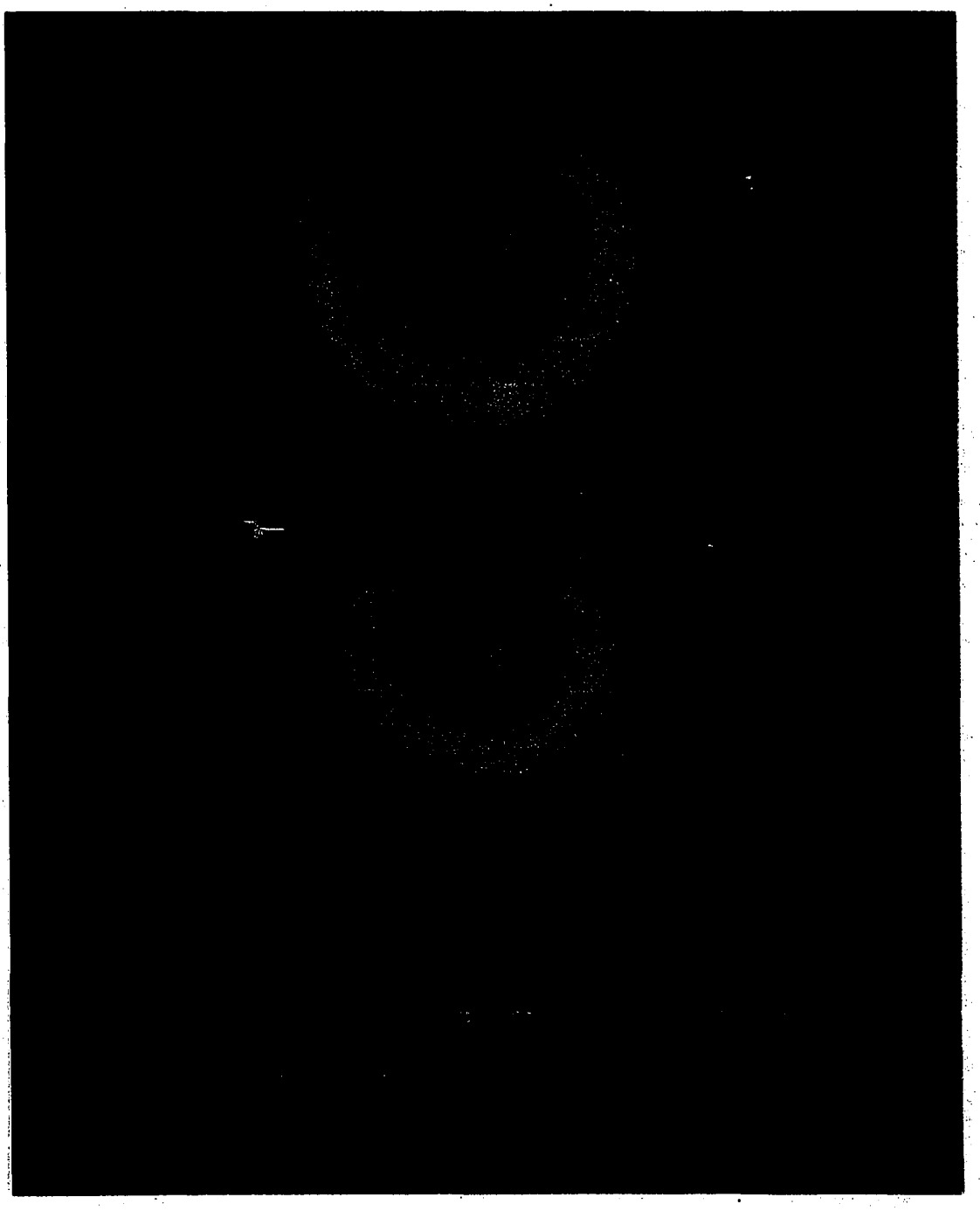

Figure 80. 10X
Solder preforms which were reflowed at 215°C with a soldering time of 80 seconds on a cleaned and fluxed cobalt hardened gold plating. 60/40 (top) - 63/37 (middle) - antimonial (bottom).

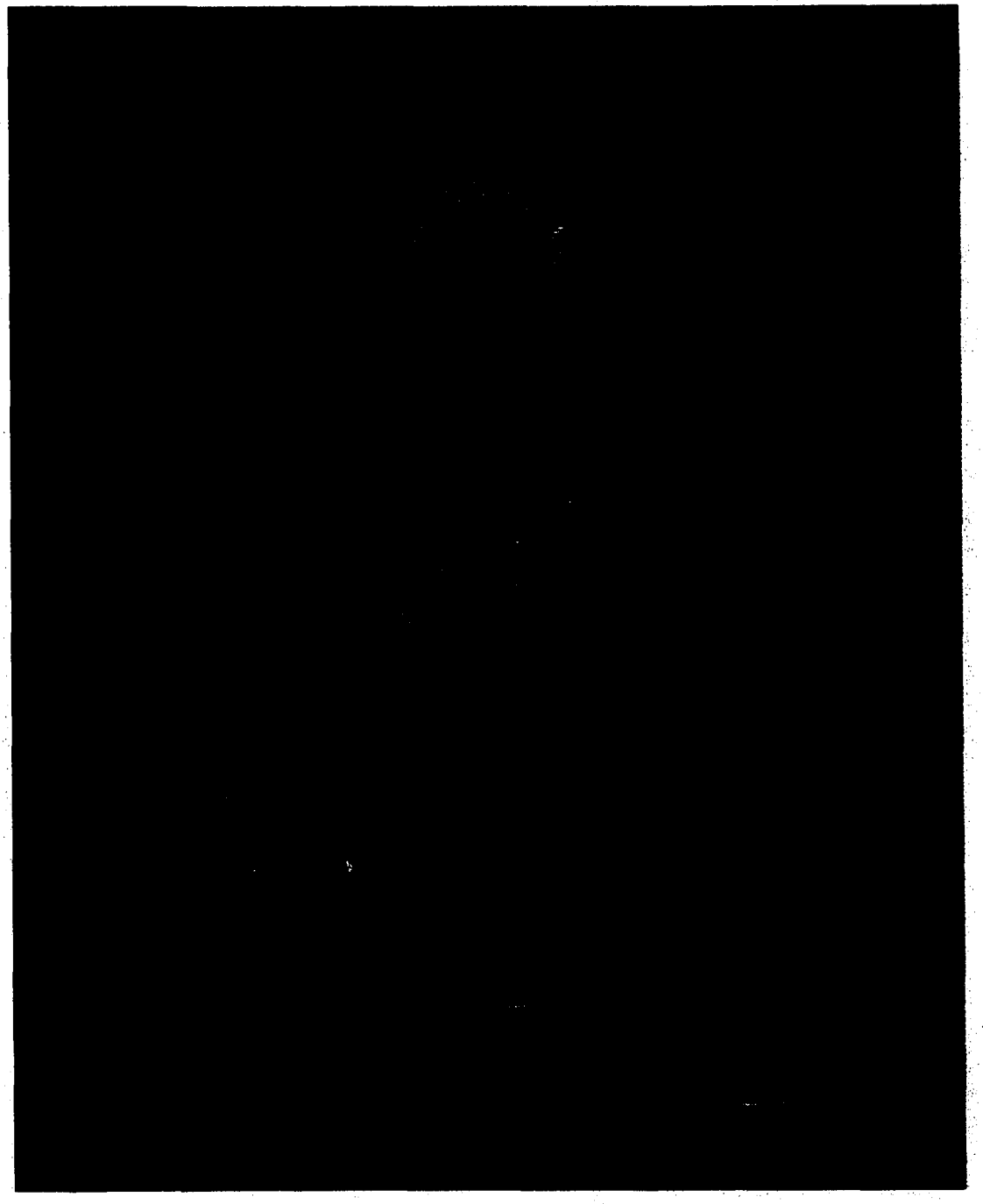

Figure 81. 10X
Solder preforms applied to a cobalt hardened gold which was cleaned but not fluxed prior to reflowing. 60/40 (top) - 63/37 (middle) - antimonial (bottom).

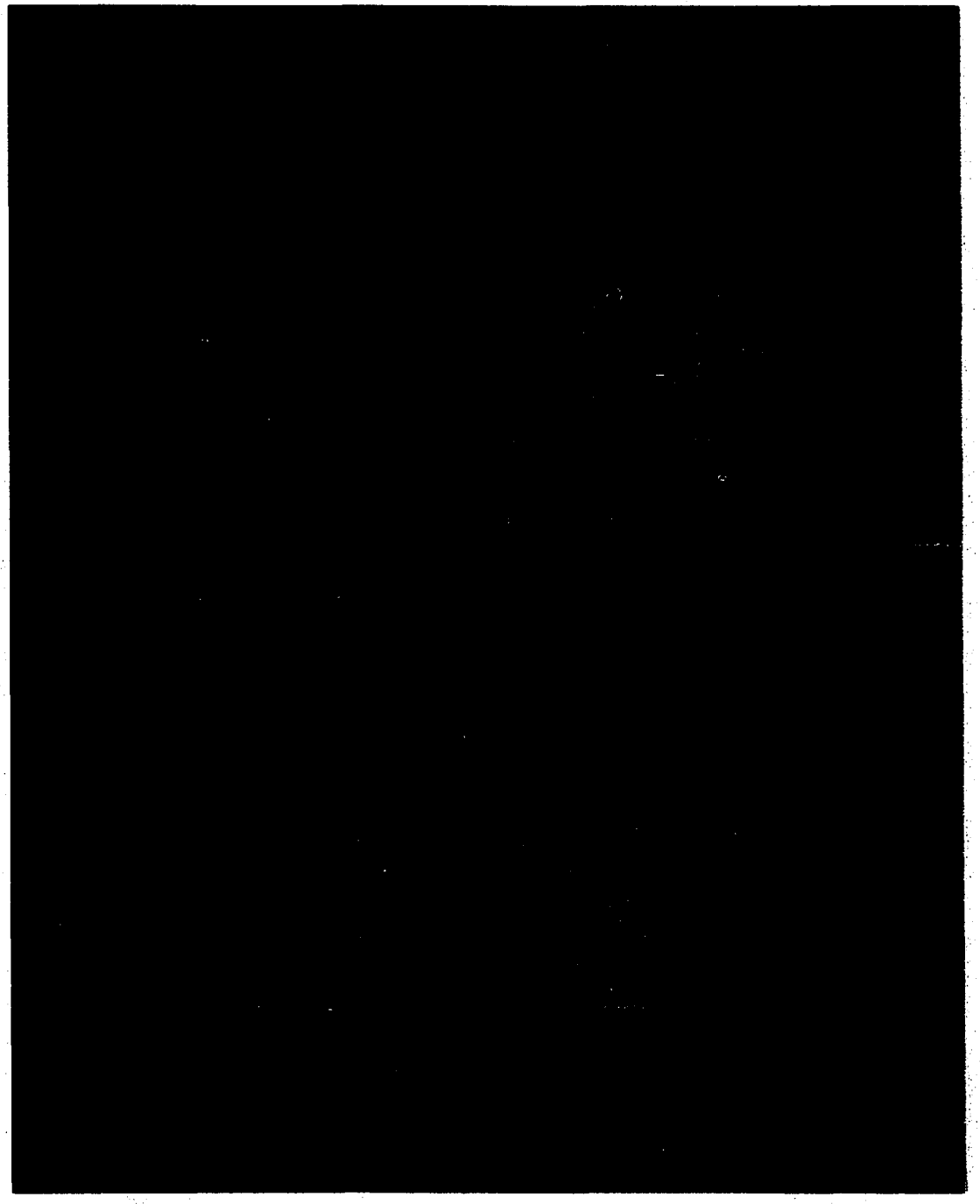

Figure 82. 10X
Solder preforms applied to a copper substrate which was cleaned with HCl but not fluxed prior to reflowing at 215°C. 60/40 (top) - 63/37 (middle) - antimonial (bottom).

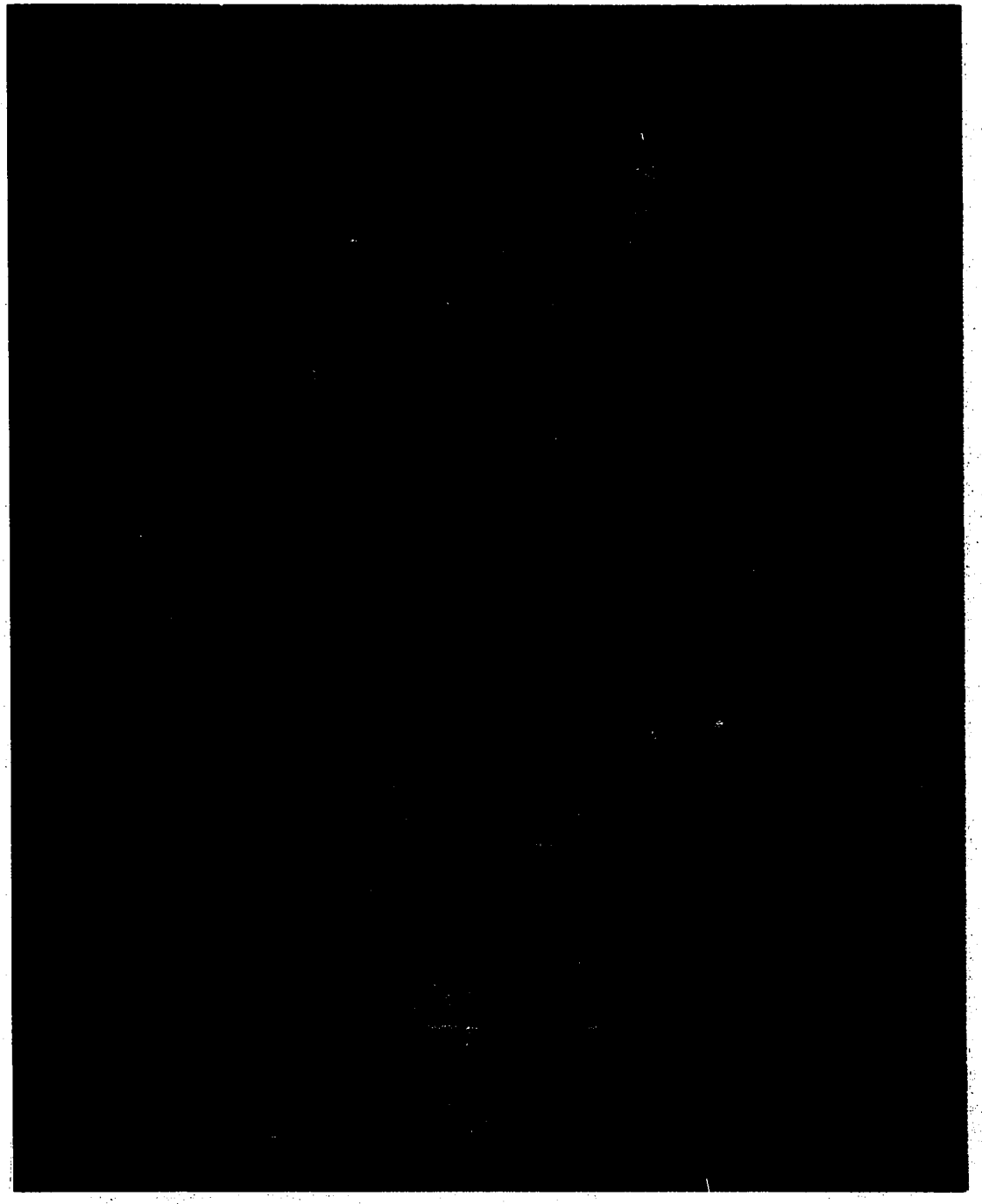

Figure 83. 7X
Comparison of spread areas on copper and gold using cleaned and fluxed substrates by reflowing solder preforms at 215°C for 80 seconds. 60/40 (top) - 50/50 (2nd) on copper. 60/40 (3rd) - 50/50 (bottom) on gold.

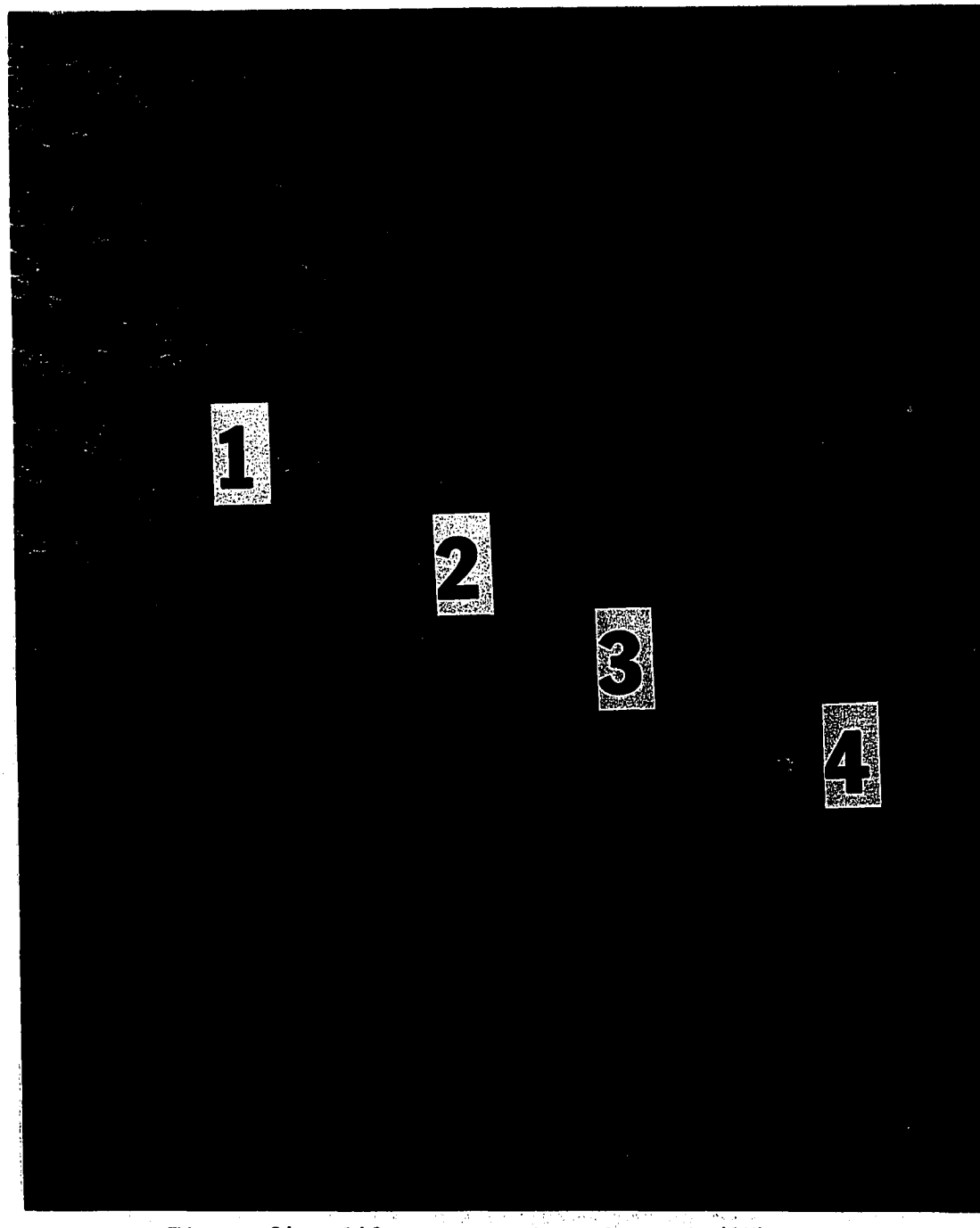

Figure 84. 140X - Peroxide and Nital (2%) Etch
A spread sample shown in Figure 77 of 60/40 solder on pure copper with 80 second reaction time at 215°C.
(1) solder mass, (2) intermetallic band, (3) diffusion band, (4) copper substrate.

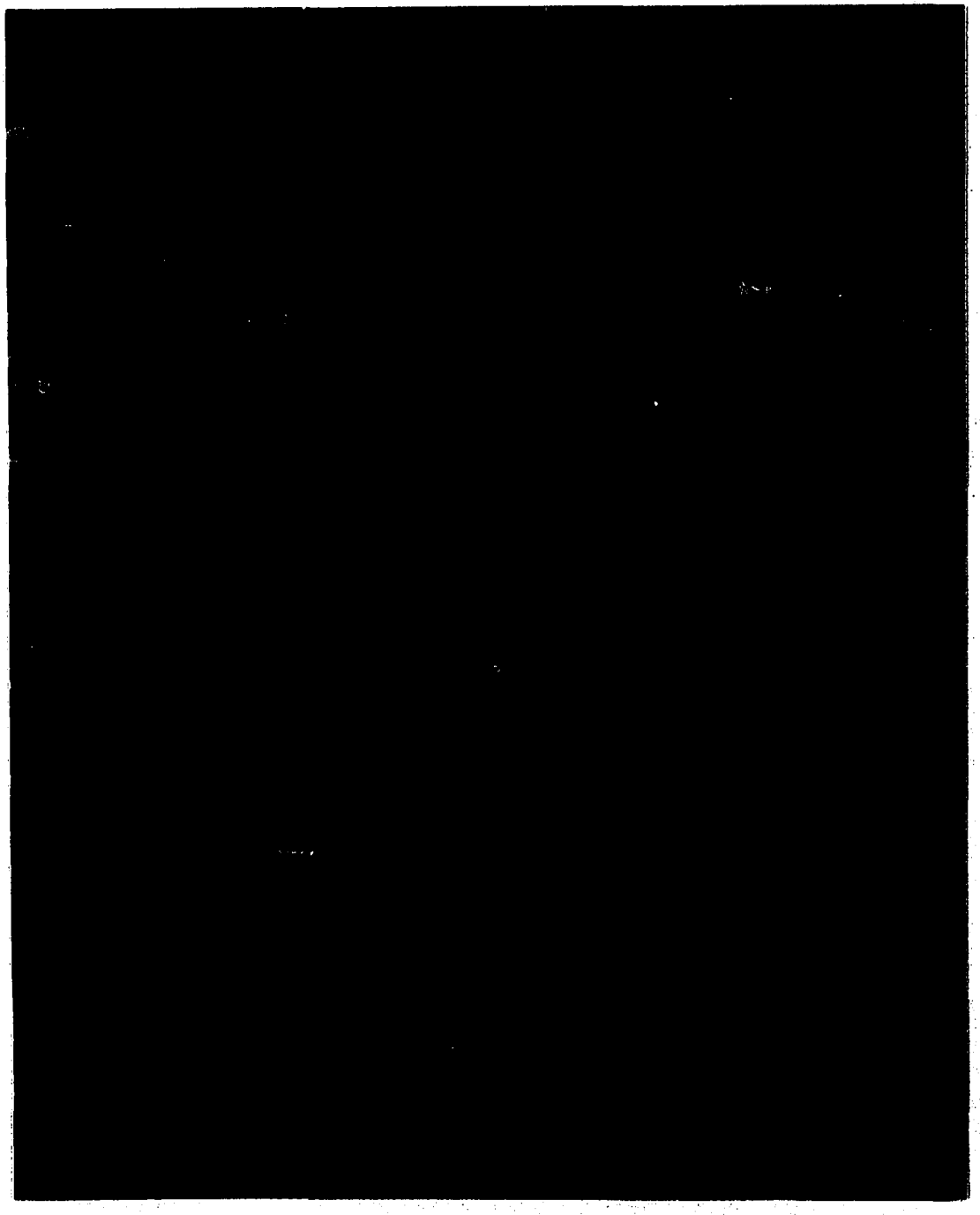

Figure 85. 1400X - Peroxide and Nital (2%) Etch
The interface between the intermetallic and diffusion bands of Figure 84 is shown.

correspond to the diffusion band observed by Bailey and Watkins in their study of the flow of liquid metals on solid substrates.

Figure 86 shows the boundary between a copper substrate and the most advanced portion of the diffusion band ahead of the 60/40 solder mass. The composition of the leading edge of the band was determined by using EDS to be 62 w/o Cu - 38 w/o Sn. The absence of lead in the structure indicates that it was formed by selective dissolution of tin by the solid copper substrate.

The inner layer of the diffusion band in the same solder substrate combination as Figures 84 and 86 is shown in Figure 87. The region is composed of nodules of composition 36 w/o Cu - 64 w/o Sn. This composition is close to η' (Cu_6Sn_5) and lies in the two phase region $\eta' + \beta$ (tin).

Figure 88 shows the boundary between the solder mass and the inner diffusion band. The solder was remarkably free of needles of Cu_6Sn_5 which would have been expected to form during the 80-second soldering period.

Figures 89 and 90 show the diffusion band surrounding a mass of 63/37 solder applied to a fluxed copper substrate. The soldering time was 80 seconds. The character of the diffusion band is comparable to that obtained with the 60/40 alloy. However, considerable Cu_6Sn_5 compound formation may be noted in the solder mass. Between the region where compounds were observed and the inner diffusion band, a light appearing band is seen (Figure 89). The composition corresponds to 83 w/o Cu - 17 w/o Sn. The significance of this band is not certain because the sample was etched prior to performing the analysis. Etching

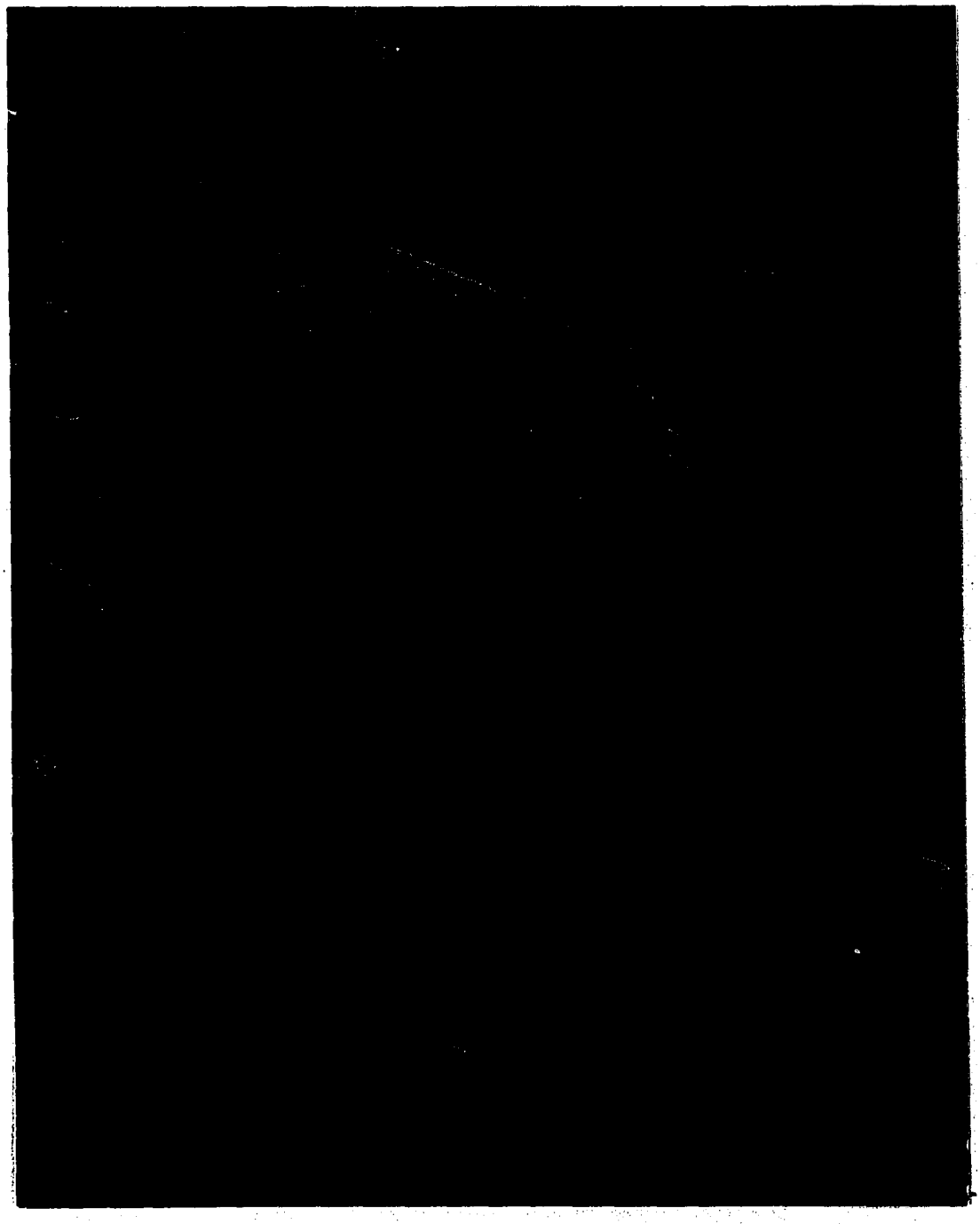

Figure 86. 1400X - Peroxide and Nital (2%) Etch
The interface between the diffusion band and copper substrate of Figure 84 is shown.

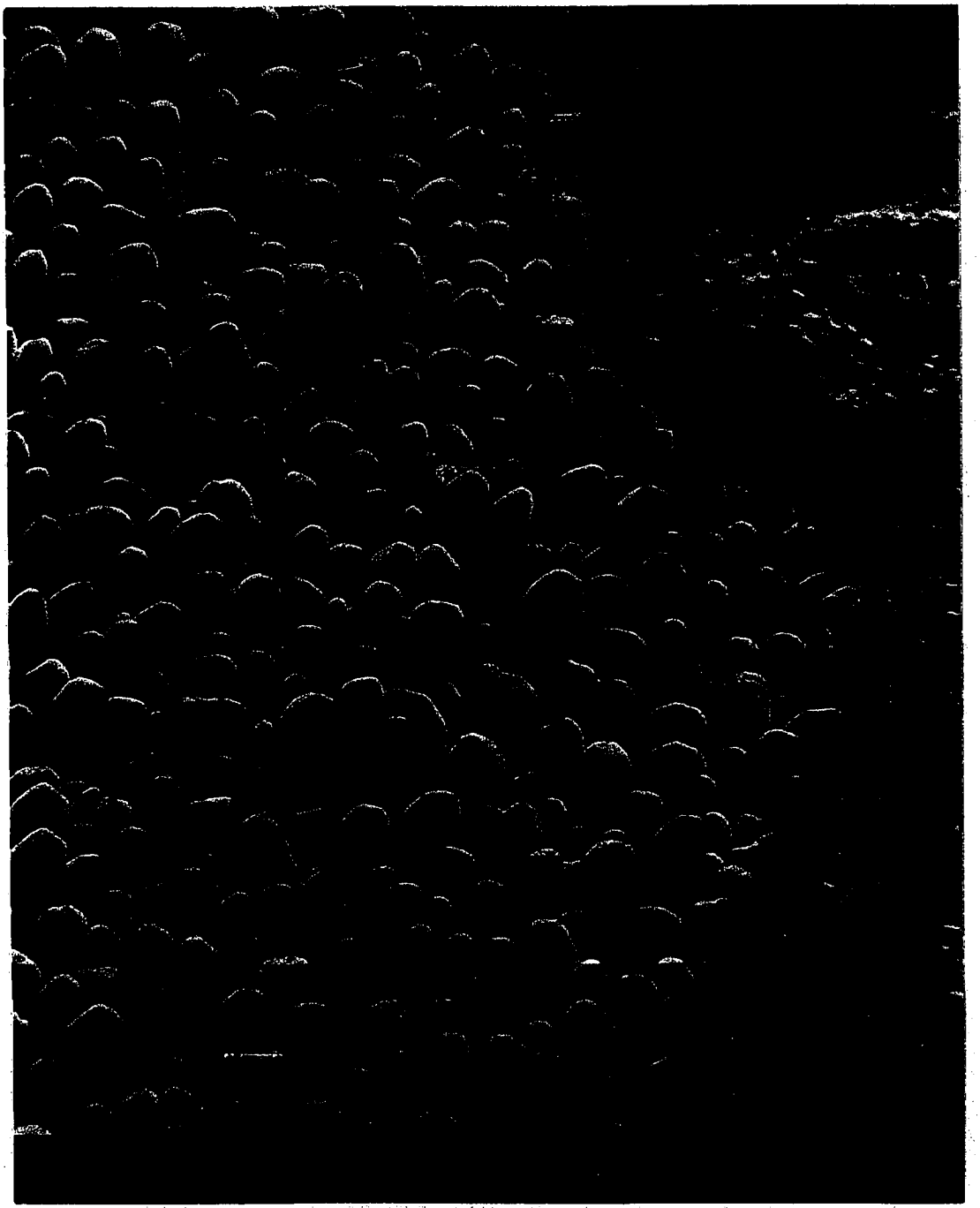

Figure 87. 1400X - Peroxide and Nital (2%) Etch The intermetallic band and the inner portion of the diffusion band shown in Figure 84.

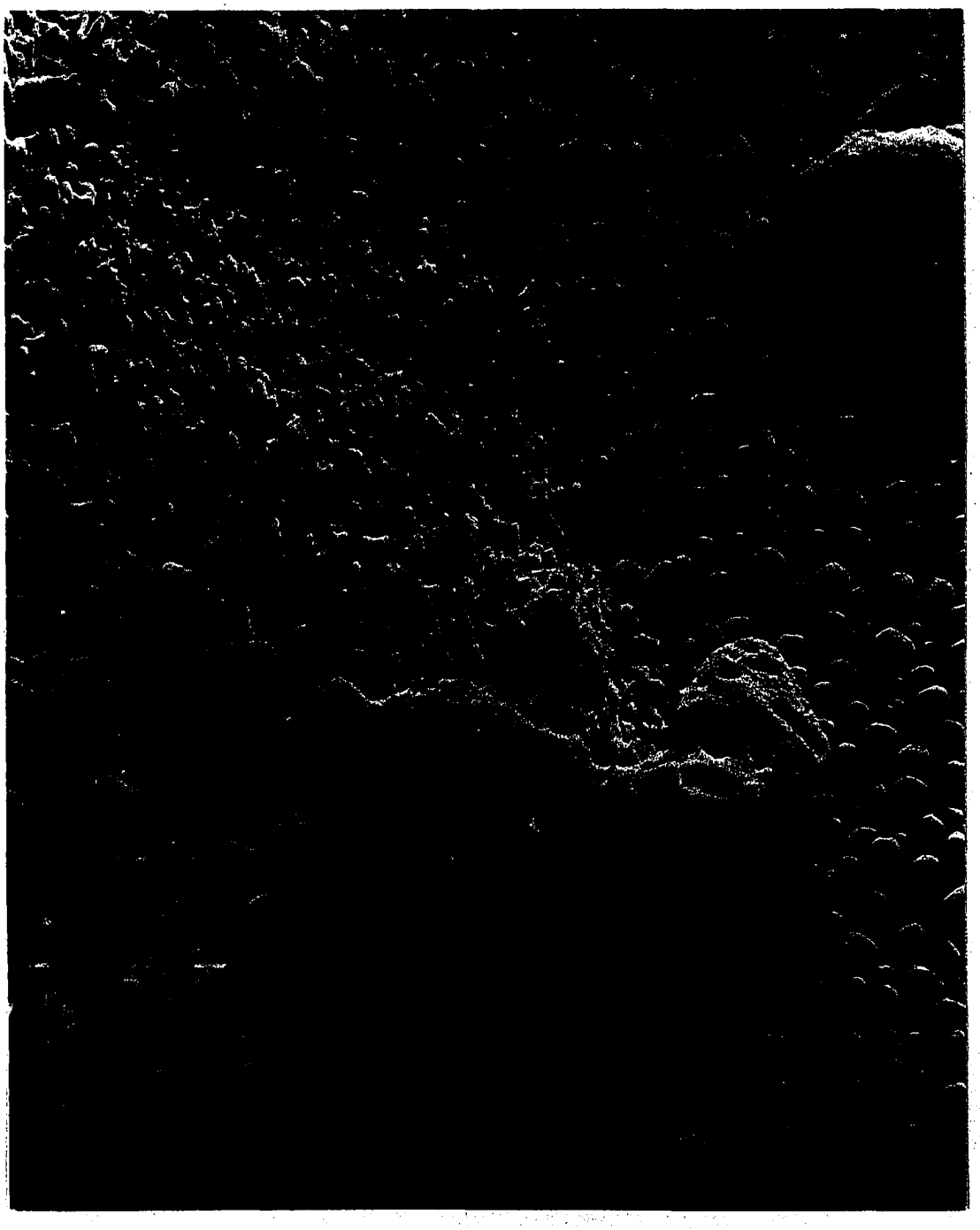

Figure 88. 1400X - Peroxide and Nital (2%) Etch
The interface between the solder mass and the intermetallic band shown in Figure 84.

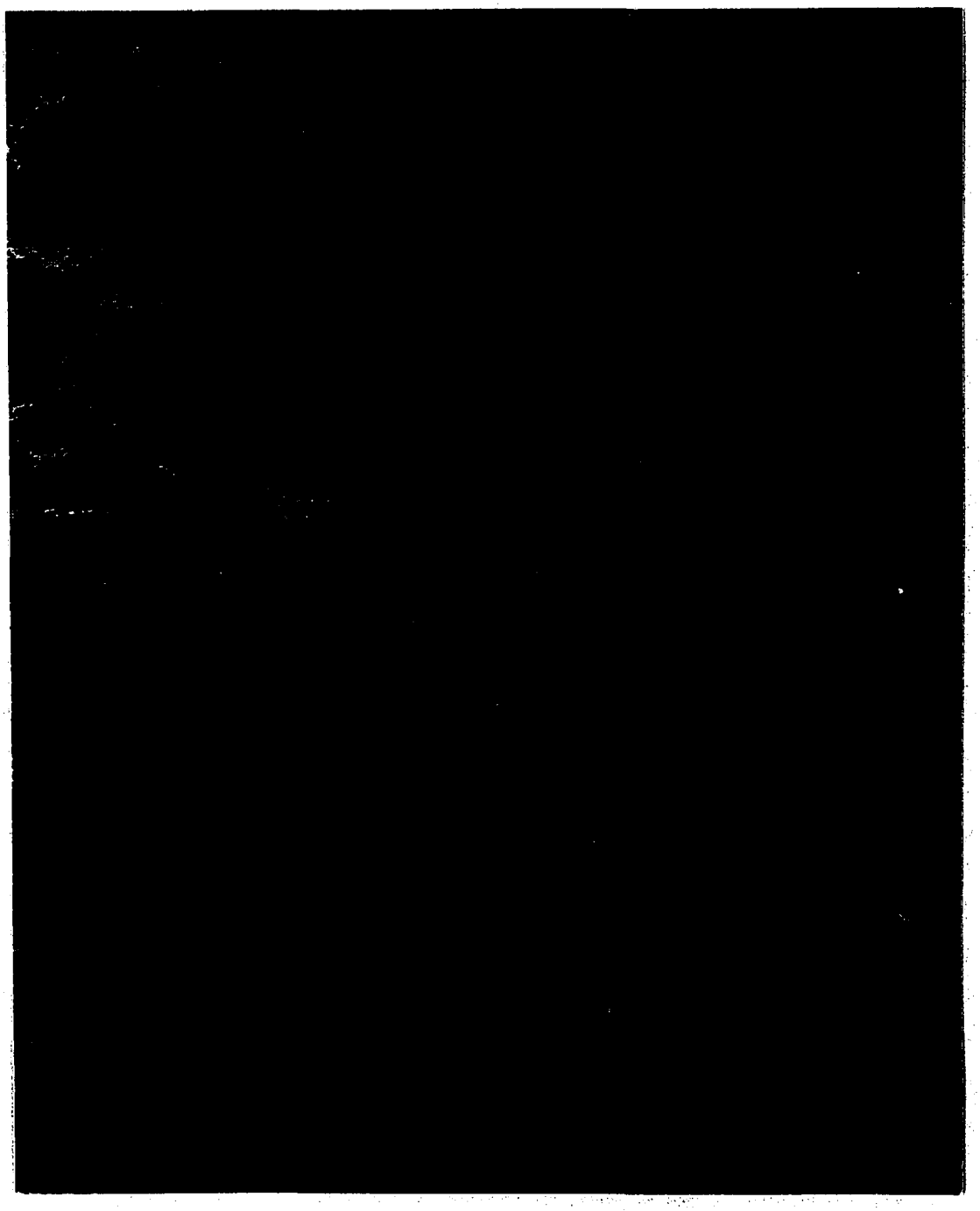

Figure 89. 420X - Peroxide and Nital (2%) Etch
A 63/37 solder preform spread area on pure copper as seen in Figure 77 after etching. The figure is similar to Figure 84; however, intermetallic compounds which appear as needles are seen in the solder mass.

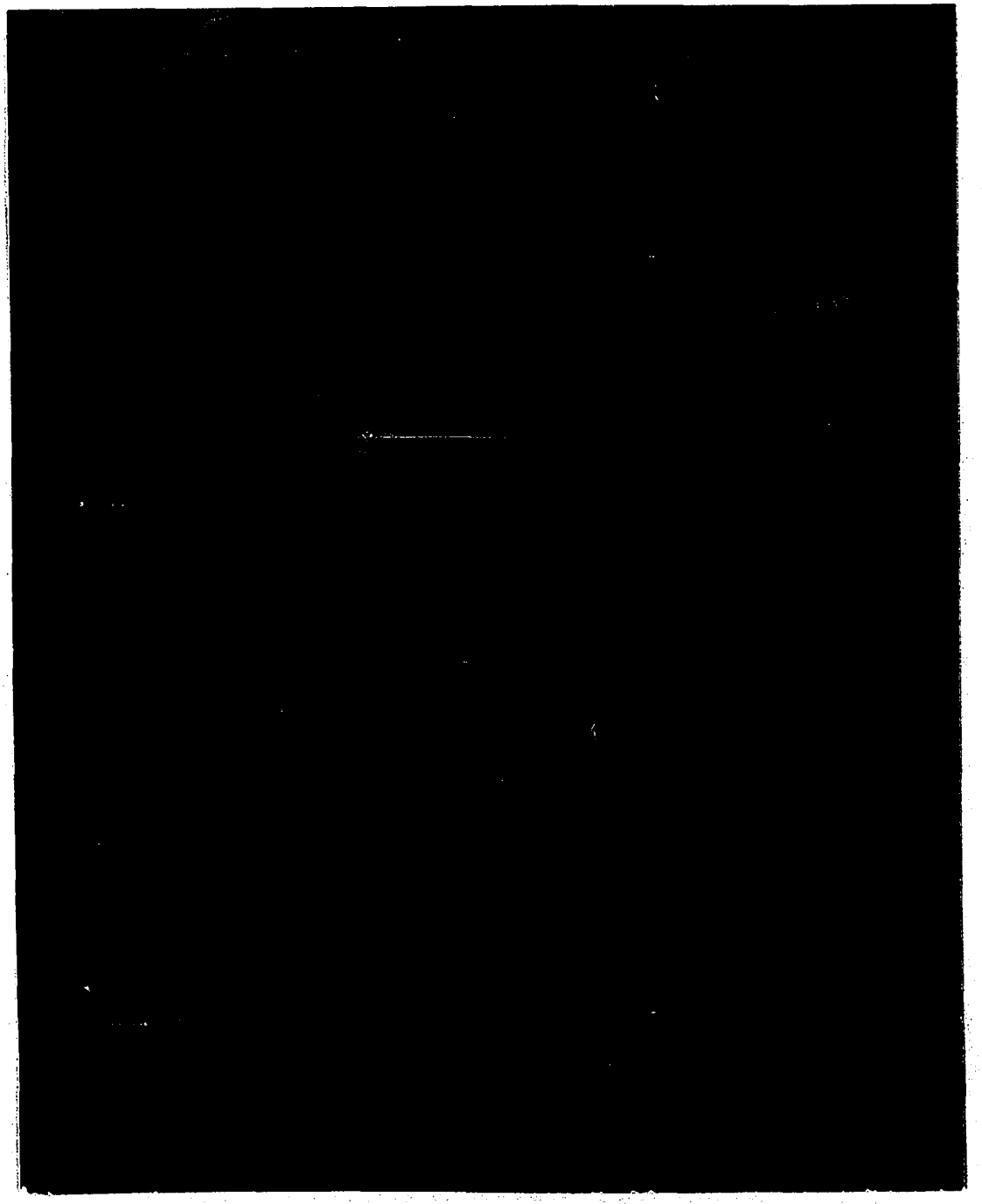

Figure 90. 980X - Peroxide and Nital (2%) Etch
The solder mass and intermetallic band interface seen in Figure 89. The intermetallic needles are seen in the solder mass.

is capable of selectively removing one of the constituents from the structure. More detailed views of the intermetallic compounds which were formed are shown in Figures 91 and 92.

The appearance of the interface obtained with the antimonial solder on a fluxed copper substrate after 80-second soldering times was somewhat different from the simple binary tin-lead alloys. Figure 93 shows an overall view of the diffusion band and adjacent substrate and solder mass. In Figure 94 the interface consists almost entirely of nodular formations and the diffusion band is very narrow. An abnormal region where the outer band is quite wide is seen near the bottom of Figure 93. The strong influence of impurities and low concentration alloy additions on contact angle is well known. Apparently antimony can also influence the diffusion rate of tin into the solid copper substrate.

Blum, Pelissier, and Silvestre (25) have proposed that there exist two types of diffusion when soldering to copper. The first process is a rapid solid-to-liquid diffusion process which commences when the liquid solder and copper come into contact. An interface develops with a copper concentration slightly greater than the eutectic composition of a Cu-Sn system and crystals of the η phase begin to develop. The second diffusion process is a solid state process which develops an ε phase (Cu_3Sn) between the η phase and the boundary of pure copper. Comparison of their micrographs and the micrographs presented here reveals similar structures.

Analysis of the aged samples (100°C - 7 days) reported here show that the η phase is 60.17 w/o Sn - 39.83 w/o Cu and the ε phase is 34.39 w/o Sn - 65.61 w/o Cu. The observed composition of the η phase is

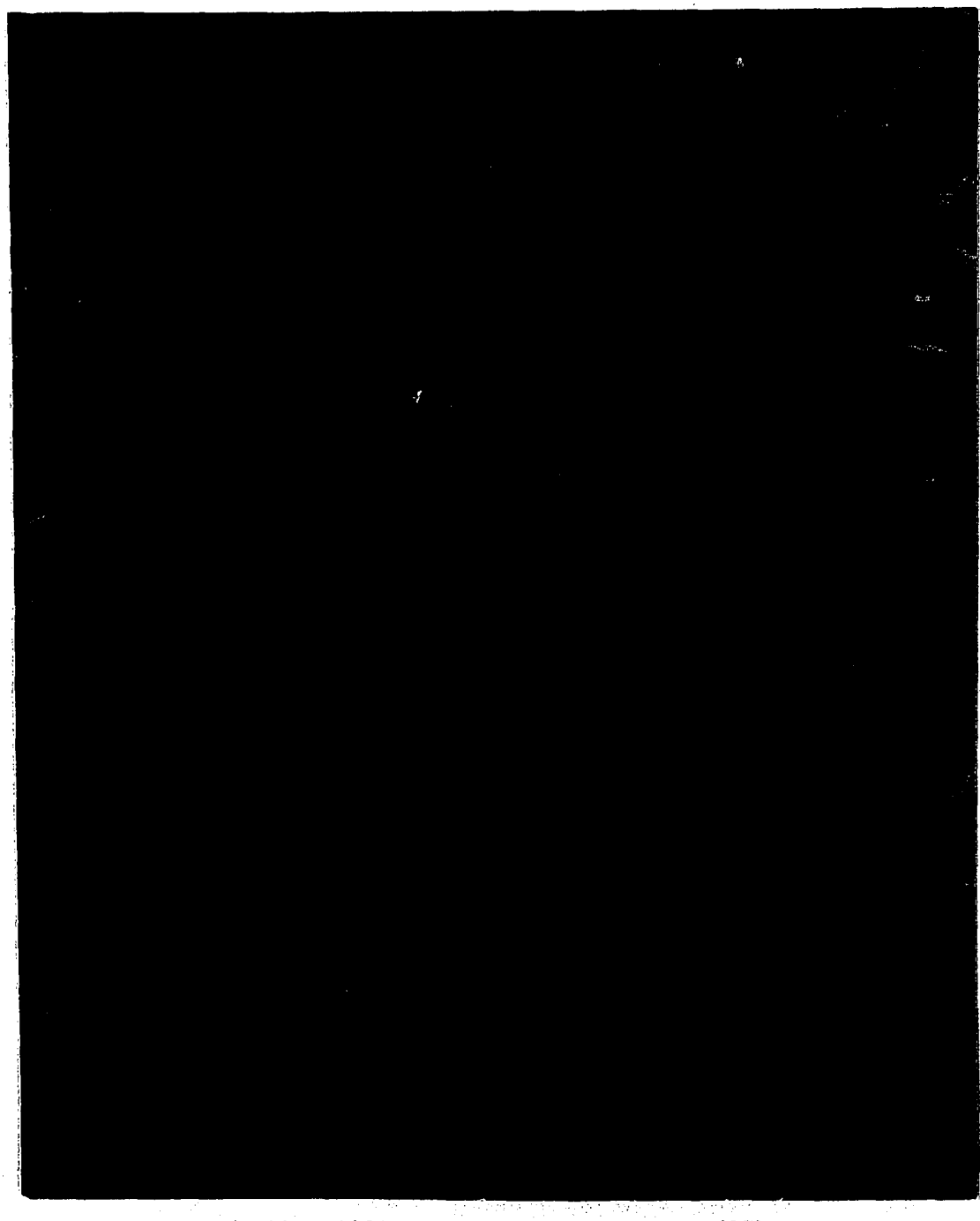

Figure 91. 1400X - Peroxide and Nital (2%) Etch
A detailed view of the intermetallic Cu_6Sn_5 compounds in the solder mass seen in Figure 90.

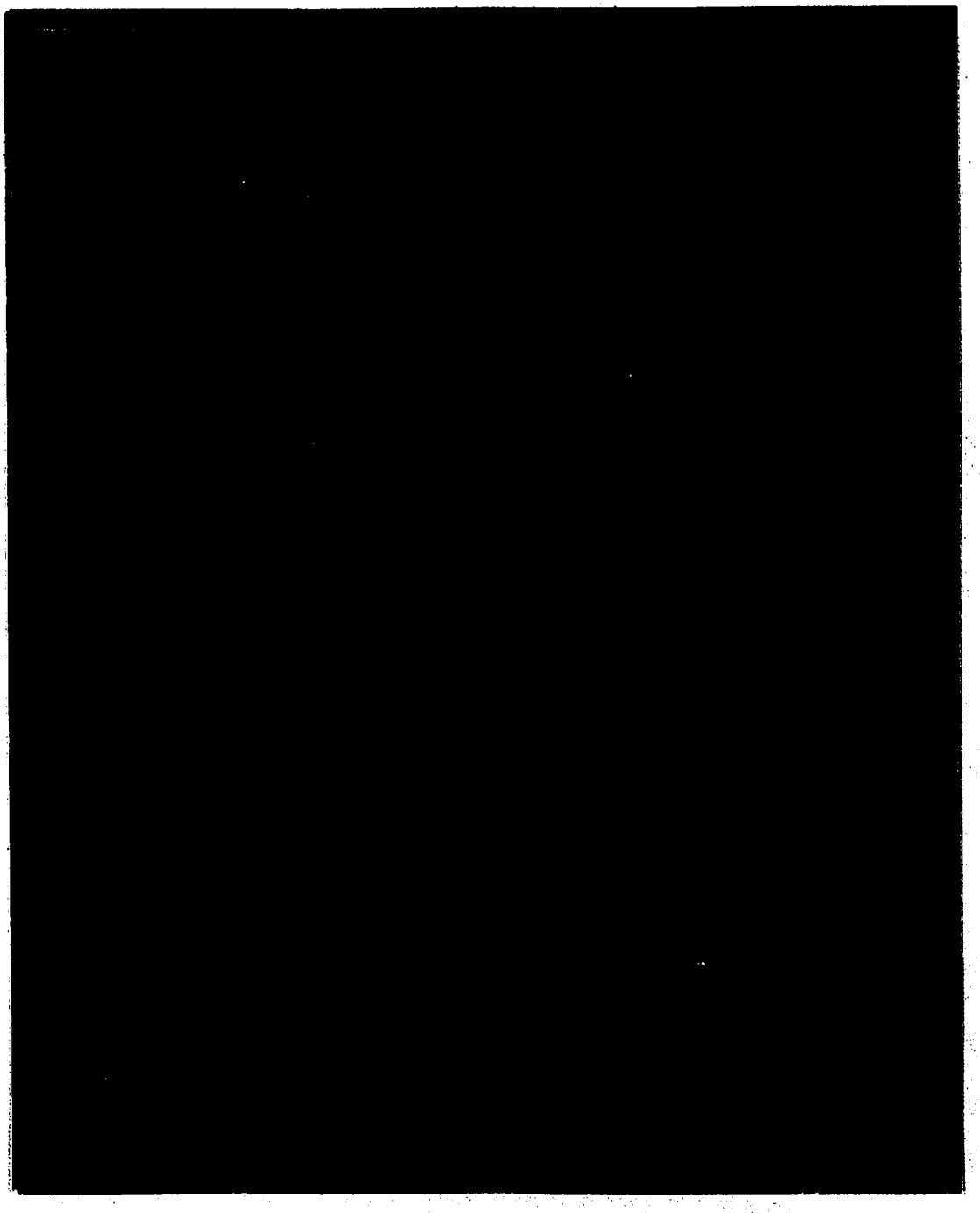

Figure 92. 5600X - Peroxide and Nital (2%) Etch
A more detailed view of the compounds shown in Figure 91.

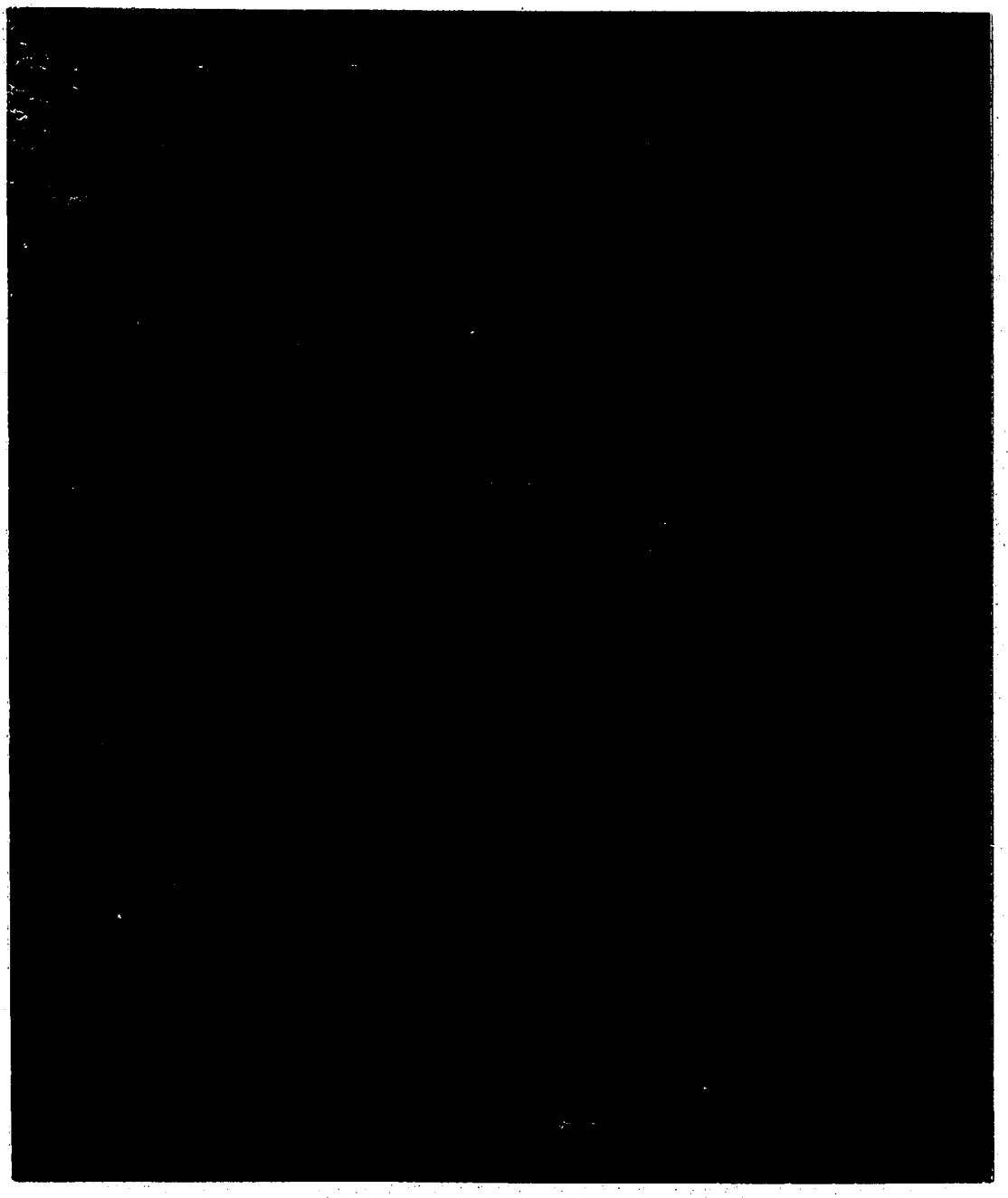

Figure 93. 420X - Peroxide and Nital (2%) Etch
The area of spread of antimonial solder as shown in Figure 77 on a pure copper substrate. Needle-like intermetallic compounds are seen in the solder mass. The intermetallic and diffusion bands as seen in Figure 84 are present, however, the diffusion band is much smaller.

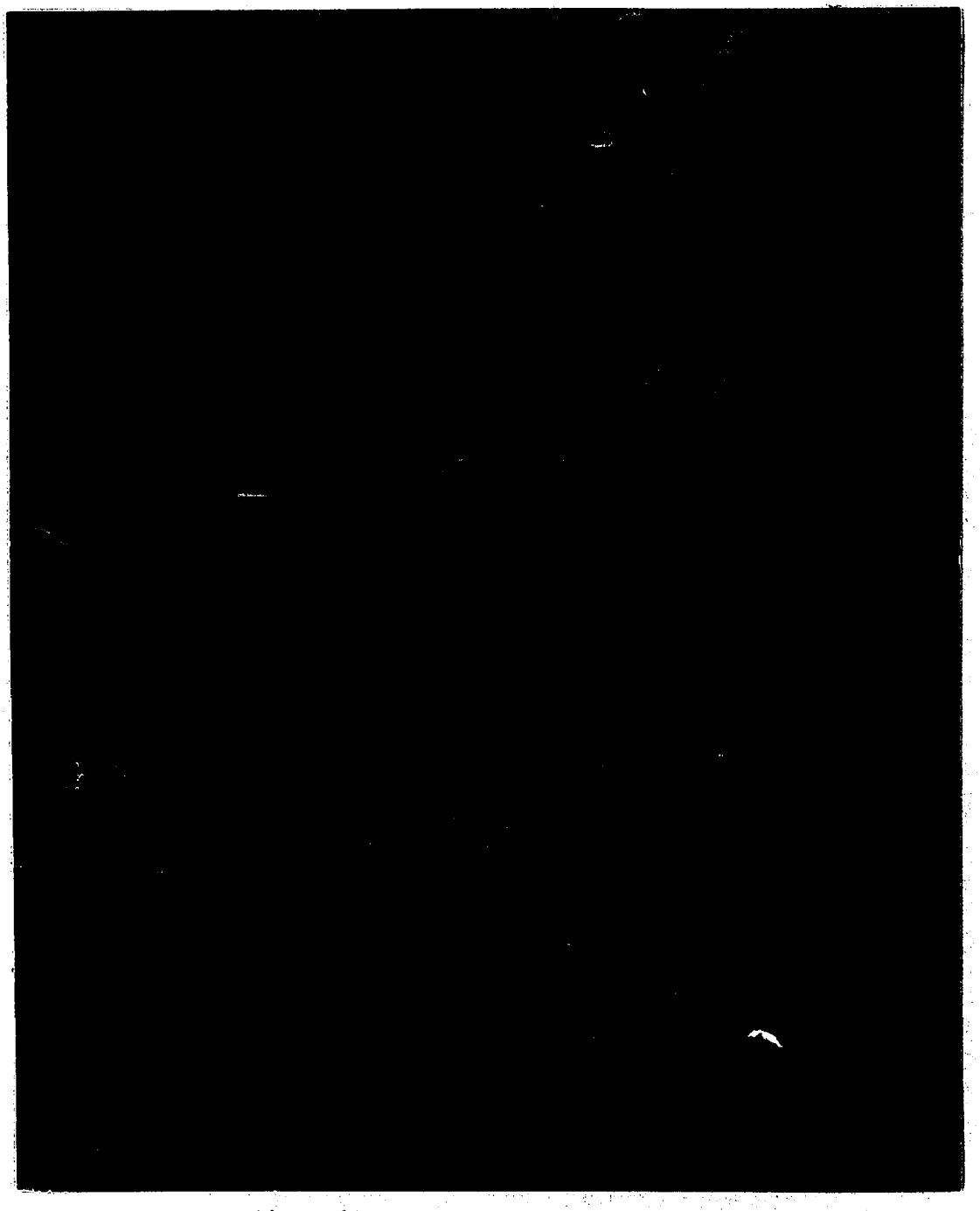

Figure 94. 5600X - Peroxide and Nital (2%) Etch
The intermetallic and diffusion band interface of Figure 93 is shown in more detail. The diffusion band is very narrow.

consistent with published phase diagrams, while the analyzed copper content of the ε phase is too high by about 4 w/o - Cu. Blum, Pelissier, and Silvestre have suggested that the width (thickness) of the η phase increases with interaction time while the ε phase remains nearly unchanged. Figures 95, 96, and 97 are SEM micrographs of the spread samples shown in Figure 76 for which the reaction time was five seconds. Comparison of the samples reacted for 80 seconds and those reacted for 5 seconds show that the width of both the η and the ε phases are indeed a function of reaction time. Zakravsek (26) has suggested that the η phase is initially much larger in thickness than the ε phase. Subsequently, due to solid state diffusion, the ε phase grows at the expense of the tin-rich η phase. Comparison of aged versus unaged samples does not demonstrate significant growth of the ε phase at the expense of the η phase.

The data presented in this study is consistent with the theory suggested by Blum, Pelissier, and Silvestre which requires a tin-rich advancing interface. The rate of dissolution of copper into the solder mass appears to create a competing reaction for tin; when the dissolution rate of copper is high a stable value is attained in the solder mass with the formation of Cu_6Sn_5 intermetallic compounds, which also competes for tin. Intermetallic compound formation reduces the availability of tin to the advancing interface and thereby reduces the area of spread which is obtained. Area spread tests made with a 50/50 solder, as shown in Figure 83 (50 w/o Sn - 50 w/o Pb), resulted in spread areas slightly larger than spreads of the 60/40 solder. These data suggest that the reduced spread area obtained with the antimonial solder is not a direct result of a lower tin content.

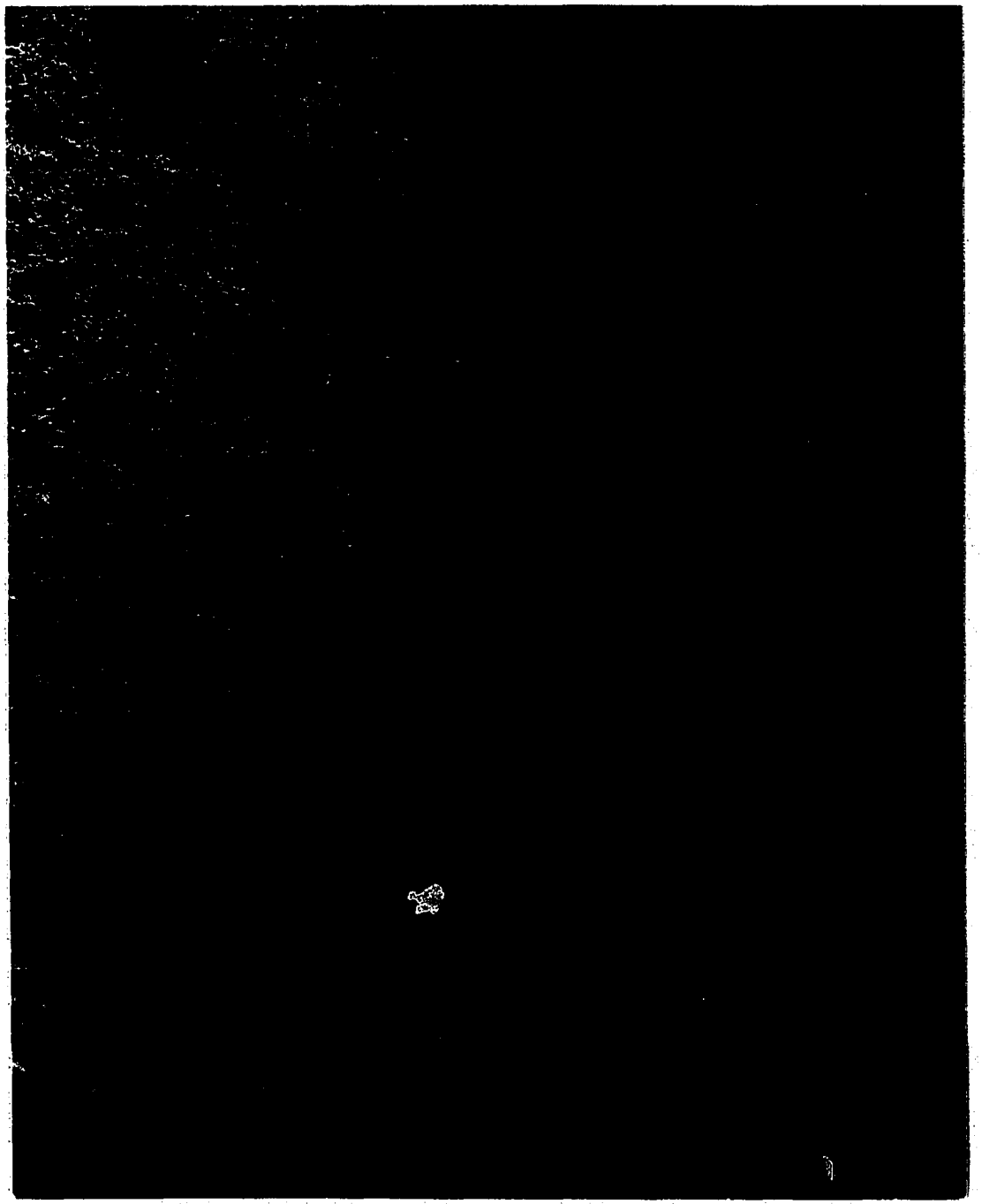

Figure 95. 140X - Peroxide and Nital (2%) Etch
The 60/40 area spread sample shown in Figure 76 after etching. Comparison with Figure 84 indicates that the width of the various bands have changed. The reaction time at 215°C was 5 seconds.

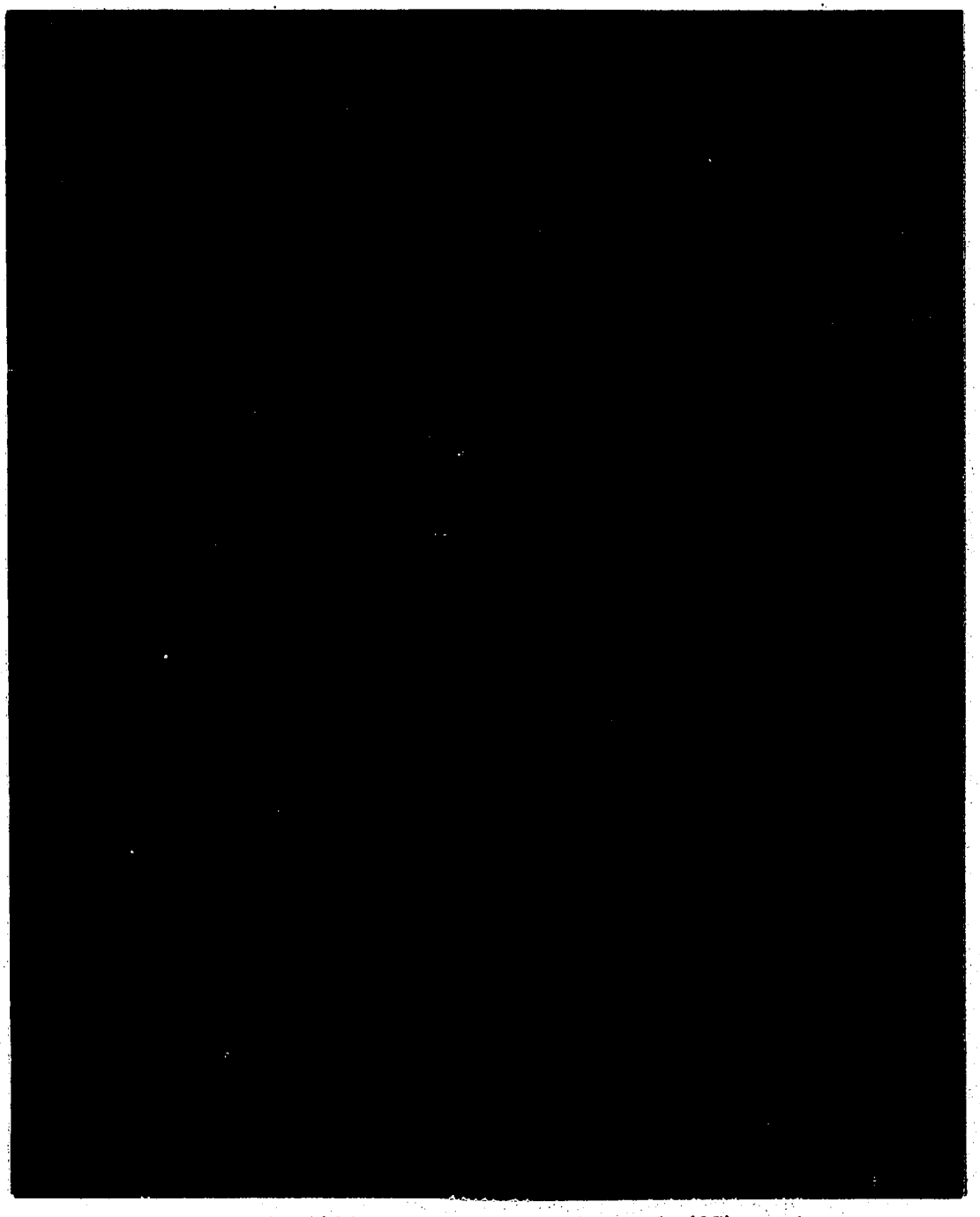

Figure 96. 420X - Peroxide and Nital (2%) Etch
The 63/37 area spread sample shown in Figure 76 with a reaction time of 5 seconds at 215°C. A comparison with Figure 89 indicates the effect of reaction time.

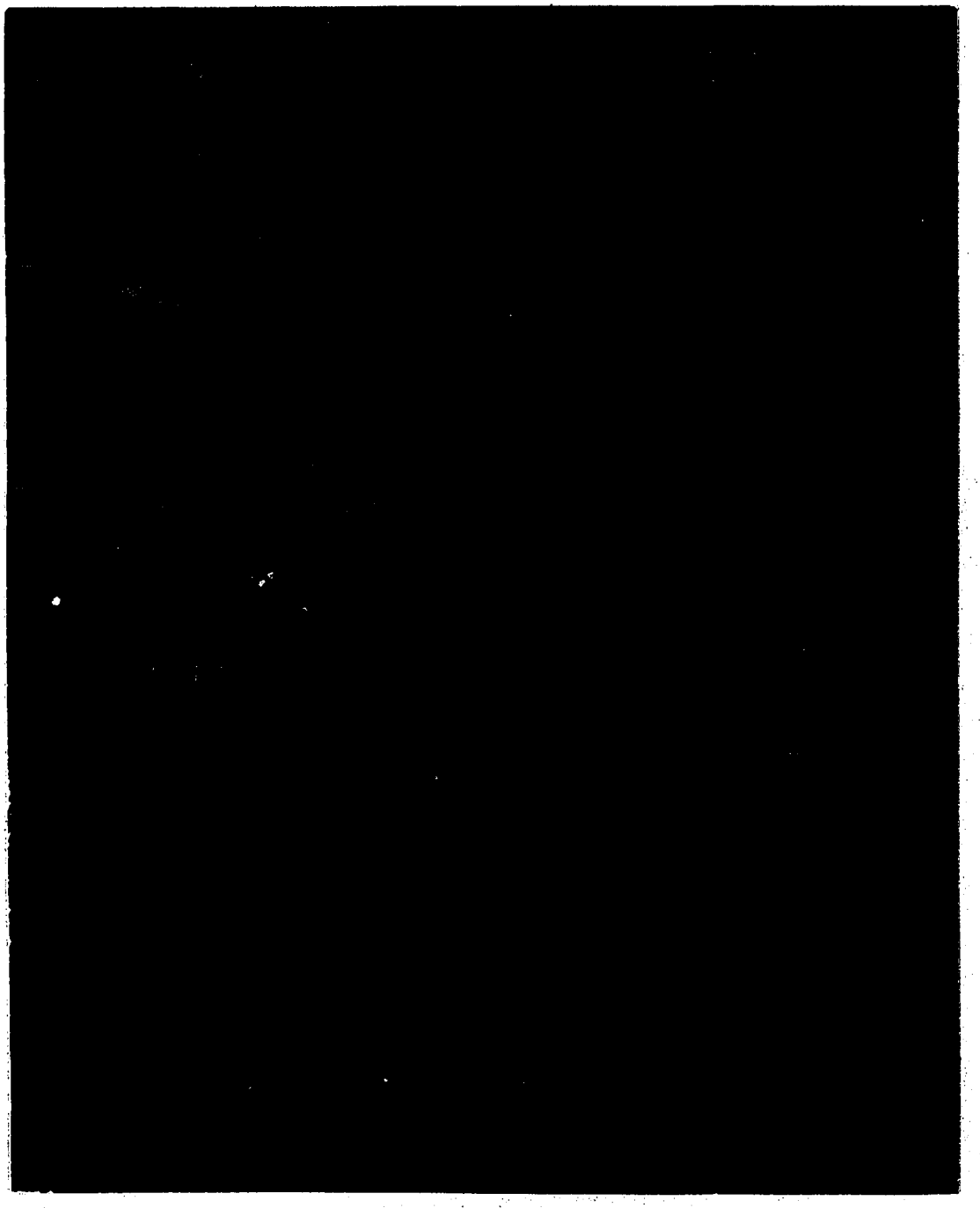

Figure 97. 420X - Peroxide and Nital (2%) Etch
The antimonial area spread sample shown in Figure 76 with a reaction time of 5 seconds at 215°C. A comparison with Figure 93 indicates the effect of reaction time.

The area spread test samples shown in Figure 78 of the various solders applied to fluxed brass substrates were etched in peroxide and in the 2% nital solution. Again, the results were unexpected as duplex interfaces and differing nodular bands were formed. Figures 98 and 99 are SEM micrographs of the 60/40 alloy applied to brass. The outer band of the advancing interface was composed of approximately 53 w/o Cu - 7 w/o Zn - 40 w/o Sn. Figures 100 and 101 are SEM micrographs of the 63/37 alloy. The advancing front is composed of two distinct bands. The outermost band had the composition 58 w/o Cu - 8 w/o Zn - 34 w/o Sn and the inner layer consisted of 55 w/o Cu - 8.2 w/o Zn - 36.8 w/o Sn. The nodules which appear to be compounds had the composition 40 w/o Cu - 3 w/o Zn - 57 w/o Sn. Figure 102 is an SEM micrograph of the antimonial alloy applied to brass. The outer band was composed of 51 w/o Cu -10 w/o Zn - 39 w/o Sn. The nodular inner band had the composition of 38 w/o Cu - 1.5 w/o Zn - 60.5 w/o Sn. This nodular region appears similar to the corresponding band which formed when soldering to copper.

Kay and MacKay [27] have obtained results from studying the reactions of tin on brass which indicated a duplex interface and an intermetallic region. Kay and MacKay have referred to the outermost region of the advancing solder interface as a pink layer which corresponded to the composition of (β) brass - 53.1 w/o Cu - 46.9 w/o Zn. They also refer to a layer (I) near the interface having a composition of 46.2 w/o Cu - (27.5 - 40.6) w/o Zn - (26.3 - 13.2) w/o Sn. The intermetallic region was of the composition 41.2 w/o Cu - 3.3 w/o Zn - 55.5 w/o Sn, and referred to as layer (II). The results reported here suggest that a duplex interface does form; however, the composition is

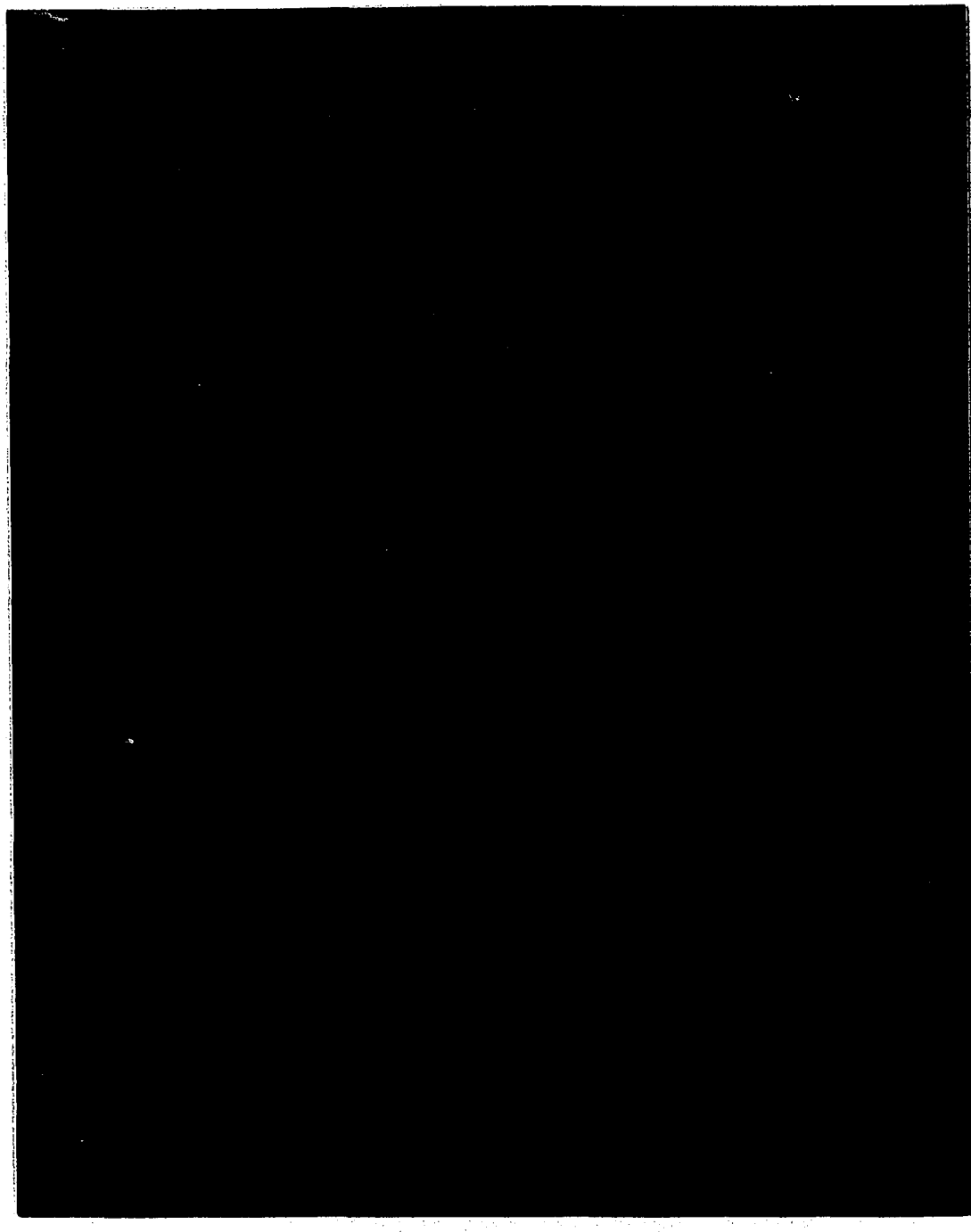

Figure 98. 2800X - Peroxide and Nital (2%) Etch
The 60/40 area spread sample shown in Figure 78 after etching. The diffusion and intermetallic bands present were produced on brass with a reaction time of 80 seconds.

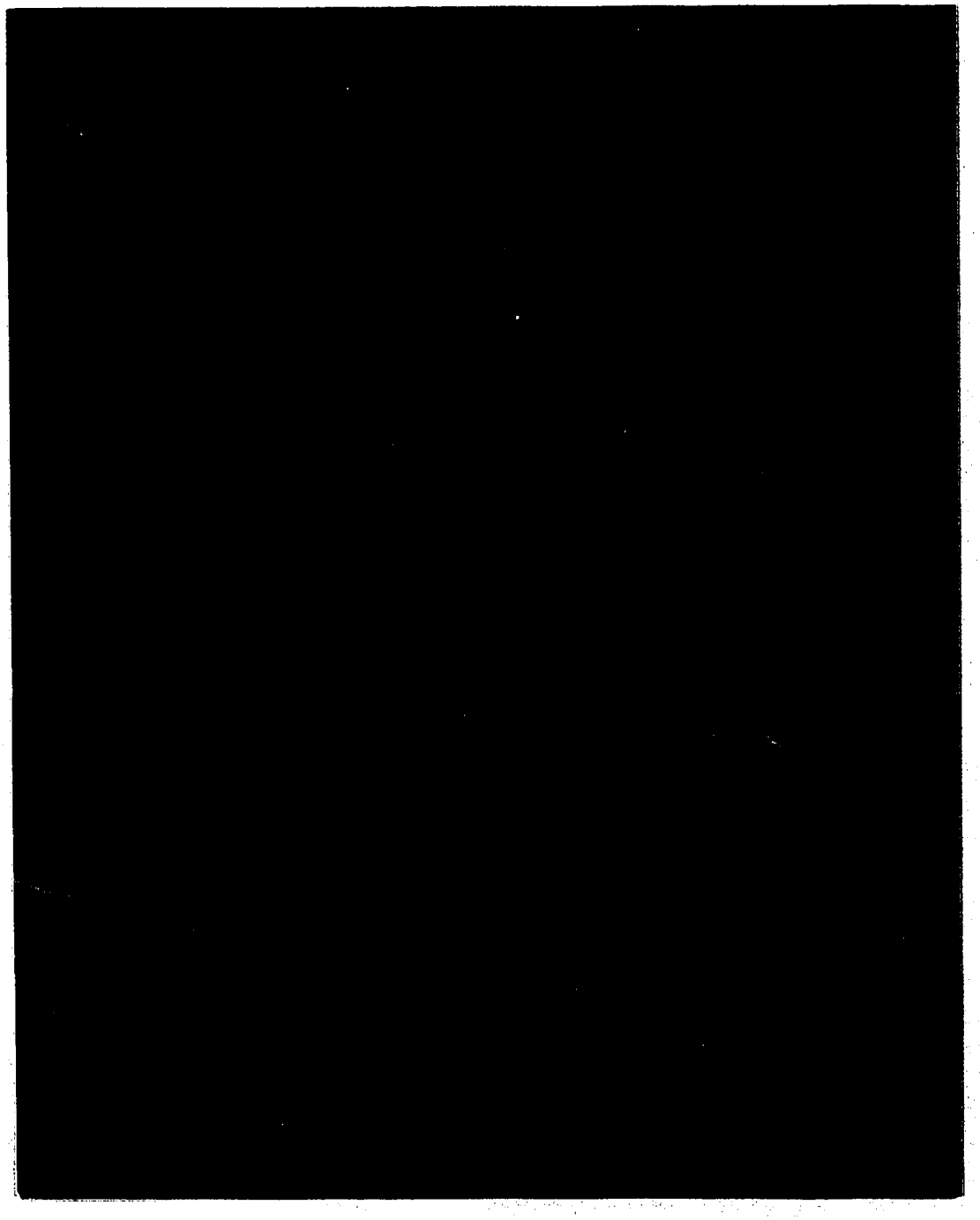

Figure 99. 5600X - Peroxide and Nital (2%) Etch
A detailed view of the intermetallic
and diffusion bands shown in Figure 97.

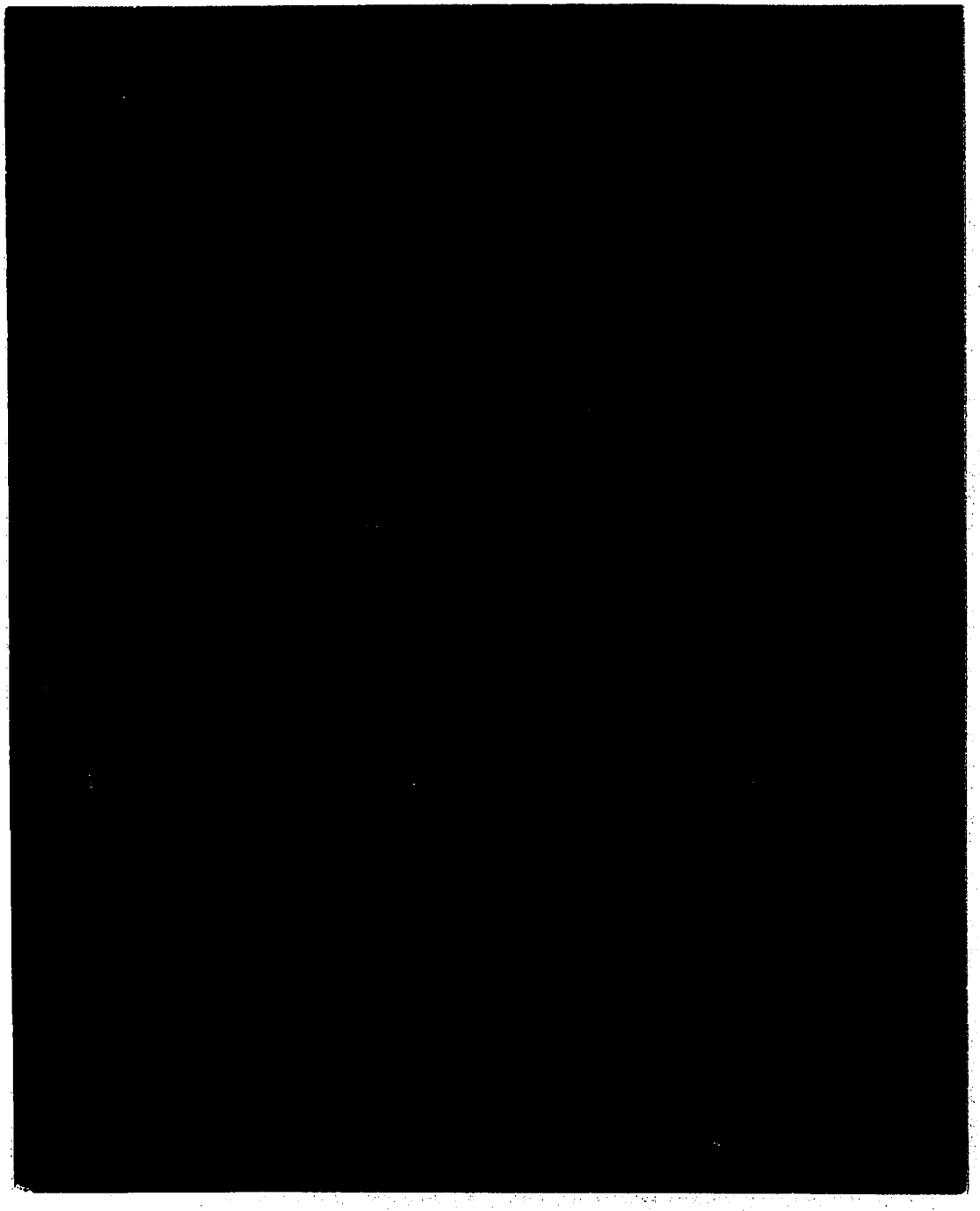

Figure 100. 1800X - Peroxide and Nital (2%) Etch
The 63/37 area spread sample on brass shown in Figure 78 after etching. The diffusion band is seen as two distinct regions.

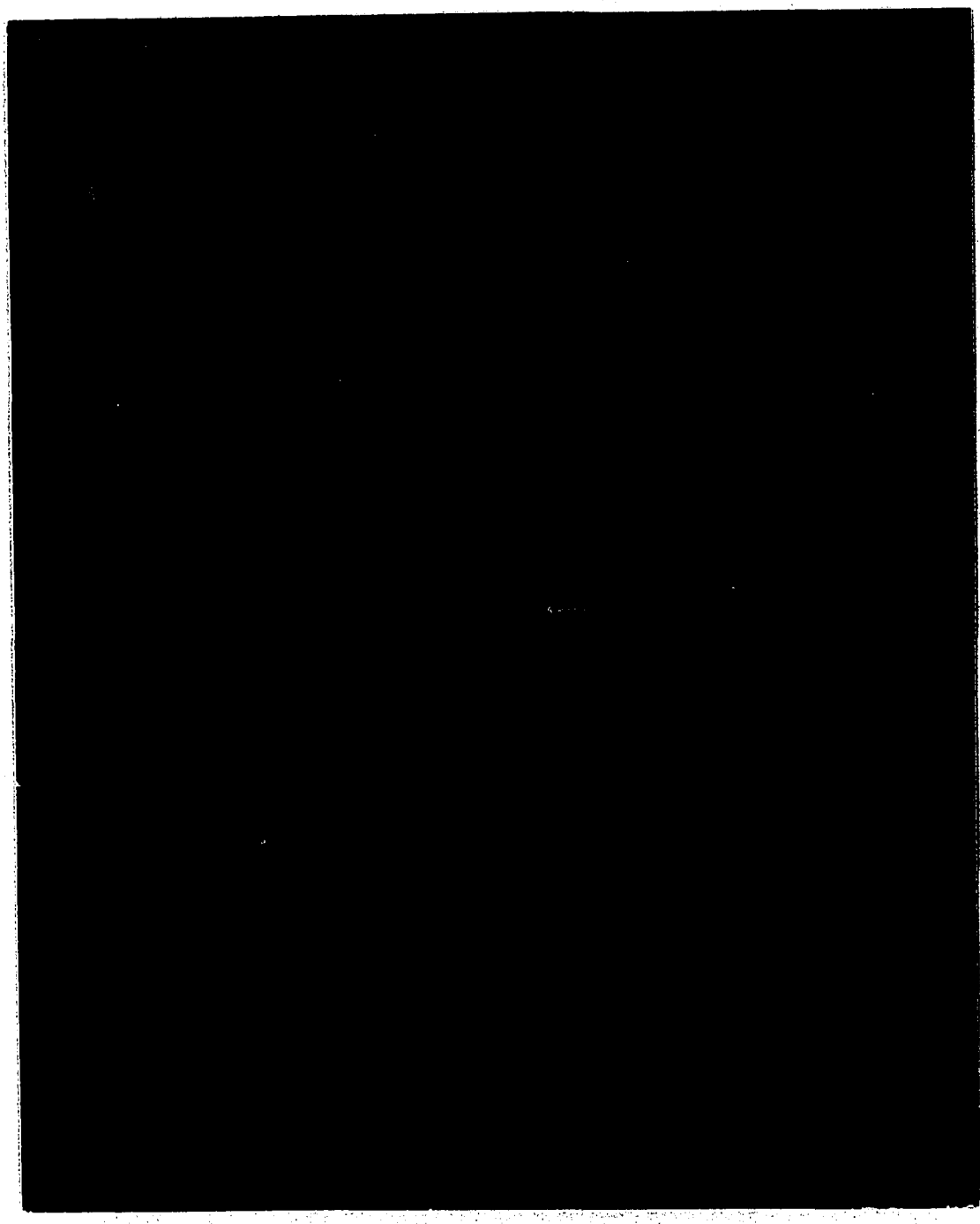

Figure 101. 3500X - Peroxide and Nital (2%) Etch
A more detailed view of the diffusion and intermetallic bands as shown in Figure 100. Two distinct regions in the diffusion band are clearly evident with the innermost band containing greater quantities of zinc.

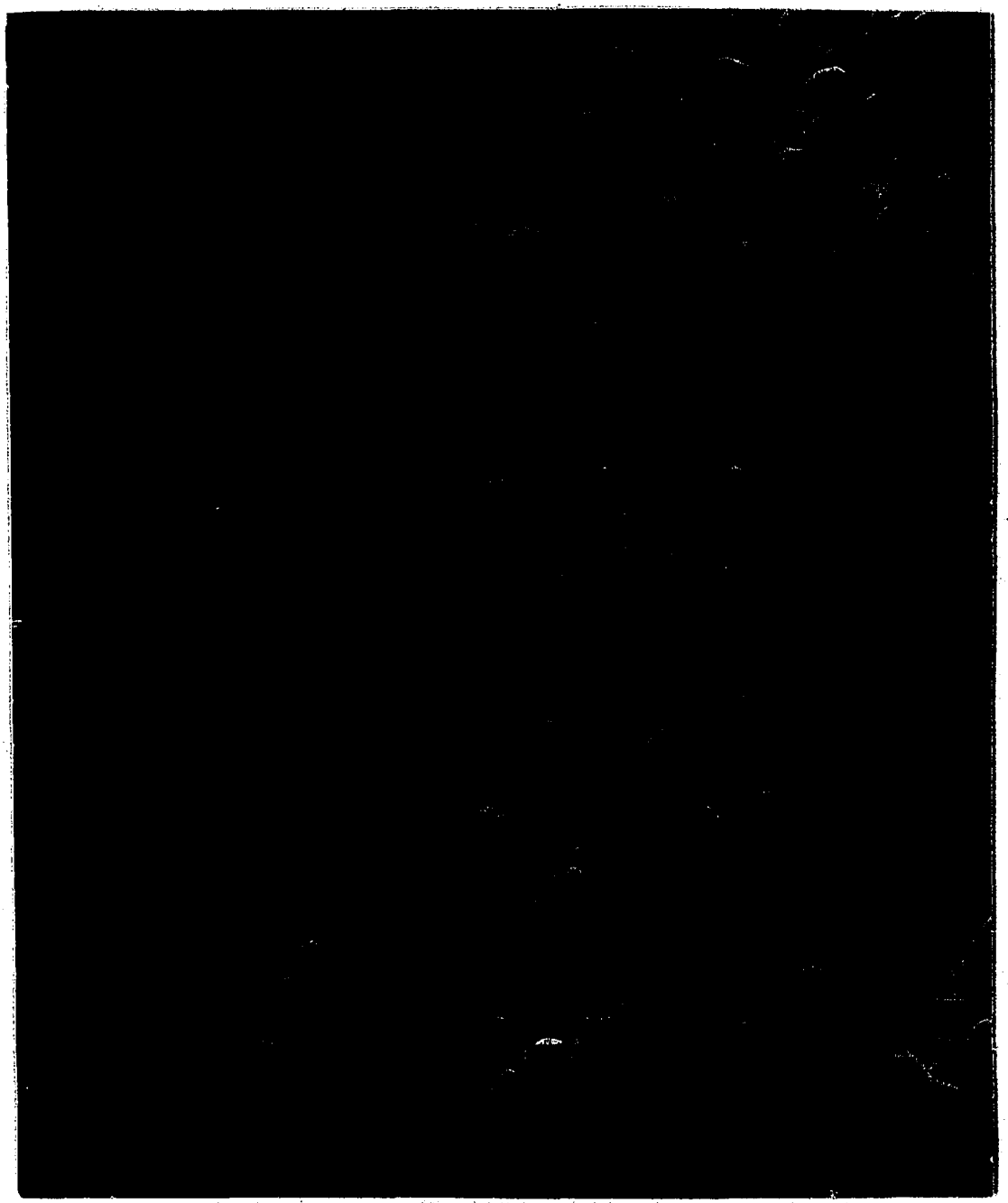

Figure 102. 1400X - Peroxide and Nital (2%) Etch
The antimonial area spread sample of Figure 78 after etching. The diffusion band (left) and the intermetallic band (right) are shown in detail. The structure of the intermetallic band is similar to the structure of the intermetallic bands which formed on copper.

not consistent with the findings of Kay and MacKay. The duplex interface was easily observed with 63/37 solder and difficult to observe with 60/40 solder. The width of the duplex interface was greater with 63/37 solder and, upon aging of the spread samples, the duplex layer in the 63/37 solder disappeared in favor of a continuous layer. The width of this continuous layer was equivalent to the width of the duplex layer before aging. The composition of this single layer was 56.30 w/o Cu - 8.54 w/o Zn - 35.16 Sn and is similar to the ε phase of copper-tin, but with incorporation of zinc into the structure. The innermost layer did not exhibit compositional changes or grow in width upon aging. This layer is similar to the η phase of copper-tin with zinc incorporation; having a composition of 39.73 w/o Cu - 2.73 w/o Zn - 57.54 w/o Sn. Comparison of the respective micrographs clearly indicates a difference in the crystal form of the η phases formed in solders applied to copper and brass.

The nature of the advancing solder interface formed on gold substrates was briefly examined. Figure 103 shows the boundary between a 60/40 solder mass and the substrate metal. Massive $AuSn_4$ intermetallic compound formation occurs close to the solder substrate boundary. Some detachment due to dewetting is also noted (adjacent to the large flat particle near the center of the photograph). Figure 104 indicates the various structures formed in the interface of the gold and advancing solder. Figure 105 reveals the interface and compounds which develop when the 60/40 solder was applied to gold. Near the right side of Figure 105 a different crystal structure is noted. EDS analysis confirmed these structures to correspond to the composition of $AuSn_2$.

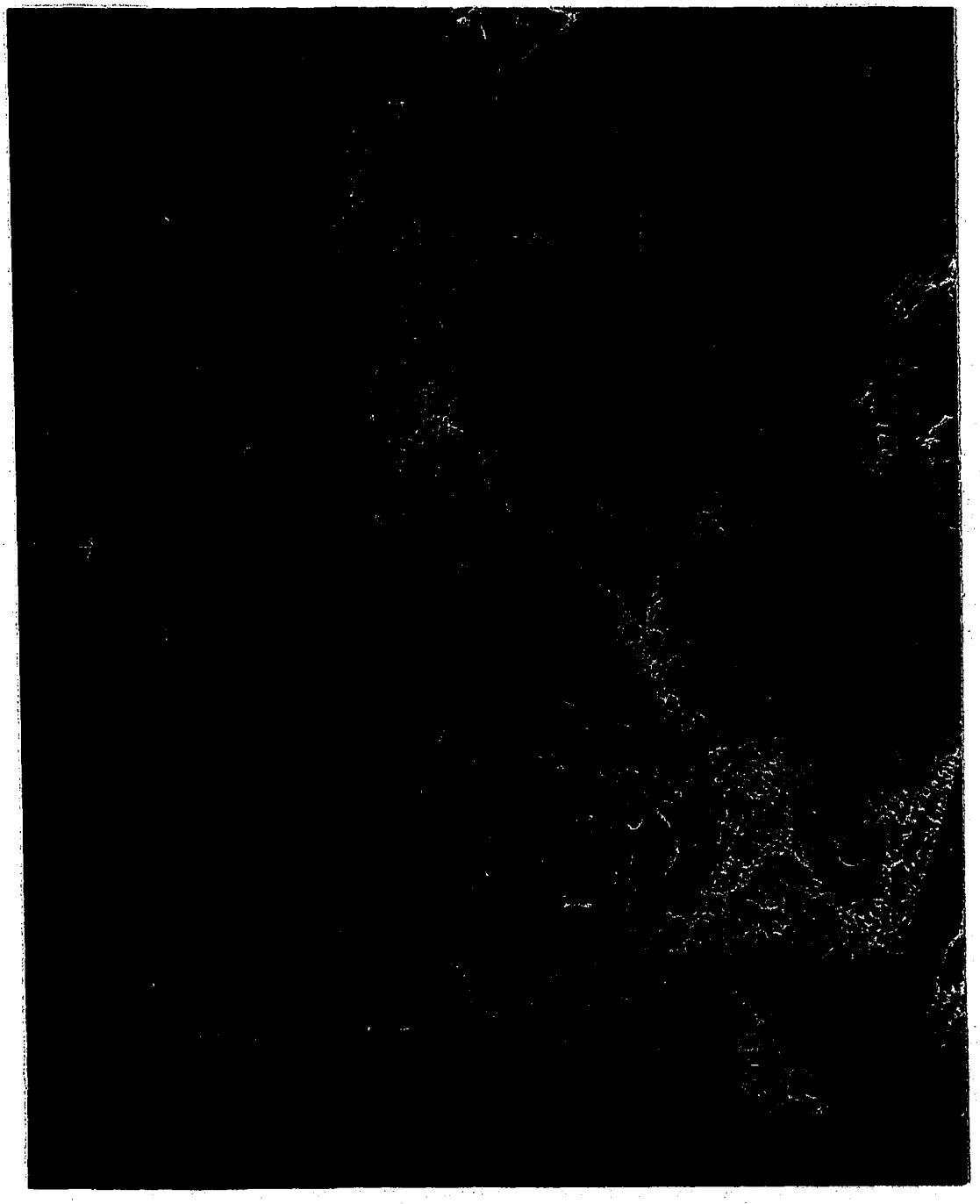

Figure 103. 420X - Peroxide and Nital (2%) Etch
The 60/40 area spread sample shown in Figure 80 after etching. Massive $AuSn_4$ intermetallic compound formation near the solder substrate boundary is evident.

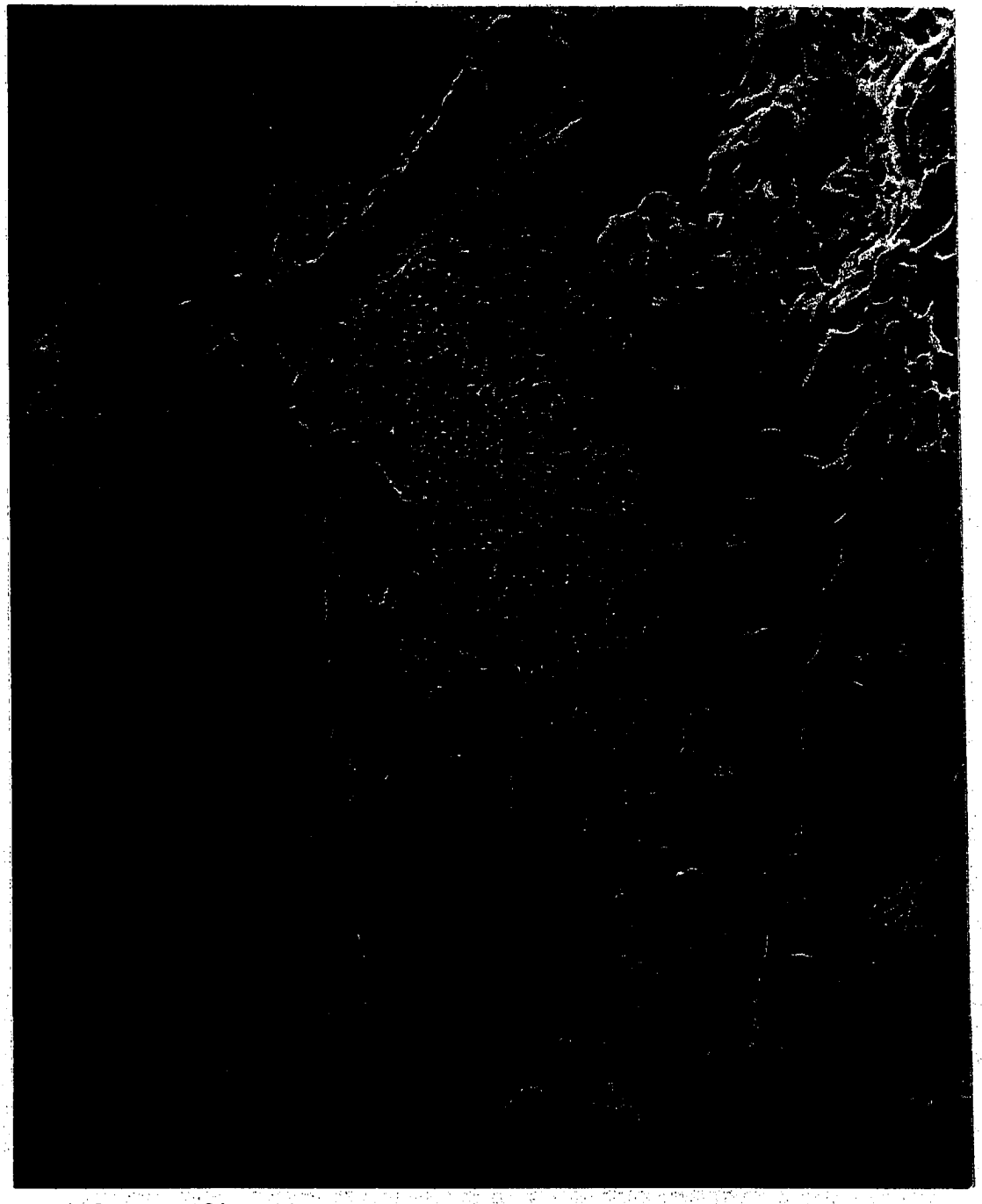

Figure 104. 840X – Peroxide and Nital (2%) Etch
A detailed view of the compounds and interface which developed when 60/40 solder was applied to a gold plated substrate.

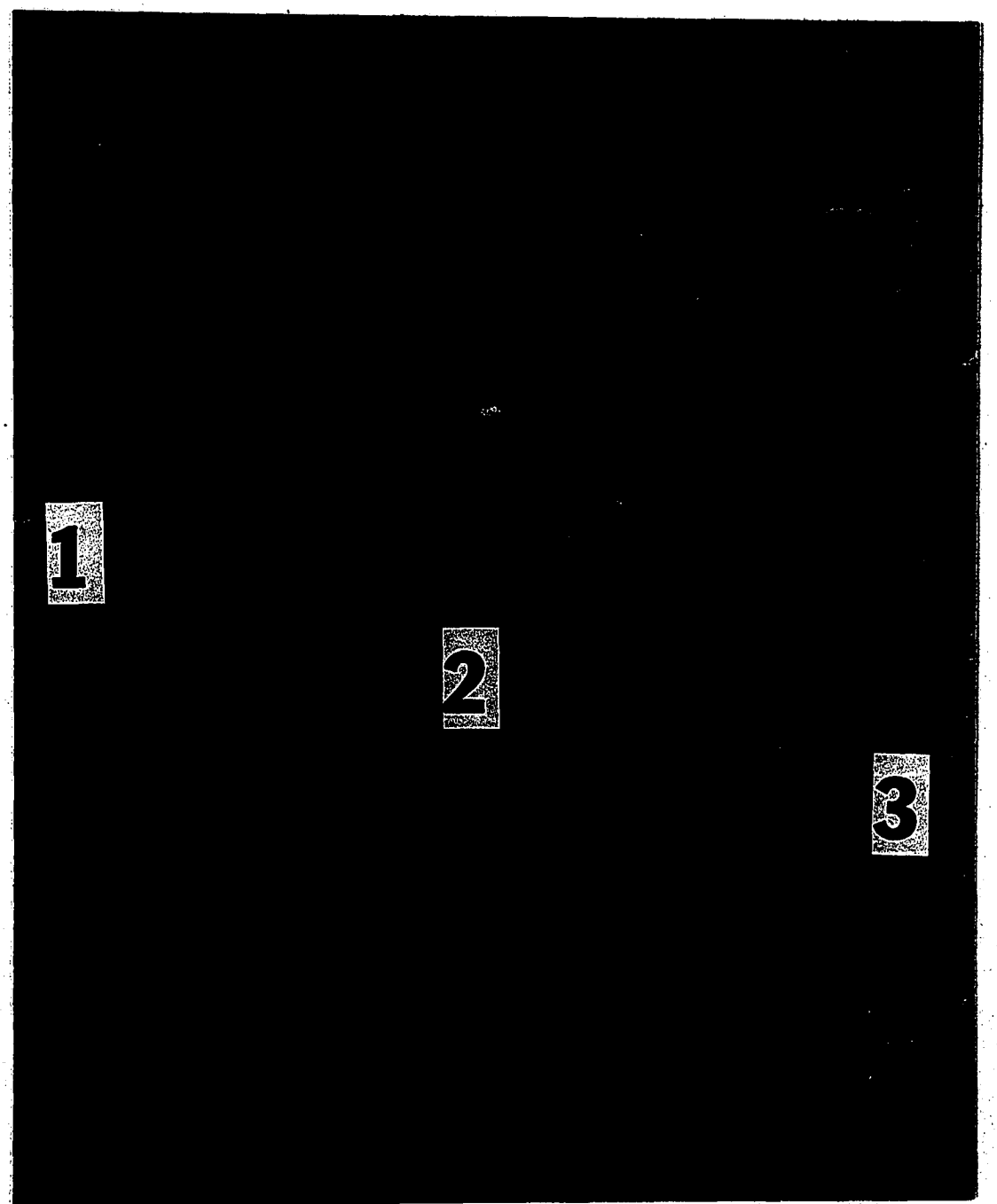

Figure 105. 2800X - Peroxide and Nital (2%) Etch
A detailed view of the ζphase (1), the AuSn compounds (2) and the $AuSn_2$ compounds (3).

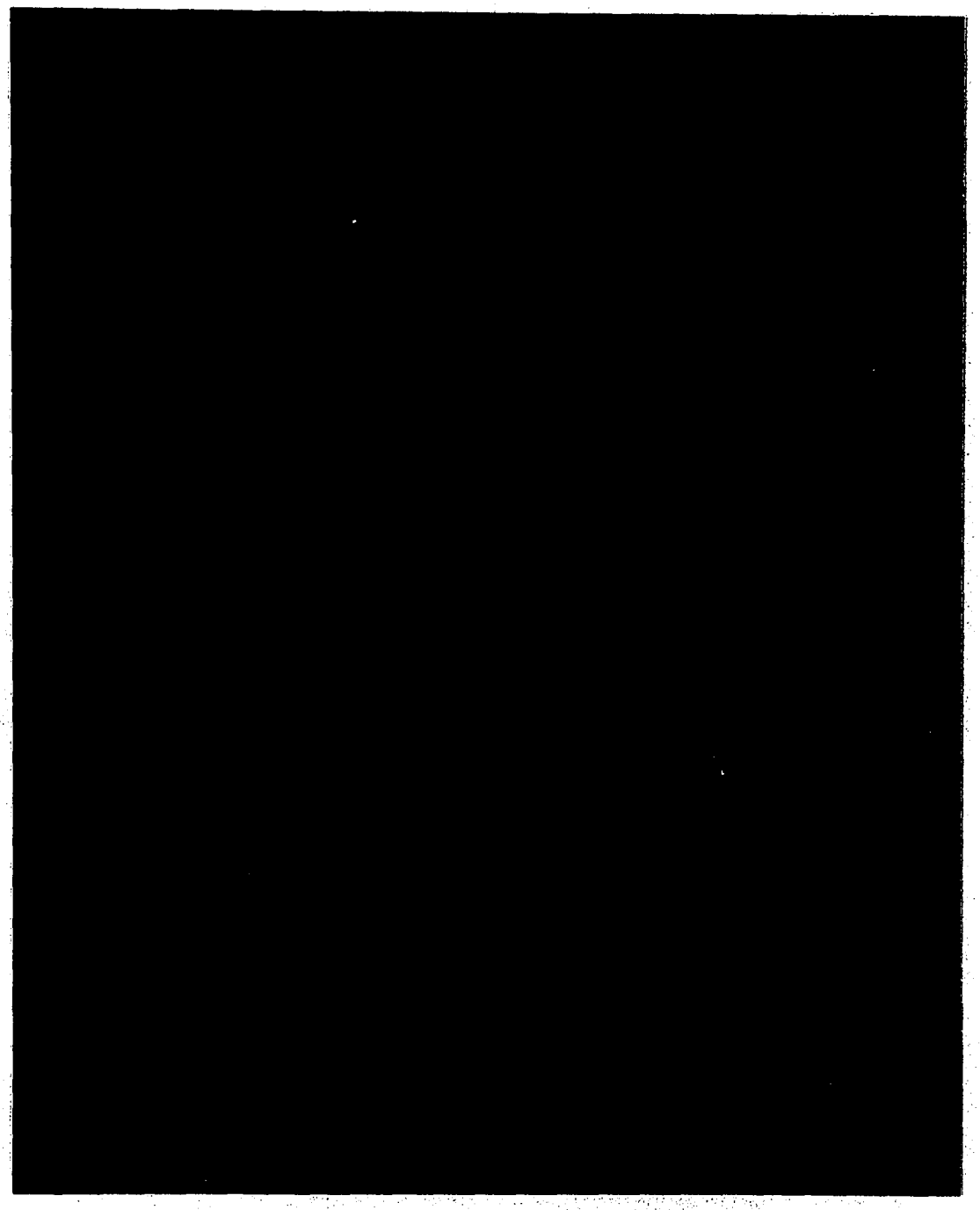

Figure 106. 8400X - Peroxide and Nital (2%) Etch
A detailed view of an area shown in Figure 105 with the AuSn compounds on the left and the $AuSn_2$ compounds on the right.

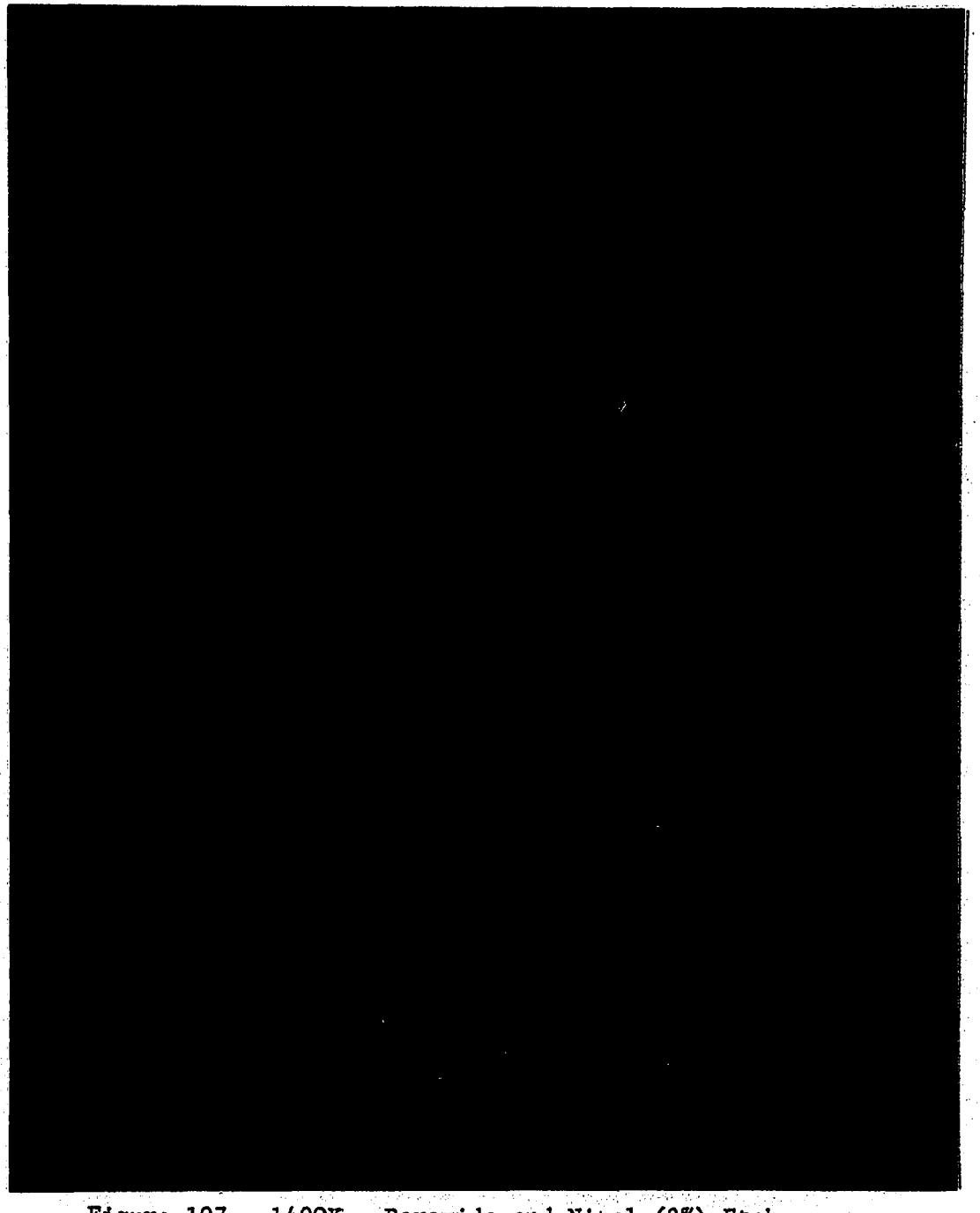

Figure 107. 1400X - Peroxide and Nital (2%) Etch Massive $AuSn_4$ compounds which formed in the solder mass.

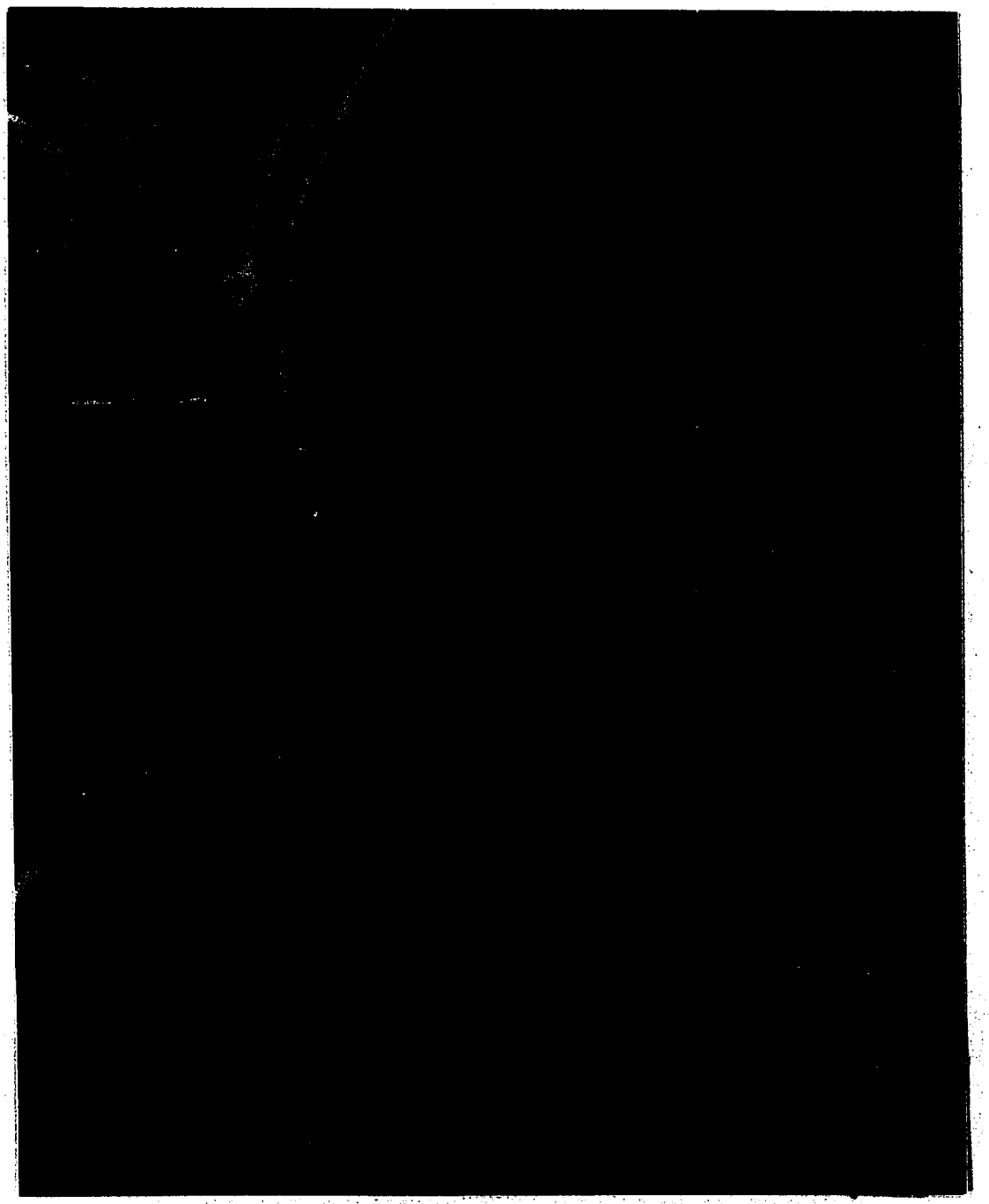

Figure 108. 12600X - Peroxide and Nital (2%) Etch
A detailed view of the $AuSn_4$ plate like structure as shown in Figure 107.

The structures noted in the center of Figure 105 were analyzed and they corresponded to the composition of AuSn. Figure 106 reveals the $AuSn_2$ compounds which formed between the massive $AuSn_4$ and AuSn compounds in the solder mass and the AuSn compound layer. The most advanced layer of the interface corresponded to the ζ phase as shown in the AuSn phase diagram. Figures 107 and 108 reveal the massive $AuSn_4$ which forms in the solder mass.

CHAPTER IV

CONCLUSIONS

The studies reported here indicate that the formation of intermetallic compounds within soldered connections is a common phenomenon which must be considered in all soldering applications. The ability of tin (as a principle solder component) to form significant quantities of intermetallic compounds in practical industrial applications is not limited to its interactions with copper and gold, but extends to nickel, silver, platinum, and palladium substrates. In addition, the interaction of tin with impurities such as iron and arsenic has also been shown to result in intermetallic compound formation. The appearance of intermetallic compound layers which form at the solder substrate boundary, has been documented and the morphology of isolated compound particles is also presented. Recognition of the microstructural appearance of the various intermetallic compounds is obviously important to analysis of failures which can result from either excessive amounts or unsatisfactory distribution of these compounds.

The substitution of antimony for tin may also result in unexpected intermetallic compound formation. Even though the formation of the solder alloy may be appropriate to achieve solid solubility of antimony within

the tin portion of the ternary alloy, conditions will change as the solder reacts with the substrate. Depletion of tin from the solder through the formation of tin-substrate compounds has been shown to result in saturation of the solder mass with respect to the tin-antimony intermetallic compound.

The formation of zinc-antimony intermetallic compounds was not observed in antimonial solders applied to brass substrates by commercial soldering processes. However, the zinc-antimony intermetallic compound was formed when the ternary alloy was applied to pure zinc substrates.

The use of gold plated substrates for soldering applications presents special problems involving the phenomena of dewetting and porosity. Dewetting has been conclusively shown to involve the formation of continuous layers of gold-tin intermetallic compounds at the solder-substrate interface. These layers are particularly susceptible to separation from the substrate because of their brittle character. In addition to disbonding during straining of the substrate, there is some evidence that separation of solder from gold plated substrates will occur spontaneously upon cooling from the soldering temperatures. Here the cause most probably involves large differences in the thermal expansion properties of the compound and substrate. This latter process may explain why gold plated substrates are sensitive to dewetting and copper substrates are not. Both will form massive interfacial compound layers. However, the copper-tin intermetallic compound does not readily detach.

The experiments demonstrate the fundamental reasons for the dependence of joint reliability on gold plating thickness. As more gold becomes available to the molten solder pool, the probability of massive gold-tin compound formation at the solder-substrate interface greatly increases and the reliability of the finished joint is proportionally reduced. This problem can be controlled to some extent by minimizing the thickness of the gold plating and allowing sufficient time at the soldering temperature to assure complete dissolution of the gold plating from the substrate. However, the implications of this relationship are particularly important in microelectronic circuit applications where the size of the solder joint must be reduced as far as possible. The results indicate that there is a practical limit on the size of a reliable soldered connection which can be achieved on a substrate plated with any given thickness of gold.

The association of porosity with thick, hard gold plated substrates has also been demonstrated. Porosity appears to result from the decomposition of a codeposited polymer in the heated solder pool. Direct evidence of the polymer is also presented.

The processes by which molten solder wets and spreads on a substrate metal is greatly complicated by the processes of intermetallic compound formation. Wetting involves dissolution of the substrate in the molten solder and dissolution of the solder components in the solid substrate. With each of these processes the solubility limits of various intermetallic compounds will generally be exceeded and the compounds will form. In the cases of the two most common substrate materials, copper and gold, common soldering temperatures are significantly

lower than the temperatures at which the room temperature stable compounds form. Consequently, solid intermetallic compounds are predicted in the molten solder masses as well as at the solder-substrate interfaces.

The current use of tin in soft solders represents a compromise between cost, wettability, low melting temperatures and its disposition toward intermetallic compound formation with common substrate materials. However, one can foresee applications in which the balance will no longer favor the simple traditional solder formulations. It would appear that alloy additions will be required to suppress undesirable reactions in solder to meet the demands of newly developing circuit technologies. It seems very likely that a great renewal of interest in solder alloy development is imminent.

LIST OF REFERENCES

1. Thwaites, C. J., Soft Soldering Handbook, Middlesex, England: Inter. Tin Res. Inst., Publ. No. 533, 1977.

2. Gerth, D., "Microprobe Studies of the Constitution of Diffusion Layers in Soft-Soldered Copper," Metall., Vol. 24, pp. 838-846, Aug. 1970.

3. Bader, W. G., "Dissolution and Formation of Intermetallics in the Soldering Process," Proc. Symp. on Phys. Metallurgy of Metal Joining, Oct. 1978.

4. Saperstein, Z. P., "The Reaction of Lead-Tin Solders with Copper Alloys," Weld. Jour., Vol. 2, pp. 80s-85s, Feb. 1969.

5. Manko, H. H., Solders and Soldering, New York's McGraw Hill, pp. 130-131, 1964.

6. Bailey, G. L. and Watkins, H. C., "The Flow of Liquid Metals on Solid Metal Surfaces and its Relation to Soldering, Brazing and Hot-Dip Coating," Jour. Inst. Metals, Vol. 80, pp. 57-76, 1952-53.

7. Gangulee, A.; Das, G. C.; and Bever, M. B., "An X-Ray Diffraction and Calorimetric Investigation of the Compound Cu_6Sn_5," Metall. Trans., Vol. 4, pp. 2063-2066, Sept. 1973.

8. Hansen, M., Constitution of Binary Alloys, New York: McGraw Hill, pp. 633-638, 1958.

9. Selected Values of the Thermodynamic Properties of Binary Alloys, American Society for Metals, Metals Park, Ohio, pp. 320-328, 1973.

10. Hansen, M., Constitution of Binary Alloys, New York: McGraw Hill, pp. 1141-1143, Ref. 12, 1958.

11. Metals Handbook, 8th Edition, Metallography, Structures and Phase Diagrams, A.S.M., Metals Park, Ohio, Vol. 8, p. 370, Ref. 2, 1974.

12. Metals Handbook, 8th Edition, Metallography, Structures and Phase Diagrams, A.S.M., Metals Park, Ohio, Vol. 8, p. 362, Ref. 2, 1974.

13. Thwaites, C. J., "Soft Solders and Soldering in the Electrical Industry," Inter. Tin Res. Inst., Publ. No. 387, 1968.

14. Duckett, H. R. and Ackroyd, M. L., "The Influence of Solder Composition on the Embrittlement of Soft-Soldered Joints on Gold Coatings," Electroplating and Metal Finishing, Vol. 29, pp. 13-20, May 1976.

15. Brewer, D. H., "Solders for Thick Gold Plating," Weld. Jour., Vol. 49, pp. 465s-470s, Oct. 1970.

16. Ainsworth, P. A., "Soft Soldering Gold Coated Surfaces," Gold Bulletin, Vol. 4, pp. 47-50, March 1971.

17. Bader, W. G., "Dissolution of Au, Ag, Pd, Pt, Cu, and Ni in a Molten Tin-Lead Solder," Weld. Jour., Vol. 48, pp. 551s-557s, Dec. 1959.

18. Thwaites, C. J., "Some Aspects of Soldering Gold Surfaces," Electroplating and Metal Finishing, Vol. 26, pp. 10-14 and pp. 21-26, Aug.-Sept. 1973.

19. Munier, G. B., "Polymer Codeposited with Gold During Electroplating," Plating, Vol 56, pp. 1151-1157, Oct. 1969.

20. Holt, L. and Stanyer, J., "Carbon Inclusion in Gold Electroplate," Trans. Inst. Met Fin., Vol. 50, pp. 24-27, Jan. 1972.

21. Antler, M.; Cohen, R. L.; and West, K. W., "Search for Gold Cyanide Inclusions in Cobalt-Hardened Gold Electrodeposits," J. Electrochem. Soc., Vol. 124, pp. 342-345, March 1977.

22. Harding, W. B. and Pressly, H. B., Tech. Proc. Am. Electroplaters Soc., Vol. 50, pp. 90-106, 1963.

23. Wassink, R. J., "Wetting of Solid-Metal Surfaces by Molten Metals," Jour. Inst. Metals, Vol. 95, pp. 38-43, 1967.

24. Okamoto, I.; Omori, A.; Miyake, M.; and Kihara, H., "Studies on Flux Action of Soldering," Trans. JWRI, Vol. 2, pp. 226-239, Feb. 1973, Vol. 3, pp. 99-109, Jan. 1974.

25. Blum, P. L.; Pelissier, J.; and Silvestre, G., "An Investigation of Soldered Copper-Tin Bond Brittleness by Electron Microscopy," Solid State Technology, Vol. 16, pp. 55-58, March 1973.

26. Zakraysek, L., "Intermetallic Growth in Tin-Rich Solders," Weld. Jour., Vol. 51, pp. 536s-541s, Nov. 1972.

27. Kay, P. J. and MacKay, C. A., "The Growth of Intermetallic Compounds on Common Basis Materials Coated with Tin and Tin-Lead Alloys," Trans. Inst. Met. Fin., Vol. 54, pp. 68-74, 1976.

APPENDIX A

BINARY PHASE DIAGRAMS

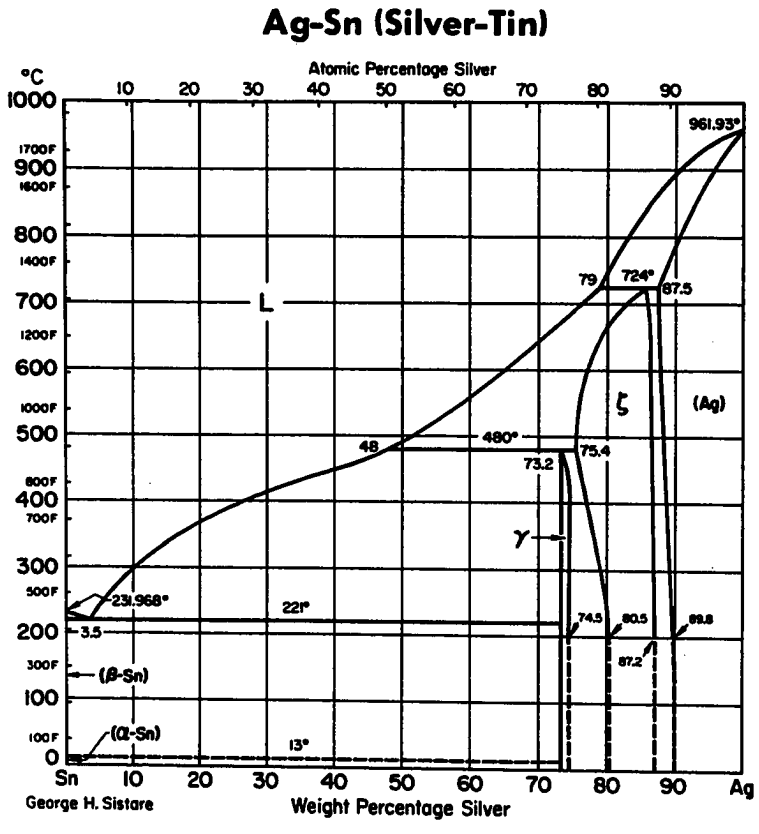

Ag-Sn (Silver-Tin)

By GEORGE H. SISTARE

The diagram is from Hansen (Gen Ref 3). Crystal-structure data are from Pearson (Gen Ref 2):

Phase	Formula	Symmetry	Symbol	Prototype
γ	ζ Ag-Sn	hcp	*A3*	Mg
ζ	γ Ag_3Sn	ortho	...	...

Figure A-1. Silver-Tin Phase Diagram
This diagram is from the Metals Handbook, Vol. 8, 8th Edition, pp. 256, 341.

As-Sn Arsenic-Tin

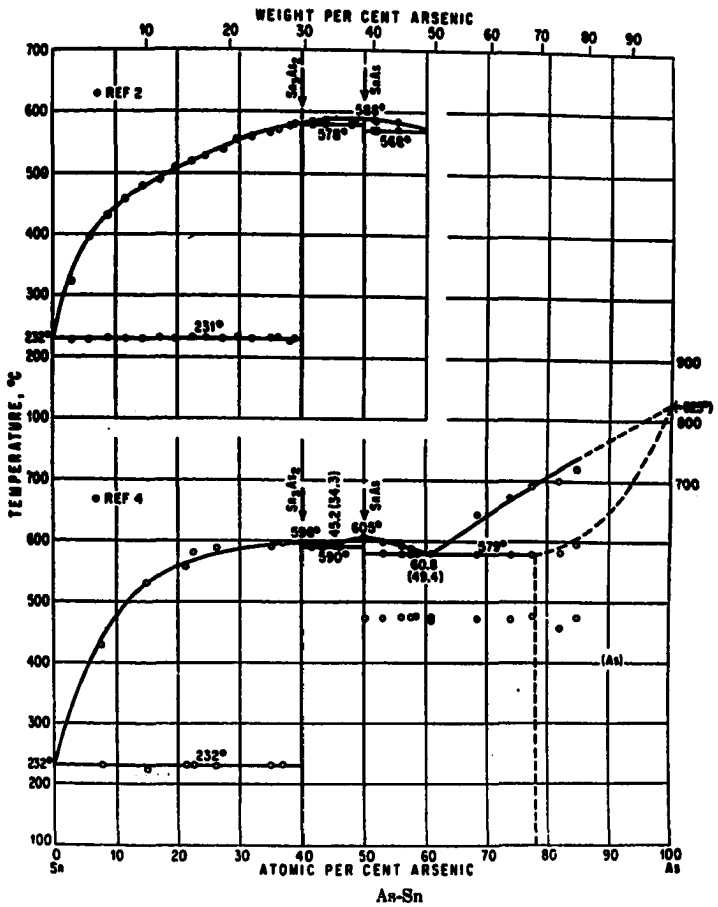

As-Sn (Arsenic-Tin)
By M. Hansen

Formula	Symmetry	Prototype
As_2Sn_3	Rhombohedral	
AsSn	Cubic	NaCl (B1)

Figure A-2. Arsenic-Tin Phase Diagram
This diagram is from the Constitution of Binary Alloys by M. Hansen, 2nd edition, p. 181.

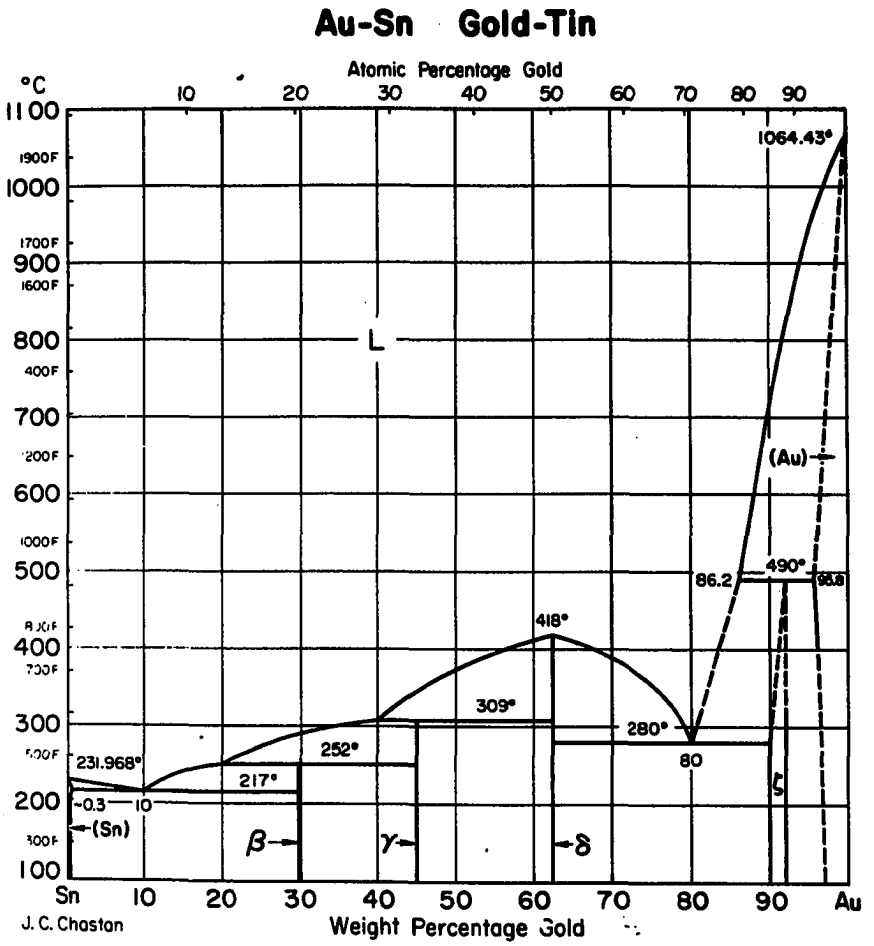

Au-Sn (Gold-Tin)

By J. C. CHASTON

The diagram is from Hansen (Gen Ref 3) and Elliott (Gen Ref 4). The decomposition temperature of the ζ phase was taken from Davies and Leach (1). Crystal-structure data are from Pearson (Gen Ref 2):

Phase	Formula	Symmetry	Symbol	Prototype
β	$AuSn_4$	fco	*D1*$_4$	$PtSn_4$
γ	$AuSn_2$	ortho	...	...
δ	AuSn	hex	*B8*$_1$	AsNi
ζ	ζ Au-Sn	hcp	*A3*	Mg

1. H. A. Davies and J. S. L. Leach, *J Inst Metals*, Vol 96, 1968, p 220-221

Figure A-3. Gold-Tin Phase Diagram
This diagram is from the Metals Handbook, Vol. 8, 8th edition, pp. 269, 347.

Cu-Sn Copper-Tin

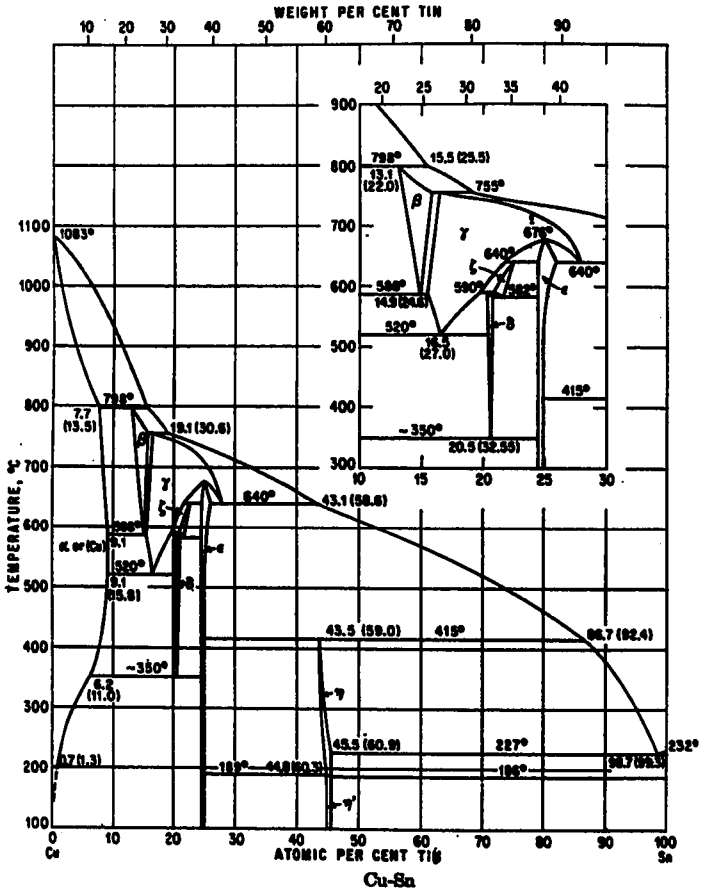

Cu-Sn

Cu-Sn (Copper-Tin)

By Robert E. Johnson

The eutectic composition is from Davey and Happ (1). The remainder of the diagram is from Hansen (Gen Ref 3). Crystal-structure data are from Pearson (Gen Ref 2):

Phase	Formula	Symmetry	Symbol	Prototype
β	...	bcc	*A2*	W
γ	γ Cu_3Sn	fcc	$D0_3$	BiF_3
δ	$Cu_{31}Sn_8$	cu	Like $D8_{1-3}$	γ brass
ε	Cu_3Sn	pseudohex	*A3*	Mg
ζ	$Cu_{20}Sn_6$	trig	...	...
η	...	unknown	...	...
η'	Cu_6Sn_5	hex	$B8_1$	AsNi

1. T. R. A. Davey and J. V. Happ, *Trans Inst Mining Met*, Ser C, Vol 78, 1969, p 108-110

Figure A-4. Copper-Tin Phase Diagram
This diagram is from the Metals Handbook, Vol. 8, 8th edition, pp. 299, 358.

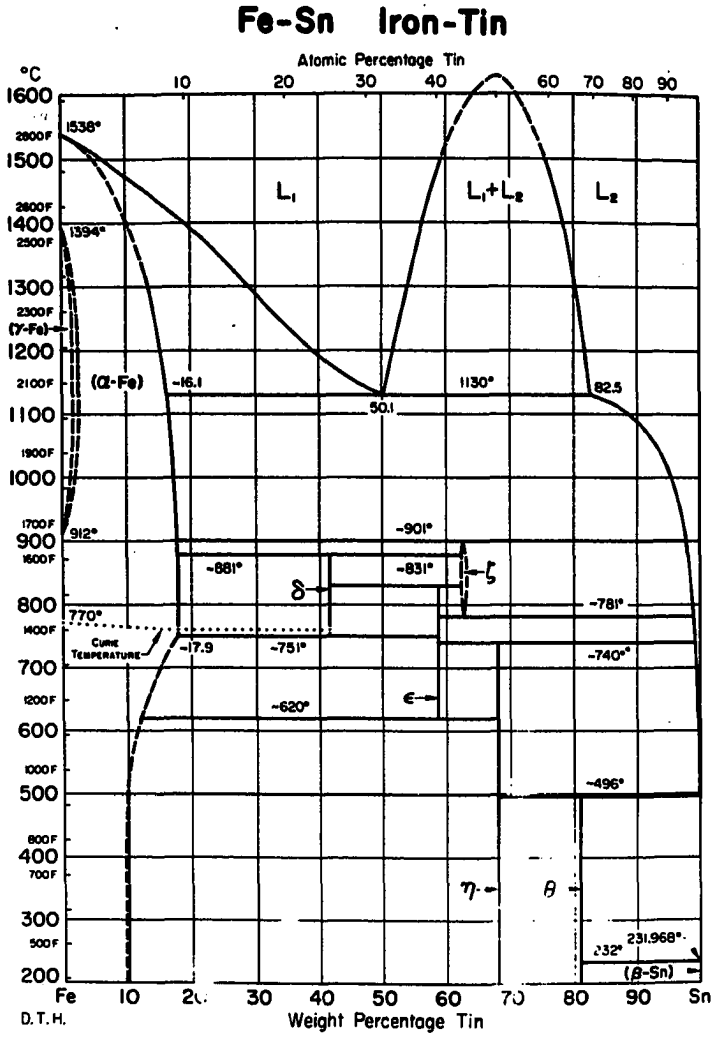

Fe-Sn (Iron-Tin)

By DONALD T. HAWKINS

The diagram is from Hansen (Gen Ref 3), Elliott (Gen Ref 4), and Shunk (Gen Ref 5), with the following exceptions: the miscibility gap is from Shiraishi and Bell (1), and the γ loop is from Davey (2). Crystal-structure data are from Pearson (Gen Ref 2):

Phase	Formula	Symmetry	Symbol	Prototype
δ	Fe_2Sn	hex	$D0_{19}$	Ni_3Sn
ι	Fe_3Sn_2	comp mono	...	...
ζ	$Fe_{1.3}Sn$	hex	$B8_2$	$InNi_2$
η	FeSn	hex	B35	CoSn
θ	$FeSn_2$	bct	C16	Al_2Cu

1. S. Y. Shiraishi and H. B. Bell, *Trans Inst Mining Met*, Ser C, Vol 77, 1968, p 104-105
2. T. R. A. Davey, *Trans Inst Mining Met*, Ser C, Vol 76, 1967, p 66-67

Figure A-5. Iron-Tin Phase Diagram
This diagram is from the Metals Handbook, Vol. 8, 8th edition, pp. 306, 362.

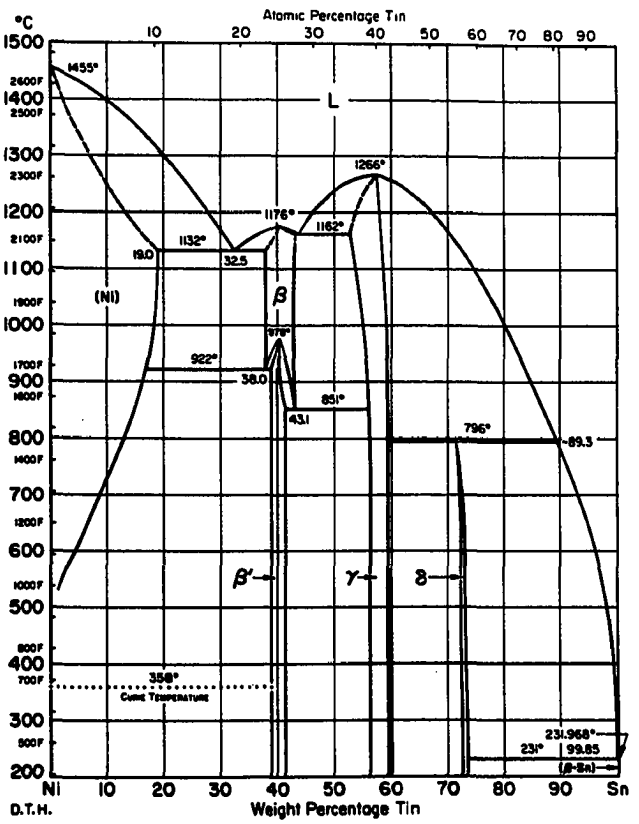

Ni-Sn (Nickel-Tin)

By DONALD T. HAWKINS

The β-β' region is from Panteleimonov, Aziz, Sokolova and Bagdasaryan (1). The remainder of the diagram is from Hansen (Gen Ref 3). Crystal-structure data are from Pearson (Gen Ref 2):

Phase	Formula	Symmetry	Symbol	Prototype
β	Ni_3Sn (HT)	cu	$D0_3$	BiF_3
β'	Ni_3Sn (LT)	hex	$D0_{19}$	Ni_3Sn
γ	$Ni_{1.4}Sn$	hex	$B8_2$	$InNi_2$
δ	δ Ni_2Sn_3	mono	...	...

1. L. A. Panteleimonov, Yu. K. Aziz, I. G. Sokolova and A. K. Bagdasaryan, *Vestn Mosk Univ, Ser II: Khim*, Vol 19, No. 4, 1964, p 49-50

Figure A-6. Nickel-Tin Phase Diagram
This diagram is from the Metals Handbook, Vol. 8, 8th edition, pp. 325, 370.

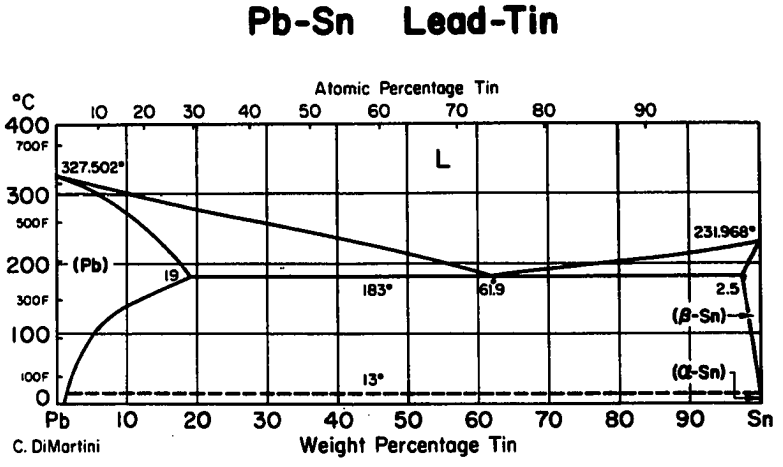

Pb-Sn (Lead-Tin)

By CARL DIMARTINI

The diagram is from Hansen (Gen Ref 3), Elliott (Gen Ref 4), and Shunk (Gen Ref 5).

Figure A-7. Lead-Tin Phase Diagram
This diagram is from the Metals Handbook, Vol. 8, 8th edition, pp. 330, 372.

Pd-Sn Palladium-Tin

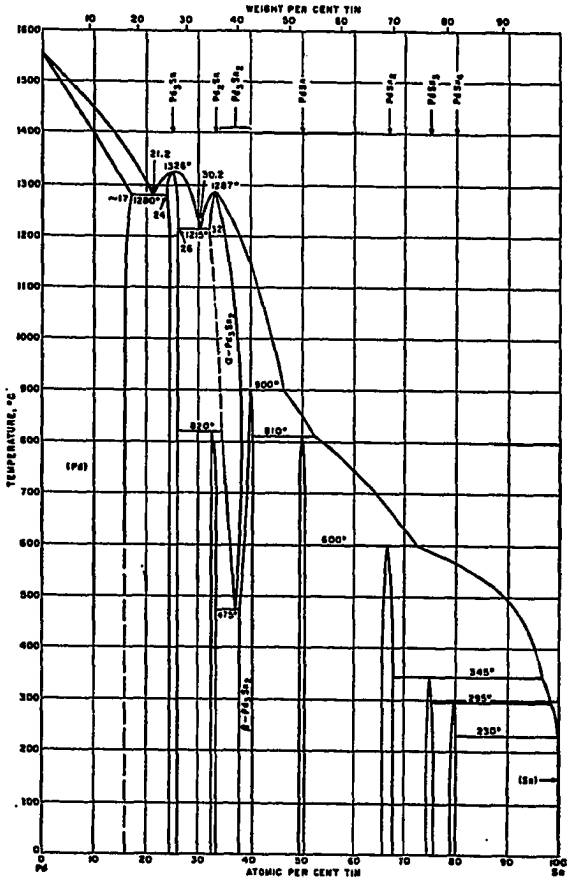

Pd-Sn

Pd-Sn (Palladium-Tin)
By R. P. Elliott

Formula	Symmetry	Prototype
Pd_3Sn	FCC	
Pd_2Sn	Orthorhombic	Ni_2Si
Pd_3Sn_2		
$PdSn$		
$PdSn_2$	Monoclinic or Tetragonal	CaF_2
$PdSn_3$	F. C. Orthorhombic	
$PdSn_4$		

Figure A-8. Palladium-Tin Phase Diagram
This diagram is from the Constitution of Binary Alloys, First Supplement by R. P. Elliott, p. 733.

Pt-Sn Platinum-Tin

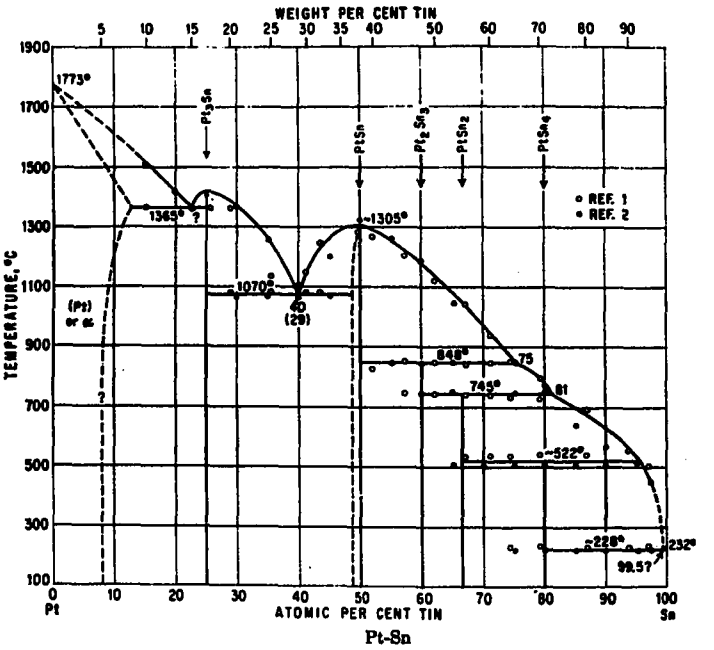

Pt-Sn (Platinum-Tin)
By M. Hansen

Formula	Symmetry	Prototype
Pt_3Sn		Cu_3Au ($L1_2$)
Pt^3Sn		NiAs (B8)
Pt_2Sn_3	Hexagonal	
Pt^2Sn_2	Cubic	CaF_2 (C1)
$Pt\ Sn_4$	Orthorhombic	

Figure A-9. Platinum-Tin Phase Diagram
This diagram is from the Constitution of Binary Alloys, by M. Hansen, 2nd edition, p. 1142.

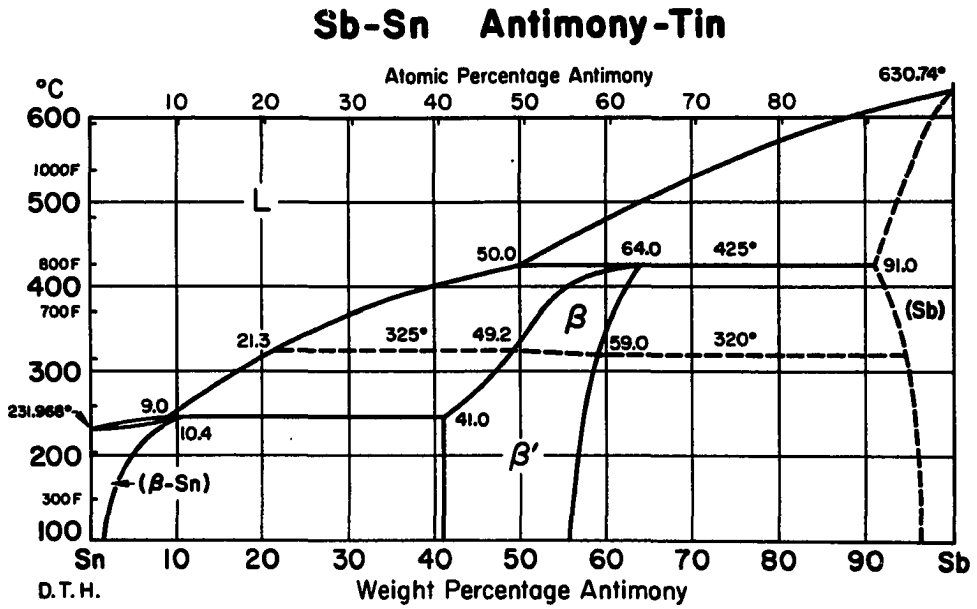

Sb-Sn (Antimony-Tin)

By DONALD T. HAWKINS

The diagram is from R. F. Smart, *Tin and Its Uses*, Vol 51, 1961, p 8-9. Hultgren *et al* (Gen Ref 6) give the formula for the β and β' phases as SbSn. The crystal symmetry is rhombohedral, nearly cubic, with no change in structure between the two phases.

Figure A-10. Antimony-Tin Phase Diagram
This diagram is from the Metals Handbook, Vol. 8, 8th edition, pp. 333, 374.

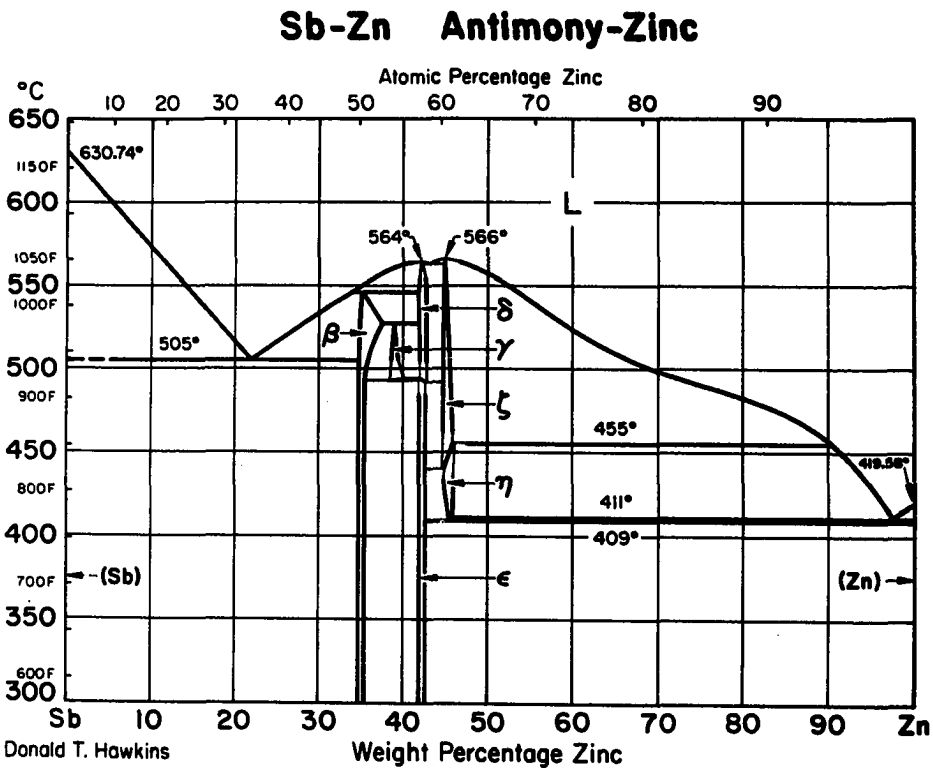

Sb-Zn (Antimony-Zinc)

By DONALD T. HAWKINS

The diagram is from Hansen (Gen Ref 3), except that the detail between 34 and 46 wt % Zn is from Vuillard and Piton (1). Crystal-structure data are from Pearson (Gen Ref 2):

Phase	Formula	Symmetry	Symbol	Prototype
β	SbZn	ortho	B_{a}	CdSb
γ	...	unknown	...	...
δ	...	unknown	...	...
ϵ	β Sb_2Zn_3	mono or hex	...	...
ζ	...	unknown	...	...
η	...	unknown	...	...

1. G. Vuillard and J. P. Piton, *Compt Rend*, Ser C, Vol 263, 1966, p 1018-1021

Figure A-11. Antimony-Zinc Phase Diagram
This diagram is from the Metals Handbook, Vol. 8, 8th edition, pp. 334, 373.

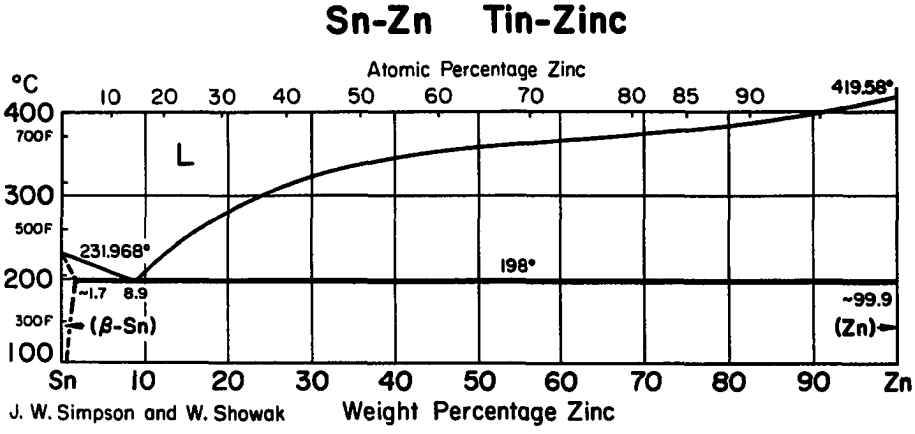

Sn-Zn (Tin-Zinc)

By J. W. SIMPSON and W. SHOWAK

The solubility of zinc in tin is from Génot and Hagège (1); the eutectic composition is from Hagège and Génot (2). The remainder of the diagram is from Hansen (Gen Ref 3) and Elliott (Gen Ref 4).

1. M. Génot, R. Hagège, *Compt Rend*, Vol 251, 1960, p 2901-2903
2. R. Hagège, M. Génot, *Compt Rend*, Vol 252, 1961, p 1002-1004

Figure A-12. Tin-Zinc Phase Diagram
This diagram is from the Metals Handbook, Vol. 8, 8th edition, pp. 336, 375.

APPENDIX B

MENISCOGRAPH MEASUREMENT OF THE SOLDERABILITY OF COMPONENT SURFACES USING 60/40 TIN-LEAD AND ANTIMONIAL SOLDERS

APPENDIX B

MENISCOGRAPH MEASUREMENT OF THE SOLDERABILITY OF COMPONENT SURFACES USING 60/40 TIN-LEAD AND ANTIMONIAL SOLDERS

Introduction

Most established solderability tests such as spread rate tests and capillary rise tests are based on a subjective appraisal of the results and do not provide simulation of modern processes. Budrys and Brick [B-1] imply that the main shortcoming of these capillary rise and solder spread tests in evaluating solderability is that they do not provide any information about the rates of wetting. The rates of wetting are of particular importance in high speed commercial soldering operations where the time allowed for complete wetting to occur is on the order of a few tenths of a second.

Due to these shortcomings in the established solderability tests, the G.E.C. (General Electric Company) Meniscograph was developed by MacKay [B-2]. The meniscograph was designed to provide a reasonable simulation of the practical conditions in soldering operations, to measure the quality of wetting achieved and not simply the attainment of

an arbitrarily defined minimum, to monitor the kinetics of the wetting process, and to produce quantitative, non-subjective results. The meniscograph test method monitors the wetting process from beginning to end by measuring the net force acting between the specimen and the solder. When recorded as a function of time this displays:

1) The time to commence wetting
2) The rate of wetting
3) The time to reach equilibrium
4) The ultimate extent of wetting

Shipley [B-3] suggests that the dependence of the wettability on each of several variables can be measured by maintaining all variables constant except the one under investigation. By this method, the influence of various flux formations, substrate materials, solder compositions, and soldering temperatures can be optimized for a given soldering system.

The principle of operation of the G.E.C. Meniscograph developed by MacKay is shown in Figure B-1. The specimen is suspended from a load cell which consists of a pair of cantilever springs between which is mounted the armature of a linear variable differential transformer. No mechanical coupling exists between the specimen and the measuring system, thus eliminating the problem of friction. The output of the load cell is a positive or negative DC signal proportional to the forces acting on the specimen. The solder bath is raised until the electrical contact is made between specimen and solder and the mechanism then immerses the specimen to variable immersion depth which is preset. A timer which is also preset comes into operation. After the set time expires the bath withdraws to its reset position. The output of the load cell is fed to

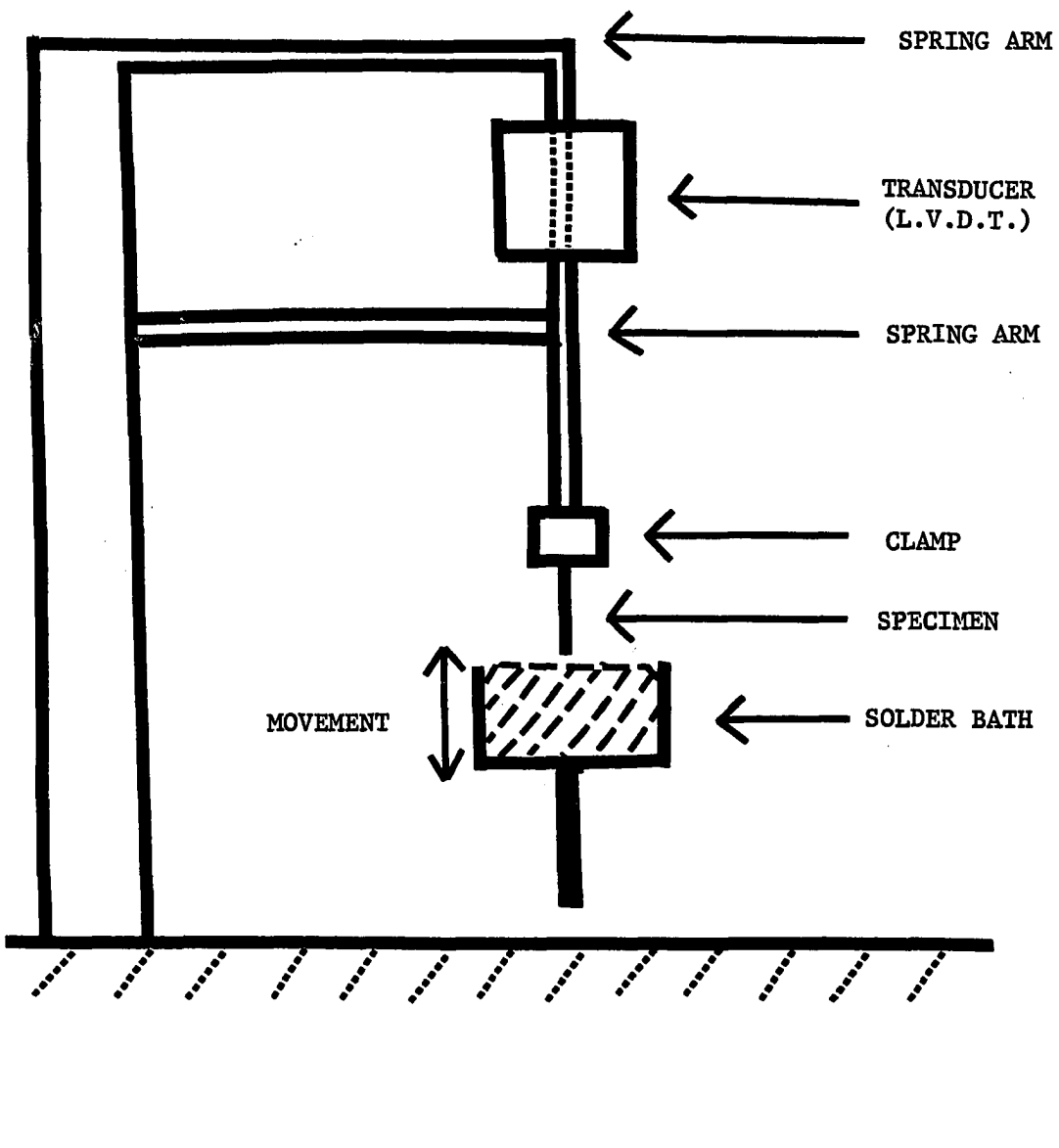

Figure B-1. The principle of operation of the G.E.C. Meniscograph

a chart recorder operating in the center zero mode. Since the initial weight of the specimen is first balanced out by means of the electrical zeroing system of the instrument, the chart recorder registers only the changing forces acting on the specimen.

Experimental

The studies reported here involved the use of the G.E.C. Meniscograph in comparing the wetting characteristics of the 60 w/o Sn - 40 w/o Pb solder commonly used in the electronics industry and an antimonial solder alloy (52 w/o Sn - 45 w/o Pb - 3 w/o Sb). The seven substrate metals used for the comparison were:

1) Pure Copper (99.999)
2) Cartridge (α) Brass (70 w/o Cu - 30 w/o Zn)
3) 2.5 micron Cobalt Hardened Gold Plating (90 w/o Cu - 8 w/o Ni - 2 w/o Sn base)
4) Copper-Nickel-Tin (90 w/o Cu - 8 w/o Ni - 2 w/o Sn)
5) Beryllium Copper (3 w/o Be - 97 w/o Cu)
6) 0.5 micron Palladium Plating (90 w/o Cu - 8 w/o Ni - 2 w/o Sn base)
7) 2.5 micron 60/40 Solder Plating (90 w/o Cu - 8 w/o Ni - 2 w/o Sn base)

The substrate metals were in the form of .025 inch square terminals.

Prior to cleaning, each terminal was fastened in the specimen holder in order to eliminate handling. The terminals were cleaned in a 10% HCl solution for 30 seconds, rinsed with distilled water for 15 seconds, immersed for 30 seconds in propanol, and allowed to dry in room air. Prior to immersion in the molten solder bath, the terminals were

dipped in Alpha 611 flux (mildly activated water-white rosin) for 15 seconds. Approximately 15 to 20 seconds after the fluxing procedure, the terminals were immersed in the molten solder bath. An immersion time of 12 seconds remained constant throughout the investigation. The terminals were immersed to a depth of 4 mm. The changes in force versus time were recorded with a 7100B Hewlett Packard strip chart recorder. Graphical force versus time recordings were obtained for five different samples of each substrate for each of the following soldering systems:

1) 60/40 Solder - 420°F (216°C)
2) 60/40 Solder - 500°F (260°C)
3) Antimonial Solder - 420°F (216°C)
4) Antimonial Solder - 500°F (260°C)

The data acquired from the five different recordings for each soldering system and substrate were averaged and compared graphically. Recordings representing nonsystematic behavior were excluded.

Results and Discussion

The graphical recordings of the force versus time data provide a quantitative measure of the wetting characteristics of the solder system. The ideal selection of cleaning, fluxing, and soldering parameters should provide conditions which approach infinite wetting. For an infinite wetting system, the terminal would be literally drawn into the bath at the moment of contact with the solder bath. The shape of the data curve for an infinite wetting specimen, as presented by Ippolito and Wolfe [B-4], is shown in Figure B-2. This figure also contains a sketch of the planar view of the contact profile between the terminal and the liquid solder.

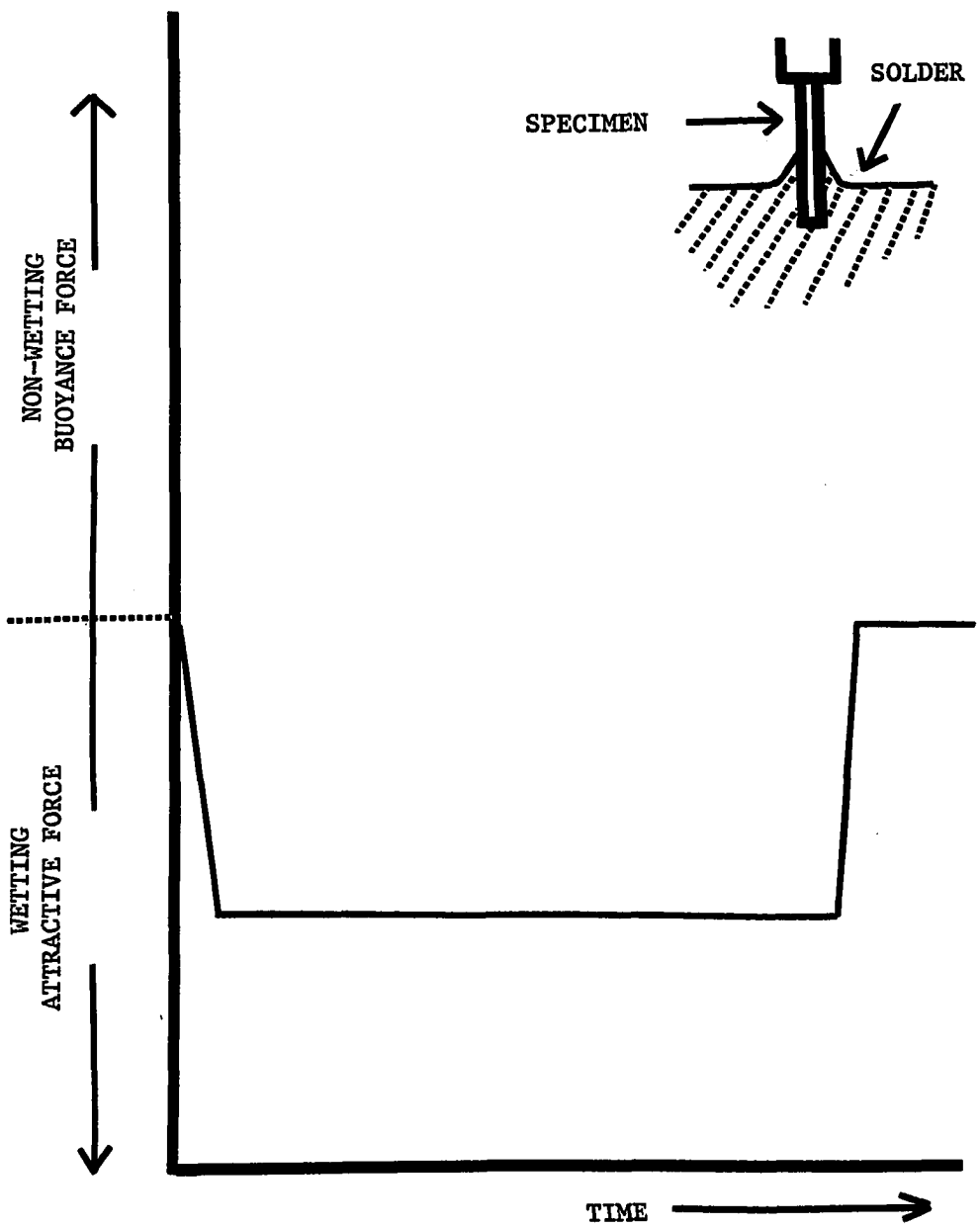

Figure B-2. Time-wetting curve for "infinite wetting"

The opposite extreme is the case of zero wetting. When the bath is brought into contact with the terminal, the terminal is buoyed upward by the bath, due to the differences in densities between the terminal and the solder. Figure B-3 reveals the shape of the data curve and a sketch of the planar view of the contact profile given by Ippolito and Wolfe for the "zero" wetting specimen. The actual solder operations in this study were characterized by a wetting time curve lying somewhere between these two extremes. Figure B-4 represents the typical curve generated by the soldering systems under investigation. This figure also serves to highlight the segments of the data curve (buoyancy peak, wetting time, and wetting rate) used to evaluate particular soldering systems. A desirable solder system is generally characterized by low buoyancy peaks, short wetting times, and high wetting rates.

Buoyancy Forces

The meniscograph recorded quantitative changes in the force exerted on the terminal as a function of time. The first force recorded was the weight of the terminal prior to entering the solder. As the terminal entered the solder a buoyancy force was exerted on the terminal by the molten solder bath. The buoyancy force was recorded as a negative change in force. A comparison of the buoyancy forces for the particular soldering systems is presented in Table B-1. The buoyancy force could be expressed in terms of dynes or newtons; however, since it is not essential for the comparison, the forces are simply given in arbitrary units. From the comparison it can be seen that in all cases except the palladium plated antimonial solder system, the buoyancy force was lower at 500°F than at 420°F. Also, the buoyancy force was higher

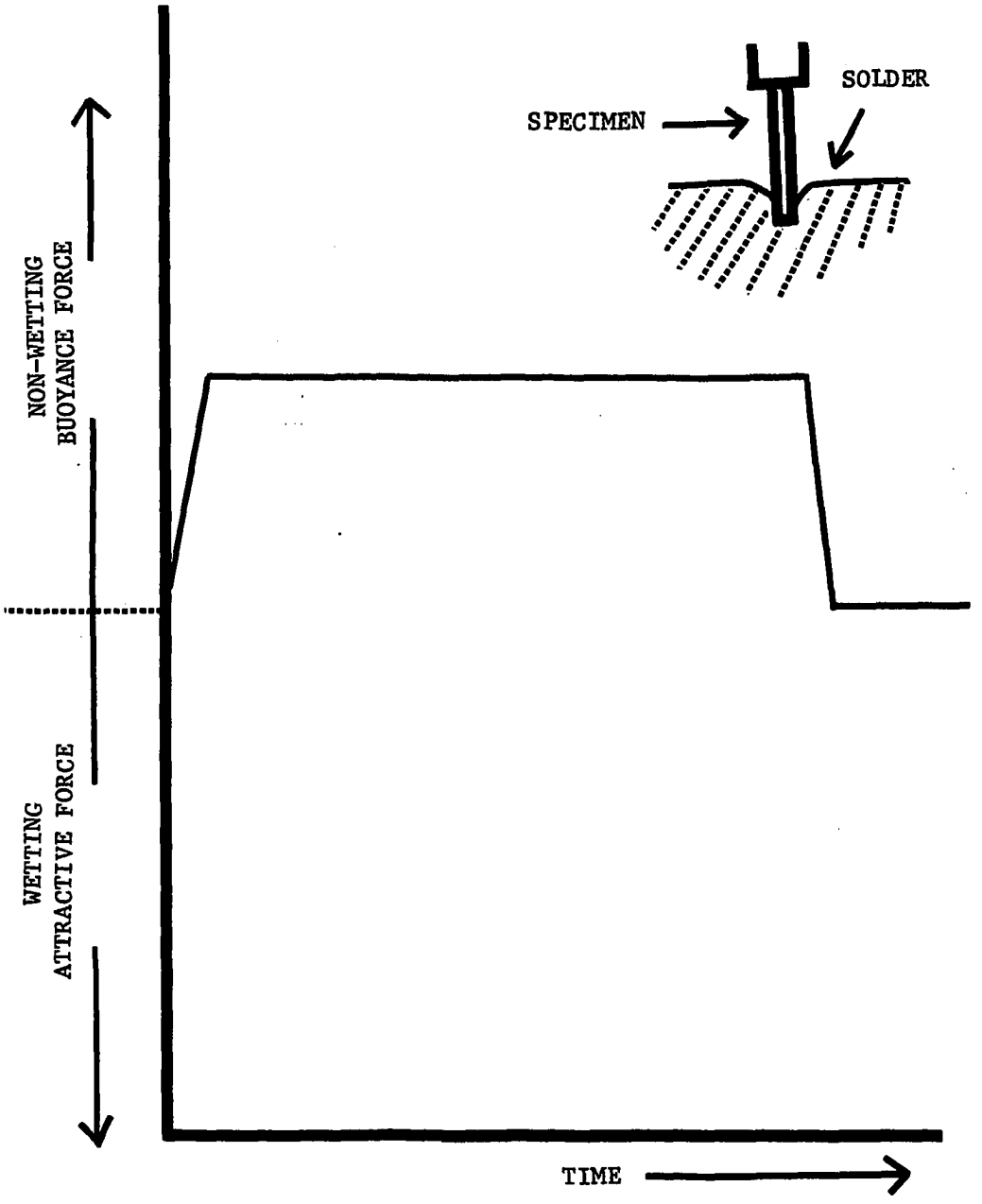

Figure B-3. Time-wetting curve for "zero wetting"

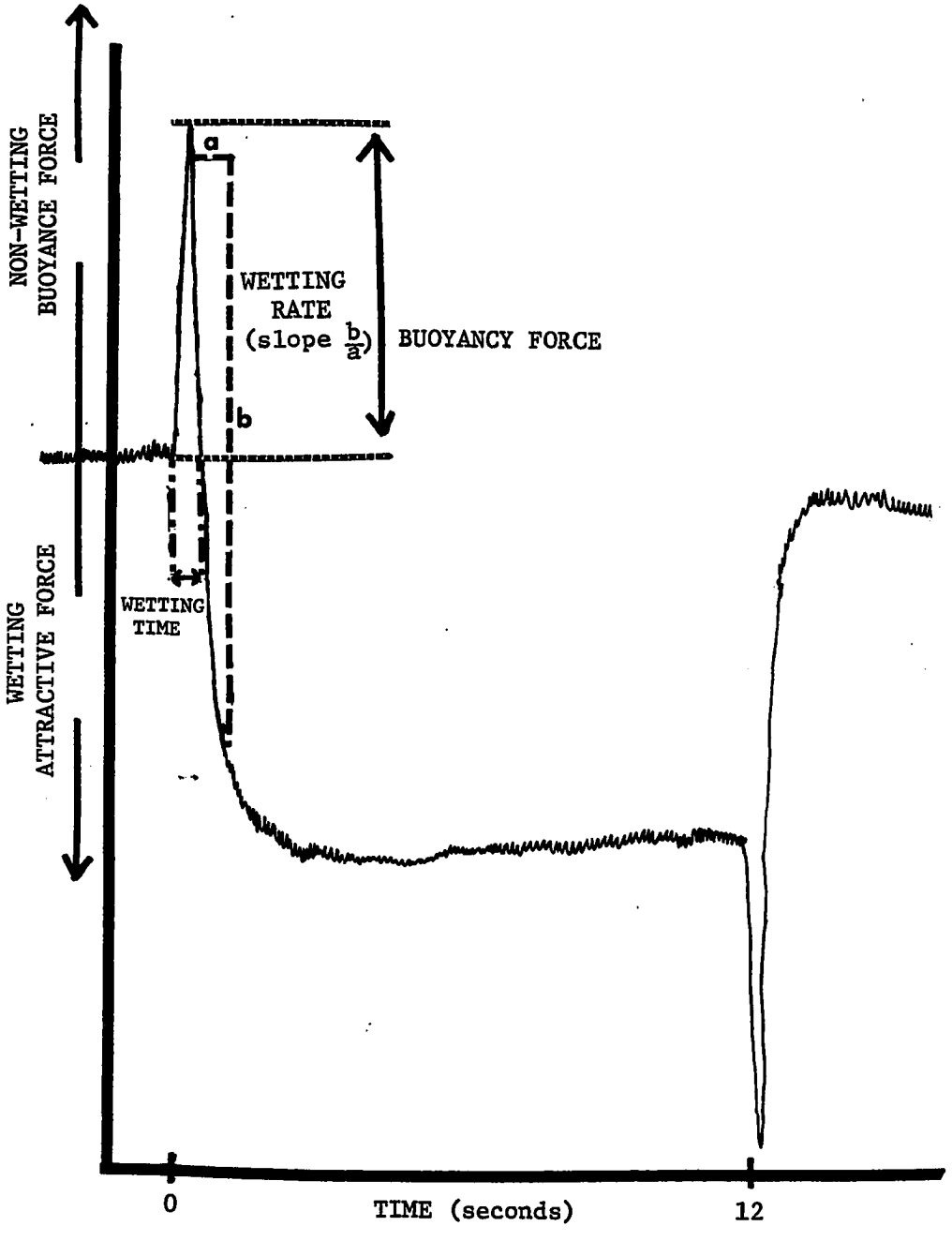

Figure B-4. A typical wetting curve generated by the soldering systems under investigation. The buoyance force, wetting time, and wetting rate (slope b/a) were used to evaluate the wetting characteristics of the soldering systems.

TABLE B-1

COMPARISON OF THE BUOYANCY FORCES
FOR THE SOLDERING SYSTEMS TESTED

SUBSTRATE	60/40 SOLDER		ANTIMONIAL SOLDER	
	420°F	500°F	420°F	500°F
Pure Copper	5.5	1.3	5.2	2.7
Cartridge (α) Brass	4.8	1.2	9.0	4.0
Gold Plated	2.6	2.0	11.2	2.2
Copper-Nickel-Tin	5.2	3.1	11.5	8.0
Beryllium Copper	8.9	1.5	13.4	2.9
Palladium Plated	9.7	5.0	10.8	14.5
Solder Plated	9.7	0.7	18.6	4.3

for the antimonial soldering systems than for the 60/40 soldering systems. An exception is evident in the case of the pure copper substrate at 420°F where the buoyancy force for the antimonial solder was slightly lower than for the 60/40 solder.

Copper, cartridge (α) brass, and cobalt-hardened gold plated terminals are very common substrate metals in the electronics industry. Therefore, a separate comparison was made of the buoyancy forces of these three substrates and is indicated by Figure B-5. In this figure, the buoyancy forces were plotted as a function of the soldering temperature for each substrate and solder. The solid lines represent the 60/40 solder systems while the dashed lines signify the antimonial solder systems.

The buoyancy forces for the gold plated 60/40 soldering system were very low due to the fact that gold dissolves rapidly in molten 60/40 solder. For the gold plated antimonial soldering system the buoyancy force plot was entirely different. At 420°F the buoyancy force for the gold plated antimonial solder system was extremely high. A possible explanation for this phenomenon, suggested by Duckett and Ackroyd [B-5], may be that the addition of antimony and the reduction of tin reduce the dissolution rate of gold in the molten solder. However, at 500°F the buoyancy force for the gold plated substrate in the antimonial solder was much lower and differed only slightly from the 60/40 solder. This suggests that at higher temperatures gold dissolves more rapidly in the antimonial solder, despite the tin reduction and the addition of antimony.

The buoyancy force for the pure copper-antimonial solder system was slightly lower than for the 60/40 solder system at 420°F. However,

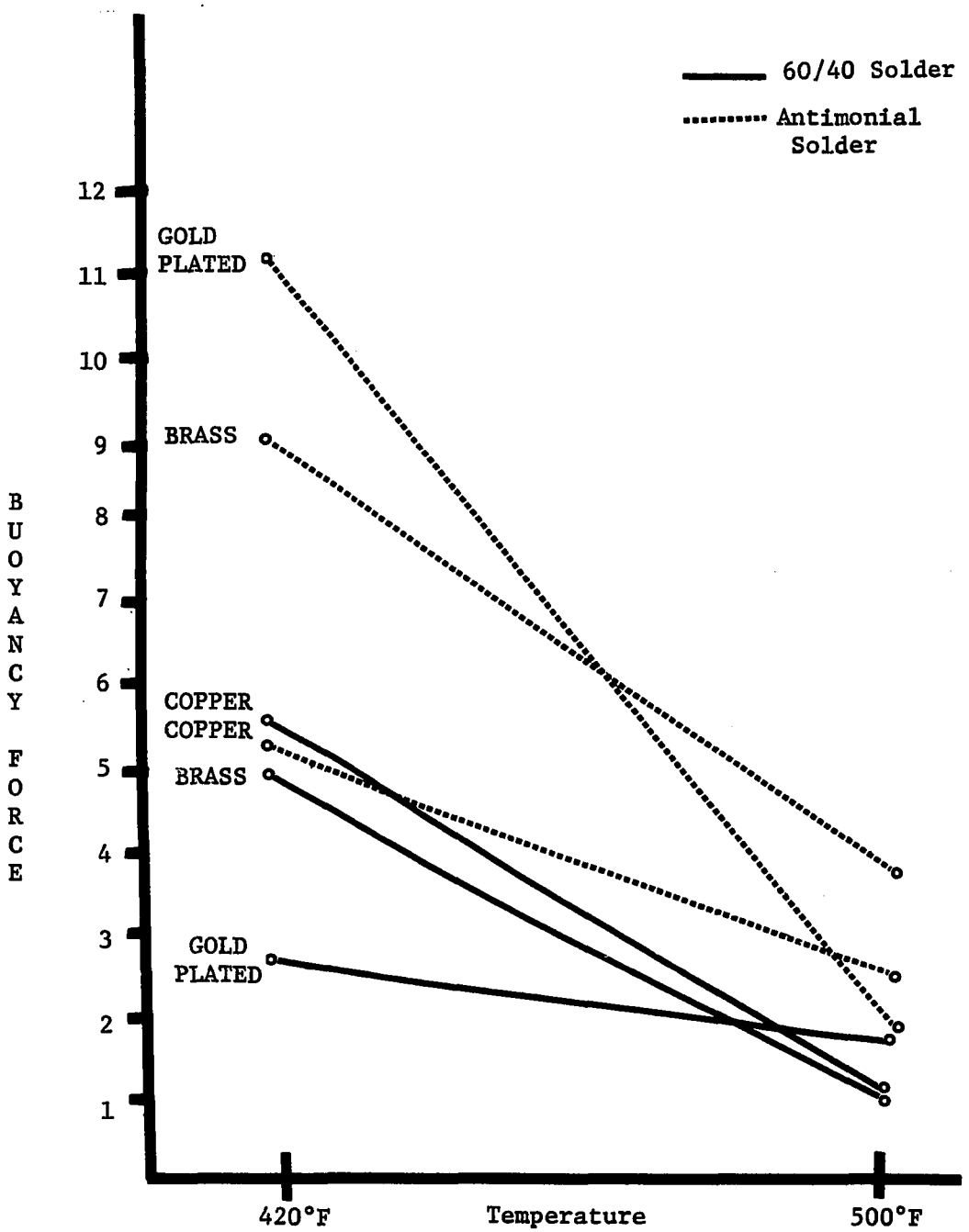

Figure B-5. Buoyancy Force vs Temperature Plot for Copper, Brass, and Gold Plated Substrates

at 500°F the buoyancy force for the 60/40 solder system was considerably lower. Gutbier [B-6] and Bader [B-7] suggest that lowering the tin content of solder reduces the dissolution rate of copper. The buoyancy force plots for the copper substrate at 500°F agree with their suggestion, while the plots at 420°F do not agree. This implies that the dissolution rate of copper in antimonial solder is temperature dependent. For the brass substrate, the buoyancy force plots were almost parallel, with the 60/40 solder system exhibiting lower buoyancy forces.

The buoyancy forces for the other four substrates (copper-nickel-tin, beryllium-copper, solder plated and palladium plated) were also compared graphically as shown in Figure B-6. The copper-nickel-tin substrate exhibited low buoyancy forces for the 60/40 solder at both 420°F and 500°F. The buoyancy force plots for the copper-nickel-tin, beryllium-copper, and the solder plated substrates decreased with increasing temperature. The plots for the 60/40 solder system and the antimonial solder system were almost parallel, with the lower plot corresponding to the 60/40 solder system. However, for the palladium plated antimonial solder system the buoyancy force plot increased with increasing temperature.

Wetting Times

The wetting time for each soldering system was determined from the force versus time data in the manner shown in Figure B-4. A comparison of the wetting times for the soldering systems is presented in Table B-2. The time is also expressed in arbitrary units, with one unit equivalent to 0.5 seconds. From the comparison, it is evident that for all soldering systems the time required for wetting was less at 500°F.

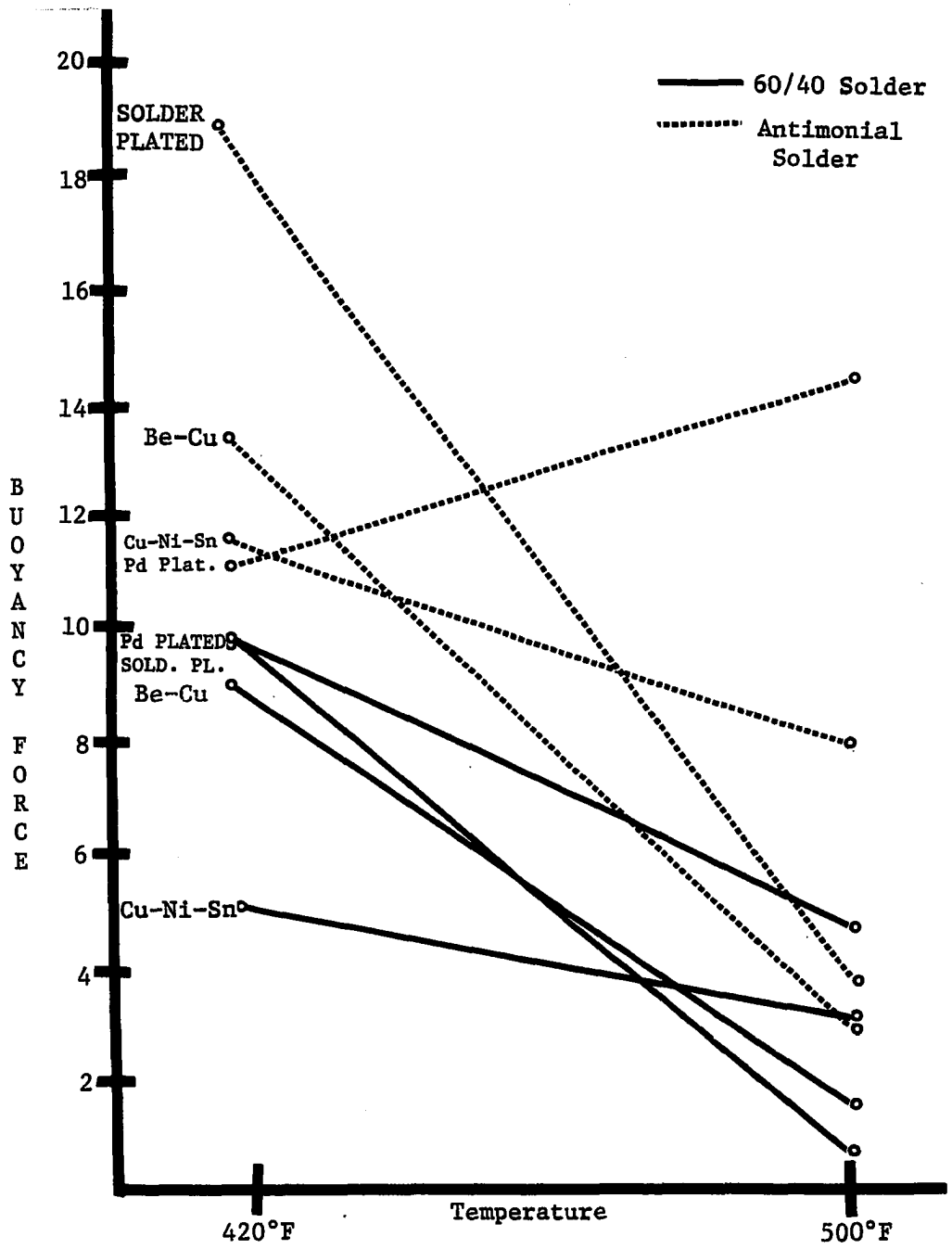

Figure B-6. Buoyancy Force vs Temperature Plot for Cu-Ni-Sn, Be-Cu, Pd Plated, and Solder Plated Substrates

TABLE B-2

COMPARISON OF THE WETTING TIMES
FOR THE SOLDERING SYSTEMS

SUBSTRATE	60/40 SOLDER 420°F	500°F	ANTIMONIAL SOLDER 420°F	500°F
Pure Copper	.60	.18	.64	.29
Cartridge (α) Brass	1.25	.24	1.20	.40
Gold Plated	.30	.10	.97	.47
Copper-Nickel-Tin	.75	.33	.98	.82
Beryllium Copper	.68	.20	.76	.30
Palladium Plated	.88	.43	1.00	.93
Solder Plated	.90	.15	1.00	.64

Also, the wetting time was shorter for the 60/40 soldering system in all cases except for the cartridge (α) brass substrate soldered at 420°F.

The wetting times for the copper, brass, and gold plated substrates are compared graphically in Figure B-7. The gold plated 60/40 soldering system had the shortest wetting time due to the high dissolution rate of gold in molten 60/40 solder. For the antimonial solder system, the gold plated substrate required a longer time for wetting, further indicating that the addition of antimony reduces the dissolution rate of gold in molten tin-lead solder.

Soldering with the antimonial alloy on the copper substrate required the shortest wetting time, which was only slightly higher than the 60/40 soldering system at both 420°F and 500°F. The brass substrate required the longest time for wetting at 420°F, with the 60/40 solder system wetting even slower than the antimonial solder system. However, at 500°F the 60/40 solder required less time for wetting the brass substrate than the antimonial solder.

The wetting times for the other four substrates were compared graphically as indicated by Figure B-8. At 420°F the beryllium-copper 60/40 soldering system had the shortest wetting time. The solder plated 60/40 soldering system required the least time for wetting at 500°F. In all cases the time required for wetting was less at 500°F than at 420°F. Furthermore, for all substrates the antimonial solder had a longer wetting time than the 60/40 solder.

Wetting Rates

The wetting rates for the soldering systems were determined from the slopes of the wetting curves by the method shown in Figure B-4.

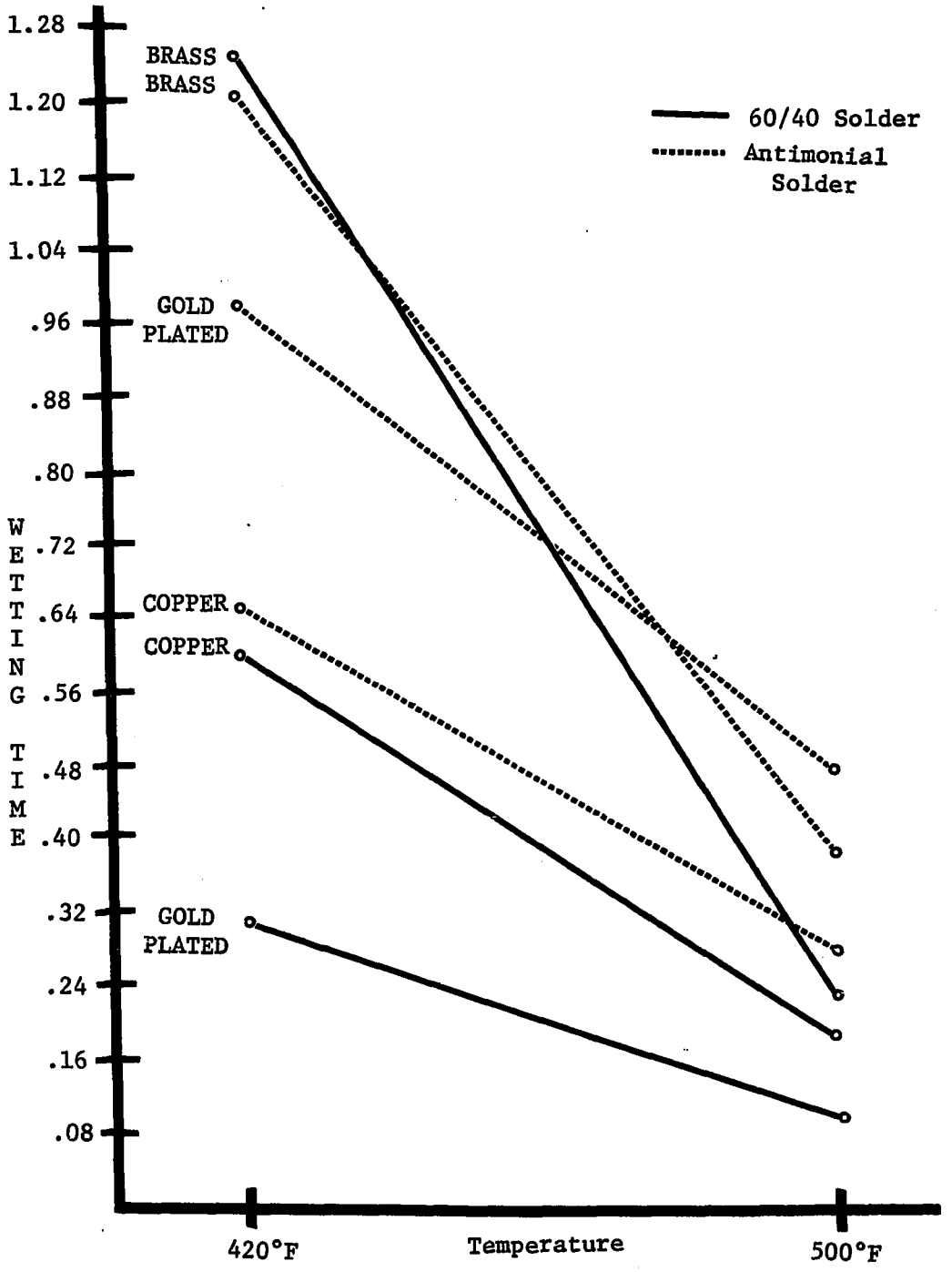

Figure B-7. Wetting Time vs Temperature Plot for Copper, Brass, and Gold Plated Substrates

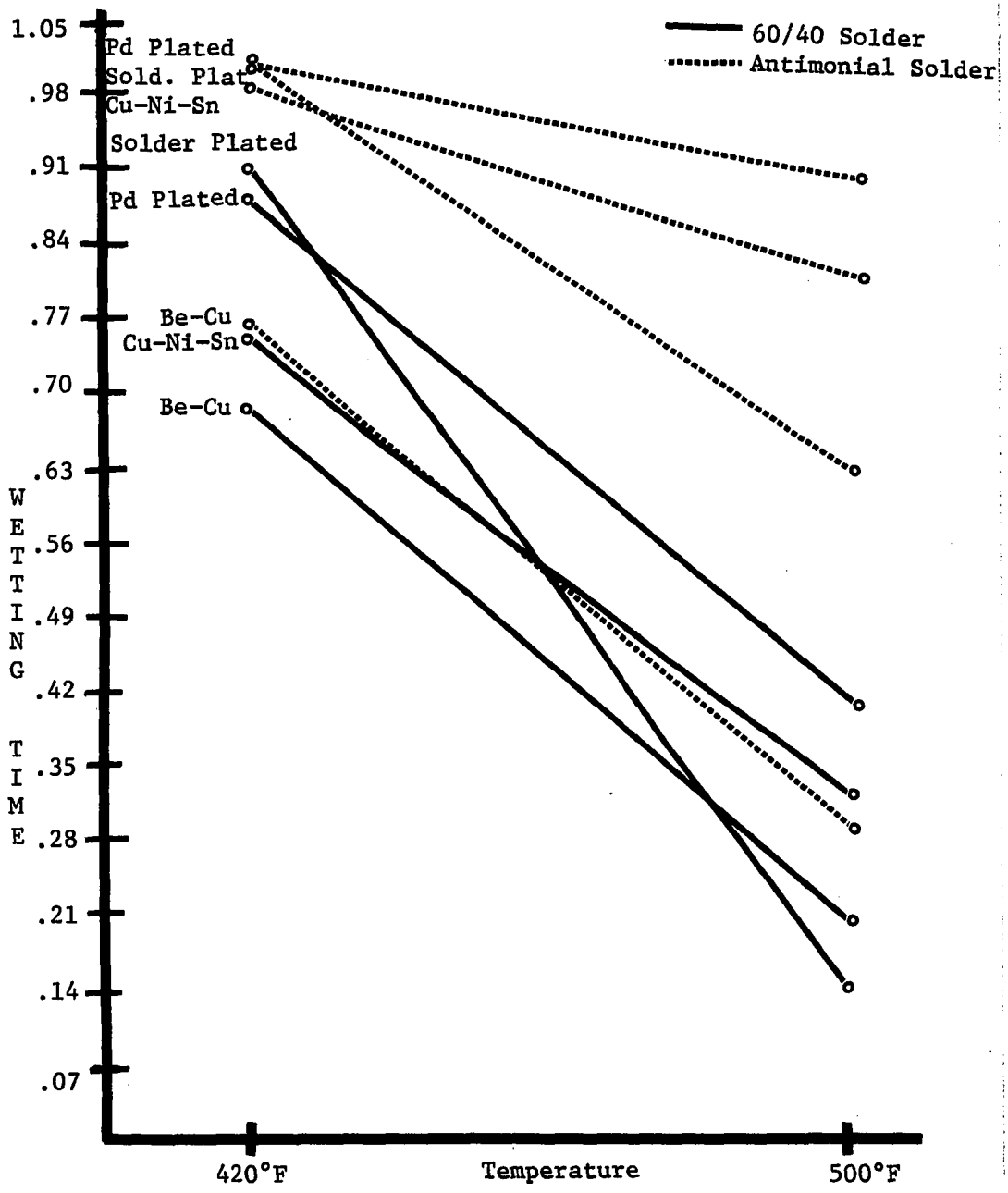

Figure B-8. Wetting Time vs Temperature Plot for Cu-Ni-Sn, Be-Cu, Pd Plated, and Solder Plated Substrates

Due to the steep slopes of the wetting curves in this study, the wetting rates were very difficult to determine accurately. Therefore, the wetting rate measurements may include a higher percentage error than the other measurements.

A comparison of the wetting rates for the soldering systems is presented in Table B-3. For the 60/40 soldering systems the wetting rates are higher at 500°F than at 420°F for all substrates except the gold plated and the palladium plated. For these substrates, the wetting rate varies only slightly with temperature. However, for the antimonial soldering systems the wetting rates are higher at 420°F than at 500°F for all substrates except the cartridge (α) brass. This implies that at higher temperatures the formation of intermetallic compounds, such as $AuSn_4$ and Cu_6Sn_5, reduced the tin content of the solder and thereby resulted in antimony exceeding the solid solubility limit in tin and the formation of antimony-tin intermetallic compounds.

The wetting rates for the copper, brass, and gold plated substrates were compared graphically as shown in Figure B-9. The gold plated 60/40 soldering system exhibited the highest wetting rate due to the extremely high dissolution rate of gold in molten 60/40 solder. The gold plated antimonial soldering system exhibited a much slower wetting rate, implying that the reduction of tin and the addition of antimony impedes the dissolution rate of gold in molten tin-lead solder. From this figure it is evident that the wetting rates for the antimonial solder are much more predictable than for the 60/40 solder. The wetting rate plots for the antimonial solder lie very close together as compared to the 60/40 solder wetting rate plots, which vary by significant amounts.

TABLE B-3

COMPARISON OF THE WETTING RATES
FOR THE SOLDERING SYSTEMS

SUBSTRATE	60/40 SOLDER 420°F	500°F	ANTIMONIAL SOLDER 420°F	500°F
Pure Copper	23.3	31.5	19.6	19.5
Cartridge (α) Brass	18.5	23.6	18.1	20.9
Gold Plated	32.0	31.0	22.6	18.4
Copper-Nickel-Tin	26.5	29.8	33.6	30.4
Beryllium-Copper	24.0	29.0	29.2	27.0
Palladium Plated	37.5	36.3	31.8	30.3
Solder Plated	25.2	36.0	32.6	27.5

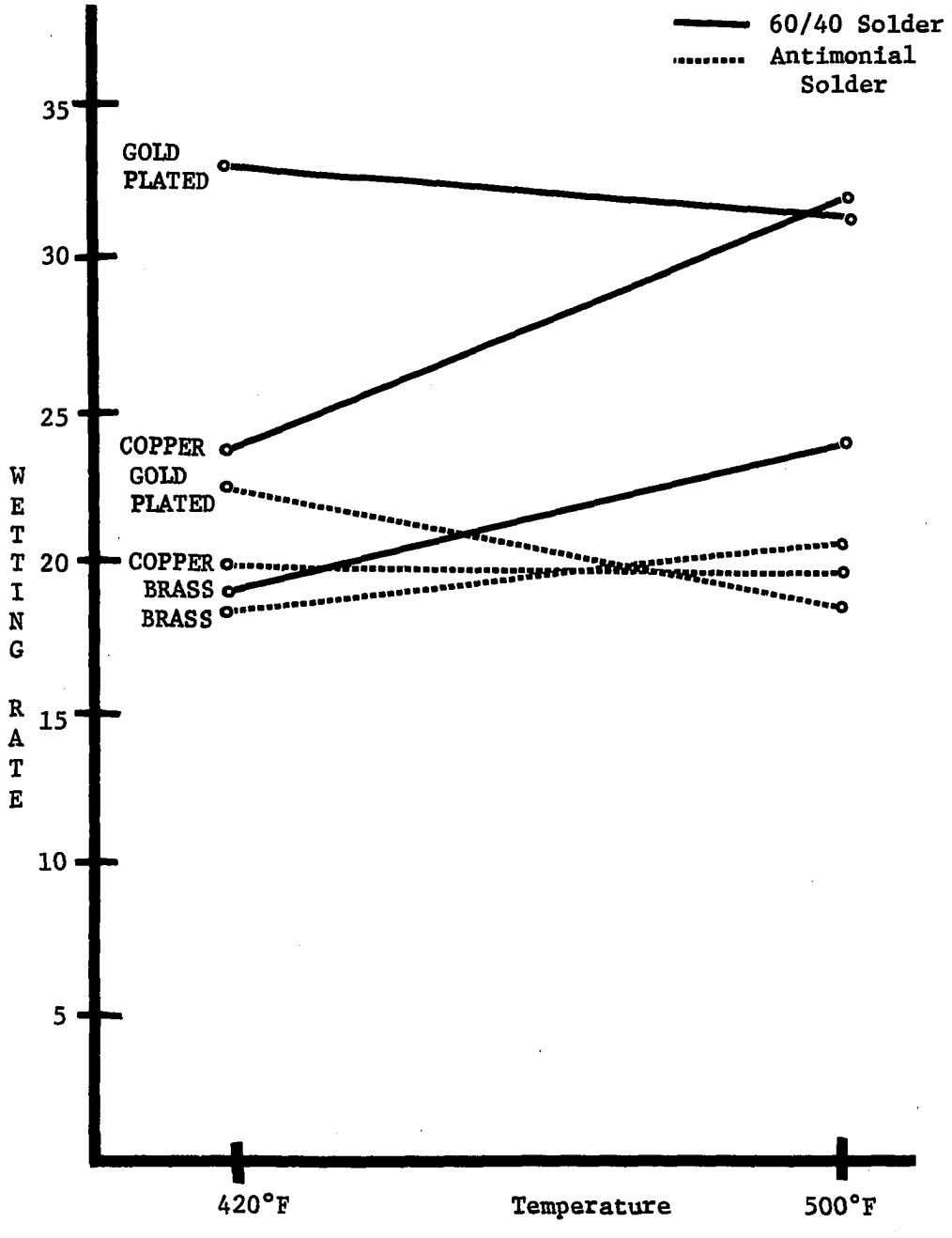

Figure B-9. Wetting Rate vs Temperature Plot for Copper, Brass, and Gold Plated Substrates

A graphical comparison of the wetting rates for the other four substrates is shown in Figure B-10. Again, the wetting rates for the antimonial solder are much more predictable than for the 60/40 solder. In all cases, except the palladium plated substrate, the wetting rates increased with increasing temperature for the 60/40 soldering system. However, for the antimonial soldering system the wetting rates decreased with increasing temperature.

Intermetallic Compound Formation

The wetting of a substrate by a tin-lead solder inevitably involves alloying between the substrate and tin at the interface between them. While a small amount of solid solution alloying can take place initially, this is quickly followed by the formation of intermetallic compounds with substrates such as gold and copper. The nature of the surface in contact with the solder thus changes with time and this may affect the wetting behavior of the system.

Abnormal fluctuations in the wetting curve represent changes in the nature of the substrate surface and suggest intermetallic compound formation. A typical wetting curve is shown in Figure B-11. A wetting curve for a gold plated terminal soldered with 60/40 solder at 500°F is shown in Figure B-12. The abnormal fluctuations (Location A) suggest the formation of gold-tin intermetallic compounds.

MacKay [B-8] studied the wetting behavior of copper substrates utilizing the meniscograph. He monitored the wetting characteristics of the compounds Cu_3Sn and Cu_6Sn_5. The wetting curves from his study are presented in Figures B-13 and B-14. His results indicate that the growth of intermetallic compounds during the soldering of copper substrates

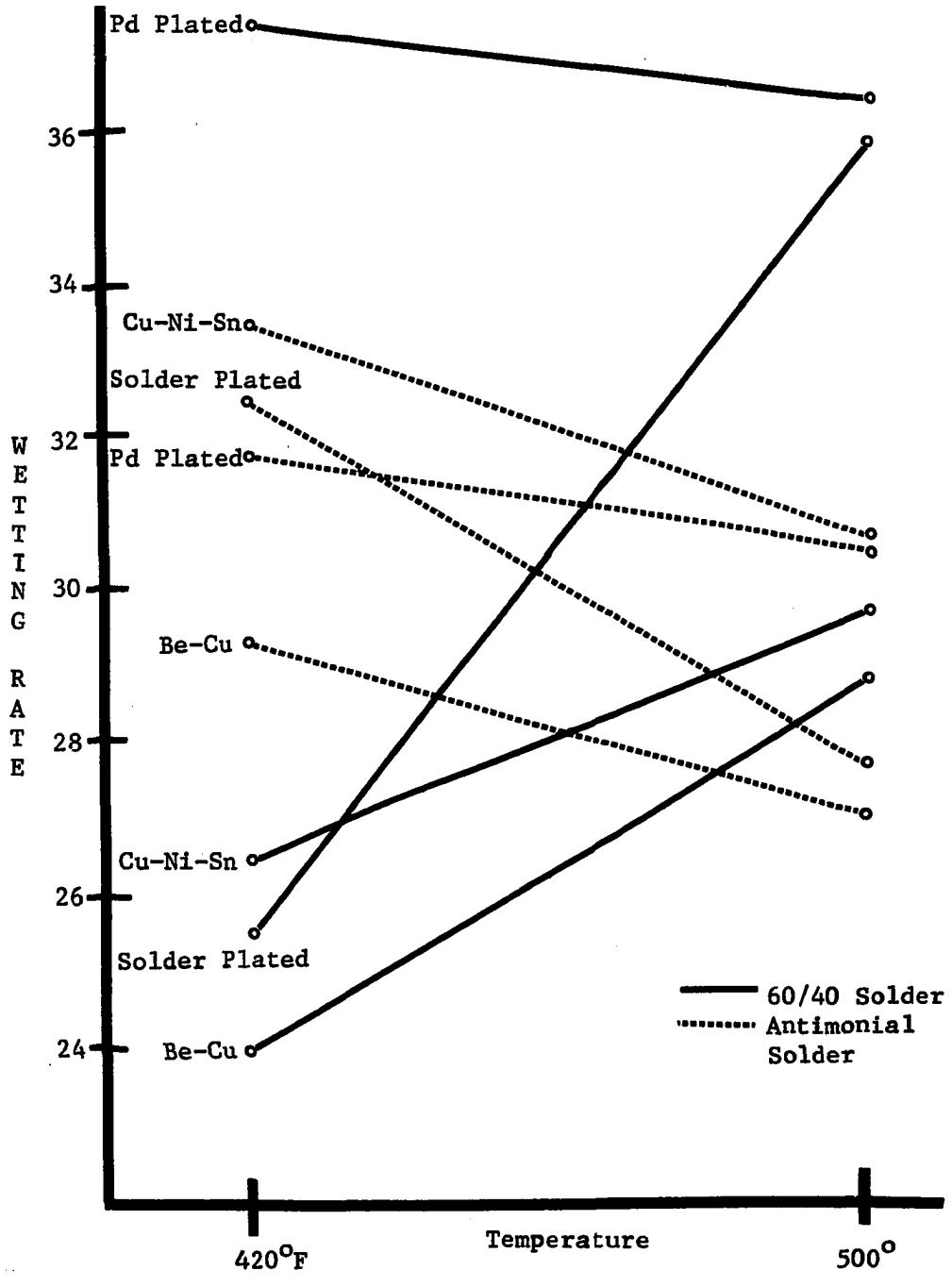

Figure B-10. Wetting Rate vs Temperature Plot for Be-Cu, Cu-Ni-Sn, Pd Plated, and Solder Plated Substrates

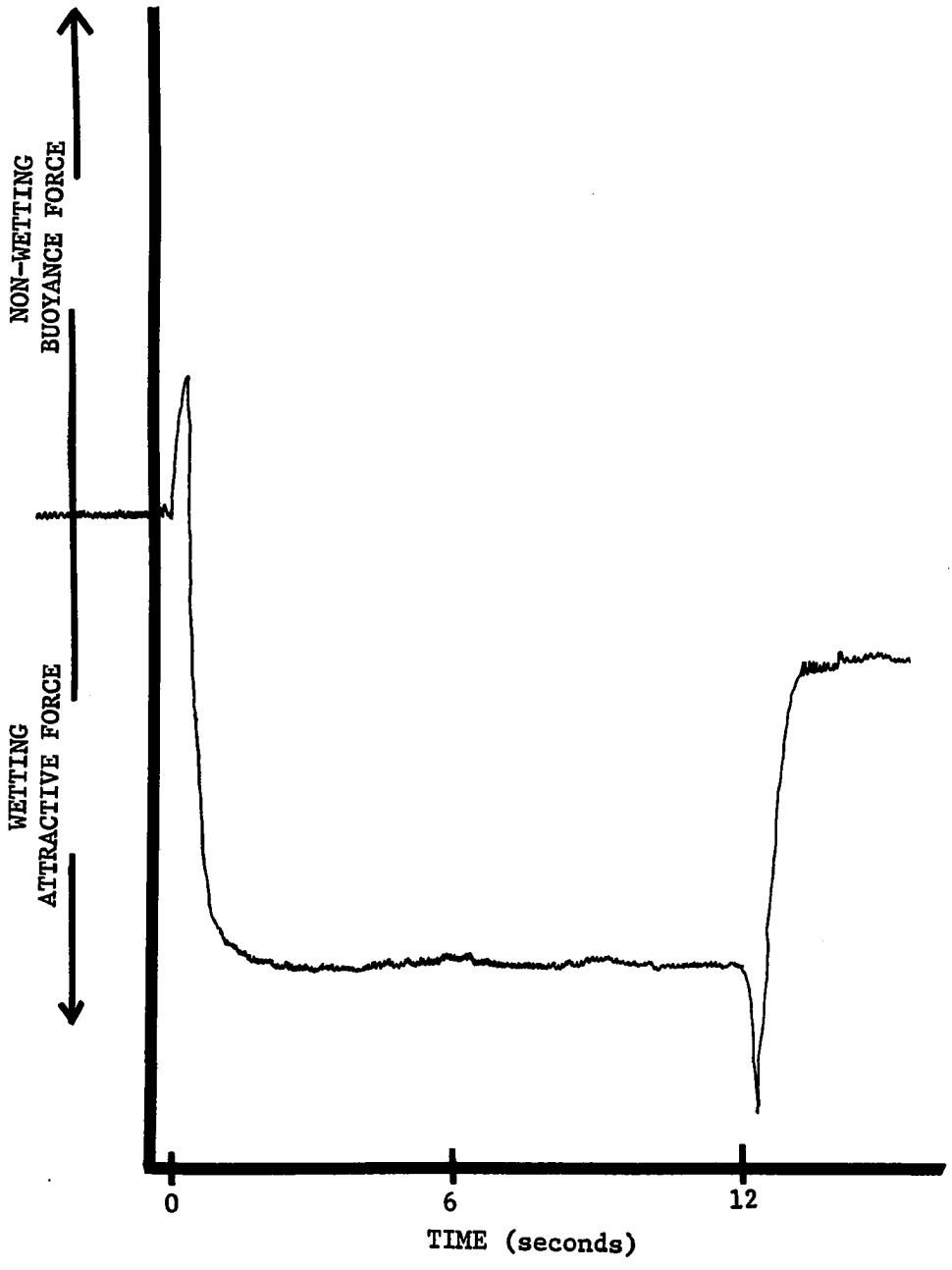

Figure B-11. A typical wetting curve. The curve is for Be-Cu soldered with 60/40 solder at 420°F (216°C).

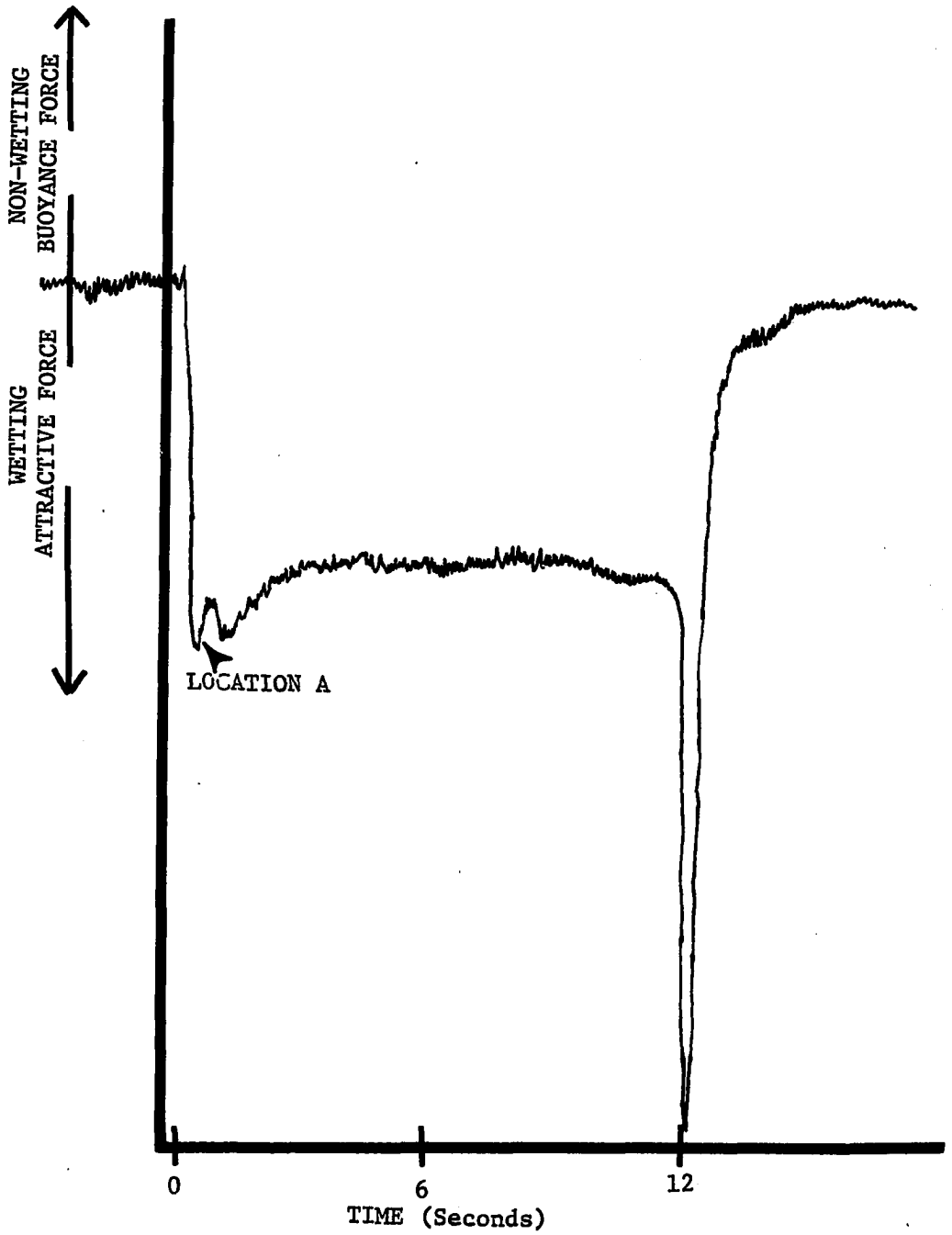

Figure B-12. Wetting curve for a gold plated terminal soldered with 60/40 solder at 500°F (260°C). Abnormal fluctuations at Location A suggest the formation of gold-tin intermetallic compounds.

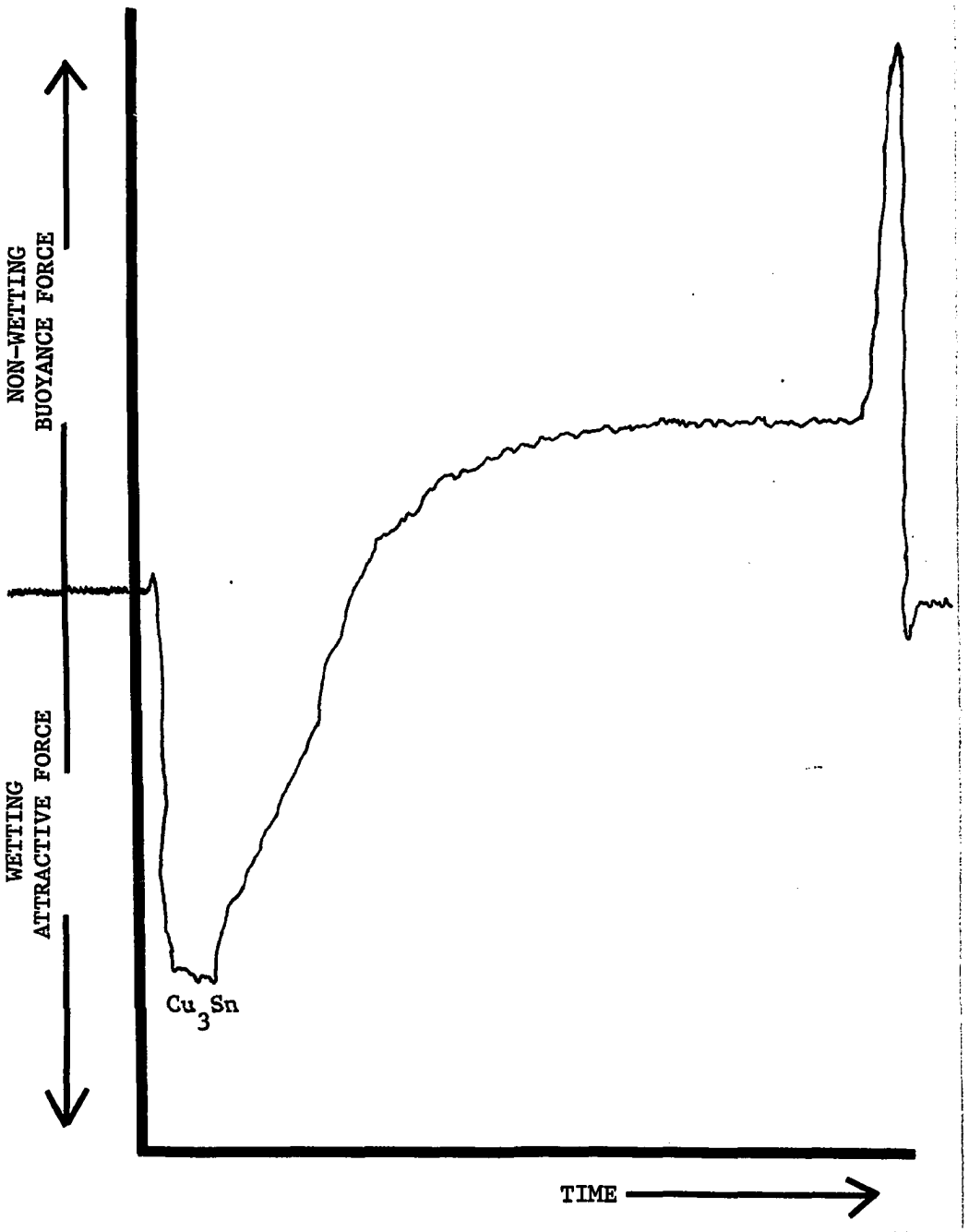

Figure B-13. The wetting curve from a study by MacKay demonstrating the wetting of Cu_3Sn at 255°C.

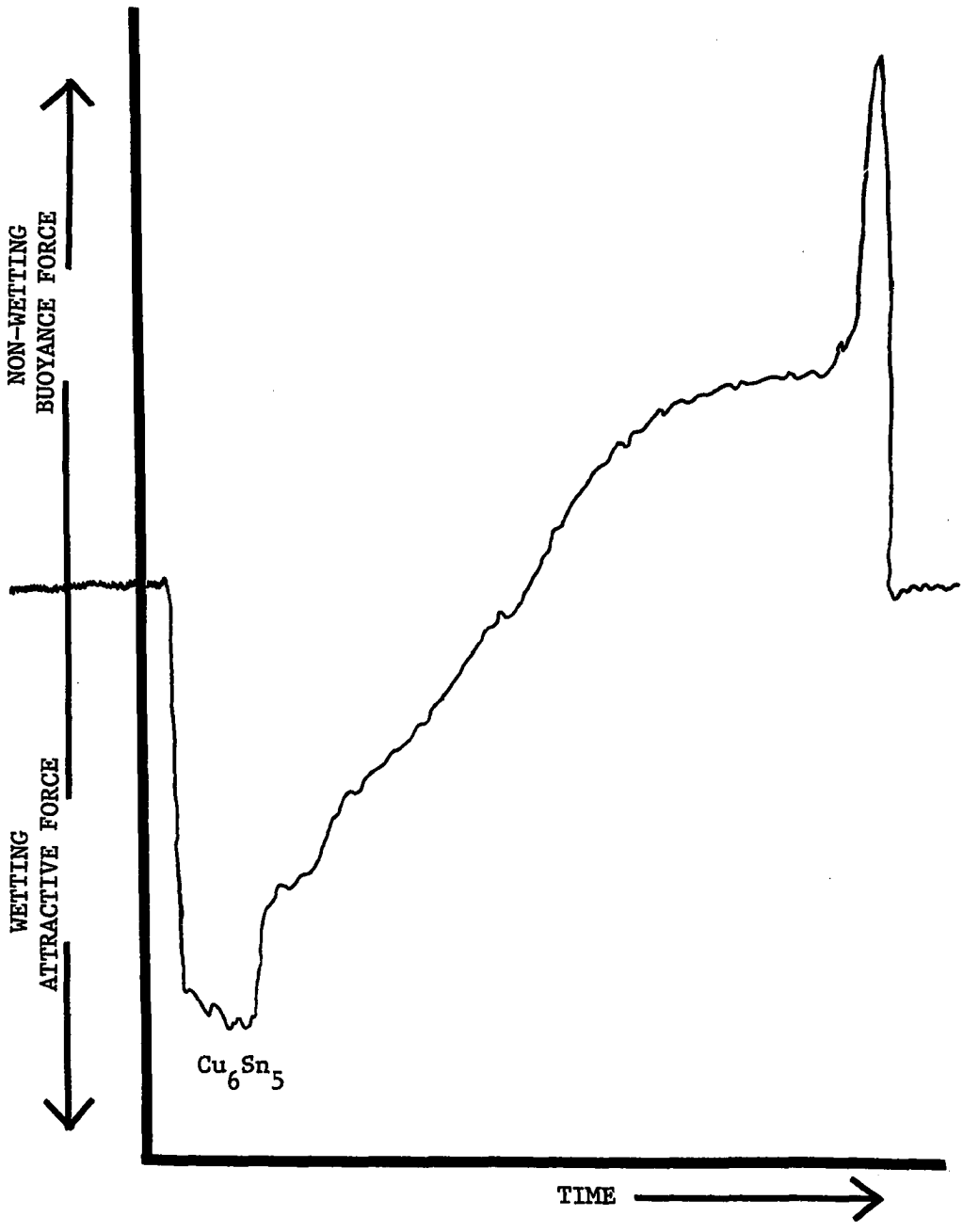

Figure B-14. The wetting curve from a study by MacKay demonstrating the wetting of Cu_6Sn_5 at 235°C.

influence the wetting behavior of the system. The wetting behavior of the soldering systems in this study may also have been influenced by the formation of intermetallic compounds.

Conclusions

An extensive study was made comparing the wetting characteristics of the 60/40 soldering system and the antimonial soldering system. The buoyancy forces, wetting times, and wetting rates were measured utilizing a meniscograph. Seven different substrate metals were used in comparing the solder systems.

The gold plated 60/40 soldering system produced the most desirable wetting characteristics with low buoyancy peaks, short wetting times, and high wetting rates at both 420°F and 500°F due to the high dissolution rate of gold in molten 60/40 solder. Abnormal fluctuations in the wetting curves for the gold plated 60/40 soldering system suggested the formation of gold-tin intermetallic compounds. The gold plated antimonial soldering system produced less desirable wetting characteristics due to the fact that the addition of the antimony and the reduction of the tin reduced the dissolution rate of gold. Duckett and Ackroyd [B-5] suggested that antimony additions would have such an effect.

The time required for wetting was less at 500°F for all substrates. The wetting time was shorter for the 60/40 soldering system in all cases except for the brass substrate soldered at 420°F. The wetting characteristics for the 60/40 solder were more desirable when soldering at 500°F than at 420°F. The wetting rates for the antimonial solder were higher at 420°F than at 500°F for all substrates except brass.

This implies that at higher temperatures antimony exceeds the solid solubility limit in tin and the formation of antimony-tin intermetallic compounds affect the wetting behavior of the substrate metals. The palladium plated substrate exhibited higher buoyancy peaks and slower wetting rates at 500°F than at 420°F. This suggests that at higher temperatures the nature of the substrate is changing possibly due to the formation of intermetallic compounds.

In general, the wetting characteristics of the 60/40 soldering systems were more desirable as compared to the antimonial soldering systems. This does not imply however that the antimonial solder alloy should not be investigated further as a substitute solder for the 60/40 alloy.

LIST OF REFERENCES

B-1. Budrys, R. S. and Brick, R. M., "Variables Affecting the Wetting of Tinplate by Sn-Pb Solders," Metall. Trans., Vol. 2, pp. 103-111, Jan. 1971.

B-2. MacKay, D., "The Meniscograph Method of Solderability Measurement," Proc. 1972 Sept. Meeting, Institute of Printed Circuits, Illinois, 1973.

B-3. Shipley, J. F., "Influence of Flux, Substrate and Solder Composition on Solder Wetting," Weld. Jour., Vol. 54, pp. 357s-362s, Oct. 1975.

B-4. Ippolito, A. D. and Wolfe, R. L., "Solderability Testing for Flux and Solder Improvement," Weld. Jour., Vol. 53, pp. 20-25, Jan. 1974.

B-5. Duckett, H. R. and Ackroyd, M. L., "The Influence of Solder Composition on the Embrittlement of Soft-Soldered Joints on Gold Coating," Electroplating and Metal Finishing, Vol. 29, pp. 13-20, May 1976.

B-6. Gutbier, E. A., "Dissolution Rates of Fine Magnet Wire in Molten Tin-Lead Solders," The Western Electric Engineer, pp. 25-33, Oct. 1977.

B-7. Bader, W. G., "Lead Alloys for High Temperature Soldering of Magnet Wire," Weld. Jour., Vol. 54, pp. 370s-375s, Oct. 1975.

B-8. MacKay, D., "The Solderability of Component Surface Tension Methods," Proc. Inter. Nepcon, Vol. II, pp. 40-51, 1970.